Universitat Autònoma de Barcelona

Searching for New Physics in Semileptonic B Meson Decays

Bernat Capdevila Soler

Searching for New Physics in Semileptonic B Meson Decays

Author: Bernat Capdevila Soler
Institut de Física d'Altes Energies (IFAE)

Thesis submitted for the degree of Philosophae Doctor (PhD)

Departament de Física
Universitat Autònoma de Barcelona

Day of Defense: 16 January 2020

Director:
Joaquim Matias Espona
Universitat Autònoma de Barcelona
Institut de Física d'Altes Energies (IFAE)
Institució Catalana de Recerca
i Estudis Avançats (ICREA)

Tutor:
Antonio Miguel Pineda Ruíz
Universitat Autònoma de Barcelona
Institut de Física d'Altes Energies (IFAE)

Abstract

In the recent years, intriguing hints of New Physics have been accumulated in semileptonic B-meson decays, mostly involving neutral-current transitions $b \to s\ell\ell$. The LHCb collaboration, other collaborations at the LHC and the Belle experiment have reported deviations from the Standard Model expectations in several observables measuring the aforementioned transition. These are commonly referred to in the literature as *B-anomalies*. Not surprisingly, some of these measurements show deviations from the SM predictions by a few standard deviations. More interesting is the fact that several of these deviations from the SM appear to be "in the same direction", in such a way that when quantified by a global fit the discrepancy with the SM is over the 5σ level.

In order to assess the significance of these anomalies and to treat them consistently, we propose a model-independent analysis based on an Effective Hamiltonian encoding the dynamics of the underlying quark level transition. This has the advantage of providing a simple systematic framework where all possible processes, mediated by the same transition, can be described with the same set of parameters, allowing for *global fits* of large numbers of observables defined in several channels.

This Thesis presents our most updated global analyses of $b \to s\ell\ell$ data. First, we describe the general framework used to compute the different types of observables, paying special attention to the treatment of the uncertainties involved. And then, we discuss both our analytical approach and the implications of the most significant results obtained from our fits.

Contents

Introduction

The discovery of the Higgs boson marked the completion of the Standard Model (SM) of particle physics, which describes the elementary constituents of matter and their interactions (strong, electromagnetic and weak) as a quantum field theory. This has led to precise predictions for measurable quantities tested experimentally with a high accuracy. However, there are compelling arguments claiming the existence of New Physics (NP) beyond the SM. Examples of these arguments are the observational evidence for the existence of dark matter and the fact that neutrinos have masses.

Therefore, we know that the SM must be extended but, since the SM provides precise determinations in most sectors, there are no obvious signals to be searched for. In this context, the field of rare decays will be a crucial tool to help us envisage effects at very high energies, which we cannot yet access at colliders, as it probes physics occurring at higher energies.

Over the last few years, many observables related to the flavour-changing neutral-current transitions $b \to s\ell\ell$ have exhibited deviations from SM expectations, constituting one of the first solid evidences of NP. On the one hand, the $b \to s\mu\mu$ flavour-changing neutral current is loop suppressed in the SM and it has been measured by several experiments, showing a collection of deviations from the SM in angular observables and branching ratios. Moreover, the comparison of $b \to s\mu\mu$ and $b \to see$ through the measurements of the observables R_K and R_{K^*}, for several values of the dilepton invariant mass, suggest a significant violation of Lepton Flavour Universality (LFU). All these deviations can be explained in a model-independent approach by NP contributions to Wilson coefficients associated with the effective operators describing $b \to s\mu\mu$ transitions, providing a consistent description of the observed pattern. More in detail, our recent combined analysis of these observables indeed singles out some NP scenarios preferred over the SM with a significance at the 5σ level, confirming the scenarios already highlighted in earlier analyses in the field.

The main goal of this Thesis is to provide a coherent and self-consistent description of all the techniques and methods needed for performing model-independent global fits to $b \to s\ell\ell$ data. To this end, this thesis can be formally divided into three parts:

- Part I (Chapters 1 to 5), where the main theoretical framework is described.
- Part II (Chapters 6 to 7), where we analyse in detail the different sources of hadronic uncertainties and construct a new basis of angular observables designed to test lepton flavour universality violating (LFUV) NP effects, without pollution coming from hadronic uncertainties in the SM.
- Part III (Chapters 8 to 9), where we present the latest results of our global fits, with a detailed anatomy of their composition and analytical strategies, and their implications

More in detail, we start by reviewing the fundamental theoretical framework used to compute the relevant observables within effective field theories, both at leading order and including higher-order QCD corrections. In Chapter 1 we describe how to construct effective field theories when different and highly hierarchised scales are involved in the physical phenomena under study. Particularly important is going to be the concept of effective Hamiltonian, which allows us to consistently treat physics at high and low energy scales. The former effects are encoded in Wilson coefficients, while effective operators contain the latter. Particularly relevant are the matrix elements of these effective operators, since they constitute one of the majors sources of uncertainty in our theory predictions. At leading order the aforementioned matrix elements can be parametrised in terms of form factors, which we discuss in Chapter 2. On the other hand, computing QCD corrections to the amplitude of our relevant processes is a major endeavour, as some of these corrections cannot be treated in perturbation theory at the typical energy scales of B-decays. However, in Chapter 3 we show, in the context of non-leptonic decays, that a systematic way of computing these corrections emerges from well-suited approximations. This very same framework is put into work for the semileptonic $B \to K^*\ell^+\ell^-$ mode in Chapter 4, where a general description of the dynamics of this decay is presented. We conclude this part in Chapter 5 by introducing the definitions and properties of the most relevant observables in our fits, both for $B \to K^*\ell^+\ell^-$ and the other channels involved. In this context, we will show that observables with optimal properties regarding their sensitivity to form factors at leading order can be constructed in the large recoil limit.

As we mentioned above, some of the QCD corrections to the amplitude admit a computation within the context of certain well-suited effective theories, but some others (often referred to as hadronic uncertainties) cannot be computed from first principles and one has to rely on partial calculations and phenomenological models. These hadronic uncertainties will set the main theme of Part II. First, following our article Ref. [1], in Chapter 6 we discuss the state-of-the-art treatment of these corrections and we critically reassess other frameworks where hadronic uncertainties are predicted to be particularly enhanced, showing that they are disfavoured as explanations for the observed anomalies. Second, we discuss how to construct a set of observables with optimal capabilities to test LFUV-NP and minimal sensitivity to hadronic uncertainties in the SM. This work was originally presented in our article Ref. [2], which we use as a reference for Chapter 7.

Finally, in Part III we discuss at length our global fits. In Chapter 8 we dissect the composition of our analyses, review the basic statistical framework used and showcase our most-updated results. Based on the structure of these results, we further investigate their potential implications for model-building and the inner tensions of the global fit itself. One of the aforementioned model-building implications precisely bridges the gap between the anomalies in the neutral-current transitions $b \to s\ell^+\ell^-$ and the tensions observed in the charged-current transitions $b \to c\tau\nu$. As we show in Chapter 9, such a connection implies huge enhancements of $b \to s\tau\tau$ mediated channels, which could be at reach of the current experiments at the LHC. Whereas Chapter 8 is a blend of the most important results of three of our papers [], Chapter 9 mostly follows the discussion in Ref. [3].

Part I

Basic Theoretical Framework

Chapter 1

Effective Hamiltonians

Weak decays of heavy mesons are characterized by three different energy scales, namely: the scale of QCD interactions Λ_{QCD}, the characteristic energy of process (usually determined by the mass of the decaying heavy quark m_Q) and finally, since we study electroweak processes, the typical scale of weak interactions given by the mass of the W boson M_W.

The order of magnitude of the above-mentioned scales is the following

$$O(\Lambda_{\mathrm{QCD}}) \sim 0.2\,\mathrm{GeV} \qquad O(m_Q) \sim 5\,\mathrm{GeV}\ \text{(regarding b quarks)} \qquad O(M_W) \sim 90\,\mathrm{GeV} \tag{1.0.1}$$

Thus, there is a strong scale hierarchy, $\Lambda_{\mathrm{QCD}} \ll m_Q \ll M_W$, meaning that processes mediated by the interactions above are mostly independent inside the meson decay. Hence, in order to study B-mesons decays, it is not necessary to use the full theory, it is enough to construct an effective field theory that allows an encapsulation all the physical phenomena at a certain scale.

1.1 Weak Effective Hamiltonian in the Standard Model

Due to the fact that W and Z bosons are very massive, weak meson decays (whose energy E is of the order of the meson's mass and thus $E \ll M_{W,Z}$) proceed at very small distances of the order of $O(1/M_W)$. Then, following the ideas of the previous section, the dynamical degrees of freedom that mediate these processes[1] can be integrated out of the Standard Model (SM) Lagrangian to define the Weak Effective Hamiltonian (WEH) for the given decay. Formally, this has the structure of an Operator Product Expansion (OPE) [4–6]

$$\mathcal{H}_{\mathrm{eff}} = \frac{G_F}{\sqrt{2}} \sum_i \mathcal{C}_i(\mu)\, \mathcal{O}_i, \tag{1.1.1}$$

where $\mathcal{O}_i$ is a set of local effective operators, μ is the renormalisation scale and $\mathcal{C}_i(\mu)$ are the corresponding Wilson coefficient functions.

In this context, the amplitude of a generic meson transition $M_1 \to M_2$ described by (1.1.1) admits the following decomposition

$$\mathcal{A}(M_1 \to M_2) = \langle M_2 | \mathcal{H}_{\mathrm{eff}} | M_1 \rangle = \frac{G_F}{\sqrt{2}} \sum_i \mathcal{C}_i(\mu) \langle M_2 | \mathcal{O}_i(\mu) | M_1 \rangle \equiv \frac{G_F}{\sqrt{2}} \sum_i \mathcal{C}_i(\mu) \langle \mathcal{O}_i(\mu) \rangle\,, \tag{1.1.2}$$

[1] These include the electroweak gauge bosons ($W^{\pm}$ and Z), the Higgs field and the top quark.

where both the initial and final state mesons M_1 and M_2 may contain more than only one meson in them (i.e. $B \to \pi\pi$).

Wilson coefficients contain the contributions from physical processes with characteristic scales higher than the renormalisation scale μ. These are perturbatively calculable functions as long as the scale μ is large enough. Therefore, the $\mathcal{C}_i$ include contributions from quantum fluctuations involving the high frequency modes of the theory that we integrated out: top quarks, W and Z bosons and the Higgs, in the SM. If we assume a particular *ultraviolet completion* of the SM, the new heavy degrees of freedom will also be integrated out of the Lagrangian, provided that they are sufficiently heavy, and thus will contribute to the Wilson coefficients. Consequently, $\mathcal{C}_i(\mu)$ typically depend on m_t, m_W, m_H and the mass scales of the heavy modes of any SM extension considered. These dependencies are identified by computing the penguin and box diagrams with fully propagating top, W, Z, Higgs and new heavy mediators exchanges. It is important to stress that also short distance QCD effects are properly taken into account in the computation of Wilson coefficients, these being the ones that introduce the μ scale dependence through the running of the QCD coupling constant α_s.

On the contrary, the matrix elements $\langle \mathcal{O}_i(\mu) \rangle$ summarise the contributions to the amplitude $\mathcal{A}(M_1 \to M_2)$ from scales lower than μ. Then, since they involve long distance interactions, it is not possible to compute them in perturbation theory and one must resort to non-perturbative methods for their assessment. Examples of such non-perturbative tools include lattice gauge theory, the $1/N_c$ expansion (where N_c is the number of colours), QCD sum rules, light-cone sum rules, chiral perturbation theory, etc. In B meson decays, we will see in Chapter 3 that certain dynamical conditions that emerge from Heavy Quark Effective Theory (HQET) and Large Energy Effective Theory (LEET) allow for systematic computations of these matrix elements.

Constructing an Effective Hamiltonian involves computing its corresponding Wilson coefficients and identifying its relevant local effective operators. Notice that all this can be fully done in perturbation theory. All physical information about the inner structure of the mesons in the decay is irrelevant for this construction and it will only become relevant when computing the matrix element of the decay, through the evaluation of the matrix elements discussed above. Thus, the Wilson coefficients, being objects that only depend on the underlying quark transition and the perturbative interactions they experience, are independent of the particular decay considered in the same way as the usual couplings of gauge theories are universal and process-independent parameters.

Precisely, the biggest advantage of this framework is that it allows to separate the problem of computing the amplitude $\mathcal{A}(M_1 \to M_2)$ into two distinct parts: the *short-distance* (perturbative) calculation of the effective couplings $\mathcal{C}_i$ and the *long-distance* (non-perturbative) computation of the matrix elements $\langle \mathcal{O}_i \rangle$. As we discussed above, the scale μ separates out short-distance contributions to the amplitude from the long-distance ones. Actually, this separation is somewhat arbitrary, since there is certain freedom in assigning which contribution is absorbed into the Wilson coefficients and which other is encoded within the matrix elements. Indeed, the only effect of changing the scale μ is to reshuffle terms from the matrix elements $\langle \mathcal{O}_i \rangle$ into the Wilson coefficients $\mathcal{C}_i$, hence there is no information loss in shifting from one scale to another. At the same time, this has the important implication that the scale dependence of the matrix elements cancels the unphysical scale dependence of the Wilson coefficients, and the other way around, so the amplitude is a physically meaningful quantity.

This completes our remarks about the main features of the WEH formalism and its building blocks. Now, from a more practical perspective, we review the standard procedure for obtaining the corresponding effective Hamiltonian to a given process (see Refs. [7–10] for more detailed discussions):

- Given a process $M_1 \to M_2$, compute the amplitude $\mathcal{A}(M_1 \to M_2)$ in the full theory up to certain order in α_s. As a result of Feynman diagrams with one or more loops, divergences will appear during the computations, which can be treated using usual renormalisation techniques by introducing a high scale $\mu_0 \sim M_W$. At this scale α_s is small, so perturbation theory works well.

- Once the computation of the amplitude is performed in the full theory and at the high scale μ_0, one can identify the effective operators $\{\mathcal{O}_i\}$. With the operators known, the OPE for the effective Hamiltonian can be written.

- Calculate the matrix elements $\langle\mathcal{O}_i\rangle$ of the operators at the high scale μ_0 and at the same order in α_s. Perturbation theory still applies at this scale and because QCD corrections are included, divergences will arise again. Some of them can be absorbed through *field renormalisation*, however in general the resulting expressions will still be divergent. Therefore an additional multiplicative renormalisation, the so-called operator renormalisation, is necessary. This method typically introduces mixing between different operators in the OPE that carry the same quantum numbers, in such a way that even new operators which were not present at tree level may arise. Moreover, since these matrix elements $\langle\mathcal{O}_i\rangle$ must be computed within a renormalisation scheme, this introduces a certain scheme dependence on the Wilson coefficients, so the overall scheme depend cancels at the amplitude level.

- Having computed the amplitude $\mathcal{A}(M_1 \to M_2)$ in the full theory and the matrix elements $\langle\mathcal{O}_i\rangle$ of the operators in the OPE, at the same order in Perturbation Theory and at the scale μ_0, the Wilson coefficients $\mathcal{C}_i(\mu_0)$ can be obtained via (1.1.1). This procedure is called *matching* the full theory onto the effective theory.

- Finally, renormalisation group evolution techniques must be used to obtain the value of the Wilson coefficients at the low scale μ. As we discussed, the μ scale is arbitrary, allowing us to choose what belongs to $\mathcal{C}_i(\mu)$ and what to $\langle\mathcal{O}_i(\mu)\rangle$. However, it is customary to choose μ of the order of the mass of the decaying meson, which for B decays means $\mu = \mu_b \sim m_b$. So μ has to be run down from $\mu_0 \sim M_W$ to $\mu_b \sim m_b$. Then, the matching conditions for the Wilson coefficients develop large logarithms $\ln(M_W^2/\mu_b^2)$ that break their computation in a perturbative expansion. Solving for this requires the use of Renormalisation Group (RG) Improved Perturbation Theory [8, 11], which we will discuss in the following section.

As a last note, it is important to stress that the description provided by a weak effective Hamiltonian is only valid up to the order in the $1/M_W$ expansion used for building the OPE and to the order in α_s in which the matching conditions of the effective theory are based on.

1.1.1 Renormalisation Group Evolution of Wilson coefficients

As we noticed above, the matching conditions for the Wilson coefficients present an important problem: the expansion parameter $\alpha_s/\pi \sim 0.1$ (at the $\mu_b \sim m_b$ scale) is always accompanied by consistent powers of $\ln(M_W^2/\mu_b^2)$, establishing $(\alpha_s/\pi)\ln(M_W^2/\mu_b^2) \sim 0.8$ as the *de facto* expansion parameter and spoiling the perturbative expansion. This is actually a generic problem of renormalisable quantum field theories with vastly different characteristic scales: perturbative expansions organise in powers of $\alpha_s \ln(M^2/\mu^2)$ rather than α_s.

In order to solve the problem of these large logarithms, they must be *resummed* to all orders by means of (RG)-evolution equations in *Renormalisation Group Improved Perturbation Theory*. This framework provides a reorganisation of perturbation theory where $\alpha_s \ln(M^2/\mu^2)$ works as the $O(1)$ parameter in the expansion. Then, at leading order all terms of the form $(\alpha_s \ln(M^2/\mu^2))^n$ (with $n = 0, \dots, \infty$) are resummed, contributing to the Wilson coefficients at order $O(1)$. Next-to-leading order contributions are obtained by resumming terms of the form $\alpha_s(\alpha_s \ln(M^2/\mu^2))^n$, which correspondingly count as $O(\alpha_s)$ in the expansion.

Great references where RG-Improved Perturbation Theory is discussed at length, alongside many other relevant topics for the study of Effective Theories, are Refs. [9, 12]. The discussion below borrows some of its elements from these two references.

Now we will explicitly show how large logarithms must be resumed up to leading order. Consider a complete set of effective operators

$$\{\mathcal{O}_i(\mu)\}\,, \qquad (\text{with } i = 1, \dots, n) \tag{1.1.3}$$

allowed by the symmetries of the theory. Since arbitrary changes of the renormalisation scale μ does not affect the physical value of the amplitude

$$\mathcal{A} = \sum_i \mathcal{C}_i(\mu)\,\langle \mathcal{O}_i(\mu)\rangle = \sum_i \mathcal{C}_i(\mu+\delta\mu)\,\langle \mathcal{O}_i(\mu+\delta\mu)\rangle \tag{1.1.4}$$

$$= \sum_i \left[\mathcal{C}_i(\mu)\,\langle \mathcal{O}_i(\mu)\rangle + \left(\frac{d}{d\mu}\mathcal{C}_i(\mu)\,\langle \mathcal{O}_i(\mu)\rangle + \mathcal{C}_i(\mu)\frac{d}{d\mu}\,\langle \mathcal{O}_i(\mu)\rangle\right)\delta\mu + \dots\right], \tag{1.1.5}$$

implying that

$$\frac{d}{d\ln\mu}\sum_i \mathcal{C}_i(\mu)\,\langle \mathcal{O}_i(\mu)\rangle = 0. \tag{1.1.6}$$

Being the basis of operators complete, we can write the derivative of every matrix element in terms of the other matrix elements in the set,

$$\frac{d}{d\ln\mu}\,\langle \mathcal{O}_i(\mu)\rangle = -\sum_j \gamma_{ij}(\mu)\,\langle \mathcal{O}_j(\mu)\rangle\,, \tag{1.1.7}$$

where γ_{ij} is usually referred to as the anomalous dimension matrix and it measures how much the matrix element changes under scale variations. It is important to stress that no large logarithms are contained in this matrix. Clearly, if there is more than one operator in the basis, in general γ_{ij} will cause operators to mix when the scale is changed. Expanding the derivative in Eq. (1.1.6) and using Eq. (1.1.7), we obtain

$$\sum_i \left[\frac{d}{d\mu}\mathcal{C}_i(\mu) - \sum_j \mathcal{C}_j(\mu)\gamma_{ji}(\mu)\right]\langle \mathcal{O}_i(\mu)\rangle = 0 \tag{1.1.8}$$

Therefore, because the operators are linearly independent, Eq. (1.1.8) necessarily implies the following renormalisation group equation for the Wilson coefficients

$$\frac{d}{d\mu}\mathcal{C}_i(\mu) - \sum_j \mathcal{C}_j(\mu)\gamma_{ji}(\mu) = 0, \tag{1.1.9}$$

which can be rewritten in matrix form as

$$\frac{d}{d\mu}\boldsymbol{\mathcal{C}}(\mu) = \hat{\gamma}^T(\mu)\,\boldsymbol{\mathcal{C}}(\mu), \tag{1.1.10}$$

Because the anomalous dimension matrix controls the scale variation of the matrix elements and scale dependence gets introduced in them as a result of QCD corrections, $\hat{\gamma}$ depends on the scale μ only through the running of the $\alpha_s(\mu)$ coupling constant. Then, we can change variables from μ to α_s in Eq. (1.1.10) to find

$$\frac{d}{d\alpha_s(\mu)}\boldsymbol{\mathcal{C}}(\mu) = \frac{\hat{\gamma}^T(\alpha_s(\mu))}{\beta(\alpha_s(\mu))}\,\boldsymbol{\mathcal{C}}(\mu), \tag{1.1.11}$$

where $\beta \equiv d\alpha_s(\mu)/d\ln\mu$ is the QCD *beta function.* Eqs. (1.1.10) and (1.1.11) are differential equations controlling the running of the Wilson coefficients with initial conditions set by the values of the Wilson coefficients at the high scale, i.e. $\boldsymbol{\mathcal{C}}(M_W)$.

Notice that Eq. (1.1.11) is formally identical to the Heisenberg equation of motion for time-dependent operators, with the anomalous dimension matrix playing the role of the Hamiltonian. Therefore, the general solution to equation Eq. (1.1.11) with the aforementioned initial conditions reads

$$\boldsymbol{\mathcal{C}}(\mu) = T_\alpha \exp\left[\int_{\alpha_s(M_W)}^{\alpha_s(\mu)} d\alpha_s \frac{\hat{\gamma}^T(\alpha_s(\mu))}{\beta(\alpha_s(\mu))}\right]\boldsymbol{\mathcal{C}}(M_W), \tag{1.1.12}$$

with the formal definition of the exponential above given by its Taylor expansion and T_α being an operator that organises the powers of $\hat{\gamma}^T(\alpha_s)$ such that those terms evaluated at larger values of α_s stand to the left of those with smaller values of α_s. Keeping a well-defined ordering of the powers of $\hat{\gamma}^T(\alpha_s)$ is needed since, in general, two realisations of $\hat{\gamma}^T$ at different α_s will not commute.

Now we apply Eq. (1.1.12) to the simplified case of having a theory with only one Wilson coefficient (i.e. no mixing), this will explicitly show how resummation of large logarithms works. First, we write the perturbative expansion of the relevant quantities in the RG-evolution

$$\mathcal{C}(M_W) = 1 + O(\alpha_s), \tag{1.1.13}$$

$$\gamma(\alpha_s) = \gamma_0\frac{\alpha_s}{4\pi} + O(\alpha_s^2), \tag{1.1.14}$$

$$\beta(\alpha_s) = -2\alpha_s\left(\beta_0\frac{\alpha_s}{4\pi} + O(\alpha_s^2)\right), \tag{1.1.15}$$

where we have assumed the effective operator we are dealing with is such that it represents a process operating at leading order in the full theory, hence $C(M_W) = 1$. Notice that none of these quantities are afflicted by large logarithms.

Then, we find the leading order result

$$\mathcal{C}(\mu) = \left(\frac{\alpha_s(\mu)}{\alpha_s(M_W)}\right)^{-\frac{\gamma_0}{2\beta_0}} \mathcal{C}(M_W) = \left(\frac{\alpha_s(\mu)}{\alpha_s(M_W)}\right)^{-\frac{\gamma_0}{2\beta_0}} \Big(1 + O(\alpha_s)\Big). \tag{1.1.16}$$

The resummation of the large logarithm can be made explicit by expanding the evolution factor in the equation above,

$$\left(\frac{\alpha_s(\mu)}{\alpha_s(M_W)}\right)^{-\frac{\gamma_0}{2\beta_0}} \approx \left(1 + \beta_0 \frac{\alpha_s}{4\pi} \ln \frac{M_W^2}{\mu^2}\right)^{-\frac{\gamma_0}{2\beta_0}} = 1 - \frac{\gamma_0}{2}\frac{\alpha_s}{4\pi} \ln \frac{M_W^2}{\mu^2} + O\left(\alpha_s^2 \ln^2 \frac{M_W^2}{\mu^2}\right). \tag{1.1.17}$$

Hence, in RG-Improved Perturbation Theory the characteristic large logarithms that appear in the running of Wilson coefficients are encapsulated in ratios comparing the strength of QCD interactions between the high and low scales through the QCD β-function.

If one wants to compute similar expressions for the RG-evolution of Wilson coefficients at higher orders (i.e. next-to-leading order and beyond), it is enough to write consistent perturbative expansions for $\mathcal{C}(\mu)$, $\gamma(\alpha_s)$ and $\beta(\alpha_s)$,

$$\mathcal{C}(M_W) = 1 + \sum_{n=1}^{\infty} c_n \left(\frac{\alpha_s(M_W)}{4\pi}\right)^n, \tag{1.1.18}$$

$$\gamma(\alpha_s) = \sum_{n=0}^{\infty} \gamma_n \left(\frac{\alpha_s}{4\pi}\right)^{n+1}, \tag{1.1.19}$$

$$\beta(\alpha_s) = -2\alpha_s \sum_{n=0}^{\infty} \beta_n \left(\frac{\alpha_s}{4\pi}\right)^{n+1}, \tag{1.1.20}$$

up to the desired order in α_s and proceed as detailed above. Generalisations of this procedure to cases with more than one operator, where mixing between operators is expected, can be found in Ref. [13].

1.2 The Weak Effective Hamiltonian Beyond The Standard Model

Current available knowledge on possible *New Physics* (NP) seems to suggest that such phenomena must be expected at very high scales of the order of $\Lambda_{\rm NP} \sim$ few TeV. In this regard, the SM may be understood as an effective field theory of a more general theory describing the physics at energies around $\Lambda_{\rm NP}$. Therefore, the effective field theory formalism can be used to introduce NP contributions into our description in a general and model independent way.

Once NP operators are added to the effective Hamiltonian (1.1.1), the value of the Wilson coefficients will be shifted away form their SM values when matching the full theory onto the effective theory. This is crucial since, if it is possible to obtain precise determinations of the values of the Wilson coefficient from experiments, it allows us to test the presence of NP and to constrain its contributions. This type of analyses, applied to the most updated experimental data on rare B meson decays mediated by the *flavour changing neutral current* (FCNC) transition $b \to s\ell^+\ell^-$, constitute the most important results of this Thesis and will be discussed in Chapter 8.

In principle, the effective Hamiltonian $\mathcal{H}_{\rm eff}^{\rm NP}$ that keeps track of the presence of NP might contain an infinite set of operators. However, the complexity of $\mathcal{H}_{\rm eff}^{\rm NP}$ is reduced once the next requirements and assumptions are imposed.

- The building blocks of the effective operators in $\mathcal{H}_{\rm eff}^{\rm NP}$ are necessarily the relevant SM fields to the process considered. Recall that the low energy degrees of freedom are the SM particles with masses below M_W.

- For the same reason, all the operators must be invariant under $SU(3)_{\rm C} \otimes SU(2)_{\rm L} \otimes U(1)_{\rm Y}$, the gauge group of the SM. Moreover, other global symmetries might be imposed to preserve certain phenomenological facts (i.e. avoid proton decay, etc).

- There are still an infinite set of operators satisfying (i) and (ii), so a prescription to cut this infinite set is in order. This prescription consists in dropping the operators with very high dimensions. A suppression factor $\Lambda_{\rm NP}^{D-6}$ is added to the NP effective Hamiltonian so that the larger the dimension D of the operator becomes, the smaller are the coupling constants $\mathcal{C}_i^{[D]}/\Lambda_{NP}^{D-6}$. Since $\Lambda_{\rm NP}$ is very large, this prescription provides indeed a good constraint on the operators that are relevant in $\mathcal{H}_{\rm eff}^{\rm NP}$.

According to the previous points, the most general form for the NP effective Hamiltonian should be cast as

$$\mathcal{H}_{\rm eff}^{\rm NP} = \sum_{D=7}^{\infty} \sum_i \frac{\mathcal{C}_i^{[D]}}{\Lambda_{\rm NP}^{D-6}} \mathcal{O}_i^{[D]}. \tag{1.2.1}$$

Even though this top-down prescription drastically simplifies the description of NP in the form of an effective Hamiltonian, the number of operators in Eq. (1.2.1) is still too large for most of its applications. Therefore, bottom-up procedures are usually followed in most NP studies. These consist in writing down a model or a family of models, which formally are represented by the addition of a new piece $\delta\mathcal{L}^{\rm SM}$ to the SM Lagrangian consistent with the symmetries assumed, integrating out the heavy modes (both coming from the SM and NP) and using the corresponding set of Wilson coefficients and effective operators obtained to perform phenomenological analyses with experimental data. In this thesis, only NP effects proceeding through SM-like and chirally-flipped operators will be considered.

1.3 Introduction to Heavy-Quark Effective Theory

Hadronic systems with a *heavy-quark* constituent are naturally characterised by two relevant energy scales: the heavy-quark mass m_Q and the scale of hadronic physics $\Lambda_{\rm QCD}$, defined by the typical momenta of gluons exchanged in a bound state. These two scales are clearly hierarchised $\Lambda_{\rm QCD} \ll m_Q$ and thus allow for a description of heavy-quark systems within the Effective Field Theory formalism discussed above, with the resulting theory being called *Heavy-Quark Effective Theory* (HQET) [14–21]. Educational lectures on this topic can be found in Refs. [8, 11, 12].

More in detail, HQET provides a simplified description of physical processes involving the interaction of a heavy-quark ($m_Q \to \infty$) with *light degrees of freedom* (light-quarks and/or antiquarks and gluons) predominantly through the exchange of *soft* (low energy) gluons. This underlying assumption on the nature of gluon exchanges between heavy and light degrees of freedom is usually known as *soft dominance*. At energy scales of the order of m_Q or higher (i.e. short-distances), the QCD coupling constant is small and strong interactions can be computed in a perturbative expansion. On the other hand, at scales below the heavy-quark mass (i.e. long distances), QCD becomes strongly coupled due to *confinement*, rendering no perturbative computation as reliable. Precisely, the main purpose of HQET is to provide a reliable theoretical framework for these scales. As it is standard with effective theories, short- and long-distance effects are separated by introducing a separation scale μ such that $\Lambda_{\rm QCD} \ll \mu \ll m_Q$. Then, HQET is constructed in such a way that it is equivalent to QCD in the long-distance region, i.e. scales below μ. As a result, this framework will fail at explaining short-distance interactions, since all heavy modes have been integrated out. But we can deal with these contributions consistently by using the renormalisation group techniques in Section 1.1.1.

Since $\Lambda_{\rm QCD}/m_Q \sim 0.1 \ll 1$ for heavy quarks ($Q = c,\, b$), this defines a good expansion parameter for an OPE-type of structure. However, because in heavy-quark physics we are interested in the properties of the heavy-quark, the heavy-quark degrees of freedom cannot be completely removed from the theory in HQET, as the heavy-quark is not virtual and carries flavour charge. In this sense, it is not fair to regard HQET as a proper OPE. Instead, what deserves to be eliminated from the theory are the quantum numbers of the heavy-quark that cannot be resolved by the light degrees of freedom.

Now we will derive the basics of HQET following Refs. [8, 11]. It is convenient to start by writing down the QCD Lagrangian

$$\mathcal{L}_{\rm QCD} = \bar{q}(x)\left(i\not{D}_s - m_q\right) q(x), \tag{1.3.1}$$

with $D_s^\mu \equiv \partial^\mu - igT^a A_s^{a,\mu}(x)$ the covariant derivative (being g the QCD coupling constant and a the colour indices), T^a the $SU(3)_{\rm C}$ generators, $A_s^{a,\mu}(x)$ the soft gluon field and m_q the corresponding mass term of the quark field $q(x)$. Notice that the covariant derivative contains only the soft gluon field since we have already integrated out all contributions coming from hard gluons. We purposely do not include the gluon field kinetic term as we are only interested in processes with quarks in the initial and final states.

A softly interacting heavy-quark in a *heavy-meson*[2] is nearly on-shell, as it carries most of the hadron's momentum. Therefore, its momentum can be decomposed as

$$p_Q^\mu = m_Q v^\mu + k^\mu, \tag{1.3.2}$$

where v^μ is the velocity of the meson (recall that $v^2 = 1$ for any four-velocity), m_Q is the heavy-quark mass and k^μ is the so-called residual momentum, accounting for the fluctuations in the heavy-quark momentum stemming from its interactions with the rest of the meson. Assuming we work from a reference frame where $v \sim O(1)$ (i.e. the meson rest frame), then k^μ must be of the order of the scale of light interactions $k \sim \Lambda_{\rm QCD}$, which implies that changes in the heavy-quark velocity vanish as $\Lambda_{\rm QCD}/m_Q \to 0$.

Being $Q(x)$ the heavy-quark field in the QCD Lagrangian, we define the *large-* and *small-component* fields $h_v(x)$ and $H_v(x)$ as

$$h_v(x) \equiv {\rm e}^{im_Q v\cdot x} P_+ Q(x), \qquad H_v(x) \equiv {\rm e}^{im_Q v\cdot x} P_- Q(x), \tag{1.3.3}$$

[2] This actually also applies for baryons, we restrict ourselves to mesons since in this Thesis we will mostly work with mesons. Then, by heavy-hadron we understand a hadron that is composed by a heavy-quark and light-quarks only. We do not consider here the case where two or more heavy-quarks take part in the same hadronic state.

where the projection operators $P_\pm$ read[3]

$$P_\pm = \frac{1 \pm \slashed{v}}{2}. \tag{1.3.4}$$

Using the definitions in (1.3.3), the heavy-quark field takes the form

$$Q(x) = \mathrm{e}^{-im_Q v\cdot x}\left[h_v(x) + H_v(x)\right]. \tag{1.3.5}$$

Notice that $h_v(x)$ and $H_v(x)$ correspond to the two *upper* and two *lower components* of the heavy-quark spinor $Q(x)$. This is transparent in the rest frame of the heavy-quark, where $v = (1, 0, 0, 0)$. In this frame, using the Dirac representation of the gamma matrices, $\slashed{v} = \gamma_0$ and thus P_+ (P_-) leaves the two upper (lower) components of $Q(x)$ untouched, while it cancels the lower (upper) ones. Moreover, although it may look like an arbitrary choice, the phase factor $\mathrm{e}^{im_Q v\cdot x}$ in $h_v(x)$ and $H_v(x)$ has been introduced in order to remove the high-frequency modes of the x-dependence in $Q(x)$ coming from the large momentum mv. As a result, the residual x-dependence of $h_v(x)$ and $H_v(x)$ is attached to the residual momentum k, so derivatives acting on both fields count as $O(\Lambda_{\mathrm{QCD}})$.

Following the QCD Lagrangian in Eq. (1.3.1), the equation of motion describing the dynamics of the heavy-quark reads

$$\left(i\slashed{D}_s - m_Q\right) Q(x) = 0, \tag{1.3.6}$$

which can be rewritten in the following way by means of Eq. (1.3.5)

$$\mathrm{e}^{-im_Q v\cdot x}\left[i\slashed{D}_s - (1 - \slashed{v})m_Q\right]\left[h_v(x) + H_v(x)\right] = 0, \tag{1.3.7}$$

with even further rearrangements possible due to the properties of the large and small component fields $\slashed{v}h_v = h_v$ and $\slashed{v}H_v = -H_v$,

$$i\slashed{D}_s h_v(x) + (i\slashed{D}_s - 2m_Q)H_v(x) = 0. \tag{1.3.8}$$

The anticommutation relations defining the Dirac algebra $\{\gamma^\mu, \gamma^\nu\} = 2g^{\mu\nu}$ imply

$$\slashed{v}\slashed{D}_s = \gamma^\mu\gamma^\nu v_\mu D_{s\nu} = (2g^{\mu\nu} - \gamma^\nu\gamma^\mu)v_\mu D_{s\nu} = 2v\cdot D_s - \slashed{D}_s\slashed{v}, \tag{1.3.9}$$

leading to the useful property

$$P_\pm \slashed{D}_s = \slashed{D}_s P_\mp \pm v\cdot D_s. \tag{1.3.10}$$

Now, acting over Eq. (1.3.8) with $P_\pm$ by the left and using the relations in Eqs. (1.3.10), yields the following coupled system of equations

$$iv\cdot D_s h_v(x) = -i\slashed{D}_{s\perp} H_v(x), \tag{1.3.11}$$
$$(iv\cdot D_s + 2m_Q)H_v(x) = i\slashed{D}_{s\perp} h_v(x), \tag{1.3.12}$$

[3] Recall that $P_\pm$ being projection operators, they fulfill the following properties: $P_\pm^2 = \mathbb{1}$, $P_\pm P_\mp = 0$ and $P_+ + P_- = \mathbb{1}$.

where the so-called *spatial derivative* $\not{D}_{s\perp}$ stands for

$$D^{\mu}_{s\perp} \equiv D^{\mu}_{s} - v^{\mu} v \cdot D_s. \tag{1.3.13}$$

Looking at the derivative terms in Eqs. (1.3.11) and (1.3.12), their interpretation is that the field h_v describes a massless fermion, while the spinor field H_v encodes the dynamics of a fermion with mass $2m_Q$. These two modes are not independent and they mix through their interactions, as it is explicit from the right-hand side of Eqs. (1.3.11) and (1.3.12).

Solving the classical equation of motion for the field H_v we obtain

$$H_v(x) = \frac{i\not{D}_{s\perp} h_v}{iv \cdot D_s + 2m_Q}, \tag{1.3.14}$$

where one can clearly observe that $H_v(x) = O(\Lambda_{\text{QCD}}/m_Q)\, h_v(x)$, as the numerator of Eq. (1.3.14) contains a derivative of the $h_v(x)$ field while there is a mass term m_Q in the denominator. Hence $H_v(x)$ is suppressed with respect to $h_v(x)$, in the heavy-quark limit. This motivated the use of the terms large- and small-component fields for $h_v(x)$ and $H_v(x)$.

Finally, inserting Eq. (1.3.1) in the QCD Lagrangian and removing $H_v(x)$ by means of Eq. (1.3.14), we obtain the HQET effective Lagrangian

$$\mathcal{L}_{\text{HQET}} = \bar{h}_v(x)\, iv \cdot D_s\, h_v(x) + \bar{h}_v(x) i\not{D}_{s\perp} \frac{1}{iv \cdot D_s + 2m_Q} i\not{D}_{s\perp} h_v(x) \tag{1.3.15}$$

The second term on the right-hand side contains the non-local operator $(iv \cdot D_s + 2m_Q)^{-1}$. In order to obtain a local theory, this operator must be expanded in powers of Λ_{QCD}/m_Q

$$\mathcal{L}_{\text{HQET}} = \bar{h}_v(x)\, iv \cdot D_s\, h_v(x) + \frac{1}{2m_Q} \sum_{n=0}^{\infty} \bar{h}_v(x) i\not{D}_{s\perp} \left(-\frac{iv \cdot D_s}{2m_Q} \right)^n i\not{D}_{s\perp} h_v(x). \tag{1.3.16}$$

Considering only the first term in the expansion and using the identity

$$P_+ i\not{D}_{s\perp} i\not{D}_{s\perp} P_+ = P_+ \left[(iD_{s\perp})^2 + \frac{g_s}{2} \sigma_{\mu\nu} G^{\mu\nu} \right] P_+, \tag{1.3.17}$$

with $\sigma^{\mu\nu} = \frac{i}{2}[\gamma^\mu, \gamma^\nu]$ and the gluon field-strength tensor $i[D^\mu_s, D^\nu_s] = g_s G^{\mu\nu}_s$, the effective Lagrangian $\mathcal{L}_{\text{HQET}}$ at order $O(\Lambda^2_{\text{QCD}}/m^2_Q)$ becomes

$$\mathcal{L}_{\text{HQET}} = \bar{h}_v(x)\, iv \cdot D_s\, h_v(x) + \frac{1}{2m_Q} \bar{h}_v(x) \left(iD_{s\perp}\right)^2 h_v(x) + \frac{g_s}{4m_Q} \bar{h}_v(x) \sigma_{\mu\nu} G^{\mu\nu}_s h_v(x) + O\left(\frac{\Lambda^2_{\text{QCD}}}{m^2_Q} \right) \tag{1.3.18}$$

To conclude, we use the HQET Lagrangian for discussing some of its most important features.

- At leading order in the heavy-quark expansion, the HQET reads

$$\mathcal{L}_{\text{HQET}} = \bar{h}_v(x)\, iv \cdot D_s\, h_v(x) + O\left(\frac{\Lambda_{\text{QCD}}}{m_Q} \right). \tag{1.3.19}$$

  This Lagrangian describes the ”residual” heavy-quark QCD dynamics, once the kinematic dependence on its mass is removed. Since by construction Eq. (1.3.19) does not depend on the heavy-quark mass, the HQET Lagrangian is *flavour symmetric* at leading order.

Furthermore, no gamma-matrices are present in the operator $v \cdot D_s$, therefore the leading order term in HQET is also *spin symmetric*. From a physical perspective, this means that the properties of hadronic systems containing a heavy quark do not depend neither on the flavour nor the spin of the heavy quark, in the limit $m_Q \to \infty$. These two properties constitute the spin-flavour symmetries of HQET, which lead to several relations among heavy-meson form factors and give rise to important concepts such as the Isgur-Wise function [22, 23]. It is important to stress that spin-flavour symmetries only hold at leading order, as higher order corrections in Λ_{QCD}/m_Q break these symmetries.

- Explicitly writing the covariant derivative in Eq. (1.3.19)

$$\bar{h}_v(x)\, iv \cdot D_s\, h_v(x) = \bar{h}_v(x) i v^\mu \partial_\mu h_v(x) + g_s \bar{h}_v(x) T^a v^\mu A^a_{s\,\mu}(x) h_v(x), \tag{1.3.20}$$

one can extract the HQET Feynman rules, as displayed in Fig. 1.1.

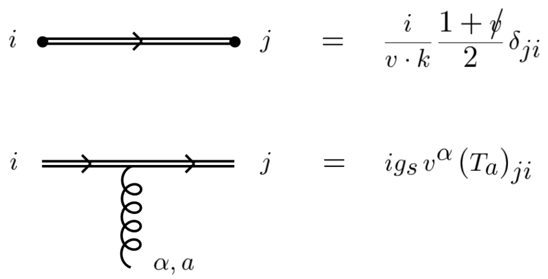

Figure 1.1: HQET Feynman rules (i, j are color indices) [12]. Double lines represent a heavy-quark with velocity v. The residual momentum k is defined in Eq. (1.3.2).

- Weak currents can be easily written in terms of HQET fields and thus it provides a good framework for the study of weak interactions. For instance, a generic heavy-to-light weak transition current $\bar{q}(x)\Gamma Q(x)$, usually appearing in semileptonic decays, can be written as

$$\bar{q}(x)\Gamma Q(x) = \bar{q}(x)\Gamma h_v(x) + O\left(\frac{\Lambda_{\text{QCD}}}{m_Q}\right), \tag{1.3.21}$$

where the heavy-quark field $Q(x)$ has been replaced by the HQET field $h_v(x)$ using Eq. (1.3.5).

1.4 Introduction to Large Energy Effective Theory

The defining property of heavy-to-light meson transitions is the large energy E transmitted by the parent meson to the daughter, in almost the whole physical phase space [24]. This is certainly the case of some of the main channels studied in this Thesis, for instance $B \to K^{(*)}\ell^+\ell^-$ at *large recoil* (see Section 2.1.4 for a definition of this term). Then, the final active quark is very energetic (in the rest frame of the parent meson) and it can be assumed to predominantly interact with the light degrees of freedom of the recoiling meson via soft gluon exchanges. This is another instance of the soft dominance assumption already used in the construction of HQET. Within this context, the recoiling quark carries most of the momentum of the emission light meson and thus the fast degrees of freedom become essentially classical [24]. Again, this resembles the HQET case, where the heavy-quark carries almost all the heavy-meson momentum due to its large mass. Following these ideas, the *Large Energy Effective Theory* (LEET) was introduced in Ref. [25], which provides a framework for studying heavy-to-light processes with fast recoiling emission mesons as an OPE using $1/E$ as the expansion parameter.

Therefore, in order to study heavy meson decays into energetic light mesons, one needs the combined framework of HQET and LEET. The former being used for describing the dynamics of the parent meson and the latter accounting for the behaviour of the energetic emission meson. Similarly to the symmetry relations that emerge among heavy-meson form factors in HQET through the Isgur-Wise function, this approach applied to B meson decays of the type $B \to V$ and $B \to P$ (with V and P vector and pseudoscalar mesons, respectively) yields a set of relations between the relevant form factors in these decay channels at order $1/M$ and $1/E$ that reduce all form factors to just a few scalar functions called *soft form factors* [24]. This is going to be discussed more in detail in Section 2.1.4.

The relevant energy scales here are the energy of the recoiling light meson E, as seen from the heavy meson rest frame, and the low scale of strong interactions $\Lambda_{\rm QCD}$. If E is large enough, then $\Lambda_{\rm QCD}/E \ll 1$, which allows for an OPE expansion of the full theory in powers of this parameter. Hard momenta, with virtualities between the separation scale μ introduced and E, will be integrated out, whereas soft contributions, with characteristic scales below μ, will be incorporated in the matrix elements of the LEET operators.

The formal development of the LEET shares a lot of similarities with the construction of the HQET. Its basis relies on the heavy-quark limit for the initial meson and the large energy limit for the final one

$$\{\Lambda_{\rm QCD},\, m\} \ll \{M,\, E\}\,, \tag{1.4.1}$$

being m and E the mass and energy of the light meson and M the mass of the heavy meson.

The momentum of the heavy meson is taken as

$$P^\mu = M v^\mu. \tag{1.4.2}$$

On the other hand, the light meson is recoiling really fast and almost all its energy is actually kinetic energy, so its 4-momentum p^μ must satisfy the condition $p^2 \simeq 0$. Therefore, by defining an almost light-like vector n^μ ($n^2 \simeq 0$), the momentum of the light meson can be written as $p^\mu = E n^\mu$. Moreover, the direction vector n^μ also fulfils the identity $v \cdot n = 1$. So, the energy of the light meson reads

$$E = v \cdot p. \tag{1.4.3}$$

The energetic quark in the emission light-meson is assumed to interact with the soft degrees of freedom of the meson only via soft QCD processes, hence its momentum p_q^μ aligns with the momentum of the whole light meson plus some small corrections $k \sim \Lambda_{\rm QCD}$ due to the aforementioned soft interactions

$$p_q^\mu = E n^\mu + k^\mu. \tag{1.4.4}$$

Following the HQET spirit, two auxiliary fields $q_n(x)$ and $Q_n(x)$, based on the energetic light quark field $q_\ell(x)$, constitute the fundamental building blocks of the effective theory

$$q_n(x) \equiv \mathrm{e}^{iEn\cdot x} P_+ q_\ell(x), \qquad Q_n(x) \equiv \mathrm{e}^{iEn\cdot x} P_- q_\ell(x), \tag{1.4.5}$$

with the the following definitions for the projection operators $P_\pm$,

$$P_+ \equiv \frac{\not{n}\not{v}}{2}, \qquad P_- \equiv \frac{\not{v}\not{n}}{2}, \tag{1.4.6}$$

One can easily show that these operators follow the characteristic properties of projection operators, i.e. $P_\pm^2 = \mathbb{1}$, $P_+P_- = 0$ and $P_+ + P_- = \mathbb{1}$. To this end, the relations below prove useful

$$v^2 = 1, \qquad v \cdot n = 1, \qquad n^2 \simeq 0. \tag{1.4.7}$$

In terms of $q_n(x)$ and $Q_n(x)$, the energetic light quark field reads

$$q_\ell(x) = \mathrm{e}^{-iEn\cdot x}[q_n(x) + Q_n(x)]. \tag{1.4.8}$$

It is worth noticing that the phase $\mathrm{e}^{iEn\cdot x}$ in Eq. (1.4.8) cancels the high frequency terms of the exponential coming from the space-time evolution of $q_\ell(x)$, since $\mathrm{e}^{-ip_q\cdot x} = \mathrm{e}^{-iEn\cdot x}\mathrm{e}^{-ik\cdot x}$. Consequently, the x-dependence of $q_n(x)$ and $Q_n(x)$ is reduced to the small residual momentum k^μ, so derivatives acting on both fields count as $O(\Lambda_{\mathrm{QCD}})$.

Now we start building the LEET Lagrangian. Take the equation of motion for a light energetic quark, which is the same as Eq. (1.3.6) but replacing $Q(x)$ by $q_\ell(x)$ and m_Q by m_q (light quark mass), and write $q_\ell(x)$ in terms of $q_n(x)$ and $Q_n(x)$ by means of Eq. (1.4.8). Then

$$\mathrm{e}^{-iEn\cdot x}\left[i\not{D}_s - m_q + E\not{n}\right][q_n(x) + Q_n(x)] = 0. \tag{1.4.9}$$

Since[4] $\not{n}^2 \simeq 0$, one trivially concludes that $\not{n}q_n(x) = 0$. So, using this property, we can re-express the previous equation as

$$\left[i\not{D}_s - m_q\right] q_n(x) + \left[i\not{D}_s - m_q + E\not{n}\right] Q_n(x) = 0. \tag{1.4.10}$$

Using the anticommutation properties of the gamma matrices, very much in the same fashion as in the proof of Eq. (1.3.9), it can be shown that

$$P_\pm \not{D}_s = \pm v \cdot D_s \not{n} \mp n \cdot D_s \not{v} + \not{D}_s P_\pm. \tag{1.4.11}$$

Now, projecting the equation of motion Eq. (1.4.10) onto the subspace defined by $P_\pm$ and performing some simplifications, one obtains the following coupled system of equations. By virtue of Eq. (1.4.11) and the kinematic conditions $\not{n}^2 = 0$ and $\not{v}^2 = 1$

$$i\not{v}n \cdot D_s q_n(x) + [i\not{D}_s - m_q - \not{v}(2iv \cdot D_s - in \cdot D_s)]Q_n(x) = 0, \tag{1.4.12}$$

$$(i\not{D}_s - m_q - i\not{v}n \cdot D_s)q_n(x) + \not{v}(2E + 2iv \cdot D_s - in \cdot D_s)Q_n(x) = 0. \tag{1.4.13}$$

Thus, the second equation can be formally solved to give an expression for $Q_n(x)$ in terms of $q_n(x)$

$$Q_n(x) = \not{v}\frac{i\not{D}_s - m_q - i\not{v}n \cdot D_s}{2E + 2iv \cdot D_s - in \cdot D_s} q_n(x). \tag{1.4.14}$$

[4]Recall that $\not{a}^2 = a^2\,\mathbb{1} = a^2$, $\forall a^\mu$.

Observe that $Q_n(x) \sim O(\Lambda_{\rm QCD}/E) q_n(x)$, since the numerator in Eq. (1.4.14) contains a derivative while the denominator has a factor E. This implies that, in the high energy limit $E \to \infty$, the field component $Q_n(x)$ gets suppressed with respect to $q_n(x)$. In the rest frame of the heavy meson, where $v^\mu = (1,0,0,0)$ and $n^\mu = (1,0,0-1)$ (assuming the z-axis as the propagation direction), the projection operators read $P_\pm = \pm\gamma_3\gamma_0$. Then, if $q_\ell(x)$ is a Dirac spinor with positive energy, $Q_n(x)$ corresponds to its negative energy counterpart.

Finally, introducing the energetic light quark field decomposition of Eq. (1.4.8) in the QCD Lagrangian of Eq. (1.3.1) (and exploiting Eq. (1.4.14) in order to write all dependencies on $Q_n(x)$ in terms of $q_n(x)$ fields) and expanding up to $O(\Lambda_{\rm QCD}/E)$, we obtain the leading order LEET Lagrangian [24]

$$\mathcal{L}_{\rm LEET} = \bar{q}_n(x)\, i\not{v} n \cdot D_s\, q_n(x) + O\left(\frac{\Lambda_{\rm QCD}}{E}\right). \tag{1.4.15}$$

Note that there is no mass term in the LEET Lagrangian for the $q_n(x)$ field, however no assumption has been made on the mass of the light quark in deriving Eq. (1.4.15). The mass term $\bar{q}_n m_q q_n$ just vanishes because of the action of the projector P_+. Building the LEET only requires a strong hierarchy between the light quark and recoiling meson masses and the energy of the meson, i.e. $m_q \ll E$ and $m' \ll E$ with m' the mass of the emission meson.

Some additional final remarks about the LEET are in order here:

- LEET and HQET provide the basic framework for the study of weak heavy-to-light quark decays (mainly $b \to u, d, s$), as long as the assumption of soft QCD interactions remains true. The joint theory admits perturbative corrections to all orders in α_s, accounting for the short-distance QCD interactions between heavy/energetic quarks and the soft degrees of freedom within the meson, while non-perturbative contributions come from higher order terms in the expansions in $\Lambda_{\rm QCD}/m_Q$ and $\Lambda_{\rm QCD}/E$.

- Since $\mathcal{L}_{\rm LEET}$ has no mass dependence, it is flavour symmetric. Unlike the HQET effective Lagrangian, Eq. (1.4.15) is not $SU(2)$ spin symmetric because of the presence of gamma matrices in $\mathcal{L}_{\rm LEET}$. But, since these gamma matrices are not dynamical (not coupled to the covariant derivative D^μ), LEET is invariant under chiral transformations

$$q_n(x) \to \mathrm{e}^{i\alpha\gamma^5/2} q_n(x). \tag{1.4.16}$$

  Actually, it can be proved that the LEET symmetry group is in fact larger than $U(1)_{\rm chiral}$, turning out that $\mathcal{L}_{\rm LEET}$ possesses a global $SU(2)$ symmetry [24, 25].

- Writing the covariant derivative explicitly, we can find the corresponding Feynman rules to the LEET Lagrangian

$$\bar{q}_n(x)\, i\not{v} n \cdot D_s\, q_n(x) = \bar{q}_n(x)\, i\not{v} n^\mu \partial_\mu\, q_n(x) + g_s \bar{q}_n(x) \not{v} T^a n^\mu A^a_{s\,\mu}(x) q_n(x), \tag{1.4.17}$$

  where we have only written the soft-gluon field for the same reasons argued in Section 1.3. Therefore, LEET quark propagator: $$\frac{i\not{v}}{n \cdot k}\frac{\not{n}\not{v}}{2}\delta_{ji} \tag{1.4.18}$$

LEET quark-gluon vertex: $$ig_s\not{v}\,(T_a)_{ji}\,n^\alpha \tag{1.4.19}$$

Chapter 2

Non-perturbative Elements

As we discussed in Chapter 1, Effective Field Theories are characterised by a given factorisation scale that separates short- and long-distance contributions. The former are encoded in the Wilson coefficients of the theory, which formally admit a computation in perturbation theory, while the latter are pushed into the matrix elements of the effective operators. These are non-perturbative objects whose determination is crucial for obtaining precise theory determinations of relevant physical observables. Therefore, we need systematic methods able to generate reliable predictions for the matrix elements.

Usually, one simplifies the complex structure of the aforementioned matrix elements by identifying the Lorentz structures in them and parametrising the unknown energy-dependent functions weighting these structures as so-called form factors. This has the advantage of reducing the complexity of the matrix elements to just a few scalar functions, which usually appear in different although related matrix elements. Currently, the most successful theoretical approaches for computing form factors include the likes of lattice gauge theory and QCD sum rules (either pure SVZ-like types of sum rules or light-cone sum rules). Good reviews of the latter non-perturbative computational methods can be found in the lectures [26–28].

Here we will not discuss at length any of these paradigms, but rather we present an anatomy of the relevant form factors in B meson decays to pseudoscalar and vectors mesons. Plus, we discuss the relations between form factors due to the symmetries that emerge in the heavy quark and large energy limits.

2.1 Meson Form Factors

2.1.1 Fundamentals

A *form factor* is a function of scalar variables that appears in the most general decomposition of the matrix element of a current that is consistent with Lorentz and gauge invariance. In the context of weak heavy-to-light meson decays, form factors are naturally required when decomposing the matrix elements of the weak current mediating the transition from a heavy meson H into a lighter one L. They can be understood as a measure of the overlap between the initial and final states of the decay:

$$\langle L|\, \bar{q}\,\Gamma Q\, |H\rangle \sim \mathrm{e}^{F_{H\to L}}. \tag{2.1.1}$$

Here, q and Q stand for the fields of the weakly produced light quark in the emitted meson L and the initial heavy quark in H, respectively. On the other hand, Γ represents an irreducible representation of the Dirac algebra component describing the Lorentz quantum numbers of the process, once the indices of the weak vertex have been contracted into a local one. And $F_{H\to L}$ is the form factor.

The term form factor is reminiscent of the functions used for parametrising the inner structure of the proton in scattering processes, since those actually contain information about the "form" of the proton. This physical interpretation is not representative in our case and we should understand the form factors along the ideas above. For this reason, in the context of weak decays it is common to use the most accurate term *transition form factor*.

Quarks in the initial and final state mesons of a decay interact among themselves via gluon exchanges. These include in general high- and low-energy exchanges, but for heavy meson decays (i.e. heavy-to-heavy and heavy-to-light transitions) the leading contribution comes from soft gluons. Therefore, form factors enter our computations as a non-perturbative input.

2.1.2 $B \to P$ Form Factors

Here P means any *pseudoscalar meson*. The following decomposition of bilinear quark matrix elements define the relevant form factors for this type of B meson decays [29]

$$\kappa \langle P(p')|\, \bar{q}\gamma_\mu b\, |\bar{B}(p)\rangle = \left[(p+p')_\mu - \frac{m_B^2 - m_P^2}{q^2} q_\mu\right] f_+(q^2) + \frac{m_B^2 - m_P^2}{q^2}\, q^\mu f_0(q^2), \qquad (2.1.2)$$

$$\kappa \langle P(p')|\, \bar{q}\sigma_{\mu\nu}q^\nu b\, |B(p)\rangle = \frac{i}{m_B + m_K}\left[q^2(p+p')_\mu - (m_B^2 - m_P^2)q_\mu\right] f_T(q^2), \qquad (2.1.3)$$

with m_B and p the mass and momentum of the B meson, m_P and p' the mass and momentum of the pseudoscalar meson in the final state and $q = p - p'$. The three q^2-structures $f_{+,0,T}(q^2)$ are the $B \to P$ form factors.

Using the equations of motion for the s and b quarks, one can transform Eq. (2.1.2) and obtain the following useful relation

$$\kappa \langle P(p')|\, \bar{q}b\, |B(p)\rangle = \frac{m_B^2 - m_P^2}{m_b - m_q} f_0(q^2), \qquad (2.1.4)$$

being m_q the mass of the q quark in the current.

2.1.3 $B \to V$ Form Factors

The relevant form factors for $B \to V$ transitions (where V stands for any *vector meson*) can be defined through the following matrix elements [1] [29]

[1]The sign convention used for the Levi-Civita symbol is such that $\epsilon^{0123} = -\epsilon_{0123} = -1$. Then $\gamma_5 = \frac{i}{4!}\epsilon_{\mu\nu\rho\sigma}\gamma^\mu\gamma^\nu\gamma^\rho\gamma^\sigma = i\gamma^0\gamma^1\gamma^2\gamma^3$.

$$\kappa \langle V(p',\varepsilon^*)|\, \bar q \gamma_\mu b \,|\bar B(p)\rangle = \frac{2iV(q^2)}{m_B+m_V}\epsilon_{\mu\nu\rho\sigma}\varepsilon^{*\nu}p'^{\rho}p^{\sigma}, \tag{2.1.5}$$

$$\begin{aligned}\kappa \langle V(p',\varepsilon^*)|\, \bar q \gamma_\mu\gamma_5 b \,|\bar B(p)\rangle &= 2m_V A_0(q^2)\frac{\varepsilon^*\cdot q}{q^2}q_\mu + (m_B+m_V)A_1(q^2)\left[\varepsilon^*_\mu - \frac{\varepsilon^*\cdot q}{q^2}q_\mu\right] \\ &- A_2(q^2)\frac{\varepsilon^*\cdot q}{m_B+m_V}\left[(p+p')_\mu - \frac{m_B^2-m_V^2}{q^2}q_\mu\right],\end{aligned} \tag{2.1.6}$$

$$\kappa \langle V(p',\varepsilon^*)|\, \bar q \sigma_{\mu\nu}q^\nu b \,|\bar B(p)\rangle = -2T_1(q^2)\epsilon_{\mu\nu\rho\sigma}\varepsilon^{*\nu}p'^{\rho}p^{\sigma}, \tag{2.1.7}$$

$$\begin{aligned}\kappa \langle V(p',\varepsilon^*)|\, \bar q \sigma_{\mu\nu}q^\nu\gamma_5 b \,|\bar B(p)\rangle &= -iT_2(q^2)\left[(m_B^2-m_V^2)\varepsilon^*_\mu - (\varepsilon^*\cdot q)(p+p')_\mu\right] \\ &- iT_3(q^2)(\varepsilon^*\cdot q)\left[q_\mu - \frac{q^2}{m_B^2-m_V^2}(p+p')_\mu\right],\end{aligned} \tag{2.1.8}$$

where m_V, p'^μ and ε^μ are the mass, the 4-momentum and the polarization vector of the vector meson V in the final state, m_B and p^μ are the mass and the 4-momentum of the B meson and $q_\mu = p_\mu - p'_\mu$ is the momentum transfer. The constant κ is defined such that it takes the value $\sqrt{2}$ for ρ^0, while it is equal to 1 for all the other mesons. Finally, the seven independent q^2-functions V, $A_{0,1,2}$ and $T_{1,2,3}$ are the corresponding form factors.

It is important to notice that while V and $A_{1,2,3}$ are scale-independent quantities, $T_{1,2,3}$ have a scale dependence [30, 31]. This is because non-factorisable corrections to the amplitude of the decay $B\to K^*\gamma^*$, with γ^* off-shell, enter the amplitude precisely through the form factors $T_{1,2,3}$ (more details on this can be found in Section 4.4).

Eqs. (2.1.5) and (2.1.8) can be combined in order to obtain expressions for the matrix elements of the typical bilinear quark currents

$$\begin{aligned}\kappa \langle V(p',\varepsilon^*)|\, \bar q \gamma_\mu P_{L,R}\, b \,|\bar B(p)\rangle = \varepsilon^{*\nu}\Bigg\{ &- i\epsilon_{\nu\mu\rho\sigma}p'^{\rho}q^{\sigma}\frac{V(q^2)}{m_B+m_V} \mp \frac{1}{2}\Bigg[\frac{2m_V}{q^2}q_\nu q_\mu A_0(q^2) \\ &+ (m_B+m_V)\left(g_{\nu\mu} - \frac{q_\nu q_\mu}{q^2}\right)A_1(q^2) \\ &- \frac{q_\nu}{m_B+m_V}\left((2p'+q)_\mu - \frac{m_B^2-m_V^2}{q^2}q_\mu\right)A_2(q^2)\Bigg]\Bigg\},\end{aligned} \tag{2.1.9}$$

$$\begin{aligned}\kappa \langle V(p',\varepsilon^*)|\, \bar q\, i\sigma_{\mu\nu}q^\nu P_{L,R}\, b \,|\bar B(p)\rangle = \varepsilon^{*\nu}\Bigg\{ &i\epsilon_{\nu\mu\rho\sigma}p'^{\rho}q^{\sigma}T_1(q^2) \\ &\pm \frac{1}{2}\Bigg[\Big((m_B^2-m_V^2)g_{\nu\mu} - q_\nu(2p'+q)_\mu\Big)T_2(q^2) \\ &+ q_\nu\left(q_\mu - \frac{q^2}{m_B^2-m_V^2}(2p'+q)_\mu\right)T_3(q^2)\Bigg]\Bigg\},\end{aligned} \tag{2.1.10}$$

where the chirality projectors are defined as usual by $P_{L,R} \equiv \frac{1}{2}(1\mp\gamma_5)$.

To conclude the section, we shall present the derivation of two additional matrix elements, which will prove to be useful later on. Let's start by multiplying both sides of Eq. (2.1.9) by q^μ,

$$\kappa \langle V(p', \varepsilon^*)| \, \bar{q} \, \not{q} P_{L,R} \, b \, |\bar{B}(p)\rangle = \epsilon^{*\nu} \left\{ \mp m_V q_\nu A_0(q^2) \right\}. \tag{2.1.11}$$

Now, taking advantage of the fact that γ_5 anticommutes with all the other Dirac matrices, $\{\gamma_\mu, \gamma_5\} = 0$, and using the equations of motion for the b quark and for the $\bar{q}$ antiquark, one transforms the quark current in Eq. (2.1.11) into

$$\left. \begin{array}{r} (\not{p} - m_b) \, b = 0 \\ \bar{q} \, (\not{p}' - m_q) = 0 \end{array} \right\} \quad \Rightarrow \quad \bar{q} \, \not{q} P_{L,R} \, b = m_b \, \bar{q} \, P_{R,L} \, b - m_q \, \bar{q} \, P_{L,R} \, b. \tag{2.1.12}$$

In the heavy-quark limit, the b quark is assumed to be much heavier than the emission quark q ($m_q \ll m_b$), hence terms of the order of m_q/m_b can be neglected. Then, using the results in Eqs. (2.1.11) and (2.1.12), it follows that

$$\kappa \langle V(p', \varepsilon^*)| \, \bar{q} \, P_{L,R} \, b \, |\bar{B}(p)\rangle \simeq \epsilon^{*\nu} \left\{ \pm \frac{m_V}{m_b} q_\nu A_0(q^2) \right\}. \tag{2.1.13}$$

Finally, we also take Eqs. (2.13)-(2.14) from [32] and rearranange them into

$$\begin{aligned} \kappa \langle V(p', \varepsilon^*)| \, \bar{q} \, \sigma_{\mu\nu}\gamma_5 \, b \, |\bar{B}(p)\rangle = \frac{1}{2} i \epsilon_{\mu\nu\rho\sigma} \epsilon_{\alpha\beta}{}^{\rho\sigma} \Bigg\{ & \varepsilon^{*\alpha} (2p' + q)^\beta T_1(q^2) \\ & - \frac{m_B^2 - m_V^2}{q^2} \varepsilon^{*\alpha} q^\beta [T_1(q^2) - T_2(q^2)] \\ & + \frac{2(\varepsilon^* \cdot q)}{q^2} p'^\alpha q^\beta \left[T_1(q^2) - T_2(q^2) - \frac{q^2}{m_B^2 - m_V^2} T_3(q^2) \right] \Bigg\}, \end{aligned} \tag{2.1.14}$$

which, by means of the identity $\sigma_{\mu\nu}\gamma_5 = -\frac{i}{2} \epsilon_{\mu\nu\alpha\beta} \sigma^{\alpha\beta}$, can be recast as

$$\begin{aligned} \kappa \langle V(p', \varepsilon^*)| \, \bar{q} \, \sigma_{\mu\nu} \, b \, |\bar{B}(p)\rangle = \varepsilon^{*\rho} \Bigg\{ & - \epsilon_{\mu\nu\rho\beta} (2p' + q)^\beta T_1(q^2) \\ & + \epsilon_{\mu\nu\rho\beta} \, q^\beta \frac{m_B^2 - m_V^2}{q^2} [T_1(q^2) - T_2(q^2)] \\ & - q_\rho \, \epsilon_{\mu\nu\alpha\beta} \, p'^\alpha q^\beta \frac{2}{q^2} \left[T_1(q^2) - T_2(q^2) - \frac{q^2}{m_B^2 - m_V^2} T_3(q^2) \right] \Bigg\}. \end{aligned} \tag{2.1.15}$$

Eqs. (2.1.11), (2.1.12), (2.1.13) and (2.1.15) are important as they characterise the decomposition of the matrix elements of the most relevant operators in the $b \to s\ell^+\ell^-$ effective Hamiltonian.

2.1.4 Heavy-to-light Form Factors in HQET/LEET: Soft Form Factors

In $b \to q$ transitions where the final quark q can be considered light with respect to the b quark (i.e. $q = u, d, s$), the initial b and final q quarks will interact with the *spectator quark* inside the B meson[2] and the other light degrees of freedom mainly via soft-gluon exchanges. This is a consequence of the b quark being heavy and the recoiling quark very energetic. Therefore, HQET can be used to described the dynamics of the b quark and the LEET formalism applies to the

[2] The quark in the B meson that does not undergo a weak transition during the whole process.

light energetic quark. Following Eqs. (1.4.2) and (1.4.4), neglecting the residual momentum k^μ, the relevant dynamical variables of the process read

$$p^\mu = m_B v^\mu, \qquad p_q'^\mu = E_q n^\mu, \tag{2.1.16}$$

with p^μ the momentum of the B meson and $p_q'^\mu$ and E_q the momentum and energy of the energetic light quark. Recall that the vectors v^μ and n^μ fulfil the properties in Eq. (1.4.7).

Since almost all the energy of the light meson E is carried by the quark created in the weak decay vertex (the spectator quark is soft), then $E_q \simeq E$ and the momentum of the light-meson p'^μ reads

$$p'^\mu = E n^\mu, \tag{2.1.17}$$

allowing us to write the momentum transfer in the following terms

$$q^\mu = p^\mu - p'^\mu = m_B v^\mu - E n^\mu. \tag{2.1.18}$$

Therefore,

$$q^2 = m_B^2 - 2 m_B E + m^2 \qquad \Longleftrightarrow \qquad E = \frac{m_B}{2}\left(1 - \frac{q^2}{m_B^2} + \frac{m^2}{m_B^2}\right) \tag{2.1.19}$$

where m stands for the mass of the final meson.

In the *large recoil limit*, the kinematic region where the energy of the final state meson scales with the heavy quark mass in the heavy-quark limit, the light meson is required to have an energy of order $O(m_B/2)$ or, equivalently, the momentum transfer must be such that $q^2 \ll m_B^2$. Thus, we have that $E \sim m_B \sim m_b \gg \Lambda_{\text{QCD}}$, so all the errors that arise due to the HQET and LEET double expansion in Λ_{QCD}/m_b and $\Lambda_{\text{QCD}}/E_{K^*}$ can be grouped together in a single $O(\Lambda_{\text{QCD}}/m_b)$ term.

The LEET in Section 1.4 can be applied only to those light mesons in which the quark emitted during the weak decay of the b quark carries almost all of the meson's momentum: this dynamical configuration is known as *soft* or *Feynman mechanism*. The preferred configuration for hadronisation is the one where constituent quarks in the outgoing meson have nearly the same momentum, thus the very asymmetric momentum distribution we are assuming here is an atypical one, implying that the probability for the quark-antiquark pair to *hadronise* into a light meson will be a function of its energy. For this reason, the heavy-to-light form factors at large recoil, commonly known as *soft form factors*, will be functions of the energy of the recoiling light meson $\xi(E)$ with unknown absolute normalization.

In this thesis, the explicit derivation of the large recoil soft form factors is not provided. For detailed descriptions of their construction, we refer to Refs. [24, 29]. The three relevant $B \to P$ form factors defined in Eqs. (2.1.2) and (2.1.3) reduce to a single soft form factor $\xi_P(E)$, while the seven independent $B \to V$ form factors defined through Eqs. (2.1.5)-(2.1.8) are all related to only two soft form factors, $\xi_\perp(E)$ and $\xi_\parallel(E)$. The subscripts $\perp$ and $\parallel$ are related to the polarization of the V vector meson, with $\xi_\perp(E)$ ($\xi_\parallel(E)$) being the only contribution to the form factor for a transversely (longitudinally) polarized V.

Neglecting some m_V^2/m_B^2 terms that must be neglected at leading order in $1/m_b$ for consistency, the aforementioned relations between form factors read [24, 29]

$$\langle P(p')|\,\bar q\gamma^\mu b\,|\bar B(p)\rangle = 2E\xi_P(E)n^\mu, \tag{2.1.20}$$
$$\langle P(p')|\,\bar q\sigma^{\mu\nu}q_\nu b\,|\bar B(p)\rangle = 2iE\xi_P(E)\left[(m_B-E)n^\mu - m_B v^\mu\right], \tag{2.1.21}$$

for B meson decays to pseudoscalars, and

$$\kappa\,\langle V(p',\varepsilon^*)|\,\bar q\gamma^\mu b\,|\bar B(p)\rangle = 2iE\,\xi_\perp(E)\epsilon^{\mu\nu\rho\sigma}\varepsilon^*_\nu\, n_\rho v_\sigma \tag{2.1.22}$$
$$\kappa\,\langle V(p',\varepsilon^*)|\,\bar q\gamma^\mu\gamma_5 b\,|\bar B(p)\rangle = 2E\left[\xi_\perp(E)(\varepsilon^{*\mu}-\varepsilon^*\cdot v\,n^\mu)+\xi_\parallel(E)\varepsilon^*\cdot v\,n^\mu\right] \tag{2.1.23}$$
$$\kappa\,\langle V(p',\varepsilon^*)|\,\bar q\sigma^{\mu\nu}q_\nu b\,|\bar B(p)\rangle = 2Em_B\,\xi_\perp(E)\epsilon^{\mu\nu\rho\sigma}\varepsilon^*_\nu\, v_\rho\, n_\sigma \tag{2.1.24}$$
$$\begin{aligned}\kappa\,\langle V(p',\varepsilon^*)|\,\bar q\sigma^{\mu\nu}\gamma_5 q_\nu b\,|\bar B(p)\rangle = -2iE\Big\{&\xi_\perp(E)(\varepsilon^{*\mu}-\varepsilon^*\cdot v\,n^\mu) \\ &+\xi_\parallel(E)\,\varepsilon^*\cdot v[(m_B-E)\,n^\mu - m_B v^\mu]\Big\}\end{aligned} \tag{2.1.25}$$

for decays to vector mesons. Finally, comparing Eqs. (2.1.2)-(2.1.3) with Eqs. (2.1.20)-(2.1.21) the following symmetry relations between form factors emerge

$$f_+(q^2) = \frac{m_B}{2E}f_0(q^2) = \frac{m_B}{m_B+m_P}f_T(q^2) = \xi_P(E) \tag{2.1.26}$$

for pseudoscalars. Correspondingly comparing Eqs. (2.1.5)-(2.1.8) with Eqs. (2.1.22)-(2.1.25) one finds

$$\frac{m_B}{m_B+m_V}V(q^2) = \frac{m_B+m_V}{2E}A_1(q^2) = T_1(q^2) = \frac{m_B}{2E}T_2(q^2) = \xi_\perp(E) \tag{2.1.27}$$
$$\frac{m_V}{E}A_0(q^2) = \frac{m_B+m_V}{2E}A_1(q^2) - \frac{m_B-m_V}{m_B}A_2(q^2) = \frac{m_B}{2E}T_2(q^2) - T_3(q^2) = \xi_\parallel(E) \tag{2.1.28}$$

for decays into vector mesons.

These relations are only valid for the soft contribution to the form factor at large recoil, neglecting corrections of order $\Lambda_{\rm QCD}/m_b$ and α_s.

2.1.5 $O(\alpha_s)$ symmetry breaking corrections

Corrections to the form factors of order $O(\Lambda_{\rm QCD}/m_b)$, although naive dimensional estimates assign a 10% size for them, cannot yet be computed from first principles within any of the theoretical frameworks available. Whereas, the status of $O(\alpha_s)$ corrections to the form factors is rather different. There are two sources of these corrections: *hard-vertex corrections* and *hard-spectator scattering* [29, 33]. High energy contributions of the first type are accounted for by multiplicative renormalising the current $[\bar q\Gamma b]_{\rm eff}$ in the effective theory, following the usual techniques of operator renormalisation in the construction of effective field theories [7]. Soft hard-vertex corrections cannot be treated following the same strategy, since these are contributions from soft collinear gluons to the light quark and therefore cannot be computed in perturbation theory. However, soft hard-vertex contributions respect the symmetries that emerge in the HQET/LEET, so it is possible to absorb them in the definition of the soft form factors [29]. The second type of $O(\alpha_s)$ corrections are, from a physical perspective, generated by gluon exchanges between a heavy or energetic quark and the spectator quark in the meson. Hence they allow mesons to transition into states where the momenta of their valence quarks is symmetrically distributed, being this the preferred configuration for a meson. These latter corrections can be computed within the theory of hard-scattering exclusive processes, which we review in Chapter 3.

The qualitative statement above can be mathematically synthesised into the following schematic expression

$$F(q^2) = D\xi_a(E) + \Phi_B \otimes T_H \otimes \Phi_a, \tag{2.1.29}$$

where F stands for any full QCD form factor, a runs over the possible light mesons in the final state $a = P, V^\perp, V^\parallel$, T_H is the so-called hard-scattering kernel, which can be computed in perturbation theory, $\Phi_{B,a}$ are the light-cone distribution amplitudes for a B meson and a light meson respectively and $D = 1 + O(\alpha_s)$ is a factor accounting for the hard-vertex corrections. As we will discuss in forthcoming chapters, Eq. (2.1.29) holds to all orders in $O(\alpha_s)$ but is only valid at leading order in $\Lambda_{\rm QCD}/m_b$, since it draws from the simplifications available in the context of the HQET/LEET.

2.2 Meson Decay Constants

Meson decay constants are fundamental hadronic parameters where information about the interaction strength between the valence quark q of the meson and its associated antiquark $\bar{q}'$ is encoded [34]. Alternatively, it measures how likely it is for q and $\bar{q}'$ to be at the same space-time point and thus annihilate. As a consequence, a meson decay constant is a natural parameter to appear when computing the transition amplitude from an initial meson state to a final non-hadronic state,

$$\langle 0| \bar{q}'\Gamma q |M\rangle \sim f_M \tag{2.2.1}$$

where Γ represents the irreducible Dirac matrix describing the transition process and f_M is the corresponding meson decay constant.

For a pseudoscalar meson P with momentum p', its decay constant is defined in terms of the following matrix element [29]

$$\kappa \langle P(p')| \bar{q}\gamma_\mu\gamma_5 q' |0\rangle = -if_P p'_\mu, \tag{2.2.2}$$

On the other hand, the longitudinal $f_{V,\parallel}$ and transverse $f_{V,\perp}$ decay constants of a vector meson V with momentum p'_μ and polarization vector ϵ^*_μ are defined as [29]

$$\langle V(p',\varepsilon^*)| \bar{q}\gamma_\mu q' |0\rangle = -if_{V,\parallel} m_V \varepsilon^*_\mu, \tag{2.2.3}$$

$$\langle V(p',\varepsilon^*)| \bar{q}\sigma_{\mu\nu} q' |0\rangle = f_{V,\perp}(\mu_h)(p'_\mu\varepsilon^*_\nu - p'_\nu\varepsilon^*_\mu). \tag{2.2.4}$$

Traditionally meson decay constants have been computed from two-point QCDSRs (see Refs. [27, 28]), yet nowadays some of the best computations for these quantities are obtained through Lattice QCD, because of its progress during the last few years.

Chapter 3

Fundamentals of QCD Factorization

In the context of exclusive hadronic decays of B mesons, factorisation is a concept that applies to matrix elements of the effective operators. For purely leptonic and strict semileptonic two body decays (i.e. $B \to \mu\mu$, for the former, and $B \to D\tau\nu$, for the latter), the amplitude of the process can be decomposed (*factorised*) into products of matrix elements of leptonic and quark currents. These are precisely the currents that originate from the 4-fermion operators in the effective Hamiltonian. The factorisation of the matrix elements for this type of decays is easy to understand because gluons cannot connect leptonic and quark currents. Thinking about Feynman diagrams, it is possible to cut the W boson line connecting the quark and leptonic parts of the decay and treat them separately.

However, for non-leptonic decays, since the products of the decay can interact via strong effects, "*non-factorisable*"[1] contributions, that is corrections to the amplitude that cannot be written as products of currents, must be also taken into account. Gluon exchanges with virtualities above the m_b scale are already included in the process-independent Wilson coefficients of the effective theory, as we discussed in Chapter 1. So, it is the soft QCD interactions that arise during the dynamics of the decay the ones that generate the aforementioned "non-factorisable" contributions. Moreover, these long-distance corrections are crucial for accounting for how the quark content of a given process organizes into hadron final states through the mechanism of *rescattering*. Therefore is crucial to have a systematic and model-independent treatment of two-body heavy meson decays capable of providing a consistent description of the non-perturbative input stemming from these matrix elements while allowing, at the same time, a perturbative treatment of the high-energy QCD effects.

In this section, we are going to first review one of the first attempts at computing matrix elements of two-body meson decays: the so-called *naive factorisation* approach [35, 36] and some of its extensions. Which will lead us to the technique of *QCD factorisation* (QCDf) [37], one of the theoretical frameworks able to deal with these objects with the characteristics described in the paragraph above. The collection of results we will qualitatively describe in this section will be used later on for computing radiative corrections to exclusive radiative B meson decays in the heavy quark limit, as it was shown in [29, 30]. An interested reader can find a more exhaustive review of the factorisation concept in non-leptonic decays in [38] and [39], plus Refs. [40, 41] also provide excellent discussions on QCDf from a more quantitative point of view.

[1] See footnote number 2 on page 31 for a precise definition of the meaning of the term non-factorisable between quotation marks.

3.1 Naive factorisation

For illustrative purposes, let's examine the weak decay of a B meson into two light mesons M_1 and M_2. The dynamics of this decays is governed by the weak effective Hamiltonian $\mathcal{H}_{\text{eff}}$ describing the underlying quark transition with the right quantum numbers. Therefore, the amplitude of the process $\bar{B} \to M_1 M_2$ can be written as

$$\langle M_1 M_2 | \, \mathcal{H}_{\text{eff}} \, | \bar{B} \rangle \sim \sum_i \mathcal{C}_i(\mu) \, \langle M_1 M_2 | \, \mathcal{O}_i \, | \bar{B} \rangle \, (\mu), \tag{3.1.1}$$

where $\mathcal{C}_i$ are the Wilson coefficients of the effective theory and $\mathcal{O}_i$ the corresponding effective operators. Now we will focus on the matrix elements $\langle M_1 M_2 | \, \mathcal{O}_i \, | \bar{B} \rangle$ without, at least in the beginning, thinking too much about its scale dependence.

From a field theory perspective, a meson state M_2 is generated by a quark current carrying the right flavour and Lorentz quantum numbers. For example, if M_2 is a pseudoscalar, one needs a current $\bar{q}_1 \gamma^\mu \gamma_5 q_2$ to create a state with the adequate quantum numbers. Assume that $\mathcal{O}_i$ is such that one of its currents is able to generate M_2 from the vacuum, if this operator also contains a current, say $\bar{q}\gamma^\mu b$, with the quantum numbers of a $\bar{B} \to M_1$ transition, this will contribute to the $\bar{B} \to M_1 M_2$ decay amplitude. In the naive factorisation approach [35, 36], it is assumed that the matrix element of the aforementioned effective operator can be decomposed (factorised) into the product of the matrix elements of the two currents,

$$\langle M_1 M_2 | \, (\bar{q}_1 \gamma^\mu \gamma_5 q_2)(\bar{q}\gamma_\mu b) \, | \bar{B}_q \rangle \simeq \langle M_2 | \, \bar{q}_1 \gamma^\mu \gamma_5 q_2 \, | 0 \rangle \, \langle M_1 | \, \bar{q}\gamma_\mu b \, | \bar{B}_q \rangle = f_{M_2} \cdot F^{\bar{B}_q \to M_1}. \tag{3.1.2}$$

So the matrix element, with two mesons in the final state, under the naive factorisation assumption, simplifies to the product of a decay constant f_{M_2} and a transition form factor $F^{\bar{B}_q \to M_1}$. These two quantities can be computed using elaborate techniques capable of dealing with non-perturbative quantities, like LCSRs or lattice gauge theories. Hence, this approach provides a simple prescription for estimating complicated matrix elements in terms of better known quantities.

In the previous expression, color indices are not explicitly written but understood to be summed over. Notice that, since hadrons only live in colour singlet states, naive factorisation requires both currents into which the full operator is decomposed to be colour singlets.

In general, the weak effective Hamiltonian will contain pairs of operators with the same flavour and Lorentz structures but different colour arrangements,

$$\mathcal{O}_i = (\bar{q}_{1\alpha} \Gamma_1 q_{2\alpha})(\bar{q}_\beta \Gamma_2 b_\beta), \tag{3.1.3}$$

$$\mathcal{O}_j = (\bar{q}_{1\alpha} \Gamma_1 q_{2\beta})(\bar{q}_\beta \Gamma_2 b_\alpha), \tag{3.1.4}$$

where α, β are the colour indices of the quark fields and Γ_1, Γ_2 the Lorentz structures of the currents. Usually, the operators above are referred to as the colour singlet and colour triplet operators. However, these are not the only forms one can write the two operators above. Using a Fierz transformation these operators can be rewritten as,

$$\mathcal{O}'_i = (\bar{q}_\alpha \Gamma'_1 q_{2\beta})(\bar{q}_{1\beta} \Gamma'_2 b_\alpha), \tag{3.1.5}$$

$$\mathcal{O}'_j = (\bar{q}_\alpha \Gamma'_1 q_{2\alpha})(\bar{q}_{1\beta} \Gamma'_2 b_\beta), \tag{3.1.6}$$

with Lorentz structures Γ_1', Γ_2' generally different from Γ_1, Γ_2. Since $\mathcal{O}_i$ and $\mathcal{O}_j'$ are colour singlet structures with the same overall flavour content but different arrangement in terms of currents, it is possible for the operators participating in the decay to be decomposed in the form $\mathcal{O}_i$ (as sketched in (3.1.2)), in the newly ordered form $\mathcal{O}_j'$ or in both forms. In the latter case, according to the principles of Quantum Mechanics one must consider the two possible contributions, as they represent different ways of rearranging the quark content into hadrons. Then, we define the factorised matrix elements by

$$\langle \mathcal{O}_i \rangle_F = \langle M_2 | \bar{q}_1 \Gamma_1 q_2 | 0 \rangle \langle M_1 | \bar{q} \Gamma_2 b | \bar{B}_q \rangle + \langle M_1 | \bar{q}_1 \Gamma_1 q_2 | 0 \rangle \langle M_2 | \bar{q} \Gamma_2 b | \bar{B}_q \rangle , \tag{3.1.7}$$

$$\langle \mathcal{O}_j' \rangle_F = \langle M_2 | \bar{q} \Gamma_1' q_2 | 0 \rangle \langle M_1 | \bar{q}_1 \Gamma_2' b | \bar{B}_q \rangle + \langle M_1 | \bar{q} \Gamma_1' q_2 | 0 \rangle \langle M_2 | \bar{q}_1 \Gamma_2' b | \bar{B}_q \rangle . \tag{3.1.8}$$

If $\mathcal{O}_i$ and $\mathcal{O}_j$ (or equivalently $\mathcal{O}_i'$ and $\mathcal{O}_j'$) are the only relevant operators for the decay, we can write the effective Hamiltonian as

$$\mathcal{H}_{\text{eff}} = \mathcal{C}_i \mathcal{O}_i + \mathcal{C}_j \mathcal{O}_j = \mathcal{C}_i \mathcal{O}_i' + \mathcal{C}_j \mathcal{O}_j'. \tag{3.1.9}$$

However, in order to introduce factorisation, we cannot work with the effective Hamiltonian above, as both $\mathcal{O}_j$ and $\mathcal{O}_i'$ do not admit a decomposition in terms of two separate colourless bilinear currents. Hence one should investigate the structure of these two operators. For that matter, it is convenient to work in the singlet-octet basis for the operators. Take the colour octet operator,

$$\mathcal{O}_8 = (\bar{q}_{1\alpha} T^a_{\alpha\beta} \Gamma_1 q_{2\beta})(\bar{q}_\gamma T^a_{\gamma\delta} \Gamma_2 b_\delta). \tag{3.1.10}$$

by means of the following relation between the generators of the Lie algebra of $SU(3)$,

$$T^a_{\alpha\beta} T^a_{\gamma\delta} = \frac{1}{2} \left[\delta_{\alpha\delta} \delta_{\beta\gamma} - \frac{1}{N_c} \delta_{\alpha\beta} \delta_{\gamma\delta} \right], \tag{3.1.11}$$

one can re-express the octet operator in terms of the singlet and triplet operators,

$$2\mathcal{O}_8 = \mathcal{O}_j - \frac{1}{N_c} \mathcal{O}_i. \tag{3.1.12}$$

This shows that the triplet operator $\mathcal{O}_j$ is *colour suppressed* with respect to the singlet. Plus, it is clear that for $\mathcal{O}_8$ to be able to contribute to the decay amplitude through factorisation, there must be gluon exchanges between the quarks in the operator, implying that contributions from these operators enter at order $O(\alpha_s)$. The same conclusions can be obtained for the Fierz transformed operator $\mathcal{O}_i'$, with the correspondingly transformed octet operator $\mathcal{O}_8'$. So one can schematically write

$$\mathcal{C}_j \mathcal{O}_j = \frac{1}{N_c} \mathcal{C}_j \mathcal{O}_i + O(\alpha_s) \qquad \text{and} \qquad \mathcal{C}_i \mathcal{O}_i' = \frac{1}{N_c} \mathcal{C}_i \mathcal{O}_j' + O(\alpha_s). \tag{3.1.13}$$

Therefore, the naive factorisation approach finally yields the following decomposition of the amplitude of the process,

$$\langle M_1 M_2 | \mathcal{H}_{\text{eff}} | \bar{B} \rangle = a_i(\mu) \langle \mathcal{O}_i \rangle_F + a_j(\mu) \langle \mathcal{O}_j' \rangle_F , \tag{3.1.14}$$

where the dressings $a_{1,2}(\mu)$ are defined as,

$$a_{i,j}(\mu) = \mathcal{C}_{i,j}(\mu) + \frac{1}{N_c}\mathcal{C}_{j,i}(\mu). \tag{3.1.15}$$

The application of the naive factorisation ansatz can be actually justified in highly energetic two-body decays. In this case, the mesons produced in the decay hadronise[2] when they are far apart from each other and thus the "factorisable"[3] part of the amplitude is expected to give the dominant contribution. Then, since quarks have already organized into colour singlet states, soft gluons cannot alter their arrangement. This dynamical condition is known as the colour transparency hypothesis [42]. One cannot strictly derive colour transparency from QCD [25] but it can be explained in a systematic and model-independent way within the combined framework of HQET and LEET [43]. Soft gluon exchanges between a fast recoiling meson produced in a point-like source, i.e. an operator in an effective field theory, and the other hadronic parts in a meson decay are very suppressed. Then, it is possible to study this soft-gluon interactions by means of a multipole expansion, being the first term the colour dipole. It can be seen that this contribution is suppressed by a $\Lambda_{\rm QCD}/m_b$ factor and so it vanishes in the heavy-quark limit.

As mentioned before, (3.1.14) implicitly means that "non-factorisable" corrections are neglected. The exchange of soft gluons between the mesons in final state is forbidden, making the physical phenomena of rescattering and the generation of strong phase shifts between amplitudes out of reach of this description.

However, the most obvious drawback of the naive factorisation approach has to do with the different scaling behaviour $a_{i,j}(\mu)$ and the factorised matrix elements $\langle \mathcal{O}^{(\prime)}_{i,j}\rangle_F$ enjoy. The renormalisation scale dependent matrix element $\langle \mathcal{O}^{(\prime)}_{i,j}\rangle(\mu)$ is ultimately reduced to a decay constant times a transition form factor, which are scale independent quantities. Therefore, all the scale dependence cancellations between the Wilson coefficients and matrix elements of the operators of the effective theory is lost in naive factorisation, consequently rendering an unphysical amplitude. Rather than interpreting the factorised amplitude as a physically meaningful object, one might want to take it as a proxy for the amplitude valid only within a suitable factorisation scale μ_f. No information on this scale is available from the principles of this prescription but one usually assumes this scale to be around $O(m_c)$ or $O(m_b)$, for D and B decays respectively.

More problems affect naive factorisation results beyond the leading logarithm contribution. At this order in the expansion, the Wilson coefficients become renormalisation scheme dependent quantities. In the "full" effective theory, the matrix elements are also scheme dependent quantities so that the overall scheme dependence cancels, however the factorised form of the matrix elements spoils this cancellation. Of course, this is unphysical too.

3.1.1 Generalised factorisation

These issues are addressed, more or less effectively, in various so-called *generalised factorisation* approaches [34, 44–49]. These models generalise the naive factorisation prescription by introducing

[2] By hadronisation one understands those strongly mediated interactions by which free quarks assemble in order to create hadron states.

[3] We will use the term "factorisable", between quotation marks, for referring to those contributions to the matrix elements that can be decomposed following naive factorisation, i.e. into the product of a transition form factor and a decay constant. Similarly, "non-factorisable" corrections are those which do not accept such a decomposition. We introduce this notation as in the next section, when discussing the elements of QCDf, factorisable and non-factorisable contributions will have a different meaning.

new parameters that account for the "non-factorisable" contributions, in an effort to cancel the scale and scheme dependence of the Wilson coefficients.

In Ref. [34] a more flexible approach is introduced where, instead of a fixed factorisation scale $\mu_f = m_b$ (for B decays), one introduces the scale as a process dependent parameter. Assume the amplitude of the decay $\bar{B} \to M_1 M_2$, given its dynamics and quantum numbers, can be described by the factorisation of $\mathcal{O}_i$ only, and not $\mathcal{O}'_j$. Using Fierz rearrangements, one can write the effective Hamiltonian for this process in terms of two colour single currents and two colour octet currents,

$$\mathcal{H}_{\text{eff}} \sim \left(\mathcal{C}_i + \frac{1}{N_c}\mathcal{C}_j\right)\mathcal{O}_i + 2\mathcal{C}_j\mathcal{O}_8. \tag{3.1.16}$$

One can introduce two process dependent non-perturbative hadronic parameters, $\varepsilon_1(\mu)$ and $\varepsilon_8(\mu)$, to account for the "non-factorisable" contribution that are neglected in naive factorisation

$$\varepsilon_1(\mu) \equiv \frac{\langle O_i\rangle}{\langle O_i\rangle_F} - 1, \qquad \varepsilon_8(\mu) \equiv 2\frac{\langle O_8\rangle}{\langle O_i\rangle_F}. \tag{3.1.17}$$

Whereas the naive factorisation decomposition $\mathcal{C}_i\langle\mathcal{O}_i\rangle + \mathcal{C}_j\langle\mathcal{O}_j\rangle = a_i(\mu)\langle\mathcal{O}_i\rangle_F$ is only valid up to $O(\alpha_s)$ corrections, the factorisation structure can be made exact with the aid of the parameters $\varepsilon_1(\mu)$ and $\varepsilon_8(\mu)$ in Eq. (3.1.17),

$$\mathcal{C}_i\langle\mathcal{O}_i\rangle + \mathcal{C}_j\langle\mathcal{O}_j\rangle = \left[\left(\mathcal{C}_i(\mu) + \frac{1}{N_c}\mathcal{C}_j(\mu)\right)[1+\varepsilon_1(\mu)] + \mathcal{C}_j(\mu)\varepsilon_8(\mu)\right]\langle\mathcal{O}_i\rangle_F\,. \tag{3.1.18}$$

The same can be argued for a decay proceeding through the decomposition of the operator $\mathcal{O}'_j$. In this case, one finds that

$$\mathcal{C}_i\langle\mathcal{O}'_i\rangle + \mathcal{C}_j\langle\mathcal{O}'_j\rangle = \left[\left(\mathcal{C}_j(\mu) + \frac{1}{N_c}\mathcal{C}_i(\mu)\right)[1+\varepsilon'_1(\mu)] + \mathcal{C}_i(\mu)\varepsilon'_8(\mu)\right]\langle\mathcal{O}'_j\rangle_F\,, \tag{3.1.19}$$

where the hadronic parameters $\varepsilon'_1(\mu)$ and $\varepsilon'_8(\mu)$ follow the definitions in Eq. (3.1.17) with the replacements $\mathcal{O}_i \to \mathcal{O}'_j$ and $\mathcal{O}_8 \to \mathcal{O}'_8$. In terms of these new parameters, the decay amplitude (3.1.14) can be recast as

$$\langle M_1 M_2|\,\mathcal{H}_{\text{eff}}\,|\bar{B}\rangle = a_i^{\text{eff}}\langle\mathcal{O}_i\rangle_F + a_i^{\text{eff}}\langle\mathcal{O}'_j\rangle_F\,, \tag{3.1.20}$$

with the coefficients a_1 and a_2 being replaced by the effective coefficients

$$a_i^{\text{eff}} = \left(\mathcal{C}_i(\mu) + \frac{1}{N_c}\mathcal{C}_j(\mu)\right)[1+\varepsilon_1(\mu)] + \mathcal{C}_j(\mu)\varepsilon_8(\mu), \tag{3.1.21}$$

$$a_j^{\text{eff}} = \left(\mathcal{C}_j(\mu) + \frac{1}{N_c}\mathcal{C}_i(\mu)\right)[1+\varepsilon'_1(\mu)] + \mathcal{C}_i(\mu)\varepsilon'_8(\mu). \tag{3.1.22}$$

Clearly, since the colour transparency hypothesis is a sound physical depiction when "non-factorisable" contributions can be safely neglected, any faithful generalisation of the naive factorisation approach should aim at providing a framework that reduces to (3.1.14) when "non-factorisable" corrections are put to zero. This is the case of the parametrisation presented above, as one can see taking the limit $\varepsilon_{1,8}^{(\prime)} \to 0$ in Eqs. (3.1.21) and (3.1.22).

The introduction of the hadronic parameters $\varepsilon_i^{(\prime)}(\mu)$ $(i = 1, 8)$ comes without any loss of generality and, since the factorised matrix elements do not depend on the scale, all of the scale dependence is contained inside the Wilson coefficients and the parameters $\varepsilon_i^{(\prime)}(\mu)$. Therefore, as the amplitude is a physical and hence μ-independent quantity, the hadronic parameters $\varepsilon_i^{(\prime)}(\mu)$ restore the correct μ-dependence of the matrix elements, which is lost in naive factorisation.

Even if the generalised factorisation presented in [34] manages to consistently treat the differences in the scale dependence of the Wilson coefficients and the factorised matrix elements, it is still affected by a major theoretical problem. The scheme dependence of the Wilson coefficients at next-to-leading order in the renormalisation group improved perturbation theory makes it possible to find, for any factorisation scale, a particular scheme where the hadronic parameters $\varepsilon_{1,8}^{(\prime)}$ vanish simultaneously [49]. This leads us back to the naive factorisation result and shows the inadequacy of this generalisation for properly accounting for the "non-factorisable" contributions to the matrix elements.

Another approach to combining the principles of factorisation while achieving results with the right scale and scheme dependence can be found in [45, 47, 48, 50]. For matching the effective theory to the full theory when building the effective Hamiltonian, one needs to eliminate the divergences that appear in the matrix elements of the effective operators through renormalisation of the constituent fields plus the so-called operator renormalisation (see Chapter 1 and [7] for more details). Therefore, since any $\mathcal{O}(\mu)$ in the effective Hamiltonian is a four-quark (current-current) operator renormalised at the scale μ, its matrix element can be schematically written in terms of its corresponding tree-level amplitude

$$\mathcal{C}(\mu)\left\langle\mathcal{O}(\mu)\right\rangle = \mathcal{C}(\mu)g(\mu)\left\langle\mathcal{O}\right\rangle_{\text{tree}}, \tag{3.1.23}$$

with [45]

$$g(\mu) \sim 1 + \alpha_s(\mu)\left(\gamma \ln\frac{\mu^2}{-p^2} + c\right), \tag{3.1.24}$$

where p is the off-shell momentum of the external quark lines, γ the anomalous dimension and c a momentum-independent constant term. Then, one can redefine the contribution of this operator to the amplitude,

$$\mathcal{C}(\mu)g(\mu)\left\langle\mathcal{O}\right\rangle_{\text{tree}} = \mathcal{C}^{\text{eff}}\left\langle\mathcal{O}\right\rangle_{\text{tree}}, \tag{3.1.25}$$

so that the effective coefficient $\mathcal{C}^{\text{eff}}$ is scale and scheme independent. Thus, coming back to our customary system described by the Hamiltonian in (3.1.16), one finds

$$\mathcal{C}_i\left\langle\mathcal{O}_i\right\rangle + \mathcal{C}_j\left\langle\mathcal{O}_j\right\rangle = \mathcal{C}_i^{\text{eff}}\left\langle\mathcal{O}_i\right\rangle_{\text{tree}} + \mathcal{C}_j^{\text{eff}}\left\langle\mathcal{O}_j\right\rangle_{\text{tree}} \tag{3.1.26}$$

Now it is, in principle, possible to safely apply naive factorisation to the "tree-level" matrix elements, as all scale and scheme dependence is encapsulated in the effective coefficients. Ultimately, as in Eq. (3.1.20), this procedure leads to a factorisation prescription that absorbs the "non-factorisable" contributions into some parameters $a_{i,j}^{\text{eff}}$,

$$a_{i,j}^{\text{eff}} = \mathcal{C}_{i,j}^{\text{eff}} + \frac{1}{N^{\text{eff}}}\mathcal{C}_{j,i}^{\text{eff}}, \tag{3.1.27}$$

where N^{eff} is a "non-factorisable" parameter representing the effective colour suppression that each different channel feels. Notice that, despite N^{eff} being in general a process dependent, this parameter is expected to be process-independent for energetic two body B-decays [45].

This last approach also has, however, its own drawbacks. As shown in [49], the perturbative evaluation of scheme-dependent finite contributions to the matrix elements makes the effective Wilson coefficients gauge dependent quantities and induces some infrared singularities. Of course, this makes the parametrisation in (3.1.27) unphysical and diminishes its predictive power.

Finally, some theoretical frameworks able to properly treat "non-factorisable" contributions emerged [51–54], where all the shortcomings discussed above are solved. In the remaining of this chapter we will focus on the computational method introduced by Beneke, Buchalla, Neubert and Sachrajda: the so-called QCD factorisation approach (QCDf), also known as *BBNS* after its authors. Originally this framework was devised for the analysis of the $B \to \pi\pi$ decay [37] and later it was extended and generalised to non-leptonic [55–57] and radiative decays [30, 33, 58].

3.2 QCD Factorisation

QCD factorisation is a theoretical framework for computing transition matrix elements of effective operators that relies on the usual factorisation sense used in most QCD applications: what it is factorised are the long-distance dynamical effects in the matrix elements from all those contributions that depend on the characteristic large scale of the underlying physical process. These ideas were already widely used in the 70s and 80s for the description of hadron scattering with large momentum transfer, i.e. deep inelastic scattering (DIS). In this last particular case, the amplitude for a process $e + A \to e + X$ (where A denotes a given hadron and X anything else) [59, 60]

$$W^{\mu\nu}(p,q) = \frac{1}{4\pi} \int d^4y \, \mathrm{e}^{iq\cdot y} \, \langle A(p)| \, j^\mu(y) \, |X\rangle \, \langle X| \, j^\nu(0) \, |A(p)\rangle \,, \tag{3.2.1}$$

where $j^\mu(y)$ is the electromagnetic current, can be written in a very compact form, following the factorisation theorem

$$W^{\mu\nu}(p,q) = \sum_a \int_x^1 \frac{d\xi}{\xi} f_{a/A}(\xi,\mu) \, H_a^{\mu\nu}(q,\xi p,\mu,\alpha_s(\mu)) + \text{power corrections of } O\left(\frac{1}{Q^2}\right). \tag{3.2.2}$$

In the expression above, p is the momentum of the incoming hadron A, q the momentum transfer, $Q^2 = -q^2$ and the index a runs over all *partons* composing the incoming hadron ($a =$ gluon, $u, \bar{u}, d, \bar{d}, \ldots$). The hard-scattering functions $H_a^{\mu\nu}$ contain the short-distance contributions, which can be computed perturbatively as an expansion in $\alpha_s(\sqrt{Q^2})$. Whereas, the so-called parton distribution functions $f_{a/A}(\xi,\mu)$ encode the long-distance phenomena and thus must be computed by means of non-perturbative methods or estimated experimentally. One must read $f_{a/A}(\xi,\mu)d\xi$ as the probability of finding a given parton a in the hadron A carrying a fraction ξ of its total momentum. The benefit of employing this decomposition is that generally the non-perturbative objects involved, that is the parton distribution functions in this case, are substantially simpler in structure with respect to the full amplitude and/or they are process independent.

In the QCDf context, the same idea applies. As in (3.2.2), QCDf factorises a given transition matrix element as a convolution of long- and short-distance structures. Again, long-distance contributions must be assessed with the aid of non-perturbative analytical tools, while the short-distance pieces can be computed in perturbation theory with $\alpha_s(m_b)$ as the expansion parameter.

Clearly, the factorisation properties of non-leptonic decay amplitudes must depend on the mesons in the final state. It is thus necessary to make distinctions between types of mesons and,

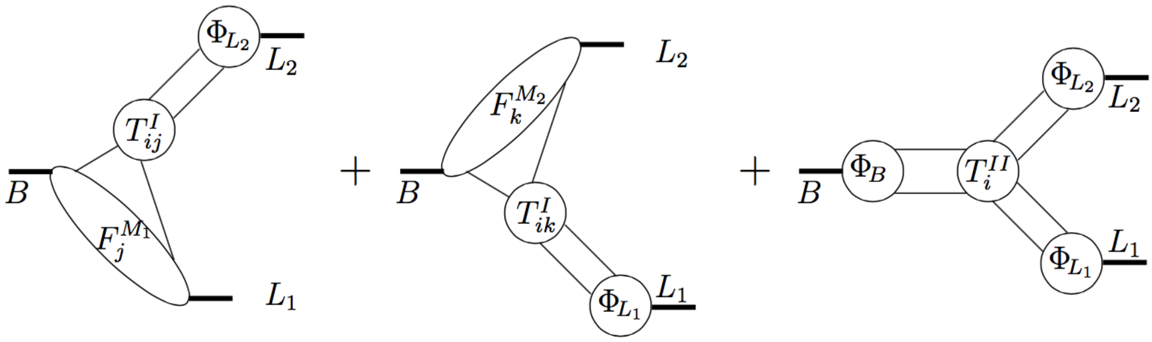

Figure 3.1: Graphical representation of the factorisation formula for B meson decays to two light mesons [55].

since m_b sets the QCDf factorisation scale, this distinction has to be expressed in meaningful terms within the heavy-quark limit. In this sense, we will call a meson "light", if its mass can be considered as finite in the heavy-quark limit. Alternatively, a meson is going to be "heavy", if its mass m scales with m_B in the same limit, so that m/m_B stays fixed.

3.2.1 The factorisation formula

The subsequent discussion contains a review of the general elements and concepts involved in QCDf mainly following [55]. We consider non-leptonic $B \to M_1 M_2$ decays mediated by an underlying weak transition in the heavy-quark limit and distinguish those cases in which both mesons in the final state are light from those where one of the mesons is heavy and the other light. Up to power corrections of order $\Lambda_{\rm QCD}/m_b$, the QCDf *factorisation formula* for the transition matrix element of an effective operator $\mathcal{O}_i$ in the WEH reads [55]

$$\begin{aligned}
\langle L_1 L_2 | \, \mathcal{O}_i \, | \bar{B} \rangle = & \sum_j F_j^{B\to L_1}(m_2^2) \int_0^1 du \; T^{\rm I}_{ij}(u) \Phi_{L_2}(u) \\
& + \sum_k F_k^{B\to L_2}(m_1^2) \int_0^1 dv \; T^{\rm I}_{ik}(v) \Phi_{L_1}(v) \qquad (3.2.3)\\
& + \int_0^1 d\xi \, du \, dv \; T^{\rm II}_i(\xi,u,v) \Phi_B(\xi) \Phi_{L_1}(u) \Phi_{L_2}(v), \\
\langle H_1 L_2 | \, \mathcal{O}_i \, | \bar{B} \rangle = & \sum_j F_j^{B\to H_1}(m_2^2) \int_0^1 du \; T^{\rm I}_{ij}(u) \Phi_{L_2}(u). \qquad (3.2.4)
\end{aligned}$$

Eq. (3.2.3), stating the factorisation of a matrix element of a B meson decay to two light mesons, is diagrammatically depicted in Fig. 3.1. On the one hand, the non-perturbative content of the factorisation formula is encoded in the form factors $F_j^{B\to L_{1,2}}(m^2_{2,1})$ modelling $B \to M_{1,2}$ transitions and the light-cone distribution amplitudes (LCDAs) $\Phi_X(u)$ for the quark-antiquark Fock state of meson X. We provide a description of the non-perturbative inputs in QCDf below. On the other hand, the hard-scattering functions $T^{\rm I}_{ij}(u)$ and $T^{\rm II}_i(\xi,u,v)$ (also known as hard-scattering kernels) are perturbatively calculable functions of the light-cone momentum fractions u, v and ξ of the quarks inside the final state mesons and the B meson respectively. There are two types of hard-scattering kernels: "type I" and "type II", accounting for "hard vertex" and "hard-spectator" contributions. Both LCDAs and hard-scattering kernels are scale and scheme dependent functions, this is not explicitly written above for the sake of keeping a simple notation. And, finally, $m_{1,2}$ denote the meson masses.

Hard interactions always enter at order $O(\alpha_s)$, therefore the third term in Eq. (3.2.3) does not contribute at $O(\alpha_s^0)$. The hard-scattering kernels $T^{\mathrm{I}}_{i,j}$ are independent of u and v at this order too, so the convolution in the factorisation formula yields the product of a form factor and a decay constant, reproducing naive factorisation. This corresponds to the lowest order topology in the effective theory (see Fig. 3.2). Hence, now we have a formalism that naturally explains the naive factorisation result at leading order while it allows us, at the same time, to systematically compute radiative corrections to this result at all orders. Additionally, this solves all the problems regarding the different scale and scheme dependencies between the different objects in generalised factorisation prescriptions.

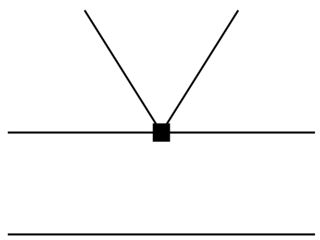

Figure 3.2: Leading order topology contributing to the decay of a B meson to two mesons. Here the black square represents the four-quark operator through which the decay proceeds [55].

In B meson decays to two light mesons, the spectator quark in the B meson can go to either of the two light mesons. This is accounted for in the first two lines of Eq. (3.2.3), each of them being one possibility. The third term in this equation contains the contributions to the matrix element coming from hard scattering interactions with the spectator quark. The two topologies in Fig. 3.3 are examples of hard-spectator scattering interactions.

The structure of the factorisation formula simplifies greatly when dealing with decays where the spectator quark goes to a heavy meson. In such a context, hard-spectator interactions (those in the third term in Eq. (3.2.3)) can be safely neglected as these contributions turn out to be power suppressed in the heavy-quark limit. Notice that it could also happen that the spectator quark goes to the light meson, while the other meson is heavy. However, in this setting QCDf does not apply because the heavy meson is neither fast nor small for it to be factorised from the decay's weak quark current. This does not pose a threat, though, since such amplitudes are power suppressed in the heavy quark limit with respect to the contributions where the spectator is captured by the heavy meson while the other is light. As a final remark, one should observe that annihilation topologies in Fig. 3.4 are not included in the factorisation formula, the reason being that these are corrections that do not contribute at leading order in the heavy-quark expansion.

Because the form factors and distribution amplitudes are all real quantities, strong phases generated via rescattering effects, of great importance in the hadronisation of mesons, must be hidden inside the perturbative hard-scattering functions or contained in the order $\Lambda_{\mathrm{QCD}}/m_b$ power corrections to the factorisation formula.

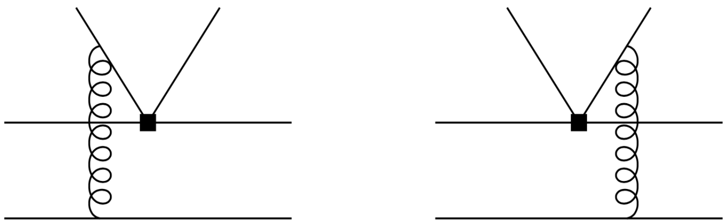

Figure 3.3: Hard-spectator scattering diagrams in the effective field theory [55].

The other great achievement of QCDf relies on its usefulness. Computing the full matrix element $\langle M_1 M_2 | \mathcal{O}_i | \bar{B} \rangle$ is a grand theoretical endeavour, however form factors and LCDAs enjoy a significantly simpler structure and they have been at the reach of many non-perturbative techniques (LCSRs, QCDSRs, lattice gauge theories, etc) since a long time already.

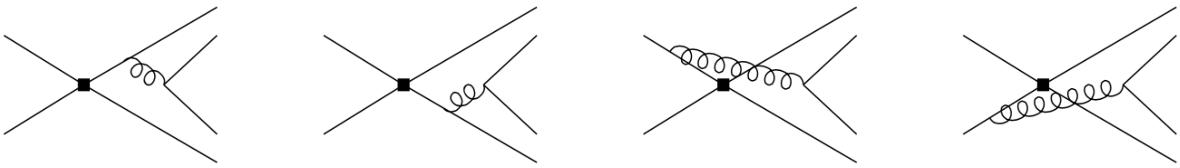

Figure 3.4: Weak annihilation topologies [55].

3.2.2 Power counting rules

Identifying which terms are leading and which are suppressed at leading power in Λ_{QCD}/m_b and at a given order in α_s is rather important in the QCDf framework. For that matter, one needs to understand the typical energy scales of the gluon exchanges between the constituent quarks inside a meson and between the quarks of the different mesons involved in the dynamics of the decay process.

For mesons, or more in general hadrons, to stay as a bound state, there must be a constant gluon exchange between the valence quarks. In the case of a heavy quark, as most of the meson's momentum is aligned with that of the heavy quark constituent, both gluon exchanges between valence quarks and the momentum of the spectator quark are soft and thus of order $q^2_{\text{soft}} \sim \Lambda^2_{\text{QCD}}$. The decay of a heavy quark is a highly energetic process, so hard-collinear gluon exchanges are expected, these being of the energy scale of the heavy quark $q^2_{\text{hard-collinear}} \sim m_b^2$. Finally, there is one last interaction possibility, which is the gluon exchange from a heavy or a fast-recoiling quark to the spectator of the heavy meson (assumed to be slow and soft), i.e. hard-spectator scattering. Typical energy scales for this type of interactions are $q^2_{\text{hard-spectator}} \sim \Lambda_{\text{QCD}} m_b$.

3.2.3 The non-perturbative quantities in QCDf

In this subsection we want to present some of the characteristics and properties of the non-perturbative inputs in the factorisation formula: form factors and light-cone distribution amplitudes.

Transition form factors

As we already discussed in Chapter 2, the general notion of a transition form factor arises in the decomposition of matrix elements of the form

$$\langle M|\,\bar{q}\Gamma b\,|\bar{B}\rangle\,, \tag{3.2.5}$$

where $\bar{q}$ and b are Dirac quark fields and Γ a given irreducible Lorentz structure linked to the vertex responsible of the $b \to q$ transition. For example, the matrix element of a vector current mediating a $B \to P$ transition can be parametrised in terms of two scalar form factors

$$\langle P(p')|\,\bar{q}\gamma^\mu b\,|\bar{B}(p)\rangle = F_+^{B\to P}(q^2)(p^\mu + p'^\mu) + \left[F_0^{B\to P}(q^2) - F_+^{B\to P}(q^2)\right]\frac{m_B^2 - m_P^2}{q^2}, \tag{3.2.6}$$

with $q = p - p'$. Here m_P is the mass of the P meson and m_B the mass of the B meson.

One can look at the form factors in the factorisation formula in a twofold way. First, one can understand that only soft contributions are accounted for in the $F_j^{B\to H_1,L_1}$ parametrising the meson transition in the factorisation formula. In this framework hard corrections to the form factors are taken to be part of the hard-scattering kernels $T^{\mathrm{I}}_{i,j}$ and T^{II}_i. Of course, this interpretation has implicit one's ability to distinguish between soft and hard contributions. Recall that "physical" form factors[4] contain both soft and hard contributions to the underlying transition. This separation is possible for B meson decays to a heavy and a light meson since one can define form factors containing only soft contributions within HQET, which can later be matched to the physical form factors. However, there is no solid procedure for doing the same for decays to two light mesons. A second approach is to equate the non-perturbative functions $F_j^{B\to H_1,L_1}$ to "physical" form factors. Then, as both soft and hard contributions are included in the "physical" form factors, hard contributions have to be omitted from type II hard-scattering kernels T^{II}_i and consistently subtracted from type I kernels $T^{\mathrm{II}}_{i,j}$, beginning at two-loop order [55].

Light mesons light-cone distribution amplitudes

Given any four-vector $k^\mu = (k^0, k^1, k^2, k^3)$, one can define its *light-cone components* (along the z-axis) by

$$k_\pm = \frac{k^0 \pm k^3}{\sqrt{2}}. \tag{3.2.7}$$

Using these components it is possible to rewrite the previous four-vector as

$$k^\mu = (k_+, k_-, \mathbf{k}_\perp), \tag{3.2.8}$$

where $\mathbf{k}_\perp$ refers to the components of $\mathbf{k} = (k^1, k^2, k^2)$ orthogonal to the axis used to define the light-cone components $k_\pm$. Clearly, these coordinates are highly dependent on the axis choice used for their definition but they provide a very powerful language for describing ultra-relativistic

[4] By "physical" form factors we understand the form factors in which we decompose transition matrix elements, i.e. $F_{+,0}^{B\to P}$ in (3.2.6) and all of the form factors discussed in Chapter 2.

phenomena where it is possible to identify a preferred axis. This is certainly the case of hard-scattering processes, being the preferred axis the collision axis. The main motivation for the use of light-cone components is their very simple transformation laws under boosts along the preferred axis (the z-axis in our case):

$$k^\mu = (k_+, k_-, \mathbf{k}_\perp) \xrightarrow{z-\text{boost}} k'^\mu = (k_+ e^{\psi}, k_- e^{-\psi}, \mathbf{k}_\perp) \tag{3.2.9}$$

with ψ an hyperbolic angle such that $v = \tanh\psi$ is the velocity of the boost. See [61] for a rather comprehensive review on the properties of light-cone components.

LCDAs play for hard-scattering processes the same role the parton distribution functions play for high-energy inclusive processes. These are universal non-perturbative objects that encode the long distance dynamics of the meson (or, more generally, hadron) considered when probed at large momentum transfer. Physically they represent the probability of finding the valence quark and antiquark inside the meson in a certain dynamical configuration.

Let us construct a light-pseudoscalar meson state out of its on-shell constituent quark components within a spin singlet-state with no net transverse momentum [55]

$$|P(k)\rangle = \int \frac{dv}{\sqrt{v\bar{v}}} \frac{d^2\ell_\perp}{16\pi^3}\, \psi(v, \boldsymbol{\ell}_\perp) \frac{1}{\sqrt{2N_c}} \left(a^\dagger_{\ell_q\uparrow} b^\dagger_{\ell_{\bar{q}}\downarrow} - a^\dagger_{\ell_q\downarrow} b^\dagger_{\ell_{\bar{q}}\uparrow} \right) |0\rangle\,. \tag{3.2.10}$$

Here $a^\dagger_{\ell\uparrow}$ ($b^\dagger_{\ell\uparrow}$) is a creation operator whose vacuum excitations are (anti)quarks with momentum ℓ and spin up, with its colour indices not explicitly stated. This is clearly a leading order representation of the quantum state of a pseudoscalar meson. The wave-function $\psi(v, \boldsymbol{\ell}_\perp)$ measures the probability for the meson to be composed of an on-shell quark and antiquark with longitudinal momentum fractions v and $\bar{v}$ and transverse momentum $\boldsymbol{\ell}_\perp$, which averages out to zero between the two quarks. The on-shell momenta of the quarks ($\ell^2_{q,\bar{q}} = 0$) are given by [55]

$$\ell_q = vk + \ell_\perp + \frac{\boldsymbol{\ell}_\perp^2}{4vE} n_-, \qquad \ell_{\bar{q}} = \bar{v}k - \ell_\perp + \frac{\boldsymbol{\ell}_\perp^2}{4\bar{v}E} n_-, \tag{3.2.11}$$

with $k = E(1,0,0,1)$ the pseudoscalar momentum, being $E = p_B \cdot k/m_B$ its energy expressed in a Lorentz invariant fashion assuming the pseudoscalar is generated in the decay of a B meson, and $n_\pm = (1,0,0,\pm 1)$ the light-cone basis vectors (along the z-axis). Notice that, as the quark's transverse momentum $\ell_\perp$ is only related to the meson soft contributions, $\ell_\perp \sim \Lambda_{\rm QCD}$ for power-counting purposes. It is also interesting to observe that the quar-antiquark invariant mass $(\ell_q + \ell_{\bar{q}})^2 = \boldsymbol{\ell}^2_\perp / v\bar{v}$ is of order $\Lambda^2_{\rm QCD}$ and thus irrelevant in the heavy quark limit.

LCDAs are defined via hadron-vacuum matrix elements of non-local operators composed by a given number of quark and gluon fields with a certain helicity structure at light-like separations. Non-local operators with different structures give rise to different LCDAs. These LCDAs are classified according to the so-called *twist*[5] of their corresponding operator. The lowest twist operator one can imagine for a pseudoscalar meson is the operator associated with its lowest Fock state. Then, explicitly using the spinorial form of the quark fields, we can write the vacuum-to-hadron matrix element defining the leading twist LCDA

[5]Roughly speaking, the twist of an operator is defined as the difference between its dimension and spin. It turns out that this quantity, rather than the dimension of the operator alone, is a more relevant quantity when classifying a given operator in an expansion near the light-cone [62, 63]. In our case, the operator with the lowest dimension compatible with gauge and Lorentz invariant follows the structure $q'_i(z)_\alpha \bar{q}_j(0)_\beta$. Since this is an operator of dimension three and spin one, the lowest or leading twist order is twist-2.

$$\langle P(k)|\, q_i'(z)_\alpha \bar{q}_j(0)_\beta \,|0\rangle_{z^2=0} = \frac{if_P}{4\kappa}\delta_{ij}\,(\gamma_5 \not{k})_{\alpha\beta}\int_0^1 dv\; \mathrm{e}^{i\bar{v}k\cdot z}\Phi_P(v), \tag{3.2.12}$$

where f_P is the pseudoscalar meson decay constant, $\kappa = \sqrt{2}$ ($\kappa = 1$) for π^0 and ρ^0 (for other mesons) and i, j and α, β are colour and spinor indices, respectively. As we mentioned earlier, LCDAs are actually probability distributions so they are normalised to unity $\int_0^1 dv\; \Phi_P(v) = 1$. Hence, the meson wave-function $\psi(v, \ell_\perp)$ in Eq. (3.2.10) is related to the leading twist pseudoscalar LCDA $\Phi_P(v)$ by integrating out its transverse momentum dependence

$$\int \frac{d^2\ell_\perp}{16\pi^3}\frac{1}{\sqrt{2N_c}}\psi(v, \boldsymbol{\ell}_\perp) = -\frac{if_P}{4\kappa}\Phi_P(v). \tag{3.2.13}$$

Similarly, vector-meson LCDAs are defined through the following matrix elements, where η^μ is the polarization vector of the vector meson V [32, 64]

$$\begin{aligned}\langle V(k,\eta)|\, q_i'(z)_\alpha \bar{q}_j(0)_\beta \,|0\rangle_{z^2=0} = &-\frac{f_V^\perp}{8\kappa}\delta_{ij}\,[\not{\eta}, \not{k}]_{\alpha\beta}\int_0^1 dv\; \mathrm{e}^{i\bar{v}k\cdot z}\Phi_V^\perp(v)\\ &-\frac{f_V^\parallel m_V}{4\kappa}\delta_{ij}\Bigg[i\,\not{k}_{\alpha\beta}\,\eta\cdot z\int_0^1 dv\; \mathrm{e}^{i\bar{v}k\cdot z}\Phi_V^\parallel(v)\\ &+\not{\eta}_{\alpha\beta}\int_0^1 dv\; \mathrm{e}^{i\bar{v}k\cdot z}g_V^{\perp(v)}(v)\\ &-\frac{1}{4}\left(\epsilon^{\mu\nu\rho\sigma}\eta_\mu k_\nu z_\rho \gamma_\sigma\gamma_5\right)\int_0^1 dv\; \mathrm{e}^{i\bar{v}k\cdot z}g_V^{\perp(a)}(v)\Bigg],\end{aligned} \tag{3.2.14}$$

with $[\not{\eta}, \not{k}] = \not{\eta}\not{k} - \not{k}\not{\eta}$ a regular commutator. The functions $\Phi_V^\perp(v)$ and $\Phi_V^\parallel(v)$ fix the leading-twist probability for a quark (or an antiquark) to carry a fraction of the total momentum v inside transversely and longitudinally polarised vector mesons, respectively. The functions $g_V^{\perp(v)}(v)$ and $g_V^{\perp(a)}(v)$ describe transverse polarisations of quarks in longitudinally polarized mesons. The latter functions, receive contributions from both matrix elements of twist-2 and twist-3 operators and their twist-2 contributions are related to the longitudinal LCDA by [64, 65]

$$g_V^{\perp(v),\mathrm{twist}-2}(v) = \frac{1}{2}\left[\int_0^v du\frac{\Phi_V^\parallel(u)}{\bar{u}} + \int_v^1 du\frac{\Phi_V^\parallel(u)}{u}\right], \tag{3.2.15}$$

$$g_V^{\perp(a),\mathrm{twist}-2}(v) = 2\left[\bar{v}\int_0^v du\frac{\Phi_V^\parallel(u)}{\bar{u}} + v\int_v^1 du\frac{\Phi_V^\parallel(u)}{u}\right]. \tag{3.2.16}$$

As explicitly stated in Eqs. (3.2.12)- (3.2.14), the space-time separation between quarks is taken to be light-like ($z^2 = 0$). The leading contributions to these matrix elements, defined on the light-cone, contain ultra-violet divergences. In order to deal with these divergences, one can regularise the aforementioned divergences, which yields non-trivial scale dependencies on these quantities that can be described by means of well-established renormalisation group methods [64, 66, 67]. The conformal symmetry of massless QCD at tree level has the important consequence that operators with different conformal spin[6] do not mix at leading logarithm [27, 64]. This can be used for expanding the LCDAs in *conformal partial waves* [68]

[6]This is how one usually refers to the quantum number associated to conformal symmetry.

$$\Phi_V^{\perp,\parallel}(v) = 6v(1-v)\left[1 + \sum_{n=2,4,\ldots} a_n^{\perp,\parallel}(\mu) C_n^{3/2}(2v-1)\right], \tag{3.2.17}$$

where $\{C_n^\lambda(x)\}$ is a family of orthogonal polynomials known as Gegenbauer polynomials

$$C_n^\lambda(x) = \binom{n+2\lambda-1}{n} \sum_{k=0}^{n} \frac{\binom{n}{k}(2\lambda+n)_k}{\left(\lambda+\frac{1}{2}\right)_k}\left(\frac{x-1}{2}\right)^k, \tag{3.2.18}$$

with the definition for the symbol $(a)_k = a\cdot(a+1)\cdot(a+2)\cdot\ldots\cdot(a+k-1)$. For a good review on the definition and properties of these polynomials we refer to Ref. [69].

Aside from the prefactor in Eq. (3.2.17), all the dependence of the LCDA on the longitudinal momentum fraction v is contained in the Gegenbauer polynomails $C_n^{3/2}$, while the transverse momentum dependence (the scale dependence) is placed in the $a_n(\mu)$ coefficients, which are multiplicatively renormalisable quantities to leading logarithm accuracy [64]

$$a_n^{\perp,\parallel}(\mu) = a_n^{\perp,\parallel}(\mu_{\text{low}})\left(\frac{\alpha_s(\mu)}{\alpha_s(\mu_{\text{low}})}\right)^{(\gamma_n^{\perp,\parallel}-\gamma_0^{\perp,\parallel})/(2\beta_0)}, \tag{3.2.19}$$

being β_0 the leading term of the QCD β-function and the one-loop anomalous dimensions [70, 71]

$$\gamma_n^{\parallel} = \frac{8}{3}\left(1 - \frac{2}{(n+1)(n+2)} + 4\sum_{j=2}^{n+1}\frac{1}{j}\right), \tag{3.2.20}$$

$$\gamma_n^{\perp} = \frac{8}{3}\left(1 + 4\sum_{j=2}^{n+1}\frac{1}{j}\right). \tag{3.2.21}$$

The combinations of anomalous dimensions in (3.2.19) are always positive and monotonically increase with n, therefore at sufficiently large scales μ only the first few terms in the Gegenbauer expansion are relevant. Usually, for applications in B physics, the expansion is truncated at $n = 2$. Furthermore, this guarantees that $a_n(\mu) \to 0$ as $\mu \to \infty$, due to the asymptotical freedom of QCD, which renders the following very simple expression for the asymptotic form of LCDAs:

$$\Phi_V^{\perp,\parallel}(v) \overset{\mu\to\infty}{=} 6v\bar{v}. \tag{3.2.22}$$

Notice that all of the results shown here correspond to vector meson LCDAs. For pseudoscalar LCDAs, the same results apply except that different anomalous dimension coefficients are required for the renormalisation of the coefficients in the conformal waves expansion (see [27] for the corresponding results for $\Phi_\pi(v)$). Indeed, the asymptotic formula $\Phi_X(v) \overset{\mu\to\infty}{=} 6v\bar{v}$ applies both for $X = P, V$.

It is important to have a solid understanding of the behaviour of the LCDAs in the *endpoint region*. This dynamical configuration is defined as the region where v or $\bar{v}$ is of order Λ_{QCD}/m_b, such that the quark or antiquark momentum is of order Λ_{QCD}. Contributions to the factorisation formula coming from this region, known as *endpoint contributions*, are dangerous because while one might be able to show the infrared safety of the hard-scattering kernels $T^{\text{I}}_{i,j}(v)$ and $T^{\text{II}}_i(\xi,u,v)$ for generic longitudinal momentum fractions and without any regards on the shape of the meson distribution functions, for $v \to 0$ or $v \to 1$ at least one of the quark propagators that were assumed to be far off-shell approaches its mass-shell. If such contributions are of leading power, perturbative computations of the hard-scattering functions are not going to be reliable.

For estimating the LCDAs endpoint structure, one can use the fact that distribution amplitudes enter the factorisation formula already at a renormalisation scale of order m_b, so it is a safe approximation to use their asymptotic form. Using (3.2.22), we count [55]

$$\Phi_X(v) \sim \begin{cases} 1; & \text{for } v \text{ away from the endpoint,} \\ \Lambda_{\text{QCD}}/m_b; & \text{for } v,\, \bar{v} \sim \Lambda_{\text{QCD}}/m_b, \end{cases} \tag{3.2.23}$$

with $X = P, V^{\perp}, V^{\parallel}$. So, for a generic longitudinal momentum fraction $v \approx 1$ the LCDA has a non-negligible contribution to the convolution integral, with well-behaved hard-scattering kernels. In the endpoint region, v and $\bar{v} \sim \Lambda_{\text{QCD}}/m_b$ then the outgoing meson momentum k is of $O(\Lambda_{\text{QCD}})$, putting its constituent quark and antiquark in a configuration dangerously close to their mass-shell. However, being the endpoint size of order Λ_{QCD}/m_b, contributions from this region are suppressed by a factor $\sim (\Lambda_{\text{QCD}}/m_b)^2$. Therefore, although this suppression has to be weighted by the possible enhancements in the amplitude due to propagators near their mass-shell, contributions to the convolution integral coming from this region are expected to be very subleading. The physical interpretation of the aforementioned suppression has to do with the fact that there is a high probability for the outgoing meson to leave the decay region already hadronised, if its valence quarks are in an endpoint-like configuration, which means that the LCDA must be very suppressed (as we have indeed observed).

B mesons light-cone distribution amplitudes

Light-cone distribution amplitudes of B mesons only appear in the hard-spectator scattering term of the factorisation formula for decays to two light mesons. The need for light meson LCDAs as functions encoding the soft physics inside the mesons conforms to our intuition, however for B mesons it is less evident. Because the b quark carries most of the B meson's momentum p, $p_b^+ = \bar{\xi} p^+ \approx p^+$, the spectator quark momentum ℓ must be of order Λ_{QCD}, $\ell^+ = \xi p^+$ with $\xi \sim O(\Lambda_{\text{QCD}}/m_b)$ and $\bar{\xi} = 1 - \xi$. Therefore, the heaviness of the b quark implies a very different internal dynamics for B mesons with respect to light mesons. Despite this fact, hard gluons connecting any of the highly energetic quarks in a fast recoiling emission meson with the spectator quark can probe the momentum distribution of the B meson, warranting the use of B mesons LCDAs for taking into account these contributions.

The most general decomposition of the B meson LCDA at leading power in $1/m_b$ uses the fact that, at the B meson rest frame, only the upper two components of the b quark field are large, whereas there is no restriction on the components of the spectator quark due to it being neither heavy nor energetic. Then, the B meson LCDA can be parametrised in terms of two scalar functions [55]

$$\begin{aligned} \langle 0 |\, \bar{q}_i(z)_\alpha [\ldots] b_j(0)_\beta \,| \bar{B}_d(p) \rangle_{z_+,\perp=0} = &- \frac{i f_B}{4} \delta_{ij} \left[(\not{p} + m_b)\gamma_5 \right]_{\beta\gamma} \\ &\times \int_0^1 d\xi \; e^{-i\xi p_+ z_-} \left[\Phi_{B_1}(\xi) + \not{n}_- \Phi_{B_2}(\xi) \right]_{\gamma\alpha} \end{aligned} \tag{3.2.24}$$

where the "dots" denote a path ordered exponential connecting the two quark fields (which is required for ensuring the gauge invariance of the matrix element), $n_- = (1, 0, 0, -1)$ and the following normalisation conditions apply

$$\int_0^1 d\xi \; \Phi_{B_1}(\xi) = 1, \qquad \int_0^1 d\xi \; \Phi_{B_1}(\xi) = 0. \tag{3.2.25}$$

While light meson distribution amplitudes are broadly understood, state-of-the-art knowledge on B meson LCDAs is still rather limited, even from the theoretical perspective. Naively, one expects B mesons to behave like light mesons at scales much larger than m_b, so B meson LCDAs should then approach the characteristic symmetric structure of light meson LCDAs. On the contrary, at scales of the order of m_b and smaller, distribution amplitudes are expected to be largely asymmetric with $\xi \sim O(\Lambda_{\text{QCD}}/m_b)$.

At leading order in α_s, the hard-spectator scattering amplitudes only depend on Φ_{B_1} (cf. Eqs. (28) and (29) from (3.2.3)). More precisely, it enters the computations through its first inverse moment [37],

$$\int_0^1 \frac{d\xi}{\xi} \Phi_{B_1}(\xi) \equiv \frac{m_B}{\lambda_B}. \tag{3.2.26}$$

Although, the moment λ_B is well-known to be a soft quantity of order Λ_{QCD}, it remains uncertain by a large margin with estimates ranging from 200^{+50}_{-00} Mev, as favoured for non-leptonic decays [57, 72], up to 460 ± 110 MeV, as predicted from QCD sum rules [73]. Measurements of the radiative decay $B \to \gamma \ell \nu_\ell$ with high statistics, an achievement particularly at reach of the BELLE II experiment, could prove to be instrumental in further constraining the value of λ_B [74].

For B meson LCDAs the asymptotic form, like Eq. (3.2.22) for light meson distributions, cannot be used for inferring the counting rules of these distributions in the endpoint region, since the scale of a B meson is already at m_b no large suppression of the parameters in the Gegenbauer expansion is obtained by setting $\mu \to \infty$. Instead, we use the first normalisation condition in (3.2.25) to obtain the following counting:

$$\Phi_{B_1}(\xi) \sim \begin{cases} 0; & \text{for } \xi \sim 1, \\ m_b/\Lambda_{\text{QCD}}; & \text{for } \xi \sim \Lambda_{\text{QCD}}/m_b. \end{cases} \tag{3.2.27}$$

The physical picture this is depicting has to do with the very low probability of finding the spectator quark with momentum of the same order as the b quark inside a B meson. This could only happen through a quantum fluctuation leading to a large momentum transfer from the b quark to the spectator, but this is very unlikely as all virtual gluon exchanges between the heavy quark and the spectator become soft in the heavy quark limit.

3.3 Strengths and limitations of QCDf

The QCDf prescription for the factorisation of non-leptonic B meson decay amplitudes is of great theoretical importance. Whereas naive factorisation and subsequent generalised factorisation frameworks heavily relied on phenomenological models, QCDf provides a model-independent paradigm for the analysis and computation of these amplitudes in an expansion in powers and logarithms of Λ_{QCD}/m_b. At leading power, but to all orders in α_s, the decay amplitudes can be decomposed according to Eqs. (3.2.3) and (3.2.4) [55, 75]. Therefore, QCDf is a well-defined limit of general QCD, based on power counting in $\Lambda_{\rm QCD}/m_b$, which allows to include $O(\alpha_s)$ contributions to the amplitudes in a systematic and rigorous fashion.

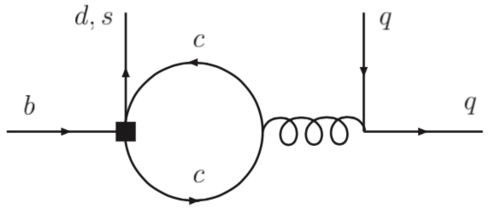

Figure 3.5: Penguin diagram with a charm-quark loop contributing to the amplitude of a non-leptonic decay $B \to M_1 M_2$. The curly line connecting the charm-quark loop to the $\bar{q}\gamma q$ current in the final state can either be a gluon or a photon, depending on whether we are dealing with a chromomagnetic or electromagnetic penguin [76].

Since the factorisation formula admits the computation of $O(\alpha_s)$ corrections to the naive factorisation decomposition, which are leading terms in the heavy quark limit, from first principles in QCD, the evolution of matrix elements follows the usual renormalisation group techniques. Hence, cancellation of scale and scheme dependencies between matrix elements and Wilson coefficients is naturally achieved in this framework. This is probably the greatest strenght of QCDf.

Despite its successes, this approach is not free of shortcomings. First, there is no proof of the factorisation formula to all orders in α_s, and first leading power in $\Lambda_{\rm QCD}/m_b$. Ref. [55] only provides a proof of QCDf up to order $O(\alpha_s^2)$. For that matter, rather than using the HQET/LEET framework, it is better to work within an effective theory specifically designed for pinning down the physical infrared degrees of freedom, so that a more straightforward power counting of infrared divergences is available. Such a theoretical framework can be found in the so-called *Soft-Collinear Effective Theory* [77, 78].

Second, there is the issue of the "charming penguins" [79]. These are topologies, like Fig. 3.5, where the quark current in a four-quark operator containing no initial states is closed in a $q\bar{q}$ loop ($q = u, c$), which is later attached to a gluon (or a photon) to produce a final state quark current. Similar topologies for semileptonic radiative decays will be the main object of discussion in a forthcoming chapter. $u\bar{u}$ loops enter the convolution integral weighted by the LCDAs close to the endpoint region, so they are very suppressed. However, $c\bar{c}$ loops, due to their mass squared being rather large $\sim 4m_c^2$, induce contributions that live in the middle of the distribution amplitudes, so they must be taken into account. Plus, no perturbative computation must be trusted for these objects as $\alpha_s(2m_c)$ is already large. Although, following the usual power counting, formally these contributions are of order $O(\Lambda_{\rm QCD}/m_b)$, it has been argued that they might be larger than expected [78–80]. In Ref. [80] an enhancement of the $c\bar{c}$ corrections was signaled as a possible explanation for the values of the decay $\mathcal{B}(B \to K\pi)$, while [78] suggested that these contributions could enter already at LO in the computation of $\mathcal{B}(B \to \pi^0\pi^0)$ within SCET. The latter claims were proven inaccurate in [76, 81], where a factor $(\Lambda_{\rm QCD}/m_b)^2$ was found to be missing in the arguments given in [78] plus charm-penguin diagrams were proven to be always parametrically suppressed in non-leptonic $B \to M_1 M_2$ decays in the heavy quark limit.

Finally, all computations in QCDf have an intrinsic error of order $O(\Lambda_{\mathrm{QCD}}/m_b)$. This is expected because QCDf is based on the theoretical frameworks of HQET and LEET, which are effective descriptions that emerge as LO terms in a $\Lambda_{\mathrm{QCD}}/m_b$ expansion. Hence, in order to have a consistent power counting, all computations involved in a QCDf result must be expanded in $1/m_b$ and only order $O(1)$ terms must be kept, of course this applies for both hard-scattering kernels and meson LCDAs. This has the advantage of greatly simplifying our computations at the cost of yielding a tower of power corrections, starting at $O(\Lambda_{\mathrm{QCD}}/m_b)$, with no systematic theoretical tools for calculating them within QCDf. In this case, one usually resorts to assigning these power corrections a flat uncertainty of the size of the naive estimate for $\Lambda_{\mathrm{QCD}}/m_b \approx 10\%$ [43]. We will comment further on these corrections and the way of parametrising them later on in this thesis, but for semileptonic B decays.

Chapter 4

Reviewing $B \to K^* \ell\ell$ at tree level and including $O(\alpha_s)$ corrections

The most important decay channel in our analyses of processes with an underlying $b \to s$ transition is the semileptonic B meson decay $\bar{B} \to \bar{K}^*(\to K\pi)\ell^+\ell^-$. This rare decay represents the bulk of experimentally available data on $b \to s\ell^+\ell^-$, plus some of the most important anomalies involve characteristic elements of this channel. More in detail, these anomalies are found in the kinematic regime where K^* meson recoils with high energy and will be extensively covered in Chapter 8.

In this section we discuss the formalism used for describing $\bar{B} \to \bar{K}^*\ell^+\ell^-$ in the aforementioned energy region of the decay. To this end, we present an anatomy of the effective Hamiltonian governing the dynamics of $b \to s\ell^+\ell^-$, and comment on possible ways of extending it for consistently including New Physics effects in the same framework, derive the structure of the relevant decay matrix element at tree level and schematically review the construction of its angular distribution. This discussion will also cover the computation of $O(\alpha_s)$ corrections to the leading order amplitude in the effective theory. Since we are mostly interested in the kinematical region where the K^* meson is rapidly recoiling, the principles of QCDf apply and will be extensively used for this matter. Central works and papers where most of these issues were discussed for the the first time include Refs. [29], [30], [82], [33], [83], [84], [31] and [85] (in chronological order).

4.1 The Weak Effective $b \to s\,\ell^+\ell^-$ Hamiltonian

As we discussed in Chapter 1, the natural language for studying weak decays of heavy mesons is given by the Effective Field Theory formalism. In particular, for $b \to s\ell^+\ell^-$ mediated transitions, the effective Hamiltonian reads [31, 83–85]

$$\mathcal{H}_{\text{eff}} = -\frac{4G_F}{\sqrt{2}}\left(\lambda_t^{(s)}\mathcal{H}_{\text{eff}}^{(t)} + \lambda_u^{(s)}\mathcal{H}_{\text{eff}}^{(u)}\right) + h.c. \tag{4.1.1}$$

with the CKM combinations $\lambda_q^{(s)} \equiv V_{qb}V_{qs}^*$. In principle, a contribution to 4.1.1 proportional to the CKM factor $\lambda_c^{(s)}$ is also expected in (4.1.1), however under the assumption that the CKM matrix is unitary even within the influence of NP, the CKM triangle holds $\lambda_u^{(s)} + \lambda_c^{(s)} + \lambda_t^{(s)} = 0$ so one can always reabsorb this contribution inside the other two terms of the Hamiltonian. The two flavour specific structures $\mathcal{H}_{\text{eff}}^{(u)}$ and $\mathcal{H}_{\text{eff}}^{(t)}$ read [31, 33, 82]

$$\mathcal{H}_{\text{eff}}^{(t)} = \mathcal{C}_1(\mu)\mathcal{O}_1^c + \mathcal{C}_2(\mu)\mathcal{O}_2^c + \sum_{i=3}^{6}\mathcal{C}_i(\mu)\mathcal{O}_i + \sum_{i=7}^{10}\Big(\mathcal{C}_i(\mu)\mathcal{O}_i + \mathcal{C}_{i'}(\mu)\mathcal{O}_{i'}\Big)$$
$$+ \sum_{i=S,PS}\Big(\mathcal{C}_i(\mu)\mathcal{O}_i + \mathcal{C}_{i'}(\mu)\mathcal{O}_{i'}\Big) + \sum_{i=T,PT}\mathcal{C}_i(\mu)\mathcal{O}_i, \tag{4.1.2}$$
$$\mathcal{H}_{\text{eff}}^{(u)} = \mathcal{C}_1(\mu)(\mathcal{O}_1^c - \mathcal{O}_1^u) + \mathcal{C}_2(\mu)(\mathcal{O}_2^c - \mathcal{O}_2^u). \tag{4.1.3}$$

In terms of the Branco and Lavoura improved Wolfenstein parametrisation of the CKM matrix [86], the CKM combinations $\lambda_q^{(s)}$ $(q = u,\, t)$ can be written as

$$\lambda_u^{(s)} = A\lambda^4(\rho + i\eta), \tag{4.1.4}$$
$$\lambda_t^{(s)} = A\lambda^2\left[-1 + \lambda^2\left(\frac{1}{2} - \rho - i\eta\right)\right] + O(\lambda^6). \tag{4.1.5}$$

Due to the enhanced dependence on the small parameter λ of $\lambda_u^{(s)}$ with respect to $\lambda_t^{(s)}$, contributions coming from $\mathcal{H}_{\text{eff}}^{(u)}$ are very suppressed (indeed $\mathcal{H}_{\text{eff}}^{(u)}$ is doubly Cabibbo-suppressed) relative to that of $\mathcal{H}_{\text{eff}}^{(t)}$. However, $\mathcal{H}_{\text{eff}}^{(u)}$ is an important source of weak phases in the SM, so it is relevant for assessing CP-violation. Thus, even though $\mathcal{H}_{\text{eff}}^{(t)}$ will be our main focus of attention, we will also discuss effects coming from $\mathcal{H}_{\text{eff}}^{(u)}$.

4.1.1 Basis of operators in the SM

Here, the operator basis we will use is the one introduced in [87–89], also known as CMM after its authors. This basis is an *irreducible* set of all dimension six operators with the quantum numbers of a $b \to s\ell^+\ell^-$ transition, compatible with Lorentz and the underlying gauge symmetries. The term *irreducible* here means that none of the operators in the basis can be transformed into combinations of the other operators in the basis through the use of equations of motion [39, 41]. Main advantage of using this basis is γ_5 not being part of the explicit Lorentz structure of the effective operators, which avoids the appearance of γ_5 in the effective theory diagrams [88] and allows to take γ_5 as fully anticommuting when computing the matching conditions. Explicitly, the relevant operators for the study presented in this thesis are

$$\mathcal{O}_1^u = (\bar{s}\gamma_\mu T^a P_L u)\,(\bar{u}\gamma^\mu T^a P_L b)\,, \tag{4.1.6}$$

$$\mathcal{O}_2^u = (\bar{s}\gamma_\mu P_L u)\,(\bar{u}\gamma^\mu P_L b)\,, \tag{4.1.7}$$

$$\mathcal{O}_1^c = (\bar{s}\gamma_\mu T^a P_L c)\,(\bar{c}\gamma^\mu T^a P_L b)\,, \tag{4.1.8}$$

$$\mathcal{O}_2^c = (\bar{s}\gamma_\mu P_L c)\,(\bar{c}\gamma^\mu P_L b)\,, \tag{4.1.9}$$

$$\mathcal{O}_3 = (\bar{s}\gamma_\mu P_L b)\sum_q(\bar{q}\gamma^\mu q)\,, \tag{4.1.10}$$

$$\mathcal{O}_4 = (\bar{s}\gamma_\mu T^a P_L b)\sum_q(\bar{q}\gamma^\mu T^a q)\,, \tag{4.1.11}$$

$$\mathcal{O}_5 = (\bar{s}\gamma_\mu\gamma_\nu\gamma_\rho P_L b)\sum_q (\bar{q}\gamma^\mu\gamma^\nu\gamma^\rho q)\,, \tag{4.1.12}$$

$$\mathcal{O}_6 = (\bar{s}\gamma_\mu\gamma_\nu\gamma_\rho T^a P_L b)\sum_q (\bar{q}\gamma^\mu\gamma^\nu\gamma^\rho T^a q)\,, \tag{4.1.13}$$

$$\mathcal{O}_7 = \frac{e}{16\pi^2} m_b(\bar{s}\sigma_{\mu\nu}P_R b)F^{\mu\nu}, \tag{4.1.14}$$

$$\mathcal{O}_9 = \frac{e^2}{16\pi^2}(\bar{s}\gamma_\mu P_L b)(\bar{\ell}\gamma^\mu\ell), \tag{4.1.15}$$

$$\mathcal{O}_{10} = \frac{e^2}{16\pi^2}(\bar{s}\gamma_\mu P_L b)(\bar{\ell}\gamma^\mu\gamma_5\ell), \tag{4.1.16}$$

where colour indices have been actively omitted, $P_{L,R} \equiv \frac{1}{2}(1 \mp \gamma_5)$ are the chirality projection operators, $F^{\mu\nu} \equiv \partial^\mu A^\nu - \partial^\nu A^\mu$ is the field strength tensor ($A^\mu(x)$ being the photon field), $\sigma^{\mu\nu} = \frac{i}{2}[\gamma^\mu, \gamma^\nu]$ and $m_b = m_b(\mu_b)$ denotes the running of the b quark mass in the $\overline{\text{MS}}$ scheme. To next-to-leading order, the relation between the b-quark $\bar{\text{M}}$S and pole masses is given by

$$m_b(\mu) = m_{b,\text{pole}}\left[1 - \frac{C_F\alpha_s(\mu)}{4\pi}\left(4 - 3\ln\frac{m^2_{b,\text{pole}}}{\mu^2}\right) + O(\alpha_s^2)\right]. \tag{4.1.17}$$

A common prescription used in computations where the b quark is nearly on-shell (with large infrared already removed) is to replace the b quark pole mass by the so-called PS scheme [90, 91],

$$m_{b,\text{PS}}(\mu) = m_{b,\text{pole}} - \frac{C_F\alpha_s}{\pi}\mu + O(\alpha_s^2), \tag{4.1.18}$$

where C_F is a colour factor.

Turning our attention to the Wilson coefficients, their specific numerical values in the SM were computed in [85], following Ref. [92] for performing the matching at the high-scale $\mu_0 \sim M_W$ and Ref. [84] for running down the values of the Wilson coefficients from the high-scale μ_0 to the relevant physical scale $\mu_b = m_b = 4.8$ GeV. This computation produced results for the Wilson coefficients at next-to-next-to-leading logarithmic order. We display the numerical values corresponding to this determination in Table 4.1.

Electromagnetic corrections can be accounted for through the introduction of five additional operators $\mathcal{O}_{3,4,5,6Q}$ and $\mathcal{O}_b$, as discussed in [93–96]. This introduces mixing among all the operators in Eqs. (4.1.6)-(4.1.16) with the same quantum numbers, leading to the introduction of two *effective coefficients* [87]

$$\mathcal{C}_7^{\text{eff}} \equiv \mathcal{C}_7 - \frac{1}{3}\mathcal{C}_3 - \frac{4}{9}\mathcal{C}_4 - \frac{20}{3}\mathcal{C}_5 - \frac{80}{9}\mathcal{C}_6, \tag{4.1.19}$$

$$\mathcal{C}_8^{\text{eff}} \equiv \mathcal{C}_8 + \mathcal{C}_3 - \frac{1}{6}\mathcal{C}_4 + 20\mathcal{C}_5 - \frac{10}{3}\mathcal{C}_6, \tag{4.1.20}$$

as the Wilson coefficients $\mathcal{C}_7$ and $\mathcal{C}_8$ always enter the matrix elements in these particular combinations of coefficients.

One can also construct an effective $\mathcal{C}_9$ coefficient with an structure such that its is both scale- and scheme-independent [97]

$$\mathcal{C}_9^{\text{eff}}(q^2) = \mathcal{C}_9 + Y(q^2), \tag{4.1.21}$$

$\mathcal{C}_1(\mu_b)$	$\mathcal{C}_2(\mu_b)$	$\mathcal{C}_3(\mu_b)$	$\mathcal{C}_4(\mu_b)$	$\mathcal{C}_5(\mu_b)$	$\mathcal{C}_6(\mu_b)$	$\mathcal{C}_7^{\rm eff}(\mu_b)$	$\mathcal{C}_8^{\rm eff}(\mu_b)$	$\mathcal{C}_9(\mu_b)$	$\mathcal{C}_{10}(\mu_b)$
-0.2632	1.0111	-0.0055	-0.0806	0.0004	0.0009	-0.2923	-0.1663	4.0749	-4.3085

Table 4.1: NNLO Wilson coefficients in the SM and at the scale $\mu_b = 4.8$ GeV [85].

where q^2 is the invariant mass squared of the lepton pair $\ell^+\ell^-$ and $Y(q^2)$ contains contributions from one-loop topologies of the four-quark operators $\mathcal{O}_1$-$\mathcal{O}_6$ in the effective theory [82]. The new effective coefficient $\mathcal{C}_9^{\rm eff}(q^2)$ indeed behaves better than the $\mathcal{C}_9$ coefficient alone. The RGE evolution of $\mathcal{C}_9$ from the high-scale μ_0 to the low-scale μ_b generates a large logarithm in $\mathcal{C}_9$, which turns out to be of order $O(1/\alpha_s)$. Hence, in order to obtain an order $O(1)$ value for $\mathcal{C}_9$ it is mandatory to go to next-to-leading logarithmic (NLL) order and build a combination of terms that cancel this logarithm. The specific combination given by the function $Y(q^2)$ accomplishes that mission

$$\begin{aligned} Y^{(t)}(q^2) = {} & h(q^2, m_c)\left(\frac{4}{3}\mathcal{C}_1 + \mathcal{C}_2 + 6\mathcal{C}_3 + 60\mathcal{C}_5\right) \\ & - \frac{1}{2}h(q^2, m_b)\left(7\mathcal{C}_3 + \frac{4}{3}\mathcal{C}_4 + 76\mathcal{C}_5 + \frac{64}{3}\mathcal{C}_6\right) \\ & - \frac{1}{2}h(q^2, 0)\left(\mathcal{C}_3 + \frac{4}{3}\mathcal{C}_4 + 16\mathcal{C}_5 + \frac{64}{3}\mathcal{C}_6\right) \\ & + \frac{4}{3}\mathcal{C}_3 + \frac{64}{9}\mathcal{C}_5 + \frac{64}{27}\mathcal{C}_6, \end{aligned} \tag{4.1.22}$$

and

$$Y^{(u)}(q^2) = \left(\frac{4}{3}\mathcal{C}_1 + \mathcal{C}_2\right)\left[h(q^2, m_c) - h(q^2, 0)\right]. \tag{4.1.23}$$

Actually, writing $h(q^2, 0)$ is a slightly abuse of notation, since what this really means is $h(q^2, m_u)$, but m_u is so small that one can set its value to 0.

The function $h(q^2, m_q)$ in (4.1.22) has the following structure

$$h(q^2, m_q) = -\frac{4}{9}\left[\ln\left(\frac{m_q^2}{\mu^2}\right) - \frac{2}{3} - z\right] - \frac{4}{9}(2+z)\sqrt{|z-1|}\begin{cases} \arctan\dfrac{1}{\sqrt{z-1}}; & z > 1, \\ \ln\dfrac{1+\sqrt{1-z}}{\sqrt{z}} - \dfrac{i\pi}{2}; & z \le 1, \end{cases} \tag{4.1.24}$$

with $z \equiv \dfrac{4m_q^2}{q^2}$.

The μ dependence contained in $h(q^2, m_q)$ comes from the scale-dependence of the calculations of the aforementioned one-loop topologies with insertions of the operators $\mathcal{O}_{1-6}$. Precisely, the logarithm in $h(q^2, m_q)$ is the one that cancels the large logarithm in $\mathcal{C}_9$ at the low-scale. At higher orders in perturbation theory, Wilson coefficients of other operators also develop potentially harmful logaritms. In order to cancel those, one must evaluate matrix elements of four quark-operators beyond the two-loop level [98].

Also, observe that $Y^{(i)}(q^2)$ $(i = u, t)$ has an absorptive component, i.e. has a non-zero imaginary part. This comes either from the limit $m_q \to 0$ in the evaluation of $h(q^2, 0)$ and also from the branch of this function when $q^2 \geq 4m_c^2$, so this last part is related with non-factorisable (potentially rescattering) effects in the open-charm region. Since imaginary phases are important in studying CP-violation, this effects must be taken into account when computing observables testing CP.

4.1.2 Basis of operators beyond the SM

Apart from the operators with a SM-like structure, given in Eqs. (4.1.6)-(4.1.16), one can imagine new operators encoding the dynamics of physical processes with conceptually different structures with respect to the SM. These are also dimension six operators consistent with Lorentz invariance but with gauge couplings of different nature. First we consider operators with different chirality, the so-called *chirally-flipped* operators or *right-handed currents*

$$\mathcal{O}_{7'} = \frac{e}{16\pi^2} m_b (\bar{s}\sigma_{\mu\nu} P_L b) F^{\mu\nu}, \tag{4.1.25}$$

$$\mathcal{O}_{9'} = \frac{e^2}{16\pi^2} (\bar{s}\gamma_\mu P_R b)(\bar{\ell}\gamma^\mu \ell), \tag{4.1.26}$$

$$\mathcal{O}_{10'} = \frac{e^2}{16\pi^2} (\bar{s}\gamma_\mu P_R b)(\bar{\ell}\gamma^\mu \gamma_5 \ell). \tag{4.1.27}$$

Actually, not all chirally-flipped are entirely forbidden in the SM but they are very suppressed (or vanish). More in detail,

$$\mathcal{C}_{7'}^{\rm SM} = \frac{m_s}{m_b} \mathcal{C}_7^{\rm SM}, \qquad \mathcal{C}_{9',10'}^{\rm SM} = 0. \tag{4.1.28}$$

Second, there are operators with *scalar* signatures (both left-handed and chirally-flipped) [31]

$$\mathcal{O}_S = \frac{e^2}{16\pi^2} m_b (\bar{s} P_R b)(\bar{\ell}\ell), \qquad \mathcal{O}_{S'} = \frac{e^2}{16\pi^2} m_b (\bar{s} P_L b)(\bar{\ell}\ell), \tag{4.1.29}$$

$$\mathcal{O}_{PS} = \frac{e^2}{16\pi^2} m_b (\bar{s} P_R b)(\bar{\ell}\gamma_5\ell), \qquad \mathcal{O}_{PS'} = \frac{e^2}{16\pi^2} m_b (\bar{s} P_L b)(\bar{\ell}\gamma_5\ell), \tag{4.1.30}$$

and finally we can also have *tensor* and *pseudotensor* operators [99]

$$\mathcal{O}_T = \frac{e}{16\pi^2} (\bar{s}\sigma_{\mu\nu} b)(\bar{\ell}\sigma^{\mu\nu}\ell), \tag{4.1.31}$$

$$\mathcal{O}_{PT} = \frac{e^2}{16\pi^2} \epsilon^{\mu\nu\rho\sigma} (\bar{s}\sigma_{\mu\nu} b)(\bar{\ell}\sigma_{\rho\sigma}\ell). \tag{4.1.32}$$

New Physics can enter the amplitude not only through the appearance of exotic operators, but also through new quantum excitations at very high scales but with NP couplings, such that they enter as shifts of the actual numerical values of the SM Wilson coefficients in Table 4.1. However, this possibility is only thought to be feasible for the operators $\mathcal{O}_{7,9,10}$. This idea will be explored in Chapter 8, where our global analyses of $b \to s\ell\ell$ data are discussed. This is not only because these operators are the dominant ones at the amplitude level for $b \to s\ell^+\ell^-$ processes, but also because Wilson coefficients of the QCD penguin operators $\mathcal{O}_{1-6}$ show a strong dependence on the value of $\mathcal{C}_2(M_W)$. Thus, changes on the values of the corresponding Wilson coefficients of the aforementioned operators would most likely mean large NP contributions to $\mathcal{C}_2(M_W)$, but this is disfavoured by data on two-body purely leptonic B meson decays.

4.2 Differential Decay Distribution and Spin Amplitudes

4.2.1 Matrix Element and Differential Decay Distribution

At tree level in the effective theory, the matrix element of the effective Hamiltonian (4.1.1) for the decay $\bar{B} \to \bar{K}^*(\to K\pi)\ell^+\ell^-$ can be written, in naive factorization[1] as [31, 83, 84]

$$\begin{aligned}\mathcal{M} = \frac{G_F\alpha}{\sqrt{2}\pi}\lambda_t^{(s)}\Bigg\{\Bigg[&\langle K\pi|\,\bar{s}\gamma^\mu(\mathcal{C}_9^{\text{eff}}P_L + \mathcal{C}_{9'}^{\text{eff}}P_R)b\,|\bar{B}\rangle \\ &- \frac{2m_b}{q^2}\langle K\pi|\,\bar{s}i\,\sigma^{\mu\nu}q_\nu\left[\left(\mathcal{C}_7^{\text{eff}} + \frac{m_s}{m_b}\mathcal{C}_{7'}^{\text{eff}}\right)P_R + \left(\frac{m_s}{m_b}\mathcal{C}_7^{\text{eff}} + \mathcal{C}_{7'}^{\text{eff}}\right)P_L\right]b\,|\bar{B}\rangle\Bigg]\langle\ell^+\ell^-|\,\bar{\ell}\gamma_\mu\ell\,|0\rangle \\ &+ \langle K\pi|\,\bar{s}\gamma^\mu(\mathcal{C}_{10}P_L + \mathcal{C}_{10'}P_R)b\,|\bar{B}\rangle\,\langle\ell^+\ell^-|\,\bar{\ell}\gamma_\mu\gamma_5\ell\,|0\rangle \\ &+ \langle K\pi|\,\bar{s}\,(\mathcal{C}_S P_R + \mathcal{C}_{S'}P_L)\,b\,|B\rangle\,\langle\ell^+\ell^-|\,\bar{\ell}\ell\,|0\rangle + \langle K\pi|\,\bar{s}\,(\mathcal{C}_{PS}P_R + \mathcal{C}_{PS'}P_L)\,b\,|B\rangle\,\langle\ell^+\ell^-|\,\bar{\ell}\gamma_5\ell\,|0\rangle \\ &+ \mathcal{C}_T\,\langle K\pi|\,\bar{s}\sigma_{\mu\nu}b\,|\bar{B}\rangle\,\langle\ell^+\ell^-|\,\bar{\ell}\sigma^{\mu\nu}\ell\,|0\rangle + i\mathcal{C}_{PT}\epsilon^{\mu\nu\rho\sigma}\,\langle K\pi|\,\bar{s}\sigma_{\mu\nu}b\,|\bar{B}\rangle\,\langle\ell^+\ell^-|\,\bar{\ell}\sigma_{\rho\sigma}\ell\,|0\rangle\Bigg\},\end{aligned} \tag{4.2.1}$$

where $\alpha \equiv \dfrac{e^2}{4\pi}$ is the fine-structure constant and all contributions from $\mathcal{H}_{\text{eff}}^{(u)}$ have been ignored for the moment.

The matrix element above is expressed in terms of $\bar{B} \to K\pi$ matrix elements, however form factors in Eqs. (2.1.9), (2.1.10), (2.1.13) and (2.1.15) are defined for $B \to V$ (V being a vector meson) transitions. Thus, we need to rewrite the matrix elements $\langle K\pi|\,\mathcal{O}_i\,|\bar{B}\rangle$ in terms of $B \to V$ form factors. In order to do so, one possibility is to assume the K^* to be produced resonantly, which warrants the use of the narrow width approximation for describing the $K^* \to K\pi$ transition. In this approximation, the full K^* propagator simplifies to

$$\frac{1}{(p_{K^*}^2 - m_{K^*}^2)^2 + (m_{K^*}\Gamma_{K^*})^2} \xrightarrow{\Gamma_{K^*} \ll m_{K^*}} \frac{\pi}{m_{K^*}\Gamma_{K^*}}\delta(k^2 - m_{K^*}^2). \tag{4.2.2}$$

This allows us to disentangle the form factors from the $K^*K\pi$ coupling $g_{K^*K\pi}$ [99, 100], because it cancels between the vertex factor and the width

$$\Gamma_{K^*} = \frac{g_{K^*K\pi}^2}{48\pi}m_{K^*}\beta^3, \tag{4.2.3}$$

being $\lambda(a,b,c) \equiv a^2 + b^2 + c^2 - 2(ab + bc + ac)$ the triangle function and the β factor is defined as [31]

$$\beta \equiv \frac{1}{m_{K^*}^2}\lambda^{1/2}(m_{K^*}^2, m_K^2, m_\pi^2). \tag{4.2.4}$$

The matrix elements in equations (2.1.9) and (2.1.10), except for the K^* polarization vector, can be written in the following compact form

$$\langle\bar{K}^*(p_{K^*})|\,J_\mu\,|\bar{B}(p)\rangle = \varepsilon^{*\nu}A_{\nu\mu}. \tag{4.2.5}$$

[1] Here using naive factorisation for decomposing the matrix elements of the electromagnetic operator $\mathcal{O}_7$ and the semileptonic operators $\mathcal{O}_{9,10}$ into products of matrix elements of currents is entirely justified. Because for all these operators one current is hadronic and the other leptonic or electromagnetic, no "non-factorisable" (in the naive-factorisation sense, see Section 3.1) interactions between final states can occur.

The $A_{\nu\mu}$ element in the previous equation is a tensor encapsulating all the form factors. Then, the corresponding $B \to K\pi$ matrix element reads

$$\langle \bar{K}(p_K)\pi(p_\pi)|\, J_\mu\, |\bar{B}(p)\rangle = -D_{K^*}(p^2_{K^*})W^\nu A_{\nu\mu}, \tag{4.2.6}$$

where [100]

$$|D_{K^*}(p^2_{K^*})|^2 = g^2_{K^*K\pi}\frac{\pi}{m_{K^*}\Gamma_{K^*}}\delta(p^2_{K^*} - m^2_{K^*}) = \frac{48\pi^2}{\beta^3 m^2_{K^*}}\delta(p^2_{K^*} - m^2_{K^*}), \tag{4.2.7}$$

$$W^\nu \equiv \left(g^{\nu\mu} - \frac{p^\nu_{K^*}p^\mu_{K^*}}{m^2_{K^*}}\right)(p_\pi - p_K)_\mu = Q^\nu_{\pi K} - \frac{m^2_K - m^2_\pi}{p^2_{K^*}}p^\mu_{K^*}, \qquad Q^\mu_{\pi K} = p^\mu_K - p^\mu_\pi. \tag{4.2.8}$$

Assuming that K^* is produced on-shell, only four independent kinematical variables are needed to fully characterize all the quantities in the decay: the dilepton mass squared q^2 and the angles θ_{K^*}, θ_ℓ and ϕ (all of them defined in Appendix A). Squaring the matrix element, summing over spins of the final states and taking advantage of several kinematics identities (see Appendix A), one obtains the full angular distribution of the $\bar{B}^0 \to \bar{K}^{*0}(\to K^+\pi^-)\ell^+\ell^-$,

$$\frac{d^4\Gamma}{dq^2 d\cos\theta_\ell d\cos\theta_{K^*} d\phi} = \frac{9}{32\pi}J(q^2, \theta_\ell, \theta_{K^*}, \phi), \tag{4.2.9}$$

where

$$\begin{aligned} J(q^2, \theta_\ell, \theta_{K^*}, \phi) = {} & J_{1s}\sin^2\theta_{K^*} + J_{1c}\cos^2\theta_{K^*} + (J_{2s}\sin^2\theta_{K^*} + J_{2c}\cos^2\theta_{K^*})\cos 2\theta_\ell \\ & + J_3\sin^2\theta_{K^*}\sin^2\theta_\ell\cos 2\phi + J_4\sin 2\theta_{K^*}\sin 2\theta_\ell\cos\phi \\ & + J_5\sin 2\theta_{K^*}\sin\theta_\ell\cos\phi \\ & + (J_{6s}\sin^2\theta_{K^*} + J_{6c}\cos^2\theta_{K^*})\cos\theta_\ell + J_7\sin 2\theta_{K^*}\sin\theta_\ell\sin\phi \\ & + J_8\sin 2\theta_{K^*}\sin 2\theta_\ell\sin\phi + J_9\sin^2\theta_{K^*}\sin^2\theta_\ell\sin 2\phi. \end{aligned} \tag{4.2.10}$$

In a similar way, the differential angular distribution of the CP-conjugate mode $B^0_d \to K^{*0}(\to K^-\pi^+)\ell^+\ell^-$ is obtained

$$\frac{d^4\bar{\Gamma}}{dq^2 d\cos\theta_\ell d\cos\theta_{K^*} d\phi} = \frac{9}{32\pi}\bar{J}(q^2, \theta_\ell, \theta_{K^*}, \phi), \tag{4.2.11}$$

with $\bar{J}(q^2, \theta_\ell, \theta_{K^*})$ having the same structure as $J(q^2, \theta_\ell, \theta_{K^*})$ but replacing [100]

$$J_{1s,1c,2s,2c,3,4,7} \longrightarrow \bar{J}_{1s,1c,2s,2c,3,4,7}, \qquad J_{5,6s,6c,8,9} \longrightarrow -\bar{J}_{5,6s,6c,8,9}, \tag{4.2.12}$$

where $\bar{J}_i$ equals J_i but with all weak phases conjugated. The extra minus sign in (4.2.12) is due to the kinematical convention used in the definition of the angles.

The angular coefficients J_i, which are functions of q^2 only, are usually expressed in term of the K^* transversity amplitudes. In the remaining of this section, we are going to define these so-called transversity amplitudes and show their relations with the angular coefficients.

4.2.2 Transversity Amplitudes

A particular context that allows for a natural introduction of the transversity amplitudes is the study of the decay $\bar{B} \to \bar{K}^* V^*$, where the $\bar{K}^{*0}$ is assumed to be on-shell while V^* is a virtual gauge boson (either a γ^* or a Z^0). Then, as in Eq. (4.2.5), the amplitude for the process takes the form [31]

$$\mathcal{M}_{(m,n)}(B \to K^* V^*) = \varepsilon^{*\mu}_{K^*}(m) M_{\mu\nu} \varepsilon^{*\nu}_{V^*}(n), \tag{4.2.13}$$

where $M_{\mu\nu}$ is the tensor associated to the hadronic current, $\varepsilon^{\mu}_{V^*}$ is the polarization vector of the virtual gauge boson and $\varepsilon^{\mu}_{K^*}$ is the K^* polarization vector.

The V^* is an off-shell gauge boson, so it has 3 (spin 1) polarisations plus an extra time-like (spin 0) polarisation. The three spin 1 components ($n = \pm, 0$) are orthogonal to the momentum q^μ transferred to V^* during the B meson decay, i.e. $q_\mu \, \varepsilon^{\mu}_{V^*}(n) = 0$, while the spin 0 component ($n = t$) is proportional to q^μ, i.e. $\varepsilon^{\mu}_{V^*}(t) = q^\mu/\sqrt{q^2}$. The set $\{\varepsilon^{\mu}_{V^*}(\pm), \varepsilon^{\mu}_{V^*}(0), \varepsilon^{\mu}_{V^*}(t)\}$ of independent polarisation vectors constitutes a basis on the polarisation space of V^*. Assuming that the gauge boson V^* propagates along the z-axis,

$$q^\mu = (q_0, 0, 0, q_z), \tag{4.2.14}$$

in the B meson rest frame, then the four polarisation vectors of this basis may be written as [99, 101]

$$\varepsilon^{\mu}_{V^*}(\pm) = \frac{1}{\sqrt{2}}(0, 1, \mp i, 0), \tag{4.2.15}$$

$$\varepsilon^{\mu}_{V^*}(0) = \frac{1}{\sqrt{q^2}}(-q_z, 0, 0, -q_0), \tag{4.2.16}$$

$$\varepsilon^{\mu}_{V^*}(t) = \frac{1}{\sqrt{q^2}}(q_0, 0, 0, q_z). \tag{4.2.17}$$

It can be proved that the polarization vectors in Eqs. (4.2.15)-(4.2.17) satisfy the following orthonormality and completeness relations

$$\varepsilon^{*\mu}_{V^*}(n) \, \varepsilon_{V^*\mu}(n') = g_{nn'}, \tag{4.2.18}$$

$$\sum_{n,n'} \varepsilon^{*\mu}_{V^*}(n) \, \varepsilon^{\nu}_{V^*}(n') g_{nn'} = g^{\mu\nu}, \tag{4.2.19}$$

with $n = \pm, 0, t$ and $g_{nn'} = \mathrm{diag}(+, -, -, -,)$.

On a different note, the K^* is on-shell, thus it has only 3 possible polarisations available and all of them are orthogonal with respect to the momentum $p^{\mu}_{K^*} = (k_0, 0, 0, k_z)$ carried by the meson. Again, in the B meson rest frame, these polarisation vectors read

$$\varepsilon^{\mu}_{V^*}(\pm) = \frac{1}{\sqrt{2}}(0, 1, \pm i, 0), \tag{4.2.20}$$

$$\varepsilon^{\mu}_{V^*}(0) = \frac{1}{m_{K^*}}(k_z, 0, 0, k_0), \tag{4.2.21}$$

$$\tag{4.2.22}$$

and satisfy the relations

$$\varepsilon^{*\mu}_{K^*}(n)\,\varepsilon_{K^*\mu}(n') = -\delta_{mm'}, \tag{4.2.23}$$

$$\sum_{m,m'} \varepsilon^{*\mu}_{K^*}(m)\,\varepsilon^{\nu}_{K^*}(m')\delta_{mm'} = -g^{\mu\nu} + \frac{p^{\mu}_{K^*}p^{\nu}_{K^*}}{m^2_{K^*}}. \tag{4.2.24}$$

The K^* helicity amplitudes H_0, H_{+1} and H_{-1} can now be projected out from $M_{\mu\nu}$ by contracting it with the explicit polarization vectors in (4.2.33), obtaining [31, 101]

$$H_{\pm 1} = \varepsilon^{*\nu}_{K^*}(\pm)\,\varepsilon^{*\mu}_{V^*}(\pm)M_{\nu\mu}, \tag{4.2.25}$$

$$H_0 = \varepsilon^{*\nu}_{K^*}(0)\,\varepsilon^{*\mu}_{V^*}(0)M_{\nu\mu}, \tag{4.2.26}$$

which are called *helicity amplitudes* as they are attached to a specific helicity value of m. Using a more compact notation

$$H_m = \mathcal{M}_{(m,m)}(B \to K^* V^*), \qquad m = 0, +1, -1 \tag{4.2.27}$$

Alternatively, one can work within a different framework provided by combinations of helicity H_m amplitudes, which we call *transversity amplitudes* [31, 83]:

$$A_{\perp,\parallel} \equiv \frac{1}{\sqrt{2}}(H_{+1} \mp H_{-1}), \qquad A_0 \equiv H_0. \tag{4.2.28}$$

However, not all the information available is contained in $A_{\pm,0}$. In $B \to K^* V^*$ with V^* being virtual there is yet another possible contraction of the hadronic tensor $M_{\mu\nu}$ with the polarization vectors in (4.2.33)

$$A_t = \varepsilon^{*\nu}_{K^*}(0)\,\varepsilon^{*\mu}_{V^*}(t)M_{\nu\mu} = \mathcal{M}_{(0,t)}(B \to K^* V^*). \tag{4.2.29}$$

This transversity amplitude has no counterpart in the K^* helicity basis, however it may be regarded to a K^* polarization vector which is longitudinal in the K^* rest frame and simultaneously time-like in the V^* rest frame.

Consider now that the V^* decays into a lepton-antilepton pair, then the amplitude becomes

$$\mathcal{M}(B \to K^* V^*(\to \ell^+\ell^-))(m) \propto \varepsilon^{*\nu}_{K^*}(m) M_{\nu\mu} \sum_{n,n'} \varepsilon^{*\mu}_{V^*}(n)\varepsilon^{\rho}_{V^*}(n') g_{nn'} \left(\bar{\ell}\gamma_\rho, P_{L,R}\ell\right), \tag{4.2.30}$$

where the $V \to \ell^+\ell^-$ coupling has been omitted, explaining the proportionality sign.

This amplitude admits a decomposition in terms of six transversity amplitudes $A^L_{\perp,\parallel,0}$ and $A^R_{\perp,\parallel,0}$, the L and R superindices refer to the chirality of the leptonic current, and also the seventh transversity amplitude A_t. This last A_t amplitude cannot be split into left- and right-handed parts since the polarization vector needed to project A_t is $\varepsilon^\mu(t) = q^\mu/\sqrt{q^2}$ and, because of current conservation, one has that

$$q^\mu \left(\bar{\ell}\gamma_\mu \ell\right) = 0, \tag{4.2.31}$$

$$q^\mu \left(\bar{\ell}\gamma_\mu\gamma_5 \ell\right) = 2im_\ell \left(\bar{\ell}\gamma_5\ell\right). \tag{4.2.32}$$

Thus, the time-like component of V^* only couples to axial vectors but not to vectors. At the same time, this proves that A_t must vanish in the limit of massless leptons.

As we have shown, this formalism incorporates all contributions to the amplitude of the decay $\bar{B} \to \bar{K}^* V^*(\to \ell\ell)$ with vector and axial-vector currents. Therefore, contributions coming from effective operators $\mathcal{O}^{(\prime)}_{7,9,10}$, including their chirally-flipped counterparts, are accounted for in the transversity amplitudes parametrising the decay.

Notice that pseudoscalar currents can be transformed into axial-vectors currents by means of the equation of motion for these currents in Eq. (4.2.32). Therefore, pseudoscalar contributions to the amplitude can be reabsorbed in the time-like transversity amplitude A_t. Unfortunately, this does not apply to the scalar contributions and need to be embedded in a new amplitude A_S. Finally, accounting for tensor and pseudotensor contributions require the addition of more transversity amplitudes (up to six new amplitudes as argued in [102]).

In summary, we have shown that the amplitude of the decay $B \to K^* V^*(\to \ell^+\ell^-)$ can be unambiguously characterised by means of seven transversity amplitudes $A^{L,R}_{\perp,\|,0}$ and A_t. If tensor and pseudotensor contributions can be neglected, then the most general framework also involves an eight amplitude accounting for scalar operators.

Given the matrix element in equation (4.2.1), the explicit form of the transversity amplitudes, up to corrections of order $O(\alpha_s)$ and $O(\Lambda_{\rm QCD}/m_b)$, reads [31, 83]

$$A^{L,R}_{\perp} = N\sqrt{2}\lambda^{1/2}\Bigg\{\Big[\left(\mathcal{C}^{\rm eff}_9 + \mathcal{C}^{\rm eff}_{9'}\right) \mp (\mathcal{C}_{10} + \mathcal{C}_{10'})\Big]\frac{V(q^2)}{m_B + m_{K^*}} + \frac{2m_b}{q^2}\left(\mathcal{C}^{\rm eff}_7 + \mathcal{C}^{\rm eff}_{7'}\right) T_1(q^2)\Bigg\}, \tag{4.2.33}$$

$$A^{L,R}_{\|} = -N\sqrt{2}\left(m_B^2 - m_{K^*}^2\right)\Bigg\{\Big[\left(\mathcal{C}^{\rm eff}_9 - \mathcal{C}^{\rm eff}_{9'}\right) \mp (\mathcal{C}_{10} - \mathcal{C}_{10'})\Big]\frac{A_1(q^2)}{m_B - m_{K^*}} + \frac{2m_b}{q^2}\left(\mathcal{C}^{\rm eff}_7 - \mathcal{C}^{\rm eff}_{7'}\right) T_2(q^2)\Bigg\}, \tag{4.2.34}$$

$$\begin{aligned} A^{L,R}_0 = -\frac{N}{2m_{K^*}\sqrt{q^2}}\Bigg\{&\Big[\left(\mathcal{C}^{\rm eff}_9 - \mathcal{C}^{\rm eff}_{9'}\right) \mp (\mathcal{C}_{10} - \mathcal{C}_{10'})\Big] \\ &\left[(m_B^2 - m_{K^*}^2 - q^2)(m_B + m_{K^*})A_1(q^2) - \lambda\frac{A_2(q^2)}{m_B + m_{K^*}}\right] \\ &+ 2m_b\left(\mathcal{C}^{\rm eff}_7 - \mathcal{C}^{\rm eff}_{7'}\right)\left[(m_B^2 + 3m_{K^*}^2 - q^2)T_2(q^2) - \frac{\lambda}{m_B^2 - m_{K^*}^2}T_3(q^2)\right]\Bigg\}, \end{aligned} \tag{4.2.35}$$

$$A_t = \frac{N}{\sqrt{q^2}}\lambda^{1/2}\left[2(\mathcal{C}_{10} - \mathcal{C}_{10'}) + \frac{q^2}{m_\ell}(\mathcal{C}_{PS} - \mathcal{C}_{PS'})\right] A_0(q^2), \tag{4.2.36}$$

$$A_S = -2N\lambda^{1/2}(\mathcal{C}_S - \mathcal{C}_{S'})A_0(q^2), \tag{4.2.37}$$

where

$$N = V_{tb}V^*_{ts}\left[\frac{G_F^2\alpha^2}{3\cdot 2^{10}\pi^5 m_B^3}q^2\lambda^{1/2}\beta_\ell\right]^{1/2}, \tag{4.2.38}$$

with the triangle function $\lambda \equiv \lambda(m_B^2, m_{K^*}^2, q^2)$ and $\beta_\ell \equiv \sqrt{1-\frac{4m_\ell^2}{q^2}}$.

It is important to stress that the amplitudes in Eqs. (4.2.33)-(4.2.37) are not physical. First, $A_\perp^{L,R}$, $A_\parallel^{L,R}$ and $A_0^{L,R}$ contain the $\mathcal{C}_9^{\rm eff}$ coefficient and it has complex contributions, which makes impossible for these amplitudes to be physical objects. Secondly, since A_t has no direct helicity amplitude counterpart, it cannot be physical either.

4.2.3 Transversity Amplitudes at Large Recoil

As stated in [83], the transversity amplitudes take a particularly simple form in the heavy quark and large energy limit. Exploiting the form factor relations in (2.1.27) and (2.1.28), up to leading order in $1/m_b$ and α_s, one obtains [31, 83, 103]

$$A_\perp^{L,R} \simeq \sqrt{2} N m_B\,(1-\hat{s})\left[\left(\mathcal{C}_9^{\rm eff}+\mathcal{C}_{9'}^{\rm eff}\right) \mp (\mathcal{C}_{10}+\mathcal{C}_{10'}) + \frac{2\hat{m}_b}{\hat{s}}\left(\mathcal{C}_7^{\rm eff}+\mathcal{C}_{7'}^{\rm eff}\right)\right]\xi_\perp(E_{K^*}), \tag{4.2.39}$$

$$A_\parallel^{L,R} \simeq -\sqrt{2} N m_B\,(1-\hat{s})\left[\left(\mathcal{C}_9^{\rm eff}-\mathcal{C}_{9'}^{\rm eff}\right) \mp (\mathcal{C}_{10}-\mathcal{C}_{10'}) + \frac{2\hat{m}_b}{\hat{s}}\left(\mathcal{C}_7^{\rm eff}-\mathcal{C}_{7'}^{\rm eff}\right)\right]\xi_\perp(E_{K^*}), \tag{4.2.40}$$

$$A_0^{L,R} \simeq -\frac{N m_B}{2\hat{m}_{K^*}\sqrt{\hat{s}}}\,(1-\hat{s})^2\left[\left(\mathcal{C}_9^{\rm eff}-\mathcal{C}_{9'}^{\rm eff}\right) \mp (\mathcal{C}_{10}-\mathcal{C}_{10'}) + 2\hat{m}_b\left(\mathcal{C}_7^{\rm eff}-\mathcal{C}_{7'}^{\rm eff}\right)\right]\xi_\parallel(E_{K^*}), \tag{4.2.41}$$

$$A_t \simeq N\frac{m_B}{2\hat{m}_{K^*}\sqrt{\hat{s}}}\,(1-\hat{s})^2\left[2(\mathcal{C}_{10}-\mathcal{C}_{10'}) + \frac{q^2}{m_\ell}(\mathcal{C}_{PS}-\mathcal{C}_{PS'})\right]\xi_\parallel(E_{K^*}), \tag{4.2.42}$$

$$A_S \simeq -N\frac{m_B^2}{\hat{m}_{K^*}}(1-\hat{s})^2(\mathcal{C}_S-\mathcal{C}_{S'})\,\xi_\parallel(E_{K^*}), \tag{4.2.43}$$

with the definitions $\hat{s} \equiv s/m_B^2$ ($s \equiv q^2$) and $\hat{m}_i = m_i/m_B$. When writing Eqs. (4.2.39)-(4.2.43) terms of $O(\hat{m}_{K^*}^2)$ have been dropped in order to be consistent with the expansions performed to obtain the form factor relations (2.1.27) and (2.1.28).

It is important to notice that in the large recoil limit each of the transversity amplitudes depends on just one soft form factor: either $\xi_\perp(E_{K^*})$ or $\xi_\parallel(E_{K^*})$.

4.3 Angular Coefficients

With the seven transversity amplitudes defined in the preceding section, the angular coefficients J_i in (4.2.41) can be written as

$$J_{1s} = \frac{(2+\beta_\ell^2)}{4}\left[|A_\perp^L|^2+|A_\parallel^L|^2+(L\to R)\right] + \frac{4m_\ell^2}{q^2}{\rm Re}\left(A_\perp^L A_\perp^{R*}+A_\parallel^L A_\parallel^{R*}\right), \tag{4.3.1}$$

$$J_{1c} = |A_0^L|^2+|A_0^R|^2+\frac{4m_\ell^2}{q^2}\left[|A_t|^2+2{\rm Re}(A_0^L A_0^{R*})\right], \tag{4.3.2}$$

$$J_{2s} = \frac{\beta_\ell^2}{4}\left[|A_\perp^L|^2+|A_\parallel^L|^2+(L\to R)\right], \qquad J_{2c} = -\beta_\ell^2\left[|A_0^L|^2+(L\to R)\right], \tag{4.3.3}$$

$$J_3 = \frac{\beta_\ell^2}{2}\left[|A_\perp^L|^2-|A_\parallel^L|^2+(L\to R)\right], \qquad J_4 = \frac{\beta_\ell^2}{\sqrt{2}}\left[{\rm Re}(A_0^L A_\parallel^{L*})+(L\to R)\right], \tag{4.3.4}$$

$$J_5 = \sqrt{2}\beta_\ell\Big[\mathrm{Re}(A_0^L A_\perp^{L*}) - (L \to R)\Big], \qquad J_{6s} = 2\beta_\ell\Big[\mathrm{Re}(A_\parallel^L A_\perp^{L*}) - (L \to R)\Big], \qquad J_{6c} = 0, \quad (4.3.5)$$

$$J_7 = \sqrt{2}\beta_\ell\Big[\mathrm{Im}(A_0^L A_\parallel^{L*}) - (L \to R)\Big], \quad J_8 = \frac{\beta_\ell^2}{\sqrt{2}}\Big[\mathrm{Im}(A_0^L A_\perp^{L*}) + (L \to R)\Big], \quad J_9 = \beta_\ell^2\Big[\mathrm{Im}(A_\parallel^{L*} A_\perp^L + (L \to R)\Big]. \quad (4.3.6)$$

The angular coefficients, in contrast to the transversity amplitudes, are physical observables. Indeed, as they parametrise the full angular distribution, they contain all the relevant physical information that can be extracted from the decay. Ultimately, every observable can be written as a combination of the angular coefficients $J_i(q^2)$. In particular, we will show in Chapter 5 how these coefficients can be combined in order to obtain observables with very limited sensitivity to form factors.

Certain relations between angular coefficients arise in the limit of massless leptons. For instance, we have $J_{1s} = 3J_{2s}$ and $J_{1c} = -J_{2c}$ in this limit. Also, $J_{6c} = 0$ only holds if scalar operators can be dismissed and lepton masses neglected.

4.4 Next-to-leading order α_s corrections from QCD factorisation

Having very precise determinations of the form factors involved in the theoretical description of a given exclusive decay is not enough. In the context of exclusive, radiative decays there exist non-factorisable[2] strong contributions to the decay amplitude that cannot be accounted for in the form factors. As it was outlined in Section 3.2, QCD factorisation [37, 55] establishes, by means of a consistent power counting in the heavy quark limit and general factorisation arguments for hard-scattering processes, a systematic framework for the computation of order α_s corrections to the matrix elements of two-body non-leptonic B meson decays. For radiative decays of the type $B \to K^*\gamma^{(*)}(\to \ell^+\ell^-)$, both factorisable and non-factorisable corrections[3] can also be computed within QCDf [30, 33, 58]. In this section, we will discuss how the aforementioned $O(\alpha_s)$ contributions can be accounted for within QCDf, since these contributions take an important part in the computation of our state-of-the-art predictions for the relevant observables in $b \to s\ell\ell$ analyses, and we will provide some of the relevant formulae.

Good references for this matter are the seminal papers [29, 30, 33], plus a wonderful review of the main results can be found in the Thesis [39]. Most discussion below is based on these works.

4.4.1 The factorisation formula: a decomposition in hadronic amplitudes

Using (2.1.9), the matrix elements of the effective vector and axial semi-leptonic operators $\mathcal{O}_{9,10}$ can be written in terms of the seven $B \to K^*$ transition form factors. Therefore, non-factorisable contributions to the decay amplitude can only be produced through the emission of a virtual

[2] Here the term non-factorisable has similar meaning to that of the same term in Section 3.1, where it was defined.

[3] By factorisable contributions we mean all those corrections that can be absorbed in the form factors via appropriate redefinitions. Whereas non-factorisable corrections are those strong interaction effects that cannot be absorbed into the form factors. The former are mainly due to hard-vertex interactions, while the latter come from topologies involving purely hadronic effective operators $\mathcal{O}_{i=1,\ldots,6,8g}$ in $\mathcal{H}_{\mathrm{eff}}$ with insertions of a virtual photon line.

photon, which subsequently produces the lepton pair in the final state. Hence, neglecting CKM-suppressed and m_s/m_b terms, the amplitude of the radiative decay $B \to K^*\gamma^*$ in the SM reads,

$$\begin{aligned}\langle\gamma^*(q,\mu)\bar{K}^*(p',\varepsilon^*)|\,\mathcal{H}_{\text{eff}}^{(t)}\,|\bar{B}(p)\rangle = \frac{e}{4\pi^2}(-2m_b)\varepsilon^{*\nu}\Bigg\{ & i\,\epsilon_{\nu\mu\rho\sigma}p'^{\rho}q^{\sigma}\mathcal{T}_1^{(t)}(q^2) \\ & + \frac{1}{2}\Bigg[\left((m_B^2-m_{K^*}^2)g_{\nu\mu}-q_\nu(2p'+q)_\mu\right)\mathcal{T}_2^{(t)}(q^2) \\ & + q_\nu\left(q_\mu-\frac{q^2}{m_B^2-m_{K^*}^2}(2p'+q)_\mu\right)\mathcal{T}_3^{(t)}(q^2)\Bigg]\Bigg\}.\end{aligned} \tag{4.4.1}$$

where m_b refers to the b quark pole mass. This equation closely resembles Eq. (6) from [30] but, for it to present the same structure as (2.1.10) (the matrix element controlling the form factor decomposition of the matrix elements of the electromagnetic operator $\mathcal{O}_7$), the following modifications have been performed: the factor $(-G_F/\sqrt{2})V_{ts}^*V_{tb}$ in Eq. (6) of Ref. [30] has been removed as it is factored out in the definition of $\mathcal{H}_{\text{eff}}$ in (4.1.2), there an addition factor of 4 in the numerator of (4.4.1) for compensating the different normalisation factor between Eqs. (4.1.14)-(4.1.16) and Eqs. (3)-(4) in [30], the notation e for the electromagnetic coupling (with $e = |e|$ the electron charge) is used instead of $-g_{\text{em}}$, contrary to Eq. (6) in Ref. [30] momentum conservation $p = p'+q$ is employed for writing (4.4.1) only in terms of final state momenta p' and q and last some indices have also been rearranged, by means of the cyclic properties of the Levi-Civita symbol. The superscript (t) explicitly states that contributions to (4.4.1) come entirely from non-CKM suppressed terms in the effective Hamiltonian.

The hadronic amplitudes $\mathcal{T}_i^{(t)}$ that parametrise the matrix element are non-perturbative functions that contain all contributions calculable in QCDf (both factorisable and non-factorisable). At leading order, the only contribution to the matrix element $\langle\gamma^*(q,\mu)\bar{K}^*(p',\varepsilon^*)|\,\mathcal{H}_{\text{eff}}^{(t)}\,|\bar{B}(p)\rangle$ comes from the electromagnetic dipole operator $\mathcal{O}_7$. The $\mathcal{T}_i^{(t)}$ amplitudes parametrising the decomposition in (4.4.1) must account for this fact and thus they follow the schematic structure $\mathcal{T}_i^{(t)} = \mathcal{C}_7 T_i(q^2) + \dots$, where $T_i(q^2)$ are the form factors defined in (2.1.9). Including also the contributions of four-quark operators, but momentarily neglecting weak annihilation, the leading logarithm expressions for the amplitudes $\mathcal{T}_i^{(t)}$ are [104]

$$\mathcal{T}_1^{(t)}(q^2) = \mathcal{C}_7^{\text{eff}}T_1(q^2) + Y(q^2)\frac{q^2}{2m_b(m_B+m_{K^*})}V(q^2), \tag{4.4.2}$$

$$\mathcal{T}_2^{(t)}(q^2) = \mathcal{C}_7^{\text{eff}}T_2(q^2) + Y(q^2)\frac{q^2}{2m_b(m_B+m_{K^*})}A_1(q^2), \tag{4.4.3}$$

$$\mathcal{T}_3^{(t)}(q^2) = \mathcal{C}_7^{\text{eff}}T_3(q^2) + Y(q^2)\left[\frac{m_B-m_{K^*}}{2m_b}A_2(q^2) - \frac{m_B+m_{K^*}}{2m_b}A_1(q^2)\right], \tag{4.4.4}$$

with $\mathcal{C}_7^{\text{eff}}$ as defined in (4.1.19).

The relevant form factors in the region where the energy of the final state meson scales with the heavy quark mass in the heavy quark limit are not those defined in the usual transversity basis (V, A_i, T_i), but rather the soft form factors that emerge due to the symmetries that apply in this kinematic limit ($\xi_\perp$, $\xi_\parallel$). Then, the various form factors involved in the decay are related according to the symmetries in Eqs. (2.1.27)-(2.1.28), allowing us to introduce a new set of hadronic amplitudes that align with the soft form factors [30]

$$\mathcal{T}_1^{(t)}(q^2) \equiv \mathcal{T}_\perp^{(t)}(q^2) = \xi_\perp(q^2)\left[\mathcal{C}_7^{\rm eff}\delta_1 + \frac{q^2}{2m_b m_B}Y(q^2)\right], \tag{4.4.5}$$

$$\mathcal{T}_2^{(t)}(q^2) = \frac{2E}{m_B}\mathcal{T}_\perp^{(t)}, \tag{4.4.6}$$

$$\mathcal{T}_3^{(t)}(q^2) - \frac{m_B}{2E}\mathcal{T}_2^{(t)}(q^2) \equiv \mathcal{T}_\parallel^{(t)} = -\xi_\parallel(q^2)\left[\mathcal{C}_7^{\rm eff}\delta_2 + \frac{m_B}{2m_b}Y(q^2)\delta_3\right], \tag{4.4.7}$$

where $E = (m_B^2 - q^2)/2m_B$ is the energy of the recoiling K^* meson, $\xi_{\perp,\parallel}$ denote the soft form factors in the heavy quark and large energy limits, as defined in (2.1.27)-(2.1.28), and $\delta_i = 1 + O(\alpha_s)$ are factors encapsulating the α_s corrections. The $\mathcal{T}_{\perp,\parallel}^{(t)}$ functions represent the amplitude for a decay to occur through the production of a transversely and longitudinally polarised vector meson, respectively.

Using this new basis for the hadronic amplitudes, one can rewrite the $B \to K^*\gamma^*$ amplitude in a more suitable form for analysing the physics of the decay in the heavy quark and large energy limits,

$$\begin{aligned}\langle\gamma^*(q,\mu)\bar{K}^*(p',\varepsilon^*)|\,\mathcal{H}_{\rm eff}^{(t)}\,|\bar{B}(p)\rangle = \frac{e}{4\pi^2}(-2m_b)\varepsilon^{*\nu}\Big\{ & i\,\epsilon_{\nu\mu\rho\sigma}p'^\rho q^\sigma \mathcal{T}_\perp^{(t)}(q^2)\\ & + \left[E_{K^*}m_B g_{\nu\mu} - p'_\mu q_\nu\right]\mathcal{T}_\perp^{(t)}(q^2)\\ & + \frac{1}{2}q_\nu\left[q_\mu - \frac{q^2}{m_B^2}(2p'+q)_\mu\right]\mathcal{T}_\parallel^{(t)}(q^2)\Big\}.\end{aligned} \tag{4.4.8}$$

In the SM (and all its extensions that preserve the left-handed nature of the theory), only two independent structures (i.e. $\mathcal{T}_{\perp,\parallel}^{(t)}$ and $\xi_{\perp,\parallel}$) are needed for describing the amplitude at large recoil because of the chirality of weak interactions and helicity conservation. So, this picture is not expected to change with the inclusion of next-to-leading order corrections [29, 105]. Therefore, the hadronic amplitudes $\mathcal{T}_{\perp,\parallel}^{(t)}$ can be factorised in the same fashion as Eq. (2.1.29)

$$\mathcal{T}_a^{(t)}(q^2) = \mathcal{C}_a^{(t)}\xi_a(q^2) + \Phi_B \otimes T_a^{(t)} \otimes \Phi_{K^*}, \tag{4.4.9}$$

with $a = \perp, \parallel$. As in the factorisation theorem for non-leptonic two-body decays, the factorisation formula above is valid to all orders in α_s but only up to leading-order in $\Lambda_{\rm QCD}/m_b$. Thus, the amplitudes $\mathcal{T}_a^{(t)}$ receive two contributions: one coming from hard-vertex corrections, encoded in the $\mathcal{C}_a^{(t)}$ coefficients (not to be confused with Wilson coefficients), weighted by the soft form factor $\xi_a(q^2)$ and another coming from the hard-kernel functions $T_a^{(t)}$, generated through hard-spectator scattering, convoluted with both B meson and K^* LCDAs, accounting for the soft physics inside the meson states.

Following the discussion in 3.2, both hard-vertex corrections and hard-scattering kernels are perturbatively calculable functions, as they are related to hard processes happening at high scales. Thus, they can be written in an expansion in α_s

$$\mathcal{C}_a^{(t)} = \mathcal{C}_a^{(0,t)} + \frac{\alpha_s C_F}{4\pi}\mathcal{C}_a^{(1,t)} + \ldots, \tag{4.4.10}$$

$$T_{a,\pm}^{(t)}(u,\omega) = T_{a,\pm}^{(0,t)}(u,\omega) + \frac{\alpha_s C_F}{4\pi}T_{a,\pm}^{(1,t)}(u,\omega) + \ldots. \tag{4.4.11}$$

Here C_F is a colour factor $C_F = (N_c^2 - 1)/2N_c = 4/3$ and u (ω) is the longitudinal momentum fraction of the b-quark (s-quark) within the B meson (K^* meson).

The soft form factors $\xi_a(q^2)$ and LCDAs Φ_{B,K^*} represent the non-perturbative input of the factorisation formula in Eq. (4.4.9). The properties of these objects have been discussed at length in Section 3.2.3, with the sole exception that one needs to use the large recoil symmetries for extracting the soft form factors from the usual full form factors.

4.4.2 Processes contributing to the factorisation formula

Topologies contributing to leading order in α_s

Leading order contributions $O(\alpha_s^0)$ to the amplitude of a $b \to s\ell\ell$ process come through insertions of a virtual photon line to purely hadronic diagrams in the effective theory. Therefore, there are three different topologies contributing at this order. First, one has the diagram with an insertion of the electromagnetic effective operator $\mathcal{O}_7$, with its photon attached to the lepton current in the final state. Second, we have topologies involving four-quark operators with a $q\bar{q}$ loop, where the virtual photon is attached. These can be generated by both operators $\mathcal{O}_{1,2}^{(u,c)}$ and $\mathcal{O}_{3-6}$. Finally, four-quark operators $\mathcal{O}_{3-6}$ can also contribute through weak annihilation topologies, with the virtual photon attached to any of the four fermion legs. Diagramatic representations of these contributions can be found in Fig. 4.1.

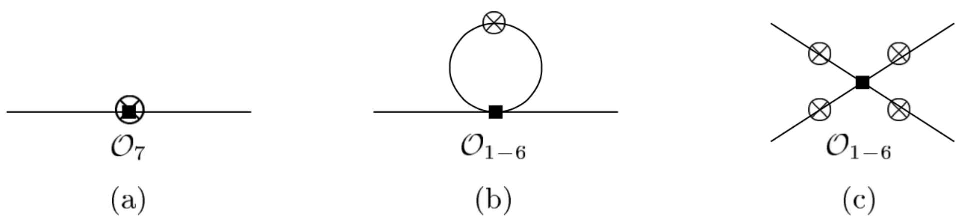

Figure 4.1: Topologies contributing to $\langle \gamma^* \bar{K}^* | \mathcal{H}_{\text{eff}} | \bar{B} \rangle$ at leading order in α_s and Λ_{QCD}/m_b. The crossed circles denote the points in the diagrams where a virtual photon line (later producing a lepton-antilepton pair) could be inserted. The spectator quark line in (a) and (b) has been omitted, being these two topologies factorisable [30].

Diagrams (a) and (b) in Fig. 4.1 are factorisable and hence they contribute to the soft form factors $\xi_\perp(E)$ and $\xi_\|(E)$. The first one actually defines the tensor form factors T_i and contributes to the amplitude with a factor $\xi_a \mathcal{C}_7$, while the second gives rise to the $Y(q^2)$ function term in Eqs. (4.4.5) and (4.4.7). As observed in Section 3.2, the four weak annihilation topologies in (c) are expected to contribute at next-to-leading order in the heavy quark expansion, and hence to be suppressed. However, the diagram in (c), where the virtual photon is attached to the spectator quark in the B meson, turns out to be leading in Λ_{QCD}/m_b [30], because this allows the quark propagator to be off-shell by an amount of order $m_b \Lambda_{\text{QCD}}$. So these will also contribute to the hard-scattering kernel $T_a^{(t)}$ at order $O(\alpha_s)$.

Since the K^* meson is produced at very high energies in the heavy-quark and large energy limits, one of the light-cone components of its momentum is going to be very light-like. We take the convention that the K^* meson momentum is nearly light-like in the minus light-cone direction. Then, the only hard-scattering kernel that will be different from zero is going to be the one projected along the minus component of the spectator quark momentum, i.e. $T^{(0,t)}_{\|,-}$.

Topologies contributing to next-to-leading order in α_s

Processes contributing to the amplitude at next-to-leading order in α_s are hard-vertex corrections and hard-spectator scattering, plus radiative corrections to weak annihilation topologies. These are shown in Fig. 4.2: (a) and (b) correspond to the latter and (c), (d) and (e) to the former type of $O(\alpha_s)$ corrections.

Hard-vertex interactions renormalise the $b \to s$ current in the effective theory. Since interactions between the heavy (or the energetic quark in the emission meson) and the spectator quark proceed through soft gluon exchanges, these contributions are proportional to the soft form factors ξ_a at the amplitude level, being responsible for the $O(\alpha_s)$ corrections to the hard-vertex coefficients $\mathcal{C}_a^{(t)}$ in Eq. (4.4.10). Amplitudes for these processes emerge from diagrams where a high-momentum gluon is emitted by the chromomagnetic effective operator $\mathcal{O}_8$ (diagram (c) in Fig. 4.2) and from topologies involving four-quark operators $\mathcal{O}_{1-6}$, with gluon exchanges between the external quark lines and the $q\bar{q}$ loop or inside the quark-antiquark loop (diagrams (d) and (e) in Fig. 4.2).

Topologies (a) and (b) in Fig. 4.2 correspond to *hard-spectator scattering* interactions. These processes involve a large momentum transfer from the heavy or energetic quark to the spectator quark, which is expected to be soft. Therefore, these gluon exchanges modify the distribution of quark momenta inside the meson and rearrange them into a more symmetric configuration, which favours hadronisation. Hence, these contributions will enter the amplitude through the convolution of the hard-scattering kernel $T^{(t)}_{a,\pm}$ with the B and K^* meson distribution amplitudes Φ_{B,K^*}. The $O(\alpha_s)$ corrections to the hard-scattering kernel in (4.4.11) are precisely coming from the aforementioned hard-gluon exchange topologies.

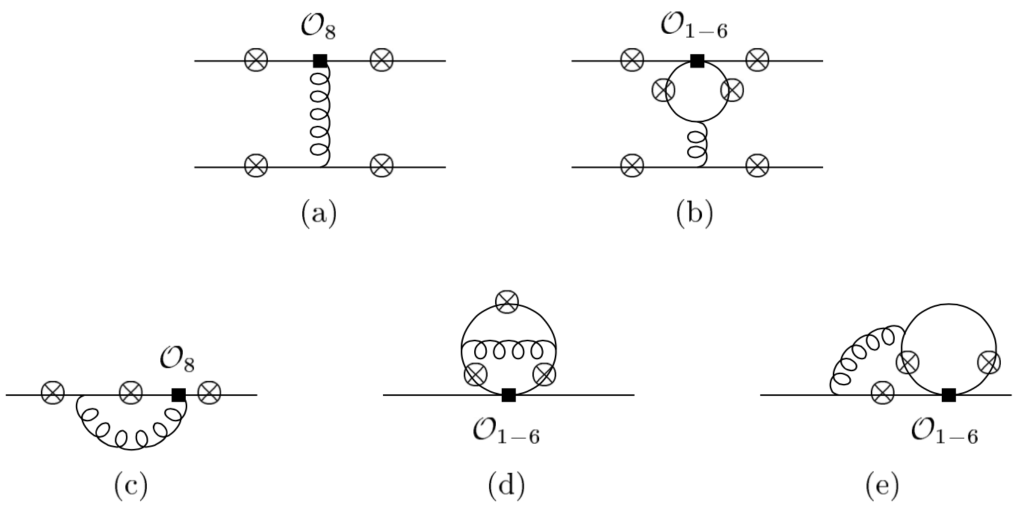

Figure 4.2: Hard-vertex factorisable contributions and hard-spectator scattering non-factorisable contributions to the amplitude $\langle \gamma^* \bar{K}^* | \mathcal{H}_{\text{eff}} | \bar{B} \rangle$. Hard-vertex topologies are depicted without explicitly drawing the spectator line for simplicity [30].

Finally, radiative QCD corrections to *weak-annihilation* topologies can be found in Fig. 4.3. Although contrary to the usual power counting in QCDf, weak annihilation diagrams contribute at leading order in $\Lambda_{\rm QCD}/m_b$, making the amplitudes in Fig. 4.3 to enter the $\langle \gamma^* \bar{K}^* | \mathcal{H}_{\rm eff} | \bar{B} \rangle$ amplitude at $O(\alpha_s)$ and not $O(\alpha_s \Lambda_{\rm QCD}/m_b)$. However, these amplitudes are still very suppressed in $b \to s$ transitions. There are three main reasons for this suppression: the small value of the strong coupling constant $\alpha_s(\mu)$ at the scale $\mu \sim m_b$, the suppression of the longitudinal transversity amplitudes in the decay rate at the low q^2 (see Eq. (4.4.8)) region and the numerically small Wilson coefficients of QCD penguin operators $\mathcal{O}_{3-6}$ (see Table 4.1) [30]. Moreover, $O(\alpha_s \Lambda_{\rm QCD}/m_b)$ corrections of the same type with endpoint divergences in the convolution integral were also shown to be small in [31]. In conclusion, order $O(\alpha_s)$ weak annihilation contributions to the factorisation of the hadronic amplitudes can, and will be, safely neglected in our computations.

4.4.3 Leading and next-to-leading order results for the amplitudes $\mathcal{T}^{(i)}_{\perp,\parallel}$

An interlude about the CKM suppressed contributions

As we argued in Section 4.1, $\mathcal{H}^{(u)}_{\rm eff}$ in the full effective Hamiltonian $\mathcal{H}_{\rm eff}$ is largely Cabibbo-suppressed with respect to $\mathcal{H}^{(t)}_{\rm eff}$, because of the relatively large CKM factor $\lambda^{(s)}_t$ with respect to $\lambda^{(s)}_u$. For this reason, effects coming from the (u) part of the Hamiltonian have been neglected in most of our results so far, including the discussion in this section about $O(\alpha_s)$ corrections to the matrix elements.

However, $\lambda^{(s)}_u$ constitutes a source of weak phases in the SM, so its impact is non-trivial when studying processes probing CP-violation. This is also the case of $b \to d$ transitions, since $\lambda^{(d)}_t$ cannot be neglected in front of $\lambda^{(d)}_u$. None of these two topics is going to be covered in this Thesis, but it warrants a brief discussion on how to include these contributions in a consistent way within the formalism developed above.

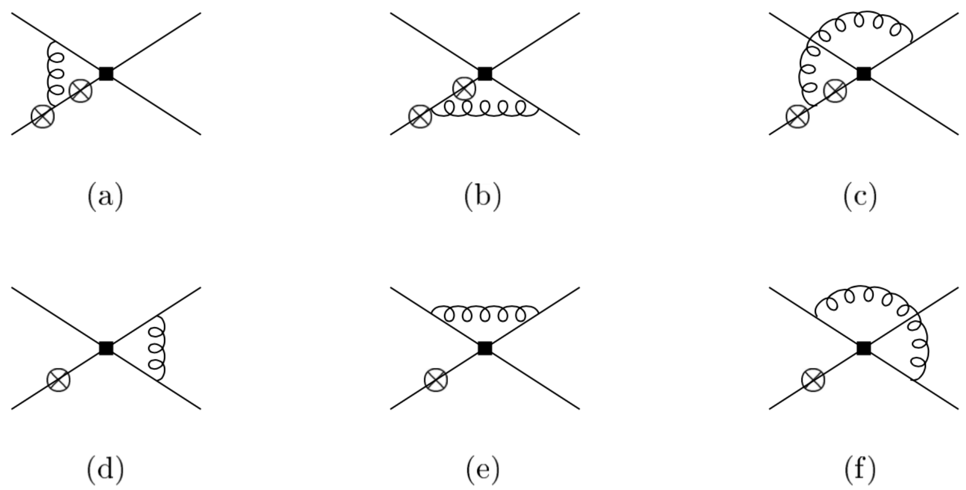

Figure 4.3: Vertex corrections to the annihilation amplitudes depicted in diagrams (c) Fig. 4.1 [30].

The extension of the factorisation formulae for including CKM suppressed terms in the effective Hamiltonian is discussed in [33]. In this reference, these contributions are put on the same footing as the "CKM allowed" terms within a unified framework. Eqs. (4.4.1), (4.4.9), (4.4.10) and (4.4.10) used for defining the relevant (t) structures, also define their (u) counterparts. This connection between the CKM allowed and suppressed modes is only formal, in general quantities wiht a (t) index will not be the same as the ones with a (u). The interested reader can find all the structures for both (t) and (u) channels in appendices A. 1 and A. 2 of [33] and [106]. Hence, from now on, we will use the notation $\mathcal{T}^{(i)}_{\perp,\parallel}$, with $i = t, u$.

Leading order result

At leading order, the explicit QCDf convolutions for the amplitudes $\mathcal{T}^{(i)}_{\perp}$ and $\mathcal{T}^{(i)}_{\parallel}$ are written by [30]

$$\mathcal{T}^{(i)}_a(q^2) = \mathcal{C}^{(0,i)}_a \xi_a(q^2) + \frac{\pi^2}{N_c}\frac{f_B f_{K^*,a}}{m_B}\,\Xi_a \sum_{\pm}\int_0^\infty \frac{d\omega}{\omega}\,\Phi_{B,\pm}(\omega)\int_0^1 du\;\Phi_{K^*,a}(u)\,T^{(0,i)}_{a,\pm}(u,\omega), \tag{4.4.12}$$

where $f_{K^*,\parallel}$ is the usual K^* meson decay constant, $f_{K^*,\perp} = f_{K^*,\perp}(\mu)$ denotes the scale-dependent transverse decay constant (defined by the matrix element of the tensor current), u (ω) is the longitudinal momentum fraction of the b-quark (s-quark) within the B meson (K^* meson), N_c is the number of colours ($N_c = 3$) and the Ξ_a parameters are defined such that $\Xi_\perp = 1$ and $\Xi_\parallel = m_{K^*}/E_{K^*}$.

Leading order hard-vertex coefficients $\mathcal{C}^{(0,i)}_a$ stem from topologies (a) and (b) in 4.1. Explicit expressions for these the coefficients can be found by comparing (4.4.12) with Eqs. (4.4.5)-(4.4.7), setting $\delta_i = 1$ for consistency,

$$\mathcal{C}^{(0,t)}_\perp = -\left(\mathcal{C}^{\rm eff}_7 + \frac{m_B}{2m_b}\,Y^{(t)}(q^2)\right), \qquad \mathcal{C}^{(0,u)}_\perp = -\frac{m_B}{2m_b}\,Y^{(u)}(q^2), \tag{4.4.13}$$

$$\mathcal{C}^{(0,t)}_\parallel = \mathcal{C}^{\rm eff}_7 + \frac{q^2}{2m_b m_B}\,Y^{(t)}(q^2), \qquad \mathcal{C}^{(0,u)}_\parallel = \frac{q^2}{2m_b m_B}\,Y^{(u)}(q^2). \tag{4.4.14}$$

To complete the result at leading order, one needs to compute the weak annihilation amplitude of 4.1 (c), with a virtual photon insertion attached to the spectator quark in the B meson. This is the only process contributing to the hard-scattering kernels at leading order. Here we will stick to the convention introduced in the previous subsection, where the K^* meson momentum is taken as nearly light-like in the minus light-cone direction. To compute these contributions, the amplitude is projected onto the B meson and K^* meson LCDAs, as shown in [29]. The result reads [30]

$$T^{(0,i)}_{\perp,+}(u,\omega) = T^{(0,i)}_{\perp,-}(u,\omega) = T^{(0,i)}_{\parallel,+}(u,\omega) = 0 \tag{4.4.15}$$

$$T^{(0,t)}_{\parallel,-}(u,\omega) = -e_q\frac{m_B\omega}{m_B\omega - q^2 - i\epsilon}\frac{4m_B}{m_b}\left(\mathcal{C}_3 + \frac{4}{3}\left(\mathcal{C}_4 + 12\mathcal{C}_5 + 16\mathcal{C}_6\right)\right), \tag{4.4.16}$$

$$T^{(0,u)}_{\parallel,-}(u,\omega) = e_q\frac{m_B\omega}{m_B\omega - q^2 - i\epsilon}\frac{4m_B}{m_b}3\delta_{qu}\mathcal{C}_2, \tag{4.4.17}$$

with e_q the electric charge of the spectator quark, so $e_q = 1/3$ for the $\bar{B}^0 \to \bar{K}^{*0}\ell^+\ell^-$ decay mode whereas $e_q = -1/3$ for the corresponding CP conjugate channel.

At leading order, weak annihilation topologies are produced via insertions of penguin operators with numerically small Wilson coefficients ($\mathcal{C}_{3-6}(\mu_b) \approx 0$), therefore these contributions are expected to be small with respect to the dominant leading order terms. This suppression of weak annihilation contributions is even stronger in $B \to K^*\gamma$, since $\mathcal{T}^{(t)}_\parallel(q^2)$ does not actually contribute to $\langle\gamma^*(q,\mu)\bar{K}^*(p',\varepsilon^*)|\,\mathcal{H}^{(t)}_{\rm eff}\,|\bar{B}(p)\rangle$ in the $q^2 \to 0$ limit, as one can see by examining Eq. (4.4.8).

It is important to emphasise that our previous discussion about weak annihilation refers only to its leading order contribution in $\Lambda_{\mathrm{QCD}}/m_b$. It is indeed a remarkable aspect of $B \to K^*\gamma^*(\to \ell\ell)$ that this process does not vanish at first order in the heavy quark limit (if $q^2 \sim m_b\Lambda_{\mathrm{QCD}}$), giving rise to a non-zero contribution to the hard-scattering kernel. We will later discuss power suppressed contributions coming from this same type of topologies.

Next-to-leading order result

At next-to-leading order, the expression of $\mathcal{T}_\perp^{(i)}$ and $\mathcal{T}_\parallel^{(i)}$ follow [30]

$$\mathcal{T}_a^{(i)}(q^2) = \left(\mathcal{C}_a^{(0,i)} + \frac{\alpha_s C_F}{4\pi}\mathcal{C}_a^{(1,i)}\right)\xi_a(q^2) \qquad (4.4.18)$$
$$+ \frac{\pi^2}{N_c}\frac{f_B f_{K^*,a}}{m_B}\,\Xi_a \sum_\pm \int_0^\infty \frac{d\omega}{\omega}\,\Phi_{B,\pm}(\omega)\int_0^1 du\,\Phi_{K^*,a}(u)\left[T_{a,\pm}^{(0,i)}(u,\omega) + \frac{\alpha_s C_F}{4\pi}T_{a,\pm}^{(1,i)}(u,\omega)\right],$$

being C_F the same colour factor defined below Eqs. (4.4.10) and (4.4.11) and again $a = \perp, \parallel$. The $O(\alpha_s)$ corrections to the hard-vertex coefficients $\mathcal{C}_a^{(1,i)}$ and hard-scattering kernels $T_{a,\pm}^{(1,i)}$ are complicated functions that can be decomposed into the sum of a *factorisable* and a *non-factorisable* part

$$\mathcal{C}_a^{(1,i)} = \mathcal{C}_a^{(\mathrm{f},i)} + \mathcal{C}_a^{(\mathrm{nf},i)}, \qquad (4.4.19)$$
$$T_{a,\pm}^{(1,i)} = T_{a,\pm}^{(\mathrm{f},i)} + T_{a,\pm}^{(\mathrm{nf},i)}, \qquad (4.4.20)$$

where the superscript f stands for factorisable while nf does so for non-factorisable.

Factorisable next-to-leading order corrections to the hard-vertex coefficients $\mathcal{C}_a^{(\mathrm{f},i)}$ originate from re-expressing the full QCD form factors in (4.4.2)-(4.4.4) in terms of soft form factors [30]. These contributions have been encoded in the δ_i terms in Eqs. (4.4.5)-(4.4.7) above. For the hard-vertex coefficients we have [30, 33]

$$\mathcal{C}_\perp^{(\mathrm{f},t)} = \mathcal{C}_7^{\mathrm{eff}}\left(\ln\frac{m_b^2}{\mu^2} - L + \Delta M\right), \qquad \mathcal{C}_\perp^{(\mathrm{f},u)} = 0, \qquad (4.4.21)$$
$$\mathcal{C}_\parallel^{(\mathrm{f},t)} = -\mathcal{C}_7^{\mathrm{eff}}\left(\ln\frac{m_b^2}{\mu^2} + 2L + \Delta M\right), \qquad \mathcal{C}_\parallel^{(\mathrm{f},u)} = 0, \qquad (4.4.22)$$

with the quantities L [30] and ΔM [33] defined as

$$L \equiv -\frac{m_b^2 - q^2}{q^2}\ln\left(1 - \frac{q^2}{m_b^2}\right), \quad \Delta M \equiv 3\ln\frac{m_b^2}{\mu^2} - 4\left(1 - \frac{\mu_h}{m_b}\right), \qquad (4.4.23)$$

where m_b in the two expressions above refers to the b-quark pole mass and μ_h is a factorisation scale. ΔM depends on the renormalisation convention for the overall m_b factor in the amplitude $\langle\gamma^*(q,\mu)\bar{K}^*(p',\varepsilon^*)|\,\mathcal{H}_{\mathrm{eff}}^{(t)}\,|\bar{B}(p)\rangle$, in [33] the authors' choice was to use the PS scheme (see Eq. (4.1.18)) and hence ΔM in Eq. (4.4.23) is written accordingly.

Hard-vertex non-factorisable corrections are obtained by computing diagrams (c)-(e) in Fig. 4.2, which correspond to matrix elements of four-quark operators and the chromomagnetic dipole operator with hard gluon exchanges. These matrix elements require to calculate two-loop diagrams with several mass scales. The non-factorisable functions presented in [30, 33] are based on the computations in [107] for topologies with the operators $\mathcal{O}_{1,2}$ and $\mathcal{O}_8$. Results for the corresponding diagrams with QCD penguin operators were not included in [30, 33] since there was no computation available, but this is expected to be a good approximation to the full results as these contributions should be small. The aforementioned corrections have the following form [30, 33]

$$\begin{aligned} C_F\, \mathcal{C}_{\perp}^{(\mathrm{nf},t)} &= -\bar{\mathcal{C}}_2 F_2^{(7)} - \mathcal{C}_8^{\mathrm{eff}} F_8^{(7)} \\ &\quad - \frac{q^2}{2m_b m_B}\left[\bar{\mathcal{C}}_2 F_2^{(9)} + 2\bar{\mathcal{C}}_1\left(F_1^{(9)} + \frac{1}{6}F_2^{(9)}\right) + \mathcal{C}_8^{\mathrm{eff}} F_8^{(9)}\right], \end{aligned} \tag{4.4.24}$$

$$\begin{aligned} C_F\, \mathcal{C}_{\parallel}^{(\mathrm{nf},t)} &= \bar{\mathcal{C}}_2 F_2^{(7)} + \mathcal{C}_8^{\mathrm{eff}} F_8^{(7)} \\ &\quad + \frac{m_B}{2m_b}\left[\bar{\mathcal{C}}_2 F_2^{(9)} + 2\bar{\mathcal{C}}_1\left(F_1^{(9)} + \frac{1}{6}F_2^{(9)}\right) + \mathcal{C}_8^{\mathrm{eff}} F_8^{(9)}\right]. \end{aligned} \tag{4.4.25}$$

The "barred" coefficients $\bar{\mathcal{C}}_{i=1-6}$ are linear combinations of the Wilson coefficients and their definitions are given in Appendix A of [30]. Also $\mathcal{C}_8^{\mathrm{eff}}$ stands for a combination of Wilson coefficients, as it is shown in Eq. (4.1.20). The functions $F_{1,2}^{(7,9)}$ can be found in Appendix B of [30] or, in an expanded form, in [107]. Corresponding expressions for $\mathcal{C}_a^{(\mathrm{nf},u)}$ are obtained by using the same expressions above with the replacements $F_8^{(7,9)} \to 0$ and $F_{1,2}^{(7,9)} \to F_{1,2}^{(7,9)} - F_{1,2,u}^{(7,9)}$, with $F_{1,2,u}^{(7,9)}$ given in [106].

The factorisable part of the next-to-leading order hard scattering functions $T_{a,\pm}^{(\mathrm{f},i)}$ also originates from re-expressing the full QCD form factors in terms of soft form factors [30]. In this case, we have [30, 33]

$$T_{\perp,+}^{(\mathrm{f},t)}(u,\omega) = \mathcal{C}_7^{\mathrm{eff}}\,\frac{2m_B}{\bar{u}E_{K^*}}, \tag{4.4.26}$$

$$T_{\parallel,+}^{(\mathrm{f},t)}(u,\omega) = \mathcal{C}_7^{\mathrm{eff}}\,\frac{4m_B}{\bar{u}E_{K^*}}, \tag{4.4.27}$$

$$T_{\perp,-}^{(\mathrm{f},t)}(u,\omega) = T_{\parallel,-}^{(\mathrm{f},t)}(u,\omega) = T_{a,\pm}^{(\mathrm{f},u)}(u,\omega) = 0. \tag{4.4.28}$$

Non-factorisable corrections to the hard-scattering kernels are obtained by performing the explicit evaluation of diagrams (a) and (b) in Fig. 4.2. These graphs correspond to the physical processes by which the spectator quark receives a hard gluon, either directly from the effective operator $\mathcal{O}_8$ or from the quark-antiquark loop one can generate with insertions of the four-quark operators $\mathcal{O}_{1-6}$. The results of such computations are later projected on the meson LCDAs, keeping only the leading term in the heavy quark limit and expanding the amplitude in powers of the spectator quark momentum whenever it is permitted by power counting. Then, one obtains [30, 33]

$$\begin{aligned} T_{\perp,+}^{(\mathrm{nf}),t}(u,\omega) &= -\frac{4e_d\,\mathcal{C}_8^{\mathrm{eff}}}{u+\bar{u}q^2/m_B^2} + \frac{m_B}{2m_b}\Big[e_u t_\perp(u,m_c)(\bar{\mathcal{C}}_2+\bar{\mathcal{C}}_4-\bar{\mathcal{C}}_6) \\ &\quad + e_d t_\perp(u,m_b)\left(\bar{\mathcal{C}}_3+\bar{\mathcal{C}}_4-\bar{\mathcal{C}}_6-\frac{4m_b}{m_B}\bar{\mathcal{C}}_5\right) + e_d t_\perp(u,0)\,\bar{\mathcal{C}}_3\Big], \end{aligned} \tag{4.4.29}$$

$$T_{\perp,-}^{(\mathrm{nf},t)}(u,\omega) = 0, \tag{4.4.30}$$

$$\begin{aligned} T_{\parallel,+}^{(\mathrm{nf}),t}(u,\omega) &= \frac{m_B}{m_b}\Big[e_u t_\parallel(u,m_c)(\bar{\mathcal{C}}_2+\bar{\mathcal{C}}_4-\bar{\mathcal{C}}_6) + e_d t_\parallel(u,m_b)(\bar{\mathcal{C}}_3+\bar{\mathcal{C}}_4-\bar{\mathcal{C}}_6) \\ &\quad + e_d t_\parallel(u,0)\,\bar{\mathcal{C}}_3\Big], \end{aligned} \tag{4.4.31}$$

$$T_{\parallel,-}^{(\mathrm{nf}),t}(u,\omega) = e_q\,\frac{m_B\omega}{m_B\omega - q^2 - i\epsilon}\left[\frac{8\,\mathcal{C}_8^{\mathrm{eff}}}{\bar{u}+uq^2/m_B^2}\right.$$

$$+\frac{6m_B}{m_b}\Big(h(\bar{u}m_B^2+uq^2,m_c)(\bar{\mathcal{C}}_2+\bar{\mathcal{C}}_4+\bar{\mathcal{C}}_6)+h(\bar{u}m_B^2+uq^2,m_b)(\bar{\mathcal{C}}_3+\bar{\mathcal{C}}_4+\bar{\mathcal{C}}_6)$$
$$+h(\bar{u}m_B^2+uq^2,0)(\bar{\mathcal{C}}_3+3\bar{\mathcal{C}}_4+3\bar{\mathcal{C}}_6)-\frac{8}{27}(\bar{\mathcal{C}}_3-\bar{\mathcal{C}}_5-15\bar{\mathcal{C}}_6)\Big)\Bigg], \tag{4.4.32}$$

where $e_u = 2/3$ and $e_d = -1/3$ are the charges of the u and d quarks, e_q refers to the charge of the spectator quark in the B meson and the function $h(s, m_q)$ is given in Eq. (4.1.24). The functions $t_a(u, m_q)$ emerge from the two loop diagrams in Fig. 4.2 (b) in which the virtual photon line is attached to the internal quark loop. They present the following structure [30]

$$t_\perp(u,m_q)=\frac{2m_B}{\bar{u}E_{K^*}}I_1(m_q)+\frac{q^2}{\bar{u}^2E_{K^*}^2}\left(B_0(\bar{u}m_B^2+uq^2,m_q)-B_0(q^2,m_q)\right), \tag{4.4.33}$$
$$t_\parallel(u,m_q)=\frac{2m_B}{\bar{u}E_{K^*}}I_1(m_q)+\frac{\bar{u}m_B^2+uq^2}{\bar{u}^2E_{K^*}^2}\left(B_0(\bar{u}m_B^2+uq^2,m_q)-B_0(q^2,m_q)\right), \tag{4.4.34}$$

and the functions $B_0(q^2, m_q)$ and $I_1(m_q)$ are also defined in [30].

The corresponding non-factorisable kernels stemming from the CKM-suppressed terms in the Hamiltonian read [33]

$$T_{\perp,+}^{(\mathrm{nf},t)}(u,\omega)=e_u\frac{m_B}{2m_b}\left(\mathcal{C}_2-\frac{1}{6}\mathcal{C}_1\right)(t_\perp(u,m_c)-t_\perp(u,0)), \tag{4.4.35}$$
$$T_{\parallel,+}^{(\mathrm{nf},t)}(u,\omega)=e_u\frac{m_B}{m_b}\left(\mathcal{C}_2-\frac{1}{6}\mathcal{C}_1\right)(t_\parallel(u,m_c)-t_\parallel(u,0)), \tag{4.4.36}$$
$$T_{\parallel,+}^{(\mathrm{nf},t)}(u,\omega)=e_q\frac{m_B\omega}{m_B\omega-q^2-i\epsilon}\frac{6m_B}{m_b}\times\left(\mathcal{C}_2-\frac{1}{6}\mathcal{C}_1\right)\left(h(\bar{u}m_B^2+uq^2,m_c)-h(\bar{u}m_B^2+uq^2,0)\right), \tag{4.4.37}$$

with $T_{\perp,-}^{\mathrm{nf},u}(u,\omega) = 0$ and $t_a(u, m_q)$ are the functions discussed above.

There is an important remark worth mentioning here. In all the computations above, the Wilson coefficients must be evaluated at the scale μ_b (as this is the scale we stop running down the four-quark operators from the high scale $\sim M_W$). Also the QCD coupling is understood to be evaluated at μ_b when multiplying the hard-vertex coefficients $\mathcal{C}_a^{(i)}$, however one needs to compute α_s at the scale $\mu_h \simeq \sqrt{m_b\Lambda_{\mathrm{QCD}}}$ when it weights the $T_{a,\pm}^{(1,i)}$ kernels, since virtualities of gluon exchanges in hard-scattering process are expected to be of order $O(m_b\Lambda_{\mathrm{QCD}})$ (see Section 3.2.2 for more information).

Finally, observe that all leading order and next-to-leading order results (except the weak annihilation contribution in Eqs. (4.4.15)-(4.4.17)) depend on which QCD form factors have been chosen to define the soft form factor ξ_a. The full form factor choice used for writing the soft form factors defines a so-called *soft form factor scheme*. We will comment on that at the end of this chapter and this subject will be extensively covered in Chapter 6.

Comments on scale- and scheme-dependence

Since the virtual photon in $\langle\gamma^*(q,\mu)\bar{K}^*(p',\varepsilon^*)|\,\mathcal{H}_{\mathrm{eff}}^{(t)}\,|\bar{B}(p)\rangle$ is off-shell, this matrix element cannot be scale- and scheme-independent (it would only be scale- and scheme-independent if the photon was taken on-shell, for which case the whole formalism developed above still applies). Therefore, it follows that the hadronic amplitudes $\mathcal{T}^{(i)}_{\perp,\parallel}$ are neither scale- nor scheme-independent. However, we can build three relevant quantities that are independent of the conventions chosen to renormalise the effective Hamiltonian [30],

$$\tilde{\mathcal{C}}_7 \equiv \frac{\mathcal{T}_\perp(0)}{\xi_\perp(0)} = \mathcal{C}_7^{\text{eff}} + \ldots, \tag{4.4.38}$$

$$\mathcal{C}_{9,\perp}(q^2) \equiv \mathcal{C}_9 + \frac{2m_b m_B}{q^2}\frac{\mathcal{T}_\perp(q^2)}{\xi_\perp(q^2)} = \mathcal{C}_9^{\text{eff}}(q^2) + \frac{2m_b m_B}{q^2}\mathcal{C}_7^{\text{eff}} + \ldots, \tag{4.4.39}$$

$$\begin{aligned}\mathcal{C}_{9,\parallel}(q^2) \equiv \mathcal{C}_9 - \frac{2m_b}{m_B}\frac{\mathcal{T}_\parallel(q^2)}{\xi_\parallel(q^2)} &= \mathcal{C}_9^{\text{eff}}(q^2) + \frac{2m_b}{m_B}\mathcal{C}_7^{\text{eff}} - e_q\frac{4m_B}{m_b}(\bar{\mathcal{C}}_3 + 3\bar{\mathcal{C}}_4)\\ &\times \frac{\pi^2}{N_c}\frac{f_B f_{K^*}}{m_B(E_{K^*}/m_{K^*})\xi_\parallel(q^2)}\int d\omega \frac{m_B\Phi_{B,-}(\omega)}{m_B\omega - q^2 - i\omega} + \ldots,\end{aligned} \tag{4.4.40}$$

where the effective, q^2-dependent coefficient $\mathcal{C}_9^{\text{eff}}$ is the same we defined in Eq. (4.1.21). The ellipses denote the $O(\alpha_s)$ corrections defined in Eq. (4.4.12), which we have discussed at lenght in this section. Notice that $\tilde{\mathcal{C}}_7$, $\mathcal{C}_{9,\perp}(q^2)$ and $\mathcal{C}_{9,\parallel}(q^2)$ depend on the soft form factor scheme chosen for our calculations, as the structure of the ratios $\mathcal{T}_{\perp,\parallel}/\xi_{\perp,\parallel}$ changes for different definitions of the soft form factors at order $O(\alpha_s)$ or higher. Moreover, $\tilde{\mathcal{C}}_7$ also depends on the b quark mass renormalisation scheme, but $m_b\tilde{\mathcal{C}}_7$ does not.

In particular, the coefficients $\tilde{\mathcal{C}}_7$, $\mathcal{C}_{9,\perp}(q^2)$ and $\mathcal{C}_{9,\parallel}(q^2)$ can be proven to be scale independent up to order $O(\alpha_s^2, \alpha_s\mathcal{C}_{3-6})$ [30], this being the order up to which the computations above hold. For consistency, when order α_s terms are explicitly included in Eqs. (4.4.43)-(4.4.40), the next-to-leading logarithmic expression for $\mathcal{C}_7^{\text{eff}}$ [87] must also be used. However, $\mathcal{C}_9$ is already needed at next-to-next-to-leading logarithmic order, since $\mathcal{C}_9 \sim \ln(M_W/\mu) \sim 1/\alpha_s$ at leading order.

4.4.4 Power suppressed corrections to the amplitudes $\mathcal{T}^{(i)}_{\perp,\parallel}$

Power corrections of order $1/m_b$ might play an important role in certain cases. On one hand, in B meson decays to charged ρ mesons power corrections to weak annihilation amplitudes should be taken into account, because they are enhanced by the large Wilson coefficient $\mathcal{C}_2$. On the other hand, since the transverse hadronic amplitude $\mathcal{T}^{(i)}_\perp$ does not depend on the charge of the spectator quark e_q, power corrections to this amplitude are expected to be a relevant source of isospin breaking. This is entirely not the case for the longitudinal amplitude $\mathcal{T}^{(i)}_\parallel$, as it manifestly depends on e_q, therefore we will assume the power corrections to this amplitude to be negligible [33].

Denoting by $\Delta\mathcal{T}^{(i)}_\perp$ the power-suppressed contributions to $\mathcal{T}^{(i)}_\perp$, weak annihilation $O(\alpha_s^0)$ corrections read [33]

$$\begin{aligned}\Delta\mathcal{T}^{(t)}_\perp\Big|_{\text{ann}} &= -e_q\frac{4\pi^2}{3}\frac{f_B f_{K^*,\perp}}{m_b m_B}\left(\mathcal{C}_3 + \frac{4}{3}(\mathcal{C}_4 + 3\mathcal{C}_5 + 4\mathcal{C}_6)\int_0^1 du\,\frac{\Phi_{K^*,\perp}(u)}{\bar{u} + u\hat{s}}\right)\\ &+ e_q\frac{2\pi^2}{3}\frac{f_B f_{K^*,\parallel}}{m_b m_B}\frac{m_{K^*}}{(1-\hat{s})\lambda_{B,+}(q^2)}\left(\mathcal{C}_3 + \frac{4}{3}\left(\mathcal{C}_4 + 12\mathcal{C}_5 + 16\mathcal{C}_6\right)\right)\end{aligned} \tag{4.4.41}$$

$$\Delta\mathcal{T}^{(u)}_\perp\Big|_{\text{ann}} = -e_q\frac{2\pi^2}{3}\frac{f_B f_{K^*,\parallel}}{m_b m_B}\frac{m_{K^*}}{(1-\hat{s})\lambda_{B,+}(q^2)}3\delta_{qu}\mathcal{C}_2, \tag{4.4.42}$$

with the reduced kinematic variable $\hat{s} = q^2/m_B^2$ and $\lambda_{B,\pm}$ are the inverse moments of the B meson distribution amplitudes $\Phi_{B,\pm}(\omega)$, defined in [30]. This result generalises the corresponding results of [108, 109].

Hard-spectator interactions enter the amplitude at order $O(\alpha_s)$, hence leading power corrections to this amplitudes will contribute at $O(\alpha_s \Lambda_{\rm QCD}/m_b)$ [33, 108, 109]

$$\begin{aligned}\Delta\mathcal{T}_\perp^{(t)}\Big|_{\rm hsa} = e_q \frac{\alpha_s C_F}{4\pi}\frac{\pi^2 f_B}{N_c m_b m_B}\Bigg[&12\mathcal{C}_8^{\rm eff}\frac{m_b}{m_B} f_{K^*,\perp} X_\perp(\hat{s}) \\ &+ 8 f_{K^*,\perp}\int_0^1 du\, \frac{\Phi_{K^*,\perp}(u)}{\bar{u}+u\hat{s}} F_{K^*}^{(t)}(\bar{u}m_B^2 + uq^2) \\ &- \frac{4 m_{K^*} f_{K^*,\parallel}}{(1-\hat{s})\lambda_{B,+}(q^2)}\int_0^1 du \int_0^u dv\, \frac{\Phi_{K^*,\parallel}(v)}{\bar{v}} F_{K^*}^{(t)}(\bar{u}m_B^2 + uq^2). \qquad (4.4.43)\end{aligned}$$

Here we have used the four-quark loop function $F_{K^*}^{(t)}$ [109]

$$\begin{aligned}F_{K^*}^{(t)}(x) = \frac{3}{4}\Bigg[&h(x,m_c)\left(-\frac{1}{6}\mathcal{C}_1 + \mathcal{C}_2 + \mathcal{C}_4 + 10\mathcal{C}_6\right) + h(x,m_b)\left(\mathcal{C}_3 + \frac{5}{6}\mathcal{C}_4 + 16\mathcal{C}_5 + \frac{22}{3}\mathcal{C}_6\right) \\ &+ h(x,0)\left(\mathcal{C}_3 + \frac{17}{6}\mathcal{C}_4 + 16\mathcal{C}_5 + \frac{82}{3}\mathcal{C}_6\right) - \frac{8}{27}\left(-\frac{15}{2}\mathcal{C}_4 + 12\mathcal{C}_5 - 32\mathcal{C}_6\right)\Bigg] \qquad (4.4.44)\end{aligned}$$

and the integral [109]

$$X_\perp(\hat{s}) = \frac{1}{3}\left[\int_0^1 du\, \frac{\Phi_{K^*,\perp}(u)}{1-u+u\hat{s}} + \int_0^1 du\, \frac{\Phi_{K^*,\perp}(u)}{(1-u+u\hat{s})^2}\right] \qquad (4.4.45)$$

This integral develops a logarithmic endpoint singularity as $u \to 1$, signaling a breakdown of factorisation in this kinematic regime. One way of treating this singularity is by introducing an infrared cutoff [109].

The corresponding (u) contribution from hard-scattering power corrections, which we denote by $\Delta\mathcal{T}_\perp^{(t)}\Big|_{\rm hsa}$ is obtained by $\mathcal{C}_8^{\rm eff} \to 0$ and $F_{K^*}^{(t)}(s) \to F_{K^*}^{(u)}(s)$, where

$$F_{K^*}^{(u)}(s) = \frac{3}{4}\left(\mathcal{C}_2 - \frac{1}{6}\mathcal{C}_1\right)\left[h(s,m_c) - h(s,0)\right]. \qquad (4.4.46)$$

4.4.5 Summary of results for $\mathcal{T}_{\perp,\parallel}^{(i)}$

Combining the next-to-leading order factorisation formula (4.4.12) with the results for power suppressed contributions $\Delta\mathcal{T}_\perp^{(i)}\Big|_{\rm ann}$ and $\Delta\mathcal{T}_\perp^{(i)}\Big|_{\rm hsa}$ given in Eqs. (4.4.41), (4.4.42) and (4.4.43), we obtain a complete description for the amplitudes $\mathcal{T}_{\perp,\parallel}^{(i)}$ at order $O(\alpha_s, \Lambda_{\rm QCD}/m_b)$,

$$\mathcal{T}_\perp^{(t),{\rm full}} = \mathcal{T}_\perp^{(t)} + \Delta\mathcal{T}_\perp^{(t)}\Big|_{\rm ann} + \Delta\mathcal{T}_\perp^{(t)}\Big|_{\rm hsa}, \mathcal{T}_\perp^{(u),{\rm full}} = \mathcal{T}_\perp^{(u)} + \Delta\mathcal{T}_\perp^{(u)}\Big|_{\rm ann} + \Delta\mathcal{T}_\perp^{(u)}\Big|_{\rm hsa}, \qquad (4.4.47)$$

which enter the amplitude according to structure of the $b \to s\ell^+\ell^-$ effective Hamiltonian

$$\mathcal{T}_\perp^{(t),{\rm full}} + \hat{\lambda}_u^{(s)}\mathcal{T}_\perp^{(u),{\rm full}}, \qquad (4.4.48)$$

$$\mathcal{T}_\parallel^{(t)} + \hat{\lambda}_u^{(s)}\mathcal{T}_\parallel^{(u)}, \qquad (4.4.49)$$

with $\hat{\lambda}_u^{(s)} = \lambda_u^{(s)}/\lambda_t^{(s)}$, being $\lambda_u^{(s)}$ and $\lambda_t^{(s)}$ as defined in (4.1.1).

4.4.6 An explicit observation about the choice of soft form factors

Soft form factors emerge from the relations between full QCD form factors in the heavy quark and large energy limits (see Eqs. (2.1.27)-(2.1.28)). These relations allow many different possible definitions for the soft form factors in terms of full form factors. Each choice sets a factorisation scheme by which one imposes the relations defining the soft form factors to hold to all orders in perturbation theory. Several conventions have been used in the literature but general consensus has been reached around the scheme defined in [33]. Clearly, physical quantities cannot depend on the particular scheme used in the calculations, however the choice of scheme certainly affects the structure of some of the functions in the factorisation formula of Eq. (4.4.18).

For instance, by choosing the scheme adopted in [29, 30], we have

$$\left.\begin{aligned} \xi_\perp(q^2) &\equiv \tfrac{m_B}{m_B+m_{K^*}} V(q^2) \\ \xi_\parallel(q^2) &\equiv \tfrac{m_{K^*}}{E_{K^*}} A_0(q^2) \end{aligned}\right\} \Rightarrow \left\{\begin{aligned} \mathcal{C}_\parallel^{(\mathrm{f},t)} &= -\mathcal{C}_7^{\mathrm{eff}}\left(4\ln\tfrac{m_b^2}{\mu^2} - 6 - 4L\right) + \tfrac{m_B}{m_b} Y^{(t)}(q^2)(1-L), \\ T_{\parallel,+}^{(\mathrm{f},t)}(u,\omega) &= \left(\mathcal{C}_7^{\mathrm{eff}} + \frac{q^2}{2m_b m_B} Y^{(t)}(q^2)\right)\frac{2m_B^2}{\bar{u}E_{K^*}^2}, \end{aligned}\right. \tag{4.4.50}$$

while fixing the scheme to the most common convention [33] leads into

$$\left.\begin{aligned} \xi_\perp(q^2) &\equiv \tfrac{m_B}{m_B+m_{K^*}} V(q^2) \\ \xi_\parallel(q^2) &\equiv \tfrac{m_B+m_{K^*}}{2E_{K^*}} A_1(q^2) - \tfrac{m_B-m_{K^*}}{m_B} A_2(q^2) \end{aligned}\right\} \Rightarrow \left\{\begin{aligned} \mathcal{C}_\parallel^{(\mathrm{f},t)} &= -\mathcal{C}_7^{\mathrm{eff}}\left(\ln\tfrac{m_b^2}{\mu^2} + 2L + \Delta M\right), \\ T_{\parallel,+}^{(\mathrm{f},t)}(u,\omega) &= \mathcal{C}_7^{\mathrm{eff}} \tfrac{4m_B}{\bar{u}E_{K^*}}, \end{aligned}\right. \tag{4.4.51}$$

In this section, we have always implicitly assumed the scheme of Ref. [33]. So, all the results presented and discussed here conform to this choice. For corresponding expressions in the scheme of Eq. (4.4.50) we refer to [30].

4.5 Transversity Amplitudes at order $O(\alpha_s)$

In order to include the $O(\alpha_s, \alpha_s\Lambda_{\mathrm{QCD}}/m_b)$ corrections computed within QCDf to the transversity amplitudes in Eqs. (4.2.33)-(4.2.37), we follow the prescription introduced in [83, 84]. Removing the perturbative quark-loop function $Y^{(t)}(q^2)$ from $\mathcal{C}_9^{\mathrm{eff}}$ and attaching it to $\mathcal{C}_7^{\mathrm{eff}}$[4], one can perform the following replacements

$$\mathcal{C}_9^{\mathrm{eff}} \to \mathcal{C}_9, \qquad (\mathcal{C}_7^{\mathrm{eff}} + \mathcal{C}_{7'}^{\mathrm{eff}})T_i \to \mathcal{T}_i^{(t)+}, \qquad (\mathcal{C}_7^{\mathrm{eff}} - \mathcal{C}_{7'}^{\mathrm{eff}})T_i \to \mathcal{T}_i^{(t)-}, \qquad (i=1,2,3) \tag{4.5.1}$$

where the superscripts $+,-$ in $\mathcal{T}_i^{(t)}$ stand for the substitution of $\mathcal{C}_7^{\mathrm{eff}} \to \mathcal{C}_7^{\mathrm{eff}} + \mathcal{C}_{7'}^{\mathrm{eff}}$ and $\mathcal{C}_7^{\mathrm{eff}} \to \mathcal{C}_7^{\mathrm{eff}} - \mathcal{C}_{7'}^{\mathrm{eff}}$, respectively. Instead of using the basis above for the hadronic amplitudes, we will use the more natural language of Eqs. (4.4.5)-(4.4.7) and use the substitutions [84]

$$\mathcal{T}_{1,\pm}^{(t)} = \mathcal{T}_{\perp,\pm}^{(t)}, \qquad \mathcal{T}_{2,-}^{(t)} = \frac{2E_{K^*}}{m_B}\mathcal{T}_{\perp,-}^{(t)}, \qquad \mathcal{T}_{3,-}^{(t)} = \mathcal{T}_{\perp,-}^{(t)} + \mathcal{T}_{\parallel,-}^{(t)} \tag{4.5.2}$$

[4] This can always be done, as both the electromagnetic dipole operator $\mathcal{O}_7$ and the semileptonic operator $\mathcal{O}_9$ have a vectorial structure.

Including the CKM-suppressed (u) contributions is an even simpler task, since the effective Hamiltonian $\mathcal{H}_{\text{eff}}^{(u)}$ in Eq. (4.1.3) does not contain any operator entering the matrix element of Eq. (4.2.1) at leading order. Then, these terms can be directly incorporated into the matrix element.

According to these instructions, the combination of hadronic functions in Eqs. (4.4.48)-(4.4.49) can be inserted in the transversity amplitudes in Eqs. (4.2.33)-(4.2.37) to obtain:

$$A_\perp^{L,R} = N\sqrt{2}\lambda^{1/2}\Bigg\{\Big[\left(\mathcal{C}_9^{\text{eff}} + \mathcal{C}_{9'}^{\text{eff}}\right) \mp (\mathcal{C}_{10} + \mathcal{C}_{10'})\Big]\frac{V(q^2)}{m_B + m_{K^*}} + \frac{2m_b}{q^2}\left(\mathcal{T}_{\perp,+}^{(t),\text{full}} + \hat{\lambda}_u^{(s)}\mathcal{T}_\perp^{(u),\text{full}}\right)\Bigg\}, \tag{4.5.3}$$

$$A_\parallel^{L,R} = -N\sqrt{2}\left(m_B^2 - m_{K^*}^2\right)\Bigg\{\Big[\left(\mathcal{C}_9^{\text{eff}} - \mathcal{C}_{9'}^{\text{eff}}\right) \mp (\mathcal{C}_{10} - \mathcal{C}_{10'})\Big]\frac{A_1(q^2)}{m_B - m_{K^*}} + \frac{2m_b}{q^2}\left[\frac{2E_{K^*}}{m_b}\left(\mathcal{T}_{\perp,-}^{(t),\text{full}} + \hat{\lambda}_u^{(s)}\mathcal{T}_\perp^{(u),\text{full}}\right)\right]\Bigg\}, \tag{4.5.4}$$

$$\begin{aligned} A_0^{L,R} = -\frac{N}{2m_{K^*}\sqrt{q^2}}\Bigg\{&\Big[\left(\mathcal{C}_9^{\text{eff}} - \mathcal{C}_{9'}^{\text{eff}}\right) \mp (\mathcal{C}_{10} - \mathcal{C}_{10'})\Big] \\ &\left[(m_B^2 - m_{K^*}^2 - q^2)(m_B + m_{K^*})A_1(q^2) - \lambda\frac{A_2(q^2)}{m_B + m_{K^*}}\right] \\ &+ 2m_b\left[\left((m_B^2 + 3m_{K^*}^2 - q^2)\frac{2E_{K^*}}{m_B} - \frac{\lambda}{m_B^2 - m_{K^*}^2}\right)\left(\mathcal{T}_{\perp,-}^{(t),\text{full}} + \hat{\lambda}_u^{(s)}\mathcal{T}_\perp^{(u),\text{full}}\right)\right] \\ &- \frac{\lambda}{m_B^2 - m_{K^*}^2}\left(\mathcal{T}_{\parallel,-}^{(t)} + \hat{\lambda}_u^{(s)}\mathcal{T}_\parallel^{(u)}\right), \end{aligned} \tag{4.5.5}$$

$$A_t = \frac{N}{\sqrt{q^2}}\lambda^{1/2}\left[2(\mathcal{C}_{10} - \mathcal{C}_{10'}) + \frac{q^2}{m_\mu}(\mathcal{C}_{PS} - \mathcal{C}_{PS'})\right]A_0(q^2), \tag{4.5.6}$$

$$A_S = -2N\lambda^{1/2}(\mathcal{C}_S - \mathcal{C}_{S'})A_0(q^2), \tag{4.5.7}$$

where the normalisation constant N is the same as in Eq. (1.3.10) and λ is the triangle function. Although Eqs. (4.5.3)-(4.5.7) are the result of a direct application of the prescription discussed above, these are not the final result as they contain $O(m_{K^*}^2/m_B^2)$ terms which need to be eliminated in order to be consistent with QCDf. At leading order in an expansion in $m_{K^*}^2/m_B^2$, the transversity amplitudes can be simplified to

$$A_\perp^{L,R} \simeq N\sqrt{2}(m_B^2 - q^2)\Bigg\{\Big[\Big(\mathcal{C}_9^{\rm eff} + \mathcal{C}_{9'}^{\rm eff}\Big) \mp (\mathcal{C}_{10} + \mathcal{C}_{10'})\Big]\frac{V(q^2)}{m_B} + \frac{2m_b}{q^2}\Big(\mathcal{T}_{\perp,+}^{(t),\rm full} + \hat{\lambda}_u^{(s)}\mathcal{T}_\perp^{(u),\rm full}\Big)\Bigg\}, \tag{4.5.8}$$

$$A_\parallel^{L,R} \simeq -N\sqrt{2}\Bigg\{\Big[\Big(\mathcal{C}_9^{\rm eff} - \mathcal{C}_{9'}^{\rm eff}\Big) \mp (\mathcal{C}_{10} - \mathcal{C}_{10'})\Big](m_B - m_{K^*})A_1(q^2) + \frac{2m_b}{q^2}\Big[(m_B^2 - q^2)\Big(\mathcal{T}_{\perp,-}^{(t),\rm full} + \hat{\lambda}_u^{(s)}\mathcal{T}_\perp^{(u),\rm full}\Big)\Big]\Bigg\}, \tag{4.5.9}$$

$$A_0^{L,R} = -N\frac{m_B^2 - q^2}{2\sqrt{q^2}}\Bigg\{\Big[\Big(\mathcal{C}_9^{\rm eff} - \mathcal{C}_{9'}^{\rm eff}\Big) \mp (\mathcal{C}_{10} - \mathcal{C}_{10'})\Big]\Bigg[\Big(1 + \frac{m_B}{m_{K^*}}\Big)A_1(q^2) - \frac{m_B}{m_{K^*}}\Big(1 - \frac{q^2}{m_B`2}\Big)A_2(q^2)\Bigg] - \frac{2m_b}{m_{K^*}}\Big(1 - \frac{q^2}{m_B`2}\Big)\Big(\mathcal{T}_{\parallel,-}^{(t)} + \hat{\lambda}_u^{(s)}\mathcal{T}_\parallel^{(u)}\Big)\Bigg\}, \tag{4.5.10}$$

$$A_t \simeq \frac{N}{\sqrt{q^2}}(m_B^2 - q^2)\Big[2(\mathcal{C}_{10} - \mathcal{C}_{10'}) + \frac{q^2}{m_\mu}(\mathcal{C}_{PS} - \mathcal{C}_{PS'})\Big]A_0(q^2), \tag{4.5.11}$$

$$A_S = -2N(m_B^2 - q^2)(\mathcal{C}_S - \mathcal{C}_{S'})A_0(q^2), \tag{4.5.12}$$

Finally, one needs to write the full QCD form factors in Eqs. (4.5.8)-(4.5.12) in terms of soft form factors. Because the equations for the transversity amplitudes above include $O(\alpha_s)$ corrections coming from QCDf, for the sake of a meaningful result one must include the $O(\alpha_s)$ corrections to the soft form factors (as defined in Eq. (2.1.29)) too. Using the scheme defined in [29]

$$V(q^2) \equiv \frac{m_B + m_K^*}{m_B}\xi_\perp(q^2), \qquad A_0(q^2) \equiv \frac{E_{K^*}}{m_{K^*}}\xi_\parallel(q^2), \tag{4.5.13}$$

and taking into account Eqs. (32)-(33) and Eqs. (59)-(60) in [29], one obtains

$$A_1(q^2) = \frac{2E_{K^*}}{m_B + m_{K^*}}\xi_\perp(q^2), \tag{4.5.14}$$

$$A_2(q^2) = \frac{m_B}{m_B - m_{K^*}}\left(\xi_\perp(q^2) - \xi_\parallel(q^2)\right) + \frac{\alpha_s}{3\pi}\frac{2m_B}{m_B - m_{K^*}}\Bigg[(1-L)\xi_\parallel(q^2) + \frac{m_{K^*}}{E_{K^*}}\frac{m_B(m_B - 2E_{K^*})}{E_{K^*}^2}\frac{\pi^2 f_B f_{K^*,\parallel}}{N_c m_B}\lambda_{B,+}^{-1}\int_0^1 du\,\frac{\Phi_{K^*,\parallel}(u)}{\bar{u}}\Bigg], \tag{4.5.15}$$

in which L is a function of q^2 already defined in Eq. (4.4.23).

Chapter 5

Observables in $b \to s\ell\ell(\gamma)$

Phenomenological analyses pretend to determine, or at least constrain, fundamental theory parameters from experimental results. The common ground where theory and experiment meet is the observable level. By observables we understand experimentally accessible quantities that admit predictions within different theoretical models in terms of their fundamental parameters. From the theory side, one aims at designing observables with maximal sensitivity to the physics we want to study and providing predictions for them with competitive uncertainties. The task of the experiments, on the other hand, is to perform precise measurements of the observables with the data obtained in particle colliders.

In this chapter we will describe all the different types of observables that are included in our global analyses of processes with underlying $b \to s\ell\ell$ and $b \to s\gamma$ transitions, paying special attention to the concept of optimised observable. In this regard, a complete presentation of the guidelines used to construct such observables will be provided and their general properties discussed.

5.1 $B \to K^*\ell^+\ell^-$: Symmetries and Optimised Observables

The main goal of this section is to provide a complete description of the four-body angular distribution of the $B \to K^*\ell^+\ell^-$ decay (see Eq. (4.2.9)) in terms of *optimised observables*. In this context, an observable is said to be optimised (or *optimal*), if it has a very limited sensitivity to uncertainties of hadronic origin throughout the relevant q^2 range of the decay. Then, since these observables are defined to depend as little as possible on the long-distance physics, they present an enhanced sensitivity to short-distance effects and thus provide excellent probes of NP.

Observables of this type have been traditionally referred to in the literature as *clean observables*. Indeed, clean observables are not new and some of them have already been known for nearly two decades now. Examples are the zero of the forward-backward asymmetry (A_{FB}) [30], as this only depends on a combination of Wilson coefficients with no form factor input, and the so-called $A_T^{(2)}$ observable [100], which was precisely built in order to have the same properties as the zero of the A_{FB} but for all the $B \to K^*\ell^+\ell^-$ large recoil region.

A systematic procedure for the construction of optimised observables can be formulated in two steps:

- Identify the irreducible building blocks from which all observables can be built by means of the symmetries of the decay distribution (see the subsection below).

- Use effective theories (i.e. HQET/LEET at low-q^2 [24, 30] and HQET at high-q^2 [110]) to build simple combinations of the aforementioned building blocks where the soft form factors cancel at leading order in the effective theory.

Complete descriptions of the theoretical formalism used to construct the above-mentioned optimised observables and thorough reviews of their properties, both in the SM and in several well-motivated NP scenarios, can be found in Refs. [103, 111–113].

5.1.1 Symmetry formalism for massless leptons

All experimental information available in the $B \to K^*\ell^+\ell^-$ decay is contained in the decay distribution, therefore the number of experimental degrees of freedom is determined by the number of angular coefficients J_i in Eq. (4.2.9). On the other hand, since all theory computations can be written in terms of transversity amplitudes in Eqs. (4.2.33)-(4.2.37), the theoretical degrees of freedom are given by the transversity amplitudes A_j. Clearly, for consistency, theoretical and experimental degrees of freedom have to match. There are two effects to consider for this: different values of the amplitudes A_j can give rise to the same differential distribution (4.2.9), being impossible to distinguish one from another (*continuous symmetries*), but also it is possible that not all angular coefficients J_i are independent, so that not all arbitrary values of the J_i are actually possible. Hence, for the theoretical and experimental degrees of freedom to match, the following is required [111]

$$n_c - n_d = 2n_A - n_s, \tag{5.1.1}$$

where n_c is the number of coefficients in the differential distribution (number of J_i), n_d the number of dependencies between the different coefficients, n_A is the number of spin amplitudes (since the amplitudes A_j are complex quantities, each of them carry 2 degrees of freedom) and n_s is the number of continuous symmetries.

Since the combination $n_c - n_d$ accounts for the number of degrees of freedom that are available from the angular analysis, we can define the experimental number of degrees of freedom as [111]

$$n_{\text{exp}} \equiv n_c - n_d = 2n_A - n_s, \tag{5.1.2}$$

Notice that n_{exp} also measures the number of independent observables required to extract all the information contained in the distribution [103]. Therefore, once a set of n_{exp} independent observables consistent with the symmetries is fixed, any angular observable can be written in terms of these observables, so the aforementioned set has the properties of a *basis* [103, 112]. Different scenarios (i.e. massless leptons, massless leptons including scalar contributions, etc) require different sets of transversity amplitudes, resulting in different number of independent observables. In this thesis we will only consider the massless lepton case, because the vast majority of our applications will only involve muons or electrons in the final state, for which the massless approximation is justified.

In this case, one has 12 angular coefficients and 6 different A_j amplitudes (with the scalar amplitude $A_S \to 0$). Considering an infinitesimal transformations of the differential distribution (4.2.9) [111], one can show that there are $n_s = 4$ continuous transformations between the $A_i^{L,R}$ that leave the angular distribution invariant. Two of these are just phase transformations ($A_i^L \to \mathrm{e}^{i\phi_L} A_i^L$

and $A_i^R \to e^{i\phi_R} A_i^R$), while the other two mix L and R amplitudes (see [111] and Appendix A of Ref. [103]). Thus, by means of Eq. (4.2.41), there must be $n_{\rm exp} = 8$ independent observables in this case. At the same time, the previous observation implies that there should be 4 relationships among the 12 angular coefficients $J_i(q^2)$. Three of them are transparent from the Eqs. (4.3.1)-(4.3.6) in Section 4.3: $J_{6c} = 0$, $J_{1s} = 3J_{2s}$ and $J_{1c} = -J_{2c}$. On the other hand, using the symmetry formalism in [111] and [103], it can be proved that the fourth relation reads

$$\begin{aligned} J_{2c} = &-2\frac{(2J_{2s}+J_3)(4J_4^2+\beta_\ell^2 J_7^2)+(2J_{2s}-J_3)(\beta_\ell^2 J_5^2+4J_8^2)}{16J_{2s}^2-(J_3^2+\beta_\ell^2 J_{6s}^2+4J_9^2)} \\ &+4\frac{\beta_\ell^2 J_{6s}(J_4J_5+J_7J_8)+J_9(\beta_\ell^2 J_5J_7-4J_4J_8)}{16J_{2s}^2-(J_3^2+\beta_\ell^2 J_{6s}^2+4J_9^2)}, \end{aligned} \tag{5.1.3}$$

where one must recall that $\beta_\ell = 1$ in the massless case (with β_ℓ defined under Eq. (4.2.38)).

5.1.2 Optimised Observables P_i

Not any observable constructed from the transversity amplitudes can be obtained from the angular distribution [103]. To this end, a well-defined observable must respect the symmetries of the angular distribution, i.e. must be formally invariant under the transformations of the transversity amplitudes. Below, we explicitly review how to construct observables with these properties in a systematic way.

First, define the following complex vectors [103, 111]

$$n_\parallel = \begin{pmatrix} A_\parallel^L \\ A_\parallel^{R*} \end{pmatrix}, \qquad n_\perp = \begin{pmatrix} A_\perp^L \\ -A_\perp^{R*} \end{pmatrix}, \qquad n_0 = \begin{pmatrix} A_0^L \\ A_0^{R*} \end{pmatrix}. \tag{5.1.4}$$

Using these vectors, one can build the products $|n_i|^2 = n_i^\dagger n_i$ and $n_i^\dagger n_j$

$$|n_\parallel|^2 = |A_\parallel^L|^2 + |A_\parallel^R|^2 = \frac{2J_{2s}-J_3}{\beta_\ell}, \qquad n_\perp^\dagger n_\parallel = A_\perp^{L*}A_\parallel^L - A_\perp^R A_\parallel^{R*} = \frac{\beta_\ell J_{6s}-2iJ_9}{2\beta_\ell^2}, \tag{5.1.5}$$

$$|n_\perp^2| = |A_\perp^L|^2 + |A_\perp^R|^2 = \frac{2J_{2s}+J_3}{\beta_\ell}, \qquad n_0^\dagger n_\parallel = A_0^{L*}A_\parallel^L + A_0^R A_\parallel^{R*} = \frac{2J_4-i\beta_\ell J_7}{\sqrt{2}\beta_\ell^2}, \tag{5.1.6}$$

$$|n_0^2| = |A_0^L|^2 + |A_0^R|^2 = -\frac{J_{2c}}{\beta_\ell^2}, \qquad n_0^\dagger n_\perp = A_0^{L*}A_\perp^L - A_0^R A_\perp^{R*} = \frac{\beta_\ell J_5-2iJ_8}{\sqrt{2}\beta_\ell^2}. \tag{5.1.7}$$

These quantities are manifestly invariant under the symmetry transformations of the transversity amplitudes, since they can be written in terms of angular coefficients. The previous equations, considering real and imaginary parts, contain nine real quantities, in which all the information of the angular distribution is codified. Their combinations provide all the possible observables consistent with the underlying symmetry. Nevertheless, these nine quantities are not all independent [103, 111],

$$|(n_\parallel^\dagger n_\perp)|n_0|^2 - (n_\parallel^\dagger n_0)(n_0^\dagger n_\perp)|^2 = (|n_0|^2|n_\parallel|^2 - |n_0^\dagger n_\parallel|^2)(|n_0|^2|n_\perp|^2 - |n_0^\dagger n_\perp|^2), \tag{5.1.8}$$

which leads to Eq. (5.1.3), when translated into J_i language. Therefore, Eqs. (5.1.5)-(5.1.7) effectively represent eight real independent quantities, as it is required by the observation above that $n_{\rm exp} = 8$.

This formalism guarantees that every observable constructed from products of the n_i vectors above will respect the symmetries of the decay distribution. Now we focus on obtaining combinations where the hadronic form factors cancel. At large recoil, the transversity amplitudes can be schematically written as [112]

$$A_\perp^{L,R} = X_\perp^{L,R}\,\xi_\perp(q^2) + O(\alpha_s, \Lambda_{\rm QCD}/m_b), \tag{5.1.9}$$

$$A_\parallel^{L,R} = X_\parallel^{L,R}\,\xi_\perp(q^2) + O(\alpha_s, \Lambda_{\rm QCD}/m_b), \tag{5.1.10}$$

$$A_0^{L,R} = X_0^{L,R}\,\xi_\parallel(q^2) + O(\alpha_s, \Lambda_{\rm QCD}/m_b), \tag{5.1.11}$$

where $X_i^{L,R}$ ($i =\perp$, $\parallel$, 0) are functions of the short-distance physics (Wilson coefficients, etc) and $\xi_{\perp,\parallel}$ are the soft-form factors defined in Eqs. (2.1.27)-(2.1.28). Notice that these equations are only a suitable and compact way of rewriting Eqs. (4.2.39)-(4.2.43). The fact that L and R transversity amplitudes are proportional to the same soft-form factor allows for the construction of several form factor independent (FFI) observables by taking corresponding ratios of the angular coefficients [103, 112].

Before discussing FFI observables, we need to make one more observation. Out of the eight independent quantities in Eq. (5.1.5)-(5.1.7), the soft form factors may be regarded as two irreducible normalisation factors in the products $n_i^\dagger n_j$. Hence, it is impossible to construct eight fully form factor independent combinations. Best-case scenario, one can build up to six clean observables, with two additional observables containing the information on the soft form factors (i.e. form factor dependent (FFD) observables).

The FFD observables we choose are the angular-integrated differential decay rate $d\Gamma/dq^2$ and the forward-backward asymmetry A_{FB} [103]

$$\frac{d\Gamma}{dq^2} = \int d\cos\theta_\ell\, d\cos\theta_{K^*}\, d\phi \frac{d^4\Gamma}{dq^2\, d\cos\theta_{K^*}\, d\cos\theta_\ell\, d\phi} = \frac{1}{4}(3J_{1c} + 6J_{1s} - J_{2c} - 2J_{2s}), \tag{5.1.12}$$

$$A_{\rm FB} = \frac{1}{d\Gamma/dq^2}\left[\int_{-1}^{0} - \int_{0}^{1}\right] d\cos\theta_\ell\,\frac{d^2\Gamma}{dq^2\,d\cos\theta_\ell} = -\frac{3J_{6s}}{3J_{1c} + 6J_{1s} - J_{2c} - 2J_{2s}}. \tag{5.1.13}$$

In the massless case, due to the relations between angular coefficients, the expressions above reduce to $d\Gamma/dq^2 = J_{1c} + 4J_{2s}$ and $A_{\rm FB} = -3J_{6s}/[4(J_{1c} + 4J_{2s})]$.

One possible choice of (clean) FFI observables is [103]

$$P_1 = \frac{|n_\perp|^2 - |n_\parallel|^2}{|n_\perp|^2 + |n_\parallel|^2} = \frac{J_3}{2J_{2s}} \tag{5.1.14}$$

$$P_2 = \frac{\mathrm{Re}(n_\perp^\dagger n_\parallel)}{|n_\perp|^2 + |n_\parallel|^2} = \frac{\beta_\ell}{8}\frac{J_{6s}}{J_{2s}} \tag{5.1.15}$$

$$P_3 = \frac{\mathrm{Im}(n_\perp^\dagger n_\parallel)}{|n_\perp|^2 + |n_\parallel|^2} = -\frac{J_9}{4J_{2s}} \tag{5.1.16}$$

$$P_4 = \frac{\mathrm{Re}(n_0^\dagger n_\parallel)}{\sqrt{|n_\parallel|^2|n_0|^2}} = \frac{\sqrt{2}J_4}{\sqrt{-J_{2c}(2J_{2s}-J_3)}} \tag{5.1.17}$$

$$P_5 = \frac{\mathrm{Re}(n_0^\dagger n_\perp)}{\sqrt{|n_\perp|^2|n_0|^2}} = \frac{\beta_\ell J_5}{\sqrt{-J_{2c}(2J_{2s}+J_3)}} \tag{5.1.18}$$

$$P_6 = \frac{\mathrm{Im}(n_0^\dagger n_\parallel)}{\sqrt{|n_\parallel|^2|n_0|^2}} = -\frac{\beta_\ell J_7}{\sqrt{-J_{2c}(2J_{2s}-J_3)}} \tag{5.1.19}$$

Then, the complete basis of observables for massless leptons above-defined reads

$$O_{m_\ell=0} = \left\{\frac{d\Gamma}{dq^2}, A_{\mathrm{FB}},\, P_{1,2,3,4,5,6}\right\}. \tag{5.1.20}$$

It is important to stress that different configurations leading to complete sets of clean observables are possible. Actually, as we will discuss in the following section, the choice above is not the most optimal and, unless otherwise stated, we will always use the new basis defined there in our analyses.

Apart from the general principles described at the beginning of this section, the optimised observables P_i are defined so that:

- They are simple ratios of the quantities in Eqs. (5.1.5)-(5.1.7) (where the form factors $\xi_{\perp,\parallel}$ cancel).
- They take values in the range $[-1, 1]$.
- They show excellent sensitivity to NP [103, 112].

5.1.3 Limitations of Optimised Observables

As it follows from the procedure we used for their construction, optimised observables P_i are only independent of the form factor input at leading order in α_s and $\Lambda_{\mathrm{QCD}}/m_b$. The exact cancellation of the soft-form factors is broken by higher-order corrections, so a residual form factor dependence is induced on the optimised observables when subleading contributions are taken into account. We can distinguish two different types of such contributions: perturbative corrections (usually from hard-gluon exchanges) and non-perturbative effects (coming from higher order $\Lambda_{\mathrm{QCD}}/m_b$ power corrections). The theoretical framework we use for dealing with these issues will be discussed at length in Chapter 6.

Furthermore, we should stress that leading order cancellation of form factors in optimised observables is only fully realised in the low-q^2 region. In general, these observables are not protected from form factor uncertainties at high-q^2 [112].

5.1.4 Further Optimising the Basis of Observables

Instead of the observable basis in Eq. (5.1.20), in our analyses we will use a slightly different one, which represents a better compromise between theoretical cleanliness and optimal experimental accessibility [103, 112, 114, 115]

$$O^{\rm opt}_{m_\ell=0} = \left\{ \frac{d\Gamma}{dq^2}, A_{\rm FB} \text{ or } F_L,\, P_{1,2,3},\, P^{(\prime)}_{4,5,6} \right\}, \tag{5.1.21}$$

where F_L is the longitudinal polarisation. See the discussion below for an explicit definition of this observable.

The unprimed basis $O_{m_\ell=0}$ is experimentally more challenging because of the difficulties these observables pose for their extraction from the angular distribution. While $P^{(\prime)}_{4,5}$ are obtained from the decay distribution by fixing F_T (transverse polarisation), $P_{4,5}$ require both the measurement of F_T and P_1, consequently reducing its discriminating power [112]. For this reason, we consider the new basis in Eq. (5.1.21) the optimal one.

There is another experimental effect we must also take into account: current experimental measurements are performed by fitting q^2-binned angular distributions (either for $B \to K^*\ell^+\ell^-$ or any other relevant decay channel). So, for a meaningful comparison of theory calculations and experimental measurements, one needs to integrate theory predictions over the kinematic ranges fixed by the experimental q^2 bins. Therefore, we define CP-averaged and CP-violating observables[1], $\langle P_i \rangle_{\rm bin}$ and $\langle P_i^{\rm CP} \rangle_{\rm bin}$, by [112]

$$\langle P_1 \rangle_{\rm bin} = \frac{1}{2}\frac{\int_{\rm bin} dq^2 [J_3 + \bar{J}_3]}{\int_{\rm bin} dq^2 [J_{2s} + \bar{J}_{2s}]}, \qquad \langle P_1^{\rm CP} \rangle_{\rm bin} = \frac{1}{2}\frac{\int_{\rm bin} dq^2 [J_3 - \bar{J}_3]}{\int_{\rm bin} dq^2 [J_{2s} + \bar{J}_{2s}]}, \tag{5.1.22}$$

$$\langle P_2 \rangle_{\rm bin} = \frac{1}{8}\frac{\int_{\rm bin} dq^2 [J_{6s} + \bar{J}_{6s}]}{\int_{\rm bin} dq^2 [J_{2s} + \bar{J}_{2s}]}, \qquad \langle P_2^{\rm CP} \rangle_{\rm bin} = \frac{1}{8}\frac{\int_{\rm bin} dq^2 [J_{6s} - \bar{J}_{6s}]}{\int_{\rm bin} dq^2 [J_{2s} + \bar{J}_{2s}]} \tag{5.1.23}$$

$$\langle P_3 \rangle_{\rm bin} = -\frac{1}{4}\frac{\int_{\rm bin} dq^2 [J_9 + \bar{J}_9]}{\int_{\rm bin} dq^2 [J_{2s} + \bar{J}_{2s}]}, \qquad \langle P_3^{\rm CP} \rangle_{\rm bin} = -\frac{1}{4}\frac{\int_{\rm bin} dq^2 [J_9 - \bar{J}_9]}{\int_{\rm bin} dq^2 [J_{2s} + \bar{J}_{2s}]}, \tag{5.1.24}$$

$$\langle P_4' \rangle_{\rm bin} = \frac{1}{\mathcal{N}'_{\rm bin}} \int_{\rm bin} dq^2 [J_4 + \bar{J}_4], \qquad \langle P_4'^{\rm CP} \rangle_{\rm bin} = \frac{1}{\mathcal{N}'_{\rm bin}} \int_{\rm bin} dq^2 [J_4 - \bar{J}_4], \tag{5.1.25}$$

$$\langle P_5' \rangle_{\rm bin} = \frac{1}{2\mathcal{N}'_{\rm bin}} \int_{\rm bin} dq^2 [J_5 + \bar{J}_5], \qquad \langle P_5'^{\rm CP} \rangle_{\rm bin} = \frac{1}{2\mathcal{N}'_{\rm bin}} \int_{\rm bin} dq^2 [J_5 - \bar{J}_5], \tag{5.1.26}$$

$$\langle P_6' \rangle_{\rm bin} = \frac{-1}{2\mathcal{N}'_{\rm bin}} \int_{\rm bin} dq^2 [J_7 + \bar{J}_7]\ , \qquad \langle P_6'^{\rm CP} \rangle_{\rm bin} = \frac{-1}{2\mathcal{N}'_{\rm bin}} \int_{\rm bin} dq^2 [J_7 - \bar{J}_7], \tag{5.1.27}$$

where $\bar{J}_i$ are the CP-conjugate angular coefficients and the normalization $\mathcal{N}'_{\rm bin}$ is defined as

$$\mathcal{N}'_{\rm bin} = \sqrt{-\int_{\rm bin} dq^2 [J_{2s} + \bar{J}_{2s}] \int_{\rm bin} dq^2 [J_{2c} + \bar{J}_{2c}]}. \tag{5.1.28}$$

An exhaustive characterisation of the q^2-binned angular distribution needs to add another observable to the basis $O^{\rm opt}_{m_\ell=0}$. This observable is called P_8' and it was defined in Ref. [115], with the

[1] Our analyses do not explicitly test CP-violation in the various $b \to s\ell\ell$ decay channels, so we will only work with CP-averaged observables. However, for completeness, here we also define their CP-violating counterparts.

following structure (in CP-averaged and CP-violating form)

$$\langle P_8' \rangle_{\rm bin} = \frac{-1}{\mathcal{N}'_{\rm bin}} \int_{\rm bin} dq^2 [J_8 + \bar{J}_8] \,, \qquad \langle P_8'^{\rm CP} \rangle_{\rm bin} = \frac{-1}{\mathcal{N}'_{\rm bin}} \int_{\rm bin} dq^2 [J_8 - \bar{J}_8] \,. \tag{5.1.29}$$

Indeed, this observable is redundant in the continuum, as it can be written in terms of the other observables in the $O^{\rm opt}_{m_\ell=0}$ basis [115]. However, the binning procedure breaks this redundancy.

Analogous definitions for the q^2-bin integrated unprimed observables $\langle P_i^{\rm CP} \rangle_{\rm bin}$ (with $i = 4, 5, 6, 8$) can be found in Appendix A of Ref. [112].

It is important to stress here that these definitions are general and also hold for the massive case ($m_\ell \neq 0$) and in presence of scalar and tensor contributions. In the infinitesimal binning limit, the observables $\langle P^{(\prime)}_{1,\ldots,6} \rangle_{\rm bin}$ in Eqs. (5.1.22)-(5.1.27) reduce to their definitions as continuous functions of q^2, with only some small differences related to lepton mass effects (such as the case of P_2 [115]).

Finally, there are some important FFD observables that should be discussed. These are the CP-averaged *branching ratio* $\mathcal{B}(B \to K^*\ell^+\ell^-)$, the *CP asymmetry* A_{CP}, both the CP-averaged and CP-violating *forward-backward asymmetry* and the *longitudinal polarisation fraction*[2] F_L of the K^* meson (again in CP-averaged and CP-violating forms).

$$\langle A_{FB} \rangle = -\frac{3}{4} \frac{\int dq^2 \, [J_{6s} + \bar{J}_{6s}]}{\langle d\Gamma/dq^2 \rangle + \langle d\bar{\Gamma}/dq^2 \rangle}, \qquad \langle A_{FB}^{\rm CP} \rangle = -\frac{3}{4} \frac{\int dq^2 \, [J_{6s} - \bar{J}_{6s}]}{\langle d\Gamma/dq^2 \rangle + \langle d\bar{\Gamma}/dq^2 \rangle}, \tag{5.1.30}$$

$$\langle F_L \rangle = -\frac{\int dq^2 \, [J_{2c} + \bar{J}_{2c}]}{\langle d\Gamma/dq^2 \rangle + \langle d\bar{\Gamma}/dq^2 \rangle}, \qquad \langle F_L^{\rm CP} \rangle = -\frac{\int dq^2 \, [J_{2c} - \bar{J}_{2c}]}{\langle d\Gamma/dq^2 \rangle + \langle d\bar{\Gamma}/dq^2 \rangle}, \tag{5.1.31}$$

$$\left\langle \frac{d\mathcal{B}}{dq^2} \right\rangle = \tau_B \frac{\langle d\Gamma/dq^2 \rangle + \langle d\bar{\Gamma}/dq^2 \rangle}{2}, \qquad \langle A_{\rm CP} \rangle = \frac{\langle d\Gamma/dq^2 \rangle - \langle d\bar{\Gamma}/dq^2 \rangle}{\langle d\Gamma/dq^2 \rangle + \langle d\bar{\Gamma}/dq^2 \rangle} \,, \tag{5.1.32}$$

where τ_B denotes the lifetime of the given B meson involved in the decay and it is to be understood that q^2-averages are taken within suitable q^2-bins fixed by experiments. Usually, we will not use the notation $\langle d\mathcal{B}/dq^2 \rangle$ for the branching ratio of a given process, but rather simply $\mathcal{B}(B \to K^*\ell^+\ell^-)$ (changing the process in parenthesis when necessary). Also, following Eq. (5.1.12), we define

$$\left\langle \frac{d\Gamma}{dq^2} \right\rangle = \frac{1}{4} \int dq^2 [3J_{1c} + 6J_{1s} - J_{2c} - 2J_{2s}]. \tag{5.1.33}$$

5.1.5 CP-averages and CP-asymmetries: S_i and A_i

Other $B \to K^*\ell^+\ell^-$ analyses are based on descriptions of the angular distribution with different observables [31, 116]. A very accessible basis from the experimental point of view can be defined by means of the CP-averaged angular coefficients S_i and the CP-asymmetries A_i [31]

$$\langle S_i \rangle = \frac{\int dq^2 \, [J_i + \bar{J}_i]}{\langle d\Gamma/dq^2 \rangle + \langle d\bar{\Gamma}/dq^2 \rangle}, \qquad \langle A_i \rangle = \frac{\int dq^2 \, [J_i - \bar{J}_i]}{\langle d\Gamma/dq^2 \rangle + \langle d\bar{\Gamma}/dq^2 \rangle}. \tag{5.1.34}$$

These observables clearly conform with the symmetries of the angular distribution, as they are defined in terms of angular coefficients. Despite their normalisation to the CP-averaged angular distribution, which may achieve some cancellations and reduce both theoretical and experimental uncertainties, these observables are not clean (unlike the optimised observables P_i). Indeed, they

[2] The *transverse polarisation fraction* F_T can be defined in terms of F_L as $F_T = 1 - F_L$.

are not constructed to exploit the form factor simplifications emerging at large recoil, so no exact cancellation of form factors is possible within them and consequently they show strong sensitivity to the choice of soft form factors. Therefore, this basis is less competitive for NP searches than descriptions based on optimised observables. See Refs. [112] and [113] for in-depth comparative studies of the properties of these two bases.

5.1.6 Theory vs LHCb conventions

As it was observed in Ref. [113], standard theory conventions [31, 103, 112] used to define the angles of the $B \to K^*\ell^+\ell^-$ decay distribution differ from the ones used by the experimental collaborations [117] (LHCb in particular). Our particular definition of the decay distribution follows the one introduced in Ref. [31]. Comparing with Refs. [118, 119], where the authors provided a dictionary connecting both theory and LHCb conventions, we find that our definition of angles is related to that of the LCHb by [113]

$$\theta_{K^*}^{\rm LHCb} = \theta_{K^*}, \qquad \theta_\ell^{\rm LHCb} = \pi - \theta_\ell, \qquad \phi^{\rm LHCb} = -\phi, \tag{5.1.35}$$

leading to the following relative signs at the level of the S_i observables

$$S_{4,6c,6s,8,9}^{\rm LHCb} = -S_{4,6c,6s,8,9}, \tag{5.1.36}$$

with the other CP-averaged angular coefficients unaffected. Regarding the optimised observables P_i, relative signs have to be combined with the fact that LHCb uses different numerical factors to define some of the P_i observables. Taking these two effects together, one obtains the following dictionary [113]

$$P_1^{\rm LHCb} = P_1, \qquad P_2^{\rm LHCb} = -P_2, \qquad P_3^{\rm LHCb} = P_3, \tag{5.1.37}$$

$$P_4^{\prime\rm LHCb} = -(1/2)P_4', \qquad P_5^{\prime\rm LHCb} = P_5', \qquad P_6^{\prime\rm LHCb} = P_6', \qquad P_8^{\prime\rm LHCb} = -(1/2)P_8'. \tag{5.1.38}$$

5.2 $B_s \to \phi\ell^+\ell^-$: tagging degeneracy and time-integrated observables

Unlike $B \to K^*\ell^+\ell^-$ decays with *neutral* B mesons, $B_s \to \phi\ell^+\ell^-$ processes very predominantly decay into CP-eigenstates[3]. Indeed, the current most precise experimental determination of this mode was obtained by the LHCb by measuring the $B_s \to \phi(\to K^+K^-)\mu^+\mu^-$ angular distribution [121]. Thus, the main difference between this decay and $B \to K^*\ell^+\ell^-$ is that the former is not self-tagging, that is, the final state does not contain enough information to discriminate whether the initial state was a B_s or its CP-conjugate $\bar{B}_s$.

Because of the aforementioned absence of self-flavour tagging in $B_s \to \phi(\to K^+K^-)\mu^+\mu^-$, and under the assumption of equal production of B_s and $\bar{B}_s$ mesons, what is actually measured at the experiments is $d\Gamma(B_s \to \phi(\to K^+K^-)\mu^+\mu^-) + d\Gamma(\bar{B}_s \to \phi(\to K^+K^-)\mu^+\mu^-)$. Therefore, because of the relative signs between J_i and $\bar{J}_i$ (see Eq. (4.2.12)), these measurements only have access to the following CP-combinations of angular coefficients J_i [122, 123]

$$\langle J_i + \bar{J}_i \rangle \qquad \text{for } i = 1s,\ 1c,\ 2s,\ 2c,\ 3,\ 4,\ 7, \tag{5.2.1}$$

$$\langle J_i - \bar{J}_i \rangle \qquad \text{for } i = 5,\ 6s,\ 6c,\ 8,\ 9, \tag{5.2.2}$$

[3] Notice that ϕ decays to K^+K^- and $K_S^0K_L^0$ make up to more than 80% of its total decay width [120].

where J_i and $\bar{J}_i$ have the same structure in terms of transversity amplitudes as for flavour-specific decays, Eqs. (4.3.1)-(4.3.6). The experimental analysis of Ref. [121] provided measurements of the CP-averaged angular coefficients $S_{3,4,7}$ and the CP-asymmetries $A_{5,6,8,9}$, where all these measurements correspond to time-integrated quantities (see the discussion below). Since we are not evaluating CP-violation in our analyses, only the first ones will be relevant for our global fits in Chapter 8, which we will recast as P_1, P_4' and P_6' using the covariance matrix in Ref. [121].

As hinted above, in $B_s \to \phi(\to K^+K^-)\mu^+\mu^-$ the final state can be produced by both the decay of a B_s or $\bar{B}_s$ meson, so $B_s - \bar{B}_s$ mixing and the direct decay interfere, from a quantum mechanical point of view. This induces additional time-dependent contributions to the decay amplitude, and hence to the angular distribution. Time dependent effects can be accounted for by introducing time-dependent transversity amplitudes $A_X(t)$ [122, 124], where $X = L\,0,\ R\,0,\ L\perp,\ R\perp,\ L\parallel,\ R\parallel$. Then, one can write the decay distribution in terms of time-dependent angular coefficients, which are obtained by replacing the usual transversity amplitudes by time-dependent ones [122–124]

$$J_i(t) = J_i(A_X \to A_X(t)), \qquad \bar{J}_i(t) = \bar{J}_i(A_X \to A_X(t)). \tag{5.2.3}$$

These time-dependent angular coefficients can be written as functions of the (non time-dependent) coefficients J_i and $\tilde{J}_i$[4], which we can determine from flavour-specific decays, and two extra angular observables s_i and h_i [122]

$$J_i(t) + \tilde{J}_i(t) = \mathrm{e}^{-\Gamma_s t}\left[(J_i + \tilde{J}_i)\cosh(y\Gamma_s t) - h_i \sinh(y\Gamma_s t)\right], \tag{5.2.4}$$

$$J_i(t) - \tilde{J}_i(t) = \mathrm{e}^{-\Gamma_s t}\left[(J_i - \tilde{J}_i)\cosh(y\Gamma_s t) - s_i \sinh(y\Gamma_s t)\right], \tag{5.2.5}$$

where $\Gamma_s \equiv (\Gamma_{L_s} + \Gamma_{H_s})/2$, $x \equiv \Delta m_s/\Gamma_s$ (with $\Delta m_s = m_{H_s} - m_{L_s}$) and $y \equiv \Delta\Gamma_s/(2\Gamma_s)$ (with $\Delta\Gamma_s \equiv \Gamma_{L_s} - \Gamma_{H_s}$), being Γ_{L_s} (Γ_{H_s}) and m_{H_s} (m_{L_s}) the width and mass of the lighter (heavier) mass eigenstate [124].

Using this formalism, theoretically accounting for measurements of time-integrated observables in hadronic experiments (like LHCb) amounts to including $O(\Delta\Gamma_s/\Gamma_s)$ corrections to the analogous $B \to K^*\ell\ell$ expressions [122]

$$\langle J_i(t) + \tilde{J}_i(t)\rangle_t = \frac{1}{\Gamma_s}\left[\frac{1}{1-y^2}(J_i + \tilde{J}_i) - \frac{y}{1-y^2}h_i\right], \tag{5.2.6}$$

$$\langle J_i(t) - \tilde{J}_i(t)\rangle_t = \frac{1}{\Gamma_s}\left[\frac{1}{1-y^2}(J_i - \tilde{J}_i) - \frac{y}{1-y^2}s_i\right], \tag{5.2.7}$$

with the notation $\langle . \rangle_t$ here meaning time-averaged quantities, not to be confused with the usual brackets $\langle . \rangle$ denoting q^2-averages. Hence, the same complete basis of optimised observables that fully characterises the $B \to K^*\ell^+\ell^-$ mode can be constructed for $B_s \to \phi\ell^+\ell^-$ by means of the corresponding replacements

$$J_i + \tilde{J}_i \longrightarrow \langle J_i(t) + \tilde{J}_i(t)\rangle_t\,, \tag{5.2.8}$$

$$J_i - \tilde{J}_i \longrightarrow \langle J_i(t) - \tilde{J}_i(t)\rangle_t\,. \tag{5.2.9}$$

in the definitions of the observables in Section 5.1.4 .

[4]The angular coefficients $\tilde{J}_i$ are defined such that $\tilde{J}_i = \zeta_i \bar{J}_i$, where the symbol ζ_i follows that $\zeta_i = 1$ for $i =$ $1s$, $1c$, $2s$, $2c$, 3, 4, 7, and $\zeta_i = -1$ for $i = 5$, $6s$, $6c$, 8, 9 [122].

5.3 $B \to K\ell^+\ell^-$: Decay Distribution and Observables

The semileptonic decay $B \to K\ell^+\ell^-$ also allows for important tests of the SM. Indeed, some of the most important anomalies involve observables defined within this decay channel, as we will discuss in Chapter 8. In this section, we will provide a general description of the dynamics governing the aforementioned decay and we will introduce its most relevant observables.

Since both $B \to K\ell^+\ell^-$ and $B \to K^*\ell^+\ell^-$ are processes driven by the same underlying $b \to s$ transition, the effective Hamiltonian of Eq. (4.1.1) can be used for their description. Therefore, proceeding as in Section 4.2.1, but now using the corresponding form factors defined in Eqs. (2.1.2)-(2.1.2), the matrix element of the $B \to K\ell^+\ell^-$ decay can be written as [125]

$$\begin{aligned}\mathcal{M}(\bar{B} \to K\ell\bar{\ell}) &= \langle \ell(p_-)\bar{\ell}(p_+)K(k)|\, \mathcal{H}_{\text{eff}}\, |\bar{B}(p)\rangle \\ &= \frac{G_F\alpha}{\sqrt{2}\pi} V_{ts}^* V_{tb} \left\{ F_S(\bar{\ell}\ell) + F_P(\bar{\ell}\gamma_5\ell) + F_V p_\mu(\bar{\ell}\gamma^\mu\ell) + F_A p_\mu(\bar{\ell}\gamma^\mu\gamma_5\ell) \right\},\end{aligned} \tag{5.3.1}$$

where p, k, p_- and p_+ are the momenta of the B meson, kaon K, lepton and anti-lepton, respectively. Correspondingly, m_B, m_K and m_ℓ will denote their masses. The Lorentz-invariant *structure functions* $F_{S,P,V,A}$ contain contributions coming from scalar, pseudo-scalar, vector and axial-vector operators. In general, tensor operators can also contribute to the matrix element, however no further consideration will be given to them here. These structure functions present the following form [125],

$$F_S = \frac{1}{2}(m_B^2 - m_K^2) f_0(q^2) \left(\frac{\mathcal{C}_S m_b + \mathcal{C}_S' m_s}{m_b - m_s} \right), \tag{5.3.2}$$

$$\begin{aligned}F_P = &-m_\ell \mathcal{C}_{10} \left\{ f_+(q^2) - \frac{m_B^2 - m_K^2}{q^2} \left(f_0(q^2) - f_+(q^2) \right) \right\} \\ &+ \frac{1}{2}(m_B^2 - m_K^2) f_0(q^2) \left(\frac{\mathcal{C}_P m_b + \mathcal{C}_P' m_s}{m_b - m_s} \right),\end{aligned} \tag{5.3.3}$$

$$F_A = \mathcal{C}_{10} f_+(q^2), \tag{5.3.4}$$

$$F_V = \mathcal{C}_9^{\text{eff}} f_+(q^2) + 2\mathcal{C}_7^{\text{eff}} m_b \frac{f_T(q^2)}{m_B + m_K}, \tag{5.3.5}$$

with $q^2 = (p_+ + p_-)^2$ the invariant mass of the dilepton pair and $\mathcal{C}_9^{\text{eff}}$ encoding both the short distance $\mathcal{C}_9$ coefficient and the leading-order four-quark loop function $Y(q^2)$, as defined in Eq. (4.1.21).

The $B \to K\ell^+\ell^-$ process gives access to a double decay distribution with respect to the dilepton mass squared q^2 and the angle θ_ℓ between the B meson and the ℓ^- line of flight, as measured from the dilepton rest frame. In the literature, the spectrum of this process is parametrised as [126–128]

$$\frac{1}{\Gamma_\ell} \frac{d\Gamma_\ell}{d\cos\theta_\ell} = \frac{3}{4}(1 - F_H^\ell)(1 - \cos^2\theta_\ell) + \frac{1}{2} F_H^\ell + A_{FB}^\ell \cos\theta_\ell. \tag{5.3.6}$$

Note that the distribution above is determined by two quantities: a *flat term* F_H^ℓ and a linear term in $\cos\theta_\ell$, containing the forward-backward asymmetry A_{FB}^ℓ. While these two observables are negligible for electrons and muons in the SM (indeed $A_{FB}^{\ell\,\text{SM}} = 0$ and $F_H^{\ell\,\text{SM}} \propto m_\ell^2$), they are sensitive to the presence of scalar/pseudoscalar and tensor operators. We make the lepton flavour ℓ explicit in all quantities as they can correspond to different leptons in the final state ($\ell = e$, μ

or τ). Actually, combinations of observables with different lepton flavours can be constructed to test whether physics is the same for all flavours (as predicted by the SM) or not. Even though it was not specifically mentioned in Section 5.1, clearly $B \to K^*\ell^+\ell^-$ observables are lepton flavour dependent and they can also be used to test differences between flavours, as we will thoroughly investigate in Chapter 7.

On the other hand, from the theory perspective, the decay distribution can be computed from the matrix element of the process. Squaring Eq. (5.3.1), averaging over all lepton polarisations and introducing the corresponding phase space factors one finds [126]

$$\frac{d^2\Gamma_\ell}{dq^2 d\cos\theta_\ell} = a_\ell(q^2) + b_\ell(q^2)\cos\theta_\ell + c_\ell(q^2)\cos^2\theta_\ell, \tag{5.3.7}$$

where the a_ℓ, b_ℓ and c_ℓ coefficients have been defined as [126]

$$\frac{a_\ell(q^2)}{\Gamma_0 \lambda^{1/2}\beta_\ell} = q^2\left(\beta_\ell^2|F_S|^2 + |F_P|^2\right) + \frac{\lambda}{4}\left(|F_A|^2 + |F_V|^2\right) \\ + (m_B^2 - m_K^2 + q^2)\mathrm{Re}\left[F_P F_A^*\right] + 4m_\ell^2 m_B^2 |F_A|^2, \tag{5.3.8}$$

$$\frac{b_\ell(q^2)}{\Gamma_0 \lambda^{1/2}\beta_\ell} = 2m_\ell \lambda^{1/2}\beta_\ell \mathrm{Re}\left[F_S F_V^*\right], \tag{5.3.9}$$

$$\frac{c_\ell(q^2)}{\Gamma_0 \lambda^{1/2}\beta_\ell} = -\frac{\lambda}{4}\beta_\ell^2\left(|F_A|^2 + |F_V|^2\right), \tag{5.3.10}$$

with

$$\Gamma_0 = \frac{G_F^2 \alpha_{\mathrm{EM}}^2}{2^9\pi^5 m_B^3}\left|V_{tb}V_{ts}^*\right|, \tag{5.3.11}$$

and the functions $\lambda = \lambda(m_B^2, m_K^2, q^2)$ and β_ℓ can be found under Eq. (4.2.38).

For a complete treatment of the $B \to K\ell^+\ell^-$ decay, where expressions for a_ℓ, b_ℓ and c_ℓ including contributions from tensor operators are given, we refer the interested reader to Refs. [126, 128]. Since in the SM scalar and pseudoscalar operators are suppressed by terms of the order of $m_\ell m_{b,s}/M_W^2$ [125], the structure function F_P in Eq. (5.3.3) simplifies considerably and $F_S = 0$ in the SM. Then, it follows that $b_\ell^{\mathrm{SM}} = 0$ and also $a_\ell^{\mathrm{SM}} = -c_\ell^{\mathrm{SM}}$, the latter holding only in the limit of massless leptons $m_\ell \to 0$.

The angular distribution is measured in integrated q^2 bins, therefore theory computations must be averaged over q^2 accordingly [126]

$$\left\langle \frac{d^2\Gamma_\ell}{dq^2 d\cos\theta_\ell} \right\rangle_{\mathrm{bin}} = \langle a_\ell \rangle_{\mathrm{bin}} + \langle b_\ell \rangle_{\mathrm{bin}}\cos\theta_\ell + \langle c_\ell \rangle_{\mathrm{bin}}\cos^2\theta_\ell, \tag{5.3.12}$$

with the phase space boundaries

$$4m_\ell^2 \le q^2 \le (m_B - m_K)^2, \qquad -1 \le \cos\theta_\ell \le 1, \tag{5.3.13}$$

and the q^2-integrated coefficients defined as [126]

$$\langle a_\ell \rangle_{\mathrm{bin}} = \int_{\mathrm{bin}} dq^2\, a_\ell(q^2), \qquad \langle b_\ell \rangle_{\mathrm{bin}} = \int_{\mathrm{bin}} dq^2\, b_\ell(q^2), \qquad \langle c_\ell \rangle_{\mathrm{bin}} = \int_{\mathrm{bin}} dq^2\, c_\ell(q^2). \tag{5.3.14}$$

Using the quantities in Eq. (5.3.14), we can write the integrated branching ratio and the normalised forward-backward asymmetry as follows [126]

$$\mathcal{B}(B \to K\ell^+\ell^-) = \tau_B \left\langle \frac{d\Gamma_\ell}{dq^2} \right\rangle = 2\tau_B \left(\langle a_\ell \rangle + \frac{1}{3} \langle c_\ell \rangle \right), \tag{5.3.15}$$

$$\langle A_{FB}^\ell \rangle \equiv \frac{1}{\langle d\Gamma_\ell/dq^2 \rangle} \left[\int_0^1 - \int_{-1}^0 \right] d\cos\theta_\ell \left\langle \frac{d^2\Gamma_\ell}{dq^2 d\cos\theta_\ell} \right\rangle = \frac{\langle b_\ell \rangle}{\langle d\Gamma_\ell/dq^2 \rangle}, \tag{5.3.16}$$

where τ_B is the B meson lifetime and the "bin" subscripts have been dropped for simplicity. Moreover, requiring the decay distribution in Eq. (5.3.7) to agree with the parametrisation in Eq. (5.3.6), one finds the structure of the flat term [126]

$$\langle F_H^\ell \rangle = \frac{2}{\langle d\Gamma_\ell/dq^2 \rangle} \left(\langle a_\ell \rangle + \langle c_\ell \rangle \right). \tag{5.3.17}$$

Observables $\langle A_{FB}^\ell \rangle$ and $\langle F_H^\ell \rangle$ are expected to have reduced uncertainties with respect to the branching ratio $\mathcal{B}(B \to K\ell^+\ell^-)$, as a result of the cancellations between the numerator in Eqs. (5.3.16) and (5.3.17) and the integrated total decay rate $\langle d\Gamma_\ell/dq^2 \rangle$ in the denominator.

Finally, we introduce a very important observable in $B \to K\ell^+\ell^-$: the lepton flavour universality ratio R_K[5]. This observable probes lepton flavour universality effects in and beyond the SM [126, 129]

$$\langle R_K \rangle \equiv \frac{\mathcal{B}(B \to K\mu^+\mu^-)}{\mathcal{B}(B \to Ke^+e^-)} = \int_{\text{bin}} dq^2 \frac{d\Gamma_\mu}{dq^2} \Big/ \int_{\text{bin}} dq^2 \frac{d\Gamma_e}{dq^2} = \frac{\langle d\Gamma_\mu/dq^2 \rangle \langle F_H^\mu \rangle - 4/3 \langle c_\mu \rangle}{\langle d\Gamma_e/dq^2 \rangle}. \tag{5.3.18}$$

If lepton masses are neglected, the SM predicts the same decay rate for processes with muons and electrons in the final state. This can be explicitly seen in branching ratios for q^2 bins such that $q^2_{\text{bin, min}} \geq 1$ GeV (since $m_\ell^2/q^2 \simeq 0$ for $\ell = \mu$ and e). Hence, $R_K^{\text{SM}} = 1$ and any deviation of R_K from one will signal to NP effects with different couplings to muons and electrons (i.e. NP with non-universal lepton couplings).

One can see that $\langle R_K \rangle$ and $\langle F_H^\ell \rangle$ are model-independently related [126]

$$\langle R_K \rangle \left(1 - \langle F_H^\mu \rangle - \Delta \right) = 1, \tag{5.3.19}$$

with

$$\Delta = \frac{4}{3} \frac{\langle c_e \rangle - \langle c_\mu \rangle}{\langle d\Gamma_\mu/dq^2 \rangle} - \frac{\langle F_H^e \rangle}{\langle R_K \rangle}. \tag{5.3.20}$$

Observe that the structure of Δ simplifies to $\Delta \propto m_\mu^2$, if chirally flipped couplings to electrons can be neglected (and in the approximation $m_e \simeq 0$), as $\langle F_H^e \rangle = 0$ and $\langle d\Gamma_e/dq^2 \rangle = -4/3 \langle c_e \rangle$ in this context. Therefore, in the SM and NP extensions that do not involve electronic right-handed currents, the relation between $\langle R_K \rangle$ and $\langle F_H^\ell \rangle$ is proportional to lepton mass effects.

5.4 Other decay channels

To conclude, we briefly review several other important observables involving exclusive and inclusive $b \to s$ decay modes. Some of them will prove very relevant for our global analyses in Chapter 8, as they pose stringent constraints on a limited number of Wilson coefficients.

[5] Here we use $\langle R_K \rangle$ for denoting the q^2-binned version of this observable. However, in a slight abuse of notation, it is also common to use R_K instead of $\langle R_K \rangle$ for its q^2-average.

$a_{(0,0)} = 3.36 \quad \delta_a = 0.23$	$a_{(0,7)} = -14.81$	$a_{(7,7)} = 16.68$	$a_{(0,7')} = -0.23$

Table 5.1: Coefficients describing the dependence of $\mathcal{B}(B \to X_s\gamma)$ on $\mathcal{C}_7$ and $\mathcal{C}_{7'}$ [85, 113].

5.4.1 $B \to X_s\gamma$ and $B \to X_s\mu^+\mu^-$

The electromagnetic and semileptonic inclusive decays $B \to X_s\gamma$ and $B \to X_s\mu^+\mu^-$ provide important constraints on the electromagnetic dipole and semileptonic operators $\mathcal{O}_{7^{(\prime)}}$ and $\mathcal{O}_{9^{(\prime)},10^{(\prime)}}$. In our analyses, we consider the branching ratio of both channels, $\mathcal{B}(B \to X_s\gamma)_{E_\gamma \geq 1.6\,\mathrm{GeV}}$ and $\mathcal{B}(B \to X_s\mu^+\mu^-)_{[1,6]}$, with the former being the observable rendering the strongest bound on the electromagnetic Wilson coefficients $\mathcal{C}_{7^{(\prime)}}$ [85, 113, 130].

We use the following parametrisation for $\mathcal{B}(B \to X_s\gamma)_{E_\gamma \geq 1.6\,\mathrm{GeV}}$ [85]

$$\mathcal{B}(B \to X_s\gamma)_{E_\gamma \geq 1.6\,\mathrm{GeV}} = \Big[a_{(0,0)} \pm \delta_a + a_{(0,7)}\delta\mathcal{C}_7 + a_{(0,7')}\delta\mathcal{C}_{7'} \tag{5.4.1}$$

$$+ a_{(7,7)}\left(\delta\mathcal{C}_7^2 + \delta\mathcal{C}_{7'}^2\right)\Big] \times 10^{-4}, \tag{5.4.2}$$

where $\delta\mathcal{C}_i = \mathcal{C}_i - \mathcal{C}_i^{\mathrm{SM}}$ and the values of the parameters $a_{(i,j)}$, with $(i,j) = (0,0), (0,7), (0,7')$, are collected in Table 5.1. This expression was first introduced in Ref. [85], based on the next-to-next-to-leading order SM computations of Refs. [92, 131, 132]. Note that $a_{(0,0)}$ and δ_a encode the SM prediction of the aforementioned observable. An update of these results was provided in Ref. [133], including all QCD corrections up to $O(\alpha_s^2)$ and new estimates of the relevant non-perturbative effects. This induced a shift on the central value of the SM prediction, which is reflected in the corresponding change on the value of $a_{(0,0)}$ with respect to that of Ref. [85].

On the other hand, the branching ratio $\mathcal{B}(B \to X_s\mu^+\mu^-)$ of the inclusive semileptonic decay at low-q^2 (from 1 to 6 GeV^2) takes following form [85]

$$\mathcal{B}(B \to X_s\mu^+\mu^-)_{[1,6]} = \left[\sum_{i,j=0,7^{(\prime)},9^{(\prime)},10^{(\prime)}} b_{(i,j)}\delta\mathcal{C}_i\delta\mathcal{C}_j \pm \delta_b\right] \times 10^{-7}, \tag{5.4.3}$$

with the definition $\delta\mathcal{C}_0 = 1$. All non-zero $b_{(i,j)}$ parameters can be found in Table 5.2. This parametrisation was obtained in terms of the computations in Refs [93] and [134], for further discussions on the details of its derivation we refer to Appendix B.4 of Ref [85]. Since the terms based on interferences between SM and chirally flipped operators are extracted from the $O(\alpha_s^0)$ calculations of Ref. [134], the error estimate presented in Table 5.2 for the central value of $\mathcal{B}(B \to X_s\mu^+\mu^-)_{[1,6]}$ accounts both for the variation of fundamental input parameters and the 5% error assignment proposed in Ref [93] for the unknown $\Lambda_{\mathrm{QCD}}/m_b$ power corrections. It is important to stress that, in our current analysis, contributions to $B \to X_s\mu^+\mu^-$ coming from logarithmically enhanced electromagnetic corrections [135] are also included.

In both cases, while the SM parameters of these observables are modified accordingly to account for the changes in their theory predictions, NP contributions have been left untouched. This is justified as NP contributions to these observables are expected to be small [113], so there is no need to include higher order contributions to these effects considering the current level of accuracy.

$b_{(0,0)} = 15.86 \quad \delta_b = 1.51$		
$b_{(0,7)} = -0.517$	$b_{(0,9)} = 2.663$	$b_{(0,10)} = -4.679$
$b_{(0,7')} = -0.680$	$b_{(0,9')} = -0.049$	$b_{(0,10')} = 0.061$
$b_{(7,7)} = b_{(7',7')} = 27.776$	$b_{(9,9)} = b_{(9',9')} = 0.534$	$b_{(10,10)} = b_{(10',10')} = 0.543$
$b_{(7,7')} = -0.399$	$b_{(9,9')} = -0.014$	$b_{(10,10')} = -0.014$
$b_{(7,9)} = b_{(7',9')} = 4.920$	$b_{(7,9')} = b_{(7',9)} = -0.113$	

Table 5.2: Coefficients describing the dependence of $\mathcal{B}(B \to X_s\mu^+\mu^-)$ on $\mathcal{C}_{7,9,10}$ and $\mathcal{C}_{7',9',10'}$ [85, 113].

$c = 4.11\%$	$\delta c = 2.52\%$
$d_0 = 1$	$d_1 = -2.51757$
$e_{(0,0)} = 1$	$e_{(1,0)} = -5.0165$
$e_{(0,1)} = -0.0919061$	$e_{(2,0)} = 6.30856$
$e_{(0,2)} = 7.49847$	

Table 5.3: Coefficients describing the dependence of $A_I(B \to K^*\gamma)$ on $\mathcal{C}_7$ and $\mathcal{C}_{7'}$ [85].

5.4.2 Exclusive $b \to s\gamma$ decays

Several exclusive radiative $b \to s\gamma$ decays are included in our analyses. The branching ratios of the decays $B \to K\gamma$, $B \to K^*\gamma$ and $B \to \phi\gamma$ are treated by using the same framework developed for studying the analogous semileptonic decays, taking the limit $q^2 \to 0$ [136]. Other $b \to s\gamma$ observables, that deserve further theory considerations, are also included: the isospin asymmetry $A_I(B \to K^*\gamma)$ and the $B \to K^*\gamma$ time-dependent CP asymmetry parameter $S_{K^*\gamma}$.

The isospin asymmetry $A_I(B \to K^*\gamma)$ vanishes within the SM in the naive factorisation limit [85]. Hence, all non-negligible SM contributions to this observable originate from non-factorisable contributions to the amplitude of the process, particularly from topologies where a photon is emitted from the spectator quark line. As a result, the observable $A_I(B \to K^*\gamma)$, being dominated by $O(\Lambda_{\rm QCD}/m_b)$ contributions, is expected to be very sensitive to hadronic uncertainties. This could be used as a discrimination criterion for not including the aforementioned observable in our analyses, however it gives direct access to the electromagnetic coefficients $\mathcal{C}_{7^{(\prime)}}$, with no interference from semileptonic operators, and thus it is a good probe for NP in these operators [85].

The corresponding numerical expression used for $A_I(B \to K^*\gamma)$ reads [85]

$$A_I(B \to K^*\gamma) = c \times \frac{\sum_k d_k\, \delta\mathcal{C}_7^k}{\sum_{k,l} e_{(k,l)}\, \delta\mathcal{C}_7^k \delta\mathcal{C}_{7'}^l} \pm \delta_c, \tag{5.4.4}$$

where $k, l = 0, 1, 2$ and the non-zero d_k and $e_{(k,l)}$ coefficients are displayed in Table 5.3.

$f = -0.0297336$	$\delta_f^u = 0.0089893$ $\delta_f^d = 0.0089767$
$g_{(0,1)} = +152.774$	$h_{(0,0)} = +39.9999$
$g_{(1,0)} = -3.17764$	$h_{(0,1)} = -4.51218$
$g_{(1,1)} = -415.441$	$h_{(1,0)} = -214.866$
$g_{(0,2)} = +8.63917$	$h_{(0,2)} = +290.553$
$g_{(2,0)} = +8.63917$	$h_{(2,0)} = +290.553$

Table 5.4: Coefficients describing the dependence of $S_{K^*\gamma}$ on $\mathcal{C}_7$ and $\mathcal{C}_{7'}$ [85].

More interesting is the CP structure of the $B \to K^*\gamma$ decay. Because of the left-handed structure of weak interactions in the SM, transitions involving a b quark will predominantly require the emission of a left-handed photon, while transitions with a $\bar{b}$ quark will demand a right-handed photon [85]. More in detail, looking at the structure of the effective operator $\mathcal{O}_7$ in Eq. (4.1.14), one can see that $b \to s\gamma$ decays with a right-handed photon are suppressed by a factor m_s/m_b[6]. This suppression can be alleviated within several NP scenarios, therefore observables characterising CP violation in $B \to K^*\gamma$ are particularly interesting for testing NP in $\mathcal{C}_{7'}$.

In our analyses, these effects are accounted for by including the parameter $S_{K^*\gamma}$ in the time-dependent CP asymmetry $A_{CP}(B^0 \to K^{*0}\gamma)$ [137, 138]

$$A_{CP}(B^0 \to K^{*0}\gamma) = \frac{\Gamma(\bar{B}^0(t) \to \bar{K}^{*0}\gamma) - \Gamma(B^0(t) \to K^{*0}\gamma)}{\Gamma(\bar{B}^0(t) \to \bar{K}^{*0}\gamma) + \Gamma(B^0(t) \to K^{*0}\gamma)} = S_{K^*\gamma}\sin(\Delta m_B t) - C_{K^*\gamma}\cos(\Delta m_B t), \tag{5.4.5}$$

with both K^{*0} and $\bar{K}^{*0}$ subsequently decaying into the CP-eigenstate $K_S\pi^0$, and the mixing parameter Δm_B being defined following Δm_s in Eqs. (5.2.4) and (5.2.5). Due to the aforementioned SM suppression of right-handed photons in $B \to K^*\gamma$, $A_{CP}(B^0 \to K^{*0}\gamma)$ is mostly dominated by the B^0 meson mixing, with reduced sensitivity to hadronic uncertainties. So, it can be used as a null-test of the SM [85, 137, 138].

Finally, we present a suitable parametrisation for $S_{K^*\gamma}$, consistent with the inputs of our analysis [85]

$$S_{K^*\gamma} = f^{+\delta_f^u}_{-\delta_f^d} + \frac{\sum_{k,l} g_{(k,l)}\, \delta\mathcal{C}_7^k \delta\mathcal{C}_{7'}^l}{\sum_{k,l} h_{(k,l)}\, \delta\mathcal{C}_7^k \delta\mathcal{C}_{7'}^l}, \tag{5.4.6}$$

where f stands for its central value SM prediction, with δ_f^u (δ_f^d) the associated upper (lower) error bar. Additionally, the coefficients $g_{(k,l)}$ and $h_{(k,l)}$ can be found in Table 5.4.

5.4.3 $B_s \to \mu^+\mu^-$

One of the most stringent constraints on axial, scalar and pseudoscalar types of NP (i.e. $\mathcal{C}_{10^{(\prime)}}$ and $\mathcal{C}_{S^{(\prime)},PS^{(\prime)}}$) is given by the measurement of the branching ratio of the purely leptonic decay $B_s \to \mu^+\mu^-$. This process is strongly helicity suppressed in the SM, so it has long been considered

[6]This explains the suppression of $\mathcal{C}_{7'}$ with respect to $\mathcal{C}_7$ in the SM, as we noted in Eq. (4.1.28)

one of the standard candles of NP in B meson decays, consequently attracting a lot of interest both from the theory and the experimental sides.

At leading order, within a generic NP model including axial, scalar and pseudoscalar contributions, the branching ratio is given by [31]

$$\mathcal{B}(B_s \to \mu^+\mu^-) = \tau_{B_s} f_{B_s}^2 m_{B_s} \frac{\alpha^2 G_F^2}{16\pi^3} |V_{tb}V_{ts}^*| \sqrt{1 - \frac{4m_\mu^2}{m_{B_s}}} \left[|S|^2 \left(1 - \frac{4m_\mu^2}{m_{B_s}^2}\right) + |P|^2 \right], \tag{5.4.7}$$

with α being the electromagnetic coupling constant, τ_{B_s} the B_s lifetime, m_{B_s} its mass and the parameters S and P defined as [31]

$$S = \frac{m_{B_s}^2}{2} (\mathcal{C}_S - \mathcal{C}_{S'}) , \qquad P = \frac{m_{B_s}^2}{2} (\mathcal{C}_{PS} - \mathcal{C}_{PS'}) + m_\mu (\mathcal{C}_{10} - \mathcal{C}_{10'}) . \tag{5.4.8}$$

Current most precise SM predictions of this observable include next-to-next-to-leading order QCD and next-to-leading order electroweak corrections [139–141], which induce a shift on both the central value and uncertainty associated to the expression in Eq. (5.4.7). Our approach for taking these corrections into account is the same used for the inclusive channels $B \to X_s\gamma$ and $B \to X_s\mu^+\mu^-$: we rescale Eq. (5.4.7) so that its central value and uncertainties reproduce the updated SM predictions, but we leave those parts of Eq. (5.4.7) that depend on the NP contributions to the coefficients $\mathcal{C}_i$ untouched. Recent computations of QED and QCD corrections to the SM value of the $B_s \to \mu^+\mu^-$ decay [142, 143] are not included in our expressions, as they are significantly small compared to both the experimental accuracy available and the errors associated to our determinations of the Wilson coefficients.

Part II

Hadronic Uncertainties and LFUV

Chapter 6

General Theoretical Framework and Hadronic Uncertainties

In Chapter 4 we described the leading contributions to the $B \to K^* \ell^+ \ell^-$ decay distribution and discussed in detail how $O(\alpha_s)$ corrections should be accounted for within the QCDf framework. These computations have an intrinsic error of order Λ_{QCD}/m_b, usually referred to as *hadronic uncertainties* in the literature, which arise from power corrections to the factorisation formula. Developing a proper theoretical treatment of these corrections is important for achieving precise theory predictions able to match the accuracy of experimental measurements, which is particularly relevant since obtaining reliable determinations of short-distance Wilson coefficients through global analyses of data depends on this premise. Factorisable hadronic corrections can be estimated by combining QCDf computations with well-grounded parametrisations, however non-factorisable contributions cannot be computed from first principles and one has to rely on partial calculations and phenomenological models for their assessment. This has motivated certain analyses to advocate for unexpectedly large hadronic effects as explanations for some of the $b \to s\ell\ell$ anomalies [144–146].

Here we will review the treatment of hadronic uncertainties, which completes the description of our theoretical framework together with a short discussion about the large-q^2 region, provide a detailed anatomy of them and collect robust arguments showing that factorisable power corrections cannot account for the observed anomalies and that an explanation through long-distance charm contributions is disfavoured.

6.1 An overview of the computation of $B \to K^* \ell^+ \ell^-$ observables

In this section, we present an overview of the general approach followed for the computation of observables in Chapter 5. This includes a complete depiction of our treatment of the various sources of uncertainties and their interplay with the computations and techniques explained in Chapter 4. This framework will be applied, e.g., in the global fit in Chapter 8. The basis of our computations highly depends on which kinematic regime of the decay we are exploring: the large recoil region ($q^2 \lesssim 7-8$ GeV) or the low recoil region ($15 \lesssim q^2 \lesssim 19$ GeV). Therefore we discuss them separately.

Whereas the $B \to K^* \ell^+ \ell^-$ decay channel and its observables will be our default context for the following discussion, at the end of the section we will comment on how these developments translate to $B_s \to \phi \ell^+ \ell^-$ and $B_s \to K \ell^+ \ell^-$

6.1.1 Theoretical framework at low-q^2

The theoretical treatment used to describe the decay $B \to K^*\ell^+\ell^-$ at low squared invariant dilepton masses q^2 (where the most significant tensions with the SM are found) is based on QCDf supplemented by a sophisticated estimate of the power corrections of order $\Lambda_{\rm QCD}/m_B$. This framework is called *improved* QCDf [113, 147], where the term "improved" stands for the fact that $O(\Lambda_{\rm QCD}/m_B)$ corrections that go beyond QCDf are also included as uncertainty estimates in our predictions.

The use of effective theories [24, 29] allows one to relate the different $B \to K^*$ form factors at leading order in $\Lambda_{\rm QCD}/m_B$ and $\Lambda_{\rm QCD}/E$, where E is the energy of the K^*. As we mentioned in Section 2.1.4, this procedure reduces the required hadronic input from seven to two independent soft form factors $\xi_\perp, \xi_\|$, which in the region of low q^2 can be calculated using LCSRs.

Two different types of LCSR form factors can be found in the literature, depending on the method adopted for their computation. On the one hand, there are form factors based on LCSRs with B-meson distribution amplitudes. Currently two form factor parametrisations of this kind are available: the calculation of form factors in [148] (KMPW), where up to leading-twist two-particle contributions were included, and the recent parametrisation presented in Ref. [149], where the leading-twist contributions are extended up to twist four. On the other hand, one can also use LCSRs with K^*-meson distribution amplitudes, which lead to results with smaller uncertainties because of the current better knowledge of light-meson LCDAs. The so-called BSZ form factors [150] were computed within the aforementioned approach, with a prevalent application of equations of motion. For in-depth analyses of the implications of using these different form factor parametrisations for the computation of relevant observables in $B \to K^*\ell^+\ell^-$ and related channels, we refer the interested reader to Refs. [113, 147]. Our default predictions rely on KMPW form factors which have larger uncertainties and thus lead to more conservative predictions for observables. By construction, the choice of the set of form factors has a relatively low impact on optimized observables but it has a large impact on the error size of form-factor sensitive observables, such as the longitudinal polarisation F_L or the CP-averaged angular coefficients S_i.

The large-recoil symmetry limit is enlightening as it allows us to understand the main behaviour of optimized observables $P_i^{(\prime)}$ [103, 112] (see also Section 5.1.2 of this Thesis) in presence of New Physics in a form-factor independent way. However, for precise predictions of these observables it has to be complemented with different kinds of corrections, separated in two classes: factorisable and non-factorisable corrections. Improved QCDf provides a systematic formalism to include the different corrections as a decomposition of the amplitude in the following form [30]:

$$\langle \ell^+\ell^-\bar{K}_i^*|H_{\rm eff}|\bar{B}\rangle = \sum_{a,\pm} \mathcal{C}_{i,a}\xi_a + \Phi_{B,\pm}\otimes T_{i,a,\pm}\otimes\Phi_{K^*,a} + O\left(\frac{\Lambda_{\rm QCD}}{m_B}\right), \qquad (6.1.1)$$

where $i = 0, \perp, \|$ and $a = \perp, \|$. The equation above is formally related to the the factorisation ansatz of the hadronic form factors in Eq. (4.4.9) and all its elements have the same meaning as the ones defined there.

Factorisable power corrections

Factorisable corrections are the corrections that can be absorbed into the (full) form factors F by means of a redefinition at higher orders in α_s and $\Lambda_{\rm QCD}/m_B$:

$$F(q^2) \;=\; F^\infty(\xi_\perp(q^2),\xi_\parallel(q^2)) \;+\; \Delta F^{\alpha_s}(q^2) \;+\; \Delta F^\Lambda(q^2). \tag{6.1.2}$$

The two types of corrections to the leading-order form factor $F^\infty(\xi_\perp,\xi_\parallel)$ are factorisable α_s-corrections ΔF^{α_s} and factorisable $O(\Lambda_{\rm QCD}/m_B)$ corrections ΔF^Λ. While the former can be computed within QCDf and are related to the prefactors $\mathcal{C}_{a,i}$ of Eq. (6.1.1), the latter, representing part of the $O(\Lambda_{\rm QCD}/m_b)$ terms of Eq. (6.1.1) that QCDf cannot predict, can be parametrised as an expansion in q^2/m_B^2 following [151]

$$\Delta F^\Lambda(q^2) = a_F \,+\, b_F\,\frac{q^2}{m_B^2} \,+\, c_F\,\frac{q^4}{m_B^4} \,+\, \ldots\,. \tag{6.1.3}$$

Whereas these corrections are expected to be small, one cannot simply neglect them as they break the symmetry relations that protect the optimised observables at leading order and reintroduce a form factor dependence at $O(\alpha_s,\Lambda_{\rm QCD}/m_b)$ in them. Therefore it is of paramount importance to have these ΔF^Λ corrections under good theoretical control. Notice that the decomposition in Eq. (6.1.2) is not unique, due to the symmetry relations in Eqs. (2.1.27) and (2.1.28) (and Eq. (2.1.26) for pseudoscalars) one can always redefine $\xi_{\perp,\parallel}$ such that some of these corrections are partly absorbed. At the practical level, in order to unambiguously define the soft form factors one needs to fix a renormalisation scheme, i.e. a specific definition for $\xi_{\perp,\parallel}$ in terms of full QCD form factors. No *a priory* restrictions exist for the definition of a particular scheme, as long as it conforms with the symmetry relations among form factors at large recoil.

Our implementation of these corrections makes particular emphasis in two aspects [147]:

- For a realistic estimation of the errors, one must consider all correlations among the parameters a_F, b_F and c_F in Eq. (6.1.3). This includes all kinematic constraints among form factors at maximum recoil (i.e. $T_1(0) = T_2(0)$) and correlations that naturally arise from the choice of scheme.

- It is relevant to choose an *appropriate scheme*. Fixing a scheme determines which corrections of $O(\alpha_s,\Lambda_{\rm QCD}/m_b)$ are absorbed into the definition of the soft form factors $F^\infty(\xi_\perp(q^2),\xi_\parallel(q^2))$ and which remain as $\Delta F^{\alpha_s}(q^2)$ and $\Delta F^\Lambda(q^2)$ symmetry breaking corrections. The $\Delta F^{\alpha_s}(q^2)$ can be computed within QCDf, but $\Delta F^\Lambda(q^2)$ power corrections need to be determined through the decomposition in Eq. (6.1.2). Hence, this introduces a scheme dependence at $O(\Lambda_{\rm QCD}/m_b)$ in the computation of the observables. In Sec. 6.2 we will further discuss the dependence of improved QCDf predictions on the scheme and we will argue that an appropriate scheme must be such that it naturally minimizes the sensitivity to power corrections in the relevant observables like P_5'. Additionally, we will also derive explicit formulae for the contribution from factorisable power corrections to the most important observables P_5', P_2 and P_1, which will allow us to confirm in an analytic way the numerical findings of Ref. [147].

In our approach we first determine the parameters a_F, b_F, c_F so that our decomposition reproduces the central values of the full QCD form factors. This has the important implication that central values of our predictions present no scheme dependence, only errors are affected. To this end, once a scheme is fixed, we fit the subsequent parametrisation to the full form factors and keep the (non-zero) correlated estimates of the parameters ($\hat{a}_F$, $\hat{b}_F$, $\hat{c}_F$) as central values. Explicit

	$\hat{a}_F$	$\hat{b}_F$	$\hat{c}_F$
A_0(KMPW)	0.002 ± 0.000	0.590 ± 0.125	1.473 ± 0.251
A_1(KMPW)	-0.013 ± 0.025	-0.056 ± 0.018	0.158 ± 0.021
A_2(KMPW)	-0.018 ± 0.023	-0.105 ± 0.022	0.192 ± 0.028
T_1(KMPW)	-0.006 ± 0.031	-0.012 ± 0.054	-0.034 ± 0.095
T_2(KMPW)	-0.005 ± 0.031	0.153 ± 0.043	0.544 ± 0.061
T_3(KMPW)	-0.002 ± 0.022	0.308 ± 0.059	0.786 ± 0.093

Table 6.1: Fit results for the power-correction parameters in the case of scheme 1 as defined in Section 6.2. The label KMPW refers to LCSR input from ref. [148]. In this scheme, V receives no power corrections and therefore the corresponding parameters vanish.

values of these estimates obtained by fitting to the full form factors in the KMPW parametrisation can be found in Table 6.1. Interestingly, this procedure yields results of typically $(5-10)\% \times F$ in size, as expected from naive power counting. We take an uncorrelated 10% error assignment to the factorisable power corrections $\Delta\hat{a}_F$, $\Delta\hat{b}_F$, $\Delta\hat{c}_F \sim F \times O(\Lambda_{\rm QCD}/m_b) \sim 0.1F$ around the central values [147], which corresponds to an error of order 100% with respect to the central values obtained through the fit. Finally, for the computation of observables the parameters are varied within the range $\hat{a}_F - \Delta\hat{a}_F \leq a_F \leq \hat{a}_F + \Delta\hat{a}_F$, and the same for b_F and c_F [147].

Notice that our assumption on the error size of power corrections is only based on dimensional arguments and, even though there is no rigorous way to validate this assignment, it was shown in Ref. [147] that this error estimation of 10% for power corrections is conservative with respect to the central values of KMPW form factors. In Sec. 6.2 we will perform the same analysis but now to extract the amount of power corrections (including errors) contained in the form factors from Ref. [150], finding them of the typical order of magnitude of 10%, in agreement with dimensional arguments.

Non-factorisable power corrections

Non-factorisable corrections refer to corrections that cannot be absorbed into the definition of the form factors due to their different structure. Thus, these corrections pose a conceptually different problem with respect to our previous discussion: even if all sources of factorisable corrections were precisely known, we would still have to deal with hadronic uncertainties of non-factorisable origin. One can identify two types of such corrections. On one side, non-factorisable α_s-corrections originating from hard-gluon exchange in diagrams with insertions of four-quark operators $\mathcal{O}_{1-6}$ and the chromomagnetic operator $\mathcal{O}_8$. And, on the other side, there are non-factorisable power corrections involving *long-distance $c\bar{c}$ loops*. First we will describe the non-factorisable power corrections associated with hard-gluon exchanges and later we will address the charm loop.

As we saw in Section 4.4, non-factorisable contributions come from four-quark and chromomagnetic operators where the dilepton is generated via the insertion of a virtual photon line. At small q^2 and at leading order in $\Lambda_{\rm QCD}/m_b$, the factorisation formula in Eq. (4.4.18) allows for their computation in terms of hard-vertex coefficients, hard-scattering kernels and the corresponding distribution amplitudes [30, 33]. However, at order $\Lambda_{\rm QCD}/m_b$ unknown non-perturbative power corrections appear. These are precisely the non-factorisable power corrections we mentioned above.

These contributions are estimated by means of a parametrisation that originally was designed to jointly account for both factorisable and non-factorisable power corrections. This approach is based on a set of complex functions that multiply each transversity amplitude [111, 152], with characteristic absolute values of the order of 10%, which again follows from dimensional arguments. Error estimates for the transversity amplitudes around singular points are usually underestimated within this framework, but it turns out to provide reasonable errors at the observable level due to interferences between the transversity amplitudes [147].

One possibility would be to use the same technique but only for the non-factorisable corrections, indeed factorisable corrections have already been taken into account with the procedure detailed above. However, this would clearly overestimate the effect as contributions that are not affected by non-factorisable power corrections, i.e. those generated by operators $\mathcal{O}_{9,10}^{(\prime)}$, would be artificially inflated.

Our procedure is based on the same idea but applied to the hadronic form factors $\mathcal{T}_i$ (generically defined through the factorisation formula in Eq. (4.4.18)) that parametrise the matrix element $\langle\gamma^*\bar{K}^*|\,\mathcal{H}_{\text{eff}}\,|\bar{B}\rangle$ [30]. First, we single out the contributions of purely hadronic origin in $\mathcal{T}_i$ by taking the limit $\mathcal{T}_i^{\text{had}} = \mathcal{T}_i|_{\mathcal{C}_7^{(\prime)}\to 0}$ and then we multiply each of these amplitudes, that will serve as a normalisation factor, by a complex q^2-dependent function

$$\mathcal{T}_i^{\text{had}} \to (1 + r_i(q^2))\,\mathcal{T}_i^{\text{had}}, \tag{6.1.4}$$

where

$$r_i(q^2) = r_i^a e^{i\phi_i^a} + r_i^b e^{i\phi_i^b}\left(\frac{q^2}{m_B^2}\right) + r_i^c e^{i\phi_i^c}\left(\frac{q^2}{m_B^2}\right)^2. \tag{6.1.5}$$

We define the central values as the ones with $r_i(q^2) \equiv 0$ and estimate the uncertainties from non-factorisable power corrections by varying $r_i^{a,b,c} \in [0, 0.1]$ and $\phi_i^{a,b,c} \in [-\pi, \pi]$ independently, which corresponds to a $\sim 10\%$ error assignment with arbitrary phase.

On the other hand, power corrections that involve long-distance $c\bar{c}$-loops correspond to one-loop contributions from the operator $\mathcal{O}_2$, which can be recast as a contribution to $\mathcal{C}_9$ depending on the squared dilepton invariant mass q^2, the transversity amplitudes $A_j^{L,R}$ $(j = 0, \perp, ||)$ and the hadronic states (as opposed to a universal contribution from New Physics). These complicated objects are included as an additional source of uncertainty, estimated on the basis of the only existing computation [148] of soft-gluon emission from four-quark operators involving $c\bar{c}$ currents. The calculation in Ref. [148] was done in the framework of LCSRs with B-meson distribution amplitudes and makes use of an hadronic dispersion relation to obtain results in the whole large-recoil region. It is important to notice that, taken at face value, the resulting correction would increase the anomaly [153]. The phenomenological model used in Ref. [148] for estimating this effect includes the perturbative leading order contribution (also coming from an insertion of the $\mathcal{O}_2$ operator). Therefore, as we are only interested in the long distance charm-loop effect, we subtract the aforementioned contribution, and proceed to shift the value of m_c according to the instructions given in Ref. [148] in order to be consistent with the value used in our analyses. Then, we introduce two parametrisations for the contribution to the transverse amplitudes [113, 147]

$$\delta\mathcal{C}_9^{\perp}(q^2) = \frac{a^{\perp} + b^{\perp} q^2 (c^{\perp} - q^2)}{q^2 (c^{\perp} - q^2)}, \qquad \delta\mathcal{C}_9^{||}(q^2) = \frac{a^{||} + b^{||} q^2 (c^{||} - q^2)}{q^2 (c^{||} - q^2)}, \tag{6.1.6}$$

and similarly for the longitudinal amplitude (with no pole at $q^2 = 0$, as expected)

$$\delta\mathcal{C}_9^0(q^2) = \frac{a^0 + b^0(q^2 + s_0)(c^0 - q^2)}{(q^2 + s_0)(c^0 - q^2)}, \tag{6.1.7}$$

being $s_0 = 1$ GeV^2. These parameters are fixed in order to cover the results from Ref. [148] in the q^2-region from 1 to 9 GeV^2. Following this approach, one obtains [113]

$$a^\perp, a^{||} = 9.25 \pm 2.25, \qquad a^0 = 33 \pm 7\,, \tag{6.1.8}$$

$$b^\perp, b^{||} = -0.5 \pm 0.3, \qquad b^0 = -0.9 \pm 0.5\,, \tag{6.1.9}$$

$$c^\perp, c^{||} = 9.35 \pm 0.25, \qquad c^0 = 10.35 \pm 0.55\,, \tag{6.1.10}$$

where all parameters are taken as uncorrelated. For the sake of being as conservative as possible in our estimate for this effect, since the sign of these contributions can be debated, for each correction to the three transversity amplitudes we introduce prefactors s_i that are scanned from -1 to $+1$. Finally, the prescription used in our theory predictions to account for the long-distance charm loop reads

$$A_i^{L,R}: \qquad \mathcal{C}_9^{\rm eff}(q^2) \to \mathcal{C}_9^{\rm eff}(q^2) + \mathcal{C}_{9\,i}^{c\bar{c}}(q^2), \qquad i = \perp, \|, 0, \tag{6.1.11}$$

with the last piece defined as

$$\mathcal{C}_{9\,i}^{c\bar{c}} = s_i \delta\mathcal{C}_9^i. \tag{6.1.12}$$

It is interesting to note that our conservative approach typically leads to larger uncertainties for observables as compared to other estimates in the literature [150, 151].

6.1.2 The large-q^2 region: lattice results and duality violation estimates

For the low-recoil region [154–156], one can perform a similar analysis based on Operator Product Expansion and Heavy-Quark Effective Theory, or using directly form factors provided by lattice QCD simulations. In the following, we will use the latter approach for the computation of the observables at low recoil. In this region, one has also to deal with resonances such as those observed by LHCb in the data of the partner channel $B^+ \to K^+\mu^+\mu^-$. This observation prevents one from taking small bins afflicted by the resonance structures. In Ref. [157] a quantitative estimate of duality violation is given. Unavoidably, one needs to use a model for this estimate, still the result is that the low recoil bin, integrated over a large energy range, gets a duality-violation impact of a few percent at the level of the branching ratio (estimated to 5% in Ref. [110] or 2% in Ref. [157]). It remains to be determined if this estimate also applies for angular observables in $B \to K^*\mu\mu$. Moreover, the exact definition of the ends of the single large bin has some impact on the analysis in the framework of the effective Hamiltonian [158]. In order to take into account such effect of duality violation for angular observables and the sensitivity to the position of the ends of the bin, we add a contribution of $O(10\%)$ (with an arbitrary phase) to the term proportional to $\mathcal{C}_9^{\rm eff}$ for each transversity amplitude. We notice that for all exclusive processes at low recoil, we include the next-to-next-to-leading logarithm corrections for $b \to s\ell\ell$ processes as described in Ref. [159].

6.2 Anatomy of factorisable power corrections

In the region of large recoil of the K^* meson, the non-perturbative form factors needed for the prediction of $B \to K^*\mu^+\mu^-$ are available from three different LCSR calculations in Refs. [148] (KMPW), [150] (BSZ) and [149]. However, our discussion here will focus only on the KMPW and BSZ parametrisations. In Ref. [150], the set of form factors has been provided together with the corresponding correlations, essential for the cancellation of the form factors at leading order in optimized observables. Instead of using the results provided in Ref. [150], *the dominant correlations can alternatively be assessed from first principles, by means of large-recoil symmetries* which relate the seven form factors among each other. Among the advantages of this second method, the correlations are free from the model assumptions entering the particular LCSR calculation and *the method can be applied also to sets of form factors for which the correlations have not been specified*, e.g., Ref. [148]. As a drawback, these correlations are obtained only at leading order, and symmetry-breaking corrections of order $O(\Lambda/m_B)$ have to be estimated using the techniques of Section 6.1.1, implying a scheme dependence of the predictions at $O(\Lambda/m_B)$. We will discuss this scheme dependence in the following.

6.2.1 Scheme dependence

Theoretical predictions for the decay $B \to K^*\ell^+\ell^-$ depend on seven hadronic form factors usually denoted as $V, A_0, A_1, A_2, T_1, T_2, T_3$. For small invariant dilepton masses $q^2 \ll m_B^2$ (large-recoil limit), and at leading order in α_s and $\Lambda_{\rm QCD}/m_B$, the set of form factors becomes linearly dependent [24, 29, 30, 160] and thus reduces to two soft form factors $\xi_\perp$ and $\xi_\|$ (see Eqs. (2.1.27) and (2.1.28) in Section 2.1.4). Then, the full set of form factors V, A_0, A_1, A_2, T_1, T_2, T_3 can be obtained as linear combinations of $\xi_\perp$, $\xi_\|$.

Eqs. (2.1.27) and (2.1.28) allow us to construct observables in which the form factors cancel at leading order. For an illustration, let us focus at $q^2 = 0$, where the first relation in Eq. (2.1.27) implies

$$\frac{A_1(0)}{T_1(0)} = \frac{T_1(0)}{V(0)} = \frac{V(0)}{A_1(0)} = 1 + O(\alpha_s, \Lambda/m_B), \tag{6.2.1}$$

while $T_1(0)/T_2(0) = 1$ holds exactly due to a kinematic identity from the definition of T_1 and T_2. Observables involving ratios like the ones in Eq. (6.2.1) are independent of the form factor input up to effects of $O(\alpha_s, \Lambda/m_B)$, and the optimized observables $P_i^{(\prime)}$ are defined following this philosophy. The reduced sensitivity to the hadronic form factor input renders these observables sensitive to subleading sources of uncertainties, i.e. to effects of $O(\alpha_s)$ and $O(\Lambda/m_B)$. As we discussed in the previous section, while $O(\alpha_s)$ corrections to Eqs. (2.1.27)-(2.1.28) can be included in the framework of QCDf, the so-called factorisable power corrections of $O(\Lambda/m_B)$ are not computable in QCDf.

Accurate QCDf predictions rely in an essential way on quantifying the uncertainty due to power-suppressed $\Lambda_{\rm QCD}/m_B$ effects. This is typically done by assigning uncorrelated errors of the size $\delta \sim 10\%$ to Eqs. (2.1.27)-(2.1.28) (and thus to the ratios in Eq. (6.2.1)). Note, however, that this cannot be done in a unique way. Let us, for instance, assume that the errors on $A_1(0)/T_1(0)$ and $T_1(0)/V(0)$ are given by δ_1 and δ_2, respectively:

$$\frac{A_1(0)}{T_1(0)} = 1 \pm \delta_1, \qquad \frac{T_1(0)}{V(0)} = 1 \pm \delta_2. \tag{6.2.2}$$

The error δ_3 on the ratio $A_1(0)/V(0)$ is then fixed by

$$1 \pm \delta_3 = \frac{A_1(0)}{V(0)} = \frac{A_1(0)}{T_1(0)}\frac{T_1(0)}{V(0)} = \begin{cases} 1 \pm \sqrt{\delta_1^2 + \delta_2^2}, & \text{quadratic error propagation} \\ 1 \pm (\delta_1 + \delta_2), & \text{linear error propagation} \end{cases}, \tag{6.2.3}$$

depending on how uncertainties are propagated. The assumption of a universal error size $\delta_1 = \delta_2 \equiv \delta$ for the first two ratios thus leads to an error $\delta_3 = \sqrt{2}\delta$ or $\delta_3 = 2\delta$ for the third one, although in principle the three ratios should be treated on an equal footing.

The same phenomenon can be understood also from a different point of view. In the QCDf approach, predictions of observables depend on the two soft form factors $\xi_\perp$ and $\xi_\parallel$ for which hadronic input (from LCSR) is needed. According to Eqs. (2.1.27)-(2.1.28), there are various possibilities to select the input among the seven full factors V, A_1, A_2, A_0, T_1, T_2, T_3, and the choice defines an input scheme. One possible choice would consist for example in defining

$$\begin{aligned} \xi_\perp(q^2) &= \frac{m_B}{m_B + m_V} V(q^2), \\ \xi_\parallel(q^2) &= \frac{m_B + m_V}{2E} A_1(q^2) - \frac{m_B - m_V}{m_B} A_2(q^2) \qquad \text{(scheme 1)}. \end{aligned} \tag{6.2.4}$$

A different choice would consist in identifying

$$\xi_\perp(q^2) = T_1(q^2), \qquad \xi_\parallel(q^2) = \frac{m_V}{E} A_0(q^2) \qquad \text{(scheme 2)}. \tag{6.2.5}$$

By definition, the form factors (or linear combinations of form factors) taken as input are exactly known to all orders in α_s and Λ/m_B. The remaining form factors are then determined from the symmetry relations in Eqs. (2.1.27)-(2.1.28) upon including $O(\alpha_s)$ corrections via QCDf and assigning an error estimate to unknown $O(\Lambda/m_B)$ corrections. Taking, for instance, as in scheme 2, $T_1(0) = T_1^{\rm LCSR}(0)$ as input for $\xi_\perp(0)$ leads to

$$V(0) = T_1^{\rm LCSR}(0) + a_V^{\alpha_s} + a_V^{\Lambda} + ..., \qquad A_1(0) = T_1^{\rm LCSR}(0) + a_{A_1}^{\alpha_s} + a_{A_1}^{\Lambda} + ..., \tag{6.2.6}$$

where $a_V^{\alpha_s}, a_{A_1}^{\alpha_s}$ and $a_V^{\Lambda}, a_{A_1}^{\Lambda}$ are α_s and $\Lambda_{\rm QCD}/m_B$ corrections to the symmetry relations in Eqs. (2.1.27)-(2.1.28) for each form factor, and the ellipsis represents terms of higher orders. If Eq. (6.2.6) was determined to all orders in α_s and $\Lambda_{\rm QCD}/m_B$, predictions for observables would not depend on the chosen input scheme. In practice, QCD corrections are known in QCDf up to $O(\alpha_s^2)$ [161, 162] while $\Lambda_{\rm QCD}/m_B$ corrections can only be estimated, implying a scheme dependence in the computation of the observables at $O(\Lambda_{\rm QCD}/m_B)$ and $O(\alpha_s^3)$.

While the form factors taken as input inherit their uncertainties directly from the LCSR calculation, the remaining form factors receive an additional error for the unknown $\Lambda_{\rm QCD}/m_B$ corrections a^Λ. In the example above (scheme 2), we have

$$T_1(0) = T_1^{\rm LCSR}(0) \pm \Delta T_1^{\rm LCSR}(0), \tag{6.2.7}$$

with $\Delta T_1^{\rm LCSR}(0)$ denoting the uncertainty of the LCSR calculation, and

$$V(0) =(T_1^{\rm LCSR}(0) + a_V^{\alpha_s} + a_V^{\Lambda}) \pm (\Delta T_1^{\rm LCSR}(0) + \Delta a_V^{\alpha_s} + \Delta a_V^{\Lambda}), \tag{6.2.8}$$

$$A_1(0) =(T_1^{\rm LCSR}(0) + a_{A_1}^{\alpha_s} + a_{A_1}^{\Lambda}) \pm (\Delta T_1^{\rm LCSR}(0) + \Delta a_{A_1}^{\alpha_s} + \Delta a_{A_1}^{\Lambda}). \tag{6.2.9}$$

In this case, $V(0)$ and $A_1(0)$ are subject to two main sources of uncertainties, namely the error $\Delta T_1^{\rm LCSR}(0)$ of the LCSR calculation and the uncertainties $\Delta a_{V,A_1}^{\Lambda}$ from unknown power corrections (we neglect the uncertainty $\Delta a_{V,A_1}^{\alpha_s}$ from the perturbative contribution). On the other hand, if we had chosen $V(0)$ or $A_1(0)$ directly as input for the soft form factor $\xi_\perp(0)$, the only source of error for $V(0)$ or $A_1(0)$ would have been the respective LCSR error $\Delta V^{\rm LCSR}(0)$ or $\Delta A_1^{\rm LCSR}(0)$. The choice of scheme thus defines the precision to which the various full form factors are known, keeping those taken as input free from a pollution by power corrections.

The freedom to choose between different input schemes is equivalent to the ambiguity in implementing the 10% requirement on the symmetry-breaking corrections to Eqs. (2.1.27)-(2.1.28) and (6.2.1). In the scheme 2, the uncertainties on the form factor ratios are:

$$\frac{A_1(0)}{T_1(0)} = 1 \pm \frac{\Delta a_{A_1}^{\Lambda}}{T_1^{\rm LCSR}}, \qquad \frac{T_1(0)}{V(0)} = 1 \pm \frac{\Delta a_{V}^{\Lambda}}{T_1^{\rm LCSR}}, \tag{6.2.10}$$

$$\frac{A_1(0)}{V(0)} = \begin{cases} 1 \pm \sqrt{\left(\dfrac{\Delta a_{A_1}^{\Lambda}}{T_1^{\rm LCSR}}\right)^2 + \left(\dfrac{\Delta a_{V}^{\Lambda}}{T_1^{\rm LCSR}}\right)^2}, & \text{quadratic error propagation} \\ 1 \pm \left(\dfrac{\Delta a_{A_1}^{\Lambda}}{T_1^{\rm LCSR}} + \dfrac{\Delta a_{V}^{\Lambda}}{T_1^{\rm LCSR}}\right), & \text{linear error propagation} \end{cases} . \tag{6.2.11}$$

In this expressions we have kept only the errors of $O(\Lambda_{\rm QCD}/m_B)$ and we have neglected uncertainties suppressed by additional powers of α_s or Λ/m_B. Note that the LCSR error $\Delta T_1^{\rm LCSR}(0)$ cancels in this approximation. Identifying $\delta_1 = \Delta a_{A_1}^{\Lambda}/T_1^{\rm LCSR}$ and $\delta_2 = \Delta a_V^{\Lambda}/T_1^{\rm LCSR}$, we find that the resulting errors are in agreement with Eqs. (6.2.2) and (6.2.3).

How can the ambiguity from the scheme dependence be solved? To answer this question, let us first have a look at the decay $B \to K^*\gamma$. The prediction of this branching ratio depends on the single form factor $T_1(0)$ and the natural choice thus consists in taking its LCSR value directly as input for the theory predictions [1]. Of course, one could take as input any other form factor to which T_1 is related through the symmetry relations in Eqs. (2.1.27)-(2.1.28), e.g. V. Unlike T_1, the choice of V would generate power corrections of $O(\Lambda_{\rm QCD}/m_B)$ in the prediction for $B \to K^*\gamma$, reflecting the fact that the identification $V = T_1$ is only an approximation, valid up to $O(\Lambda_{\rm QCD}/m_B)$, and that the "wrong" form factor, V, has been used for the prediction instead of the "correct" one, T_1. The corresponding increase in the uncertainties is thus caused artificially by an *inappropriate* choice of the input scheme. This becomes even more obvious in the hypothetical limit where the errors of the LCSR calculation go to zero: In this case, the prediction for $B \to K^*\gamma$ would be free from any form factor uncertainty (as it should be) when T_1 is taken as input, while

[1] This decay also receives a contribution from charm loops. For the sake of the argument presented in this section, we will neglect this effect, which should however be included in an actual computation of this branching ratio, contrary to the approach of Ref. [151]. We will include this contribution when discussing the fits to $c\bar{c}$ contributions, see Sec. 6.3.2 and in particular Tab. 6.7.

the wrong central value would be obtained when V is used, together with an irreducible error of order $O(|V^{\rm LCSR} - T_1^{\rm LCSR}|)$.

The example of $B \to K^*\gamma$ clearly illustrates the fact that an inappropriate choice of scheme can artificially increase the uncertainty of the theory prediction. The situation is less obvious in the case of $B \to K^*\mu^+\mu^-$, where typically all seven form factors enter the prediction of the observables. Ignoring the form factor A_0, whose contribution is suppressed by the lepton mass, we observe that the form factors V, A_1, A_2 enter the amplitudes together with the Wilson coefficients $\mathcal{C}_{9,10}^{(\prime)}$, whereas T_1, T_2, T_3 enter the amplitudes together with the coefficient $\mathcal{C}_7^{(\prime)}$. In the SM, $\mathcal{C}_7^{\rm eff} \ll {\rm Re}(\mathcal{C}_9^{\rm eff})$ (where the effective coefficients $\mathcal{C}_{7,9}^{\rm eff}$ include effects from perturbative $q\bar{q}$ loops), e.g. $\mathcal{C}_7^{\rm eff}(q_0^2) = -0.29$ and ${\rm Re}(\mathcal{C}_9^{\rm eff})(q_0^2) = 4.7$ at $q_0^2 = 6\,{\rm GeV}^2$. Hence the (axial-)vector form factors V, A_1, A_2 are in general more relevant than the tensor form factors T_1, T_2, T_3, except for the very low q^2-region where the $\mathcal{C}_7$ contribution can be enhanced by the $1/q^2$ pole from the photon propagator. In particular in the anomalous bins of the observable P_5' ($4 \le q^2 \le 8$ GeV^2), we find that the impact from $\mathcal{C}_7$ is strongly suppressed compared to the impact from $\mathcal{C}_9$. This can be seen by setting some of the Wilson coefficients to zero and determining the resulting change in the predictions: one gets a shift of $\Delta P_5'(\mathcal{C}_7 = 0)_{[4,6]} = -0.19$ when $\mathcal{C}_7$ is switched off, compared to $\Delta P_5'(\mathcal{C}_9 = 0)_{[4,6]} = +1.34$ when $\mathcal{C}_9$ is switched off. With respect to the soft form factor $\xi_\perp$, the observable P_5' is thus dominated by the ratio A_1/V suggesting the form factor V, or alternatively A_1, as a natural input for $\xi_\perp$. Defining $\xi_\perp$ from T_1, as done in Refs. [146, 151], on the other hand represents an inadequate choice: to a good approximation, the prediction of P_5' in the anomalous bins does not depend on this form factor, due to a suppression by $|\mathcal{C}_7/\mathcal{C}_9| \ll 1$.

Together with the linear propagation of errors applied in Refs. [146, 151], the choice of T_1 as input leads to an artificial inflation of the uncertainty by a factor of 2 in the anomalous bins of P_5', as we demonstrated in Eqs. (6.2.3) and (6.2.11). In other words, we conclude that the results on P_5' obtained in Ref. [146] correspond to an implicit assumption of 20% power corrections [2] because this is the size of symmetry breaking implicitly assumed for the dominant form factor ratio A_1/V [3]. The situation is different for observables that vanish in the limit $\mathcal{C}_7 \to 0$, i.e. that depend on $\mathcal{C}_7$ already at leading order in $\mathcal{C}_7/\mathcal{C}_9$, like the observable P_2. In this case, it is not clear a priory whether the observable is more sensitive to the (axial-)vector or to the tensor form factors, and the answer to this question requires a closer inspection (see Sec. 6.2.3).

In summary, in the soft-form factor approach, we expect the uncertainties of our predictions to be scheme dependent. An inappropriate choice of definition for the soft form factors will inflate the errors on the predictions. For each observable, we should thus choose a scheme as appropriate as possible to avoid an overestimation of the uncertainties.

[2] This is in contradiction with the assumption initially stated in Ref. [146] that a 10% power correction is used for all the form factors.

[3] This provides only a partial explanation to the larger uncertainties in Ref. [151]. Apart from a factor of two in the error assigned to factorisable power corrections that we have just discussed, Ref. [151] also states much larger parametric errors compared to Ref. [147] and Refs. [163, 164]. This is surprising, given the fact that the uncertainties assumed for the key parameters like m_c are compatible, while the errors for the form factors are even significantly smaller in Ref. [151] due to the extraction of $T_1(0)$ using experimental data (see also Appendix A of [1].

	a_F	b_F	c_F	$r(0\,\mathrm{GeV}^2)$	$r(4\,\mathrm{GeV}^2)$	$r(8\,\mathrm{GeV}^2)$
A_0	0.000 ± 0.000	0.054 ± 0.033	0.197 ± 0.203	0.000 ± 0.000	0.026 ± 0.020	0.055 ± 0.047
	$\pm\, 0.000$	$\pm\, 0.054$	$\pm\, 0.112$	$\pm\, 0.000$	$\pm\, 0.020$	$\pm\, 0.038$
A_1	0.020 ± 0.011	0.036 ± 0.025	0.037 ± 0.049	0.071 ± 0.043	0.086 ± 0.045	0.102 ± 0.054
	$\pm\, 0.029$	$\pm\, 0.017$	$\pm\, 0.022$	$\pm\, 0.100$	$\pm\, 0.100$	$\pm\, 0.100$
A_2	0.028 ± 0.016	0.079 ± 0.038	0.131 ± 0.079	0.116 ± 0.070	0.147 ± 0.078	0.188 ± 0.099
	$\pm\, 0.041$	$\pm\, 0.048$	$\pm\, 0.056$	$\pm\, 0.165$	$\pm\, 0.174$	$\pm\, 0.182$
T_1	-0.017 ± 0.013	-0.017 ± 0.009	-0.037 ± 0.023	0.061 ± 0.045	0.057 ± 0.038	0.054 ± 0.030
	$\pm\, 0.031$	$\pm\, 0.043$	$\pm\, 0.090$	$\pm\, 0.100$	$\pm\, 0.100$	$\pm\, 0.100$
T_2	-0.017 ± 0.012	0.007 ± 0.027	0.025 ± 0.053	0.061 ± 0.045	0.050 ± 0.045	0.036 ± 0.053
	$\pm\, 0.031$	$\pm\, 0.016$	$\pm\, 0.027$	$\pm\, 0.100$	$\pm\, 0.100$	$\pm\, 0.100$
T_3	-0.007 ± 0.021	0.014 ± 0.041	0.061 ± 0.208	0.037 ± 0.111	0.013 ± 0.132	0.016 ± 0.176
	$\pm\, 0.018$	$\pm\, 0.019$	$\pm\, 0.026$	$\pm\, 0.100$	$\pm\, 0.100$	$\pm\, 0.100$

Table 6.2: Results for the fit of the power-correction parameters a_F, b_F, c_F to the $B \to K^*$ form factors from Ref. [150], using the input scheme 1 in the transversity basis. Furthermore, the relative size $r(q^2)$ with which the power corrections contribute to the full form factors is shown for $q^2 = 0, 4, 8\,\mathrm{GeV}^2$. In the first line of each entry, the central value and the error obtained from the fit are given. In the second line, the estimate $\Delta F^\Lambda = 10\% \times F^{\mathrm{LCSR}}$ is displayed for comparison.

6.2.2 Correlated fit of power corrections to form factors

Having clarified the issue of the scheme dependence, we can turn to the question of the actual size δ of the symmetry breaking corrections. Both Refs. [147] and [146] use $\delta = 10\%$ as an error estimate. It is instructive to study how this ad-hoc value compares to the size of power corrections present in specific LCSR calculations. As we discussed in Section 6.1.1, within our standard theoretical framework, the parameters characterising the factorisable power corrections (with a scheme choice according scheme 1 in the subsection above) are extracted from the LCSR form factors in Ref. [148] (KMPW). In Ref. [147], these results were tested against the corresponding estimates one can obtain from the LCSR form factors in Ref. [165] (BZ). Here, we will discuss the results from Ref. [150] in a similar way, checking the robustness of this extraction.

The form factors F are parametrised according to Eq. (6.1.2). Following the standard method described in the beginning of this chapter, for a specific set of LCSR form factors $\{F^{\mathrm{LCSR}}(q^2)\}$, the power corrections $\Delta F^\Lambda(q^2)$ can then be determined as the difference between the full $F^{\mathrm{LCSR}}(q^2)$ and the large-recoil result $F^\infty(q^2)$ upon including α_s-corrections $\Delta F^{\alpha_s}(q^2)$ from QCDf. In practice we fit the coefficients a_F, b_F, c_F of the parametrisation in Eq. (6.1.3) to the central value of the LCSR results. In Tab. 6.2 we show the results obtained within this approach applied to the form factors from Ref. [150].

In contrast to previous LCSR calculations, Ref. [150] for the first time provided the correlations among the form factors, enabling us to fit not only the central values of the parameters a_F, b_F, c_F but also their uncertainties according to the correlation matrix of the form factors, which will serve us to illustrate the good control of our method of factorisable power corrections. Tab. 6.2 displays the results for the input scheme 1, defined in Eq. (6.2.4), and parametrising power corrections in the transversity basis $\{V, A_1, A_2, A_0, T_1, T_2, T_3\}$ (this corresponds to the default choice in Ref. [147]).

The relative size of power corrections,

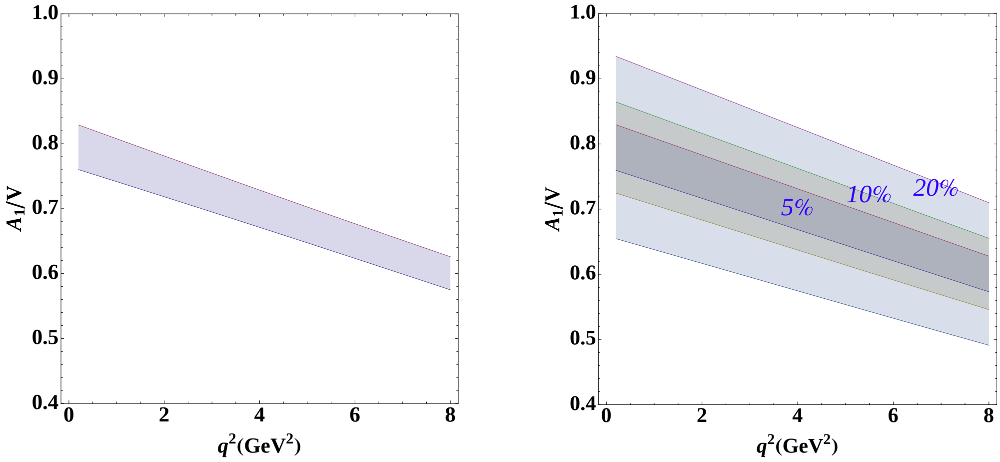

Figure 6.1: Ratio of form factors A_1/V applying the full and soft form factor approaches to the results of Ref. [150]. Left: error band according to the LCSR calculation from Ref. [150]. Right: error bands following the soft form factor approach with $\delta = 5\%, 10\%, 20\%$ power corrections.

$$r(q^2) = \left| \frac{a_F + b_F \frac{q^2}{m_B^2} + c_F \frac{q^4}{m_B^4}}{F(q^2)} \right|, \tag{6.2.12}$$

is displayed on the right-hand side of Tab. 6.2 for different invariant masses $q^2 = 0\,\text{GeV}^2$, $4\,\text{GeV}^2$, $8\,\text{GeV}^2$ of the lepton pair. Typically, the central values of the power corrections are within the range of $(5-10)\%$, with uncertainties below 5%.These findings are in line with the results for the central values of the form factors from Refs. [165] (BZ) and [148] (KMPW) obtained in Ref. [147]. Exceptions occur at large q^2 for the form factors A_2 and T_3, which are calculated as linear combination of two functions in Ref. [150]. In the case of A_2, the central values of the power corrections reach up to 19%, while the respective uncertainties still do not exceed 10%. Note that in scheme 1, the power corrections to A_2 are not an independent function, but they are fixed from the ones to A_1 as detailed in Ref. [147]. In the case of T_3, the central values are quite small but come with uncertainties that grow up to 18%. It turns out that the power corrections to these two form factors have no impact on the key observables P_5', P_1 and P_2 as can be seen from the analytic formulae in Sec. 6.2.3, where these terms are either absent or numerically suppressed.

For comparison, Tab. 6.2 also features the estimate of power corrections by a generic size of $\delta = 10\%$ following the approach of Ref. [147] to estimate the uncertainties on a_F, b_F, c_F in the absence of information on the correlations among form factors. By definition, the ratio $r(q^2)$ yields 10% for these estimates for all form factors, except for A_0 and A_2 where the power corrections are not independent but follow from correlations among form factors. The comparison with the results from the fit shows that the estimate of power corrections by a generic size of $\delta = 10\%$ in Refs. [147] is conservative compared to the procedure followed in Refs. [144, 145, 163, 164, 166] consisting in a direct extraction of the errors from the uncertainties given in Ref. [150]. This is further illustrated in Fig. 6.1, where the form factor ratio A_1/V dominating the observable P_5' is shown, comparing the direct error assessment from Ref. [150] (left plot) and our results from uncertainty assignments of $\delta = 5\%, 10\%, 20\%$ power corrections.

Let us now illustrate how the treatment of power corrections affects the uncertainties of relevant

$\langle P_5' \rangle_{[4.0,6.0]}$	scheme 1	scheme 2
a	-0.72 ± 0.05	-0.72 ± 0.15
b	-0.72 ± 0.03	-0.72 ± 0.04
c	-0.72 ± 0.03	-0.72 ± 0.03
full BSZ	-0.72 ± 0.03	

Table 6.3: SM prediction for P_5' in the anomalous bin $[4,6]\,\mathrm{GeV}^2$ together with the error from soft form factors and factorisable power corrections (all other sources of errors have been switched off). Results are shown for the three different options for the treatment of power corrections and for the two different input schemes discussed in the text. The last row contains the prediction from a direct use of the full form factors from Ref. [150].

$B \to K^* \ell\ell$ observables. Taking the above results, and following a similar procedure for the scheme 2 defined in Sec. 6.2.1, we can compute the SM prediction for P_5' in the anomalous bin $[4,6]\,\mathrm{GeV}^2$ together with the error from soft form factors and factorisable power corrections (all other sources of errors have been switched off). The results are given in Tab. 6.3 for the two schemes, with three different options for the treatment of power corrections:

a) Estimating the error size of a_F, b_F, c_F as $\sim 10\% \times F^{\mathrm{LCSR}}$ and including only the correlations dictated by the large-recoil symmetries. LCSR input is only used to extract the soft form factors $\xi_\perp$ and $\xi_\parallel$ which are considered as uncorrelated.

b) Determining the errors of a_F, b_F, c_F from the fit to the form factors from Ref. [150] but including only the correlations dictated by the large-recoil symmetries exactly as in the previous case.

c) Determining the errors of a_F, b_F, c_F from a correlated fit to the form factors from Ref. [150] and including the correlations between the a_F, b_F, c_F and the soft form factors $\xi_\perp, \xi_\parallel$ as extracted from the correlation matrix in Ref. [150].

The error estimate in option a) is mainly based on the fundamental large-recoil symmetries and thus to a large extent independent of the details of the particular LCSR calculation [150]. When going over option b) to c), we include in each step more information from Ref. [150] (the actual size of power corrections for option b), and the correlations for option c)). With option c) the full information from the particular LCSR form factors is used, implying that the result must be independent of the input scheme (apart from a residual scheme dependence from non-factorisable power corrections) and that it must coincide with the one obtained by a direct use of the correlated full form factors (displayed in the last row of Tab. 6.3). The numerical confirmation of this correspondence provides a consistency check for our implementation of the fit of the power corrections and the various methods.

In Tab. 6.3, the errors obtained in option b) are very similar to the ones using option c). From this observation we conclude that the correlations among the power correction parameters a_F, b_F, c_F and the ones among the soft form factors $\xi_\perp, \xi_\parallel$ have very little impact and that the dominant form factor correlations are indeed the ones from the large-recoil symmetries. The difference in the errors for option a) between scheme 1 and scheme 2 is easily understood: while the LCSR results of Ref. [150] end up with about $\delta \sim 5\%$ power corrections, a generic size of $\delta = 10\%$ is assumed for option a). In scheme 1, this leads to the expected increase of the errors by roughly a factor 2. On the other hand, in scheme 2, we find an increase of the errors by more than a factor 4, in accordance with the discussion in the previous section. As argued there, the implementation of option a) in scheme 2 actually corresponds to the assumption of $\delta = 20\%$ power corrections for the relevant form factor ratio A_1/V.

6.2.3 Analytic formulae for factorisable power corrections to optimised observables

We have considered a particular observable and demonstrated numerically that the prediction for observables depends on the scheme chosen for the soft form factors $\xi_{\perp,\|}$. In this section we illustrate this scheme dependence more explicitly by giving analytic formulae for the power corrections to the observables P_5', P_1 and P_2, both in the transversity and in the helicity basis. The two bases are related to each other via the relations given in Eq. (31) of Ref. [151]. In both cases we parametrise the power corrections according to Eq. (6.1.3). The formulae are given without fixing a particular scheme, i.e., before power corrections are partially absorbed into the non-perturbative input parameters $\xi_\perp$ and $\xi_\|$.

In the helicity basis, the formula for P_5' reads

$$
\begin{aligned}
P_5' = P_5'|_\infty \Bigg(1 &+ \frac{2a_{V_-} - 2a_{T_-}}{\xi_\perp} \frac{\mathcal{C}_7^{\rm eff}(\mathcal{C}_{9,\perp}\mathcal{C}_{9,\|} - \mathcal{C}_{10}^2)}{(\mathcal{C}_{9,\perp}+\mathcal{C}_{9,\|})(\mathcal{C}_{9,\perp}^2+\mathcal{C}_{10}^2)} \frac{m_b m_B}{q^2} \\
&- \frac{2a_{V_+}}{\xi_\perp} \frac{\mathcal{C}_{9,\|}}{\mathcal{C}_{9,\perp}+\mathcal{C}_{9,\|}} + \frac{2a_{V_0} - 2a_{T_0}}{\tilde{\xi}_\|} \frac{\mathcal{C}_7^{\rm eff}(\mathcal{C}_{9,\perp}\mathcal{C}_{9,\|} - \mathcal{C}_{10}^2)}{(\mathcal{C}_{9,\perp}+\mathcal{C}_{9,\|})(\mathcal{C}_{9,\|}^2+\mathcal{C}_{10}^2)} \frac{m_b}{m_B} \\
&+ \text{nonlocal terms} \Bigg) + O\left(\frac{m_{K^*}}{m_B}, \frac{\Lambda^2}{m_B^2}, \frac{q^2}{m_B^2}\right),
\end{aligned}
\tag{6.2.13}
$$

where $\tilde{\xi}_\| = (E_{K^*}/m_{K^*})\,\xi_\|$ and following Ref. [146], we have defined

$$
\mathcal{C}_{9,\perp} = \mathcal{C}_9^{\rm eff} + \frac{2m_b m_B}{q^2}\mathcal{C}_7^{\rm eff}, \qquad \mathcal{C}_{9,\|} = \mathcal{C}_9^{\rm eff} + \frac{2m_b}{m_B}\mathcal{C}_7^{\rm eff}. \tag{6.2.14}
$$

We denote the large-recoil expression as $P_5'|_\infty$ and leave aside non-local terms, corresponding to non-factorisable corrections. Our result agrees with Eq. (25) of Ref. [146] for the terms proportional to $a_{V_-}, a_{T_-}, a_{V_0}, a_{T_0}$, but we find an additional term proportional to a_{V_+}. We would like to stress that precisely this term, which is hidden in "further terms" and not discussed in Ref. [146], dominates the power corrections in the anomalous region around $q_0^2 \sim 6\,\text{GeV}^2$, as can be seen from the numerical evaluation of Eq. (6.2.13):

$$
\begin{aligned}
P_5'(6\,\text{GeV}^2) = P_5'|_\infty(6\,\text{GeV}^2) \Bigg(1 &+ 0.18\frac{2a_{V_-} - 2a_{T_-}}{\xi_\perp} - 0.73\frac{2a_{V_+}}{\xi_\perp} + 0.02\frac{2a_{V_0} - 2a_{T_0}}{\tilde{\xi}_\|} \\
&+ \text{nonlocal terms} \Bigg) + O\left(\frac{m_{K^*}}{m_B}, \frac{\Lambda^2}{m_B^2}, \frac{q^2}{m_B^2}\right).
\end{aligned}
\tag{6.2.15}
$$

This means that the discussion on the scheme dependence of P_5' in Ref. [146] only takes into account numerically subleading contributions. Converted into the transversity basis, Eq. (6.2.13) becomes

$$P_5' = P_5'|_\infty \Bigg(1 + \frac{a_{A_1} + a_V - 2a_{T_1}}{\xi_\perp} \frac{\mathcal{C}_7^{\rm eff}(\mathcal{C}_{9,\perp}\mathcal{C}_{9,\|} - \mathcal{C}_{10}^2)}{(\mathcal{C}_{9,\perp} + \mathcal{C}_{9,\|})(\mathcal{C}_{9,\perp}^2 + \mathcal{C}_{10}^2)} \frac{m_b m_B}{q^2} - \frac{a_{A_1} - a_V}{\xi_\perp} \frac{\mathcal{C}_{9,\|}}{\mathcal{C}_{9,\perp} + \mathcal{C}_{9,\|}} - \frac{a_{T_1} - a_{T_3}}{\tilde{\xi}_\|} \frac{\mathcal{C}_7^{\rm eff}(\mathcal{C}_{9,\perp}\mathcal{C}_{9,\|} - \mathcal{C}_{10}^2)}{(\mathcal{C}_{9,\perp} + \mathcal{C}_{9,\|})(\mathcal{C}_{9,\|}^2 + \mathcal{C}_{10}^2)} \frac{m_b}{m_{K^*}} + \text{nonlocal terms} \Bigg) + O\left(\frac{m_{K^*}}{m_B}, \frac{\Lambda^2}{m_B^2}\right), \tag{6.2.16}$$

with the dominant term being proportional to the combination $a_{A_1} - a_V$ of power correction parameters. If A_1 or V is chosen as input for $\xi_\perp$, the corresponding parameter a_{A_1} or a_V vanishes identically. On the other hand, if T_1 is taken as input, both a_{A_1} or a_V survive and their independent variation leads to an increase of the errors associated to power corrections. This behaviour explains part of the inflated errors in Ref. [151] and it is analytically pinned down in Eqs. (6.2.13) and (6.2.19). The formulae support the numerical analysis reported in Fig. 2 of Ref. [147], where the binned predictions for P_1, P_2, P_4', P_5' were given in the two schemes with $\xi_\perp$ defined from V or T_1, respectively. Without any further assumption on the correlations between the parameters a_F, Eqs. (6.2.13) and (6.2.19) manifest an explicit scheme dependence whose origin and interpretation was discussed in detail in Sec. 6.2.1.

For the observable P_1, which vanishes in the large-recoil limit, we find in the helicity basis

$$P_1 = -\frac{2a_{V_+}}{\xi_\perp} \frac{(\mathcal{C}_9^{\rm eff}\mathcal{C}_{9,\perp} + \mathcal{C}_{10}^2)}{\mathcal{C}_{9,\perp}^2 + \mathcal{C}_{10}^2} - \frac{2b_{T_+}}{\xi_\perp} \frac{2\mathcal{C}_7^{\rm eff}\mathcal{C}_{9,\perp}}{\mathcal{C}_{9,\perp}^2 + \mathcal{C}_{10}^2} \frac{m_b}{m_B} + \text{nonlocal terms} + O\left(\frac{m_{K^*}}{m_B}, \frac{\Lambda^2}{m_B^2}, \frac{q^2}{m_B^2}\right), \tag{6.2.17}$$

turning in the transversity basis into

$$P_1 = -\frac{a_{A_1} - a_V}{\xi_\perp} \frac{(\mathcal{C}_9^{\rm eff}\mathcal{C}_{9,\perp} + \mathcal{C}_{10}^2)}{\mathcal{C}_{9,\perp}^2 + \mathcal{C}_{10}^2} - \frac{b_{T_2} - b_{T_1}}{\xi_\perp} \frac{2\mathcal{C}_7^{\rm eff}\mathcal{C}_{9,\perp}}{\mathcal{C}_{9,\perp}^2 + \mathcal{C}_{10}^2} \frac{m_b}{m_B} + \text{nonlocal terms} + O\left(\frac{m_{K^*}}{m_B}, \frac{\Lambda^2}{m_B^2}, \frac{q^2}{m_B^2}\right). \tag{6.2.18}$$

Our result, Eq. (6.2.17), fully agrees with Eq. (26) of Ref. [146]. The authors of Ref. [146] used this result to argue that P_1 should be much cleaner than P_5' because it only involves one soft form factor and a lower number of power correction parameters a_F. However, the total number of power correction parameters is not the relevant criterion to decide whether an observable is clean: as seen before, in the case of P_5' the coefficients in front of the power correction parameters exhibit a strong hierarchy, so that in practice only one term becomes relevant. As a matter of fact, the leading power corrections for both P_5' and P_1 stem from a_{V_+} and the respective coefficients are of the same size, as seen when comparing the evaluation of Eq. (6.2.17) for $q_0^2 = 6\,\text{GeV}^2$,

$$P_1(6\,\text{GeV}^2) = -\,1.21\frac{2a_{V_+}}{\xi_\perp} + 0.05\frac{2b_{T_+}}{\xi_\perp} + \text{nonlocal terms} + O\left(\frac{m_{K^*}}{m_B}, \frac{\Lambda^2}{m_B^2}, \frac{q^2}{m_B^2}\right), \tag{6.2.19}$$

with the corresponding one for P_5' from Eq. (6.2.15). Therefore, P_1 and P_5' are on an equal footing with respect to power corrections, and all statements above, regarding the scheme dependence of P_5', also apply to P_1. Like P_5', P_1 suffers from an increase of power corrections when $\xi_\perp$ is defined from T_1 instead of from V, as already demonstrated numerically in Fig. 2 of Ref. [147] and analytically in Eq.(6.2.18).

Turning finally to the observable P_2, we find in the helicity basis

$$P_2 = P_2|_\infty \left(1 + \frac{2a_{V_-} - 2a_{T_-}}{\xi_\perp} \frac{\mathcal{C}_7^{\text{eff}}(\mathcal{C}_{9,\perp}^2 - \mathcal{C}_{10}^2)}{\mathcal{C}_{9,\perp}(\mathcal{C}_{9,\perp}^2 + \mathcal{C}_{10}^2)} \frac{m_b m_B}{q^2} + \text{nonlocal terms}\right) + O\left(\frac{m_{K^*}}{m_B}, \frac{\Lambda^2}{m_B^2}, \frac{q^2}{m_B^2}\right), \tag{6.2.20}$$

which translates into

$$P_2 = P_2|_\infty \left(1 + \frac{a_V + a_{A_1} - a_{T_1} - a_{T_2}}{\xi_\perp} \frac{\mathcal{C}_7^{\text{eff}}(\mathcal{C}_{9,\perp}^2 - \mathcal{C}_{10}^2)}{\mathcal{C}_{9,\perp}(\mathcal{C}_{9,\perp}^2 + \mathcal{C}_{10}^2)} \frac{m_b m_B}{q^2} + \text{nonlocal terms}\right) + O\left(\frac{m_{K^*}}{m_B}, \frac{\Lambda^2}{m_B^2}, \frac{q^2}{m_B^2}\right), \tag{6.2.21}$$

in the transversity basis, with $P_2|_\infty = \mathcal{C}_{9,\perp}\mathcal{C}_{10}/(\mathcal{C}_{9,\perp}^2 + \mathcal{C}_{10}^2)$. Unlike P_1 and P_5', the leading term in P_2 involves both (axial-)vector and tensor power corrections, and at first sight it seems that there is no preference whether to define $\xi_\perp$ from V or from T_1. Note, however, that the kinematic relation $T_1(0) = T_2(0)$ implies $a_{T_1} = a_{T_2}$ and that a definition from T_1 hence absorbs both a_{T_1} and a_{T_2} and leads to smaller uncertainties from corrections. Again, this is confirmed by the numerical results in Fig. 2 of Ref. [147].

We see that the scheme dependence of the angular observables can be explicitly worked out by studying the analytic dependence on the power correction parameters. Our results agree with Ref. [146] for P_1, but we have shown that the formula for P_5' in Ref. [146] actually misses the dominant and manifestly scheme-dependent term. Our analytic formulae allow us to understand how different schemes can yield significantly different uncertainties if one treats power corrections as uncorrelated, in perfect agreement with the numerical discussion in Ref. [147]. We can spot the relevant form factor(s) whose power corrections are going to have the main impact on each observable, and thus identify appropriate schemes to compute each observable accurately.

6.3 Reassessing the reappraisal of long-distance charm loops

We now turn to the second main source of hadronic uncertainties: non-factorisable Λ_{QCD}/m_B corrections associated with non-perturbative $c\bar{c}$ loops. Notice that Eq. (6.1.11) suggests that these contributions formally enter $\mathcal{C}_9$ on the same footing as possible short-distance NP effects, so they could potentially mimic a NP contribution to $\mathcal{C}_9$. Hence, disentangling one contribution from the other is of utmost importance for NP searches in $b \to s\ell\ell$ decays. While the latter would induce a q^2-independent $\mathcal{C}_9$, universal for the three different transversities $i = \perp, \|, 0$, non-factorisable long-distance effects from $c\bar{c}$ loops in general introduce a q^2- and transversity dependence that can be cast into effective coefficient functions $\mathcal{C}_{9\,i}^{c\bar{c}}(q^2)$. A promising strategy thus consists in investigating whether the $B \to K^*\mu^+\mu^-$ data points towards a q^2-dependent effect. To this end the authors of Refs. [144, 145] performed a fit of the functions $\mathcal{C}_{9\,i}^{c\bar{c}}(q^2)$ to the data using a polynomial parametrisation. In Sec. 6.3.1 we comment on the results, before presenting in Sec. 6.3.2 our own analysis based on a different, frequentist, statistical framework.

6.3.1 A thorough interpretation of charm estimates in the literature

The analysis in Refs. [144, 145] introduces for each helicity $\lambda = 0, \pm 1$ a second-order polynomial in q^2:

$$h_\lambda = h_\lambda^{(0)} + \frac{q^2}{1\ \text{GeV}^2} h_\lambda^{(1)} + \frac{q^4}{1\ \text{GeV}^4} h_\lambda^{(2)}. \tag{6.3.1}$$

The functions h_λ, with a total number of 18 real parameters, then enter the $B \to K^*\mu^+\mu^-$ transversity amplitudes as follows:

$$\begin{aligned}
A_{L,R}^0 &= A_{L,R}^0(s_i = 0) + \frac{N}{q^2}\left(\frac{q^2}{1\ \text{GeV}^2} h_0^{(1)} + \frac{q^4}{1\ \text{GeV}^4} h_0^{(2)}\right), \\
A_{L,R}^{\|} &= A_{L,R}^{\|}(s_i = 0) \\
&\quad + \frac{N}{\sqrt{2}q^2}\left[(h_+^{(0)} + h_-^{(0)}) + \frac{q^2}{1\ \text{GeV}^2}(h_+^{(1)} + h_-^{(1)}) + \frac{q^4}{1\ \text{GeV}^4}(h_+^{(2)} + h_-^{(2)})\right], \\
A_{L,R}^{\perp} &= A_{L,R}^{\perp}(s_i = 0) \\
&\quad + \frac{N}{\sqrt{2}q^2}\left[(h_+^{(0)} - h_-^{(0)}) + \frac{q^2}{1\ \text{GeV}^2}(h_+^{(1)} - h_-^{(1)}) + \frac{q^4}{1\ \text{GeV}^4}(h_+^{(2)} - h_-^{(2)})\right],
\end{aligned} \tag{6.3.2}$$

with the normalisation

$$N = V_{tb}V_{ts}^* \frac{m_B^{3/2} G_F \alpha \sqrt{q^2}}{\sqrt{3}\pi} \lambda^{1/4}(m_B^2, m_{K^*}^2, q^2)\left(1 - \frac{4m_\ell^2}{q^2}\right)^{1/4}. \tag{6.3.3}$$

Here, $s_i = 0$ indicates that only the perturbative quark-loop contribution $Y(q^2)$ has been included in the amplitudes $A_{L,R}^\lambda(s_i = 0)$ while any long-distance contribution as the one calculated in Ref. [148], which we include in our general theoretical framework [113], is switched off.

The coefficients $h_\lambda^{(i)}$ parametrise the q^2-expansion of the charm-loop contribution to the various helicity amplitudes, but can also (partially) be mimicked by NP contributions to the Wilson coefficients $\mathcal{C}_7$ and $\mathcal{C}_9$. Note that a NP contribution to $\mathcal{C}_7$ would yield a pole at $q^2 = 0$ and thus contribute to $h_\lambda^{(0)}$ and higher orders, whereas a NP contribution to $\mathcal{C}_9$ would contribute only starting from $h_\lambda^{(1)}$ and higher orders. Let us stress that both kinds of NP contributions would also contribute to $h_\lambda^{(2)}$, since they enter the transversity amplitudes as a Wilson coefficient multiplied by a q^2-dependent form factor [4]. Contrary to Refs. [144, 145], we have set $h_0^{(0)} = 0$ in order to avoid an unphysical pole at $q^2 = 0$ in $A_{L,R}^0$ (which for instance would result in a divergence in $\mathcal{B}(B \to K^*\gamma)$).

For a proper interpretation of the results obtained in Ref. [144], it is important to note that the authors study two different hypotheses:

[4] It is thus not correct to state that $h^{(2)}$ and higher coefficients can arise only due to long-distance physics as suggested in Ref. [144, 145]. Even though the form factors do not vary strongly with q^2, the presence of NP contributions to Wilson coefficients would generate terms corresponding to (small) contributions to higher orders in the polynomial expansion.

n	0		1		2		3	
$\chi^{2(n)}_{\rm min}$	70.00		52.70		51.50		51.20	
$\chi^{2(n-1)}_{\rm min} - \chi^{2(n)}_{\rm min}$	1.64	(0.5 σ)	17.30	(3.4 σ)	1.14	(0.3 σ)	0.35	(0.1 σ)
$h_+^{(0)}$	$0.17^{+1.15}_{-0.62}$	(0.3 σ)	$2.22^{+1.07}_{-1.13}$	(2.0 σ)	$1.28^{+1.45}_{-0.40}$	(3.2 σ)	$1.19^{+1.32}_{-0.62}$	(1.9 σ)
$h_+^{(1)}$			$-2.37^{+1.42}_{-0.57}$	(1.7 σ)	$-1.66^{+1.43}_{-1.03}$	(1.2 σ)	$-1.31^{+0.83}_{-1.21}$	(1.6 σ)
$h_+^{(2)}$					$-0.11^{+0.19}_{-0.14}$	(0.6 σ)	$-0.09^{+0.11}_{-0.11}$	(0.8 σ)
$h_+^{(3)}$							$-0.00^{+0.01}_{-0.00}$	(0.2 σ)
$h_-^{(0)}$	$1.30^{+1.47}_{-1.07}$	(1.2 σ)	$2.62^{+1.58}_{-2.69}$	(1.0 σ)	$2.30^{+1.68}_{-1.76}$	(1.3 σ)	$1.85^{+1.93}_{-1.09}$	(1.7 σ)
$h_-^{(1)}$			$-0.34^{+0.90}_{-0.53}$	(0.4 σ)	$-1.24^{+1.53}_{-0.21}$	(0.8 σ)	$-0.94^{+1.19}_{-0.64}$	(0.8 σ)
$h_-^{(2)}$					$0.13^{+0.06}_{-0.19}$	(0.7 σ)	$0.11^{+0.12}_{-0.18}$	(0.6 σ)
$h_-^{(3)}$							$0.00^{+0.00}_{-0.01}$	(0.0 σ)
$h_0^{(1)}$			$-1.00^{+1.69}_{-0.89}$	(0.6 σ)	$-1.35^{+1.70}_{-1.14}$	(0.8 σ)	$-0.96^{+1.01}_{-1.45}$	(0.9 σ)
$h_0^{(2)}$					$0.10^{+0.12}_{-0.10}$	(1.0 σ)	$0.11^{+0.11}_{-0.17}$	(0.6 σ)
$h_0^{(3)}$							$-0.00^{+0.01}_{-0.00}$	(0.2 σ)

Table 6.4: Fit to $B \to K^*\mu^+\mu^-$ only, with $\mathcal{C}_{9\mu}^{\rm NP} = 0$, using LCSR from Ref. [148] in the soft-form-factor approach employed by Ref. [113]. All coefficients are given in units of 10^{-4}. Different orders n of the polynomial parametrisation of the long-distance charm-loop contribution are considered. If this contribution is set to zero, the fit yields $\chi^2_{{\rm min};h=0} = 71.60$ for $N_{dof} = 59$.

- Hypothesis 1: No constraint is imposed on the long-distance charm-loop contribution represented by the coefficients $h_\lambda^{(i)}$, and the results of the LCSR computation in Ref. [148] are not used in the fit. Instead, after fitting the functions $h_\lambda(q^2)$ to the $B \to K^*\mu^+\mu^-$ data they are compared with the functions $\tilde{g}_i^{\mathcal{M}}$ calculated in Ref. [148]. We have checked the relation between the functions $\tilde{g}_i^{\mathcal{M}}$ and the long-distance charm-loop contributions h_λ, given by Eq. (2.7) in Ref. [144] (up to the correction $\mathcal{C}_1 \to \mathcal{C}_2$ noticed in Ref. [145]). Rewriting the amplitudes $\mathcal{M}_{1,2,3}$ in Ref. [148] in terms of helicity amplitudes leads to [5]:

$$\begin{aligned}
{\rm Re}\, \tilde{g}_1^{\mathcal{M}} &= -\frac{1}{2\mathcal{C}_2}\frac{16 m_B^3 (m_B + m_{K^*})\pi^2}{\sqrt{\lambda(q^2)}V(q^2)q^2}\left({\rm Re}\, h_-(q^2) - {\rm Re}\, h_+(q^2)\right), \\
{\rm Re}\, \tilde{g}_2^{\mathcal{M}} &= -\frac{1}{2\mathcal{C}_2}\frac{16 m_B^3 \pi^2}{(m_B + m_{K^*})A_1(q^2)q^2}\left({\rm Re}\, h_-(q^2) + {\rm Re}\, h_+(q^2)\right), \\
{\rm Re}\, \tilde{g}_3^{\mathcal{M}} &= \frac{1}{2\mathcal{C}_2}\frac{64\pi^2 m_B^3 m_{K^*}\sqrt{q^2}(m_B + m_{K^*})}{\lambda(q^2)A_2(q^2)q^2}\Big[{\rm Re}\, h_0(q^2) \\
&\quad - \frac{16 m_B^3 \pi^2 (m_B + m_{K^*})(m_B^2 - q^2 - m_{K^*}^2)}{\lambda(q^2)A_2(q^2)q^2}\left({\rm Re}\, h_-(q^2) + {\rm Re}\, h_+(q^2)\right)\Big]. \quad (6.3.4)
\end{aligned}$$

It is interesting to observe that the results of the fit in Ref. [144] for $\tilde{g}_i^{\mathcal{M}}$ seem to agree well with the LCSR estimates of Ref. [148] if in all amplitudes approximately the same q^2-independent shift is added to the LCSR result. This observation is in line with the conclusions from global fits [113, 163, 164], bearing in mind that in Ref. [144, 145] basically only $B \to K^*\mu^+\mu^-$ data is used and that the authors interpret this constant shift as being of hadronic origin. Notice that such a q^2-independent shift (very similar for all helicity amplitudes) is at odds with a q^2- and helicity-dependent contribution expected in the case of an hadronic effect, in particular if it is attributed to tails of resonances. Note, however, that a firm conclusion can only be

[5] Even though Eq. (6.3.4) is also valid for the imaginary part of the functions, we only consider the real part of the $\tilde{g}_i^{\mathcal{M}}$ here, as the authors of Ref. [148] consider these contributions to be real in the region of interest within their approximations.

drawn by comparing the quality of a fit for a q^2-independent contribution with the one for q^2-dependent functions, a task that was not carried out in Refs. [144, 145] and that will be performed in Sec. 6.3.2. In any case, one should keep in mind that a universal shift in $\mathcal{C}_{9\mu}$ due to NP can also explain the deviations in $B_s \to \phi\mu^+\mu^-$ and the violation of lepton-flavour universality suggested by R_K and $Q_5 = P_5^{\mu\prime} - P_5^{e\prime}$ (see Chapter 7 for more details on Q_i observables), which is not the case for hadronic $c\bar{c}$ contributions.

- Hypothesis 2: In a second analysis, the authors of Ref. [144] impose an additional constraint to the fit: they assume that the results of Ref. [148] hold exactly for $q^2 \leq 1$ GeV^2, while they do not make any assumptions for $q^2 > 1$ GeV^2 and again set all the Wilson coefficients to their SM value. The results obtained in this second approach have to be interpreted with great care:

  i) The authors of Ref. [144] decide to take the results of Ref. [148] as exact in the region $q^2 < 1$ GeV^2 but to discard them for larger q^2: this choice of range is rather arbitrary, as the LCSR approach yields a computation valid up to 2 GeV^2 according to Ref. [148], and the extrapolation via the dispersion relation is deemed appropriate up to 4 GeV^2 by the authors of Ref. [144] themselves.

  ii) The additional constraint artificially tilts the fit by forcing it to follow a behaviour at $q^2 \lesssim 1$ GeV^2 against the trend of data (which would prefer to have a constant shift $\mathcal{C}_9^{\rm NP}$, as discussed in Refs. [113, 163, 164, 167], corresponding to non-vanishing $h_\lambda^{(1)}$ in the framework of Ref. [144]). This is compensated by a spurious q^4-dependence with $h_\lambda^{(2)} \neq 0$, which is then interpreted in Refs. [144, 145] as an indication of non-local hadronic effects.

  iii) In the region below 1 GeV^2, the treatment of the distribution by LHCb means that the data correspond to slightly different observables from the optimized observables defined in Ref. [103, 112], as discussed in Sec. 2.3.1 in Ref. [113] and in the previous section. This effect, which can be taken into account by a redefinition of the optimized observables, is not considered in Ref. [144, 145] and can affect the outcome of the analysis.

  iv) Finally, the LCSR computation of Ref. [148] does not take into account all non-local effects but is an estimate of the soft gluon part with respect to the leading-order factorisable contribution, from which the imaginary part is still missing. In this sense it is not consistent to compare the absolute value of the fitted $\tilde{g}_i^{\mathcal{M}}$ obtained from data with the computation of Ref. [148], and if one still insists in doing so (ignoring all previous issues), at least one should compare their real parts rather than the absolute values.

We conclude that a fit under the second hypothesis cannot indicate whether a q^2-dependent effect is favoured over a constant one, since it artificially creates a q^2-dependence by putting a constraint on one side (below $q^2 = 1$ GeV^2). A fit under the first hypothesis can be an appropriate method, but requires to compare the quality of the fits obtained in both cases under consideration of the number of free parameters. We will address this issue in the following.

n	0		1		2		3	
$\chi^{2(n)}_{\rm min}$	62.10		51.60		50.50		50.00	
$\chi^{2(n-1)}_{\rm min} - \chi^{2(n)}_{\rm min}$	1.23	(0.3 σ)	10.50	(2.4 σ)	1.14	(0.3 σ)	0.53	(0.1 σ)
$h_+^{(0)}$	$0.66^{+1.06}_{-0.55}$	(1.2 σ)	$1.97^{+1.32}_{-0.51}$	(3.8 σ)	$1.62^{+1.22}_{-1.00}$	(1.6 σ)	$1.43^{+1.13}_{-0.80}$	(1.8 σ)
$h_+^{(1)}$			$-1.92^{+0.81}_{-0.76}$	(2.4 σ)	$-1.29^{+1.70}_{-1.75}$	(0.8 σ)	$-1.45^{+1.40}_{-0.74}$	(1.0 σ)
$h_+^{(2)}$					$-0.16^{+0.24}_{-0.09}$	(0.7 σ)	$-0.09^{+0.08}_{-0.16}$	(1.2 σ)
$h_+^{(3)}$							$0.00^{+0.01}_{-0.00}$	(0.0 σ)
$h_-^{(0)}$	$-0.14^{+1.43}_{-0.93}$	(0.1 σ)	$1.90^{+1.99}_{-1.64}$	(1.2 σ)	$1.87^{+2.71}_{-1.31}$	(1.4 σ)	$1.93^{+1.93}_{-0.93}$	(2.1 σ)
$h_-^{(1)}$			$-0.81^{+0.68}_{-0.43}$	(1.2 σ)	$-0.56^{+0.48}_{-1.32}$	(1.2 σ)	$-0.65^{+0.59}_{-0.82}$	(1.1 σ)
$h_-^{(2)}$					$-0.04^{+0.22}_{-0.07}$	(0.2 σ)	$-0.02^{+0.14}_{-0.10}$	(0.1 σ)
$h_-^{(3)}$							$-0.00^{+0.00}_{-0.00}$	(0.2 σ)
$h_0^{(1)}$			$-1.28^{+1.17}_{-1.24}$	(1.1 σ)	$-2.24^{+1.64}_{-1.43}$	(1.4 σ)	$-2.08^{+0.90}_{-1.38}$	(2.3 σ)
$h_0^{(2)}$					$0.08^{+0.17}_{-0.07}$	(1.1 σ)	$0.16^{+0.17}_{-0.12}$	(1.3 σ)
$h_0^{(3)}$							$-0.00^{+0.01}_{-0.00}$	(0.5 σ)

Table 6.5: Fit to $B \to K^*\mu^+\mu^-$ only, with $\mathcal{C}_{9\mu}^{\rm NP} = -1.1$, using LCSR from Ref. [148] in the soft-form-factor approach employed by Ref. [113]. All coefficients are given in units of 10^{-4}. Different orders n of the polynomial parametrisation of the long-distance charm-loop contribution are considered. If this contribution is set to zero, the fit yields $\chi^2_{\min;h=0} = 63.30$ for $N_{dof} = 59$.

6.3.2 A frequentist fit

We are going to perform fits using the general approach described in Section 6.1, taking LHCb data on $B \to K^*\mu\mu$ as data. We follow this theoretical framework for the predictions of the observables, but modify it slightly to remain as close as possible to the fits shown in Refs. [144, 145]: we will not use the computation of long-distance charm effects in Ref. [148]. In practice, this amounts to keeping only the perturbative function $Y(q^2)$ while setting all three $s_i = 0$. We treat the form factors using the soft-form-factor approach with the inputs of Ref. [148], and employ the same parametrisation Eq. (6.3.2) as Refs. [144, 145] for the long-distance charm contribution, extending it in a straightforward way to the order q^6 by introducing the parameters $h_\lambda^{(3)}$. We take all coefficients of the expansion as real, following Ref. [148]. Note that the results of Ref. [144, 145] favour mostly real values for h_+ and h_0, but not necessarily for h_-.

Our fits differ from the ones in Refs. [144, 145] with respect to the statistical framework. We use a frequentist approach and in particular do not assume any a-priory range for the fit parameters $h_\lambda^{(i)}$, contrary to the Bayesian approach in Refs. [144, 145] where (flat or Gaussian) priors are used for the polynomial parameters. Keeping in mind that the functions $h_\lambda(q^2)$ are expansions in q^2, we perform fits allowing for $h_\lambda^{(i)}$ with $i \leq n$, increasing progressively the degree of the polynomials n. At each order, we determine the minimum $\chi^2_{\rm min}$ as well as the difference between the $\chi^2_{\rm min}$ with polynomial degrees $n-1$ and n, and the pull of the hypothesis $h^{(n)}_{0,+,-} = 0$. This information indicates the improvement of the fit obtained by increasing the degree of the polynomial expansion.

In Tabs. 6.4 and 6.5, we provide the results in the SM case and in the NP scenario $\mathcal{C}_9^{\rm NP} = -1.1$, respectively, using only $B \to K^*\mu^+\mu^-$ data. We see that in both cases, the fit clearly improves when increasing the degree of the polynomial from $n = 0$ to $n = 1$ (the addition of the parameters $h_\lambda^{(1)}$ leads to a q^2 dependence similar to that of a NP contribution to the Wilson coefficient $\mathcal{C}_9$). On the other hand, including quadratic or cubic terms does not provide any significant improvement. This implies that the fit does not hint at a q^2-dependence beyond the one generated by the Wilson

n	0		1		2	
$\chi^{2(n)}_{\min}$	65.50		52.70		52.40	
$\chi^{2(n-1)}_{\min} - \chi^{2(n)}_{\min}$	4.31	(1.2 σ)	12.80	(2.8 σ)	0.26	(0.0 σ)
$h^{(0)}_+$	$0.05^{+1.21}_{-0.71}$	(0.1 σ)	$1.40^{+1.12}_{-0.69}$	(2.0 σ)	$1.10^{+1.66}_{-0.40}$	(2.8 σ)
$h^{(1)}_+$			$-0.82^{+0.76}_{-0.41}$	(1.1 σ)	$0.09^{+0.49}_{-1.22}$	(0.1 σ)
$h^{(2)}_+$					$-0.16^{+0.32}_{-0.06}$	(0.5 σ)
$h^{(0)}_-$	$1.24^{+1.04}_{-0.55}$	(2.2 σ)	$0.53^{+1.00}_{-0.75}$	(0.7 σ)	$0.78^{+0.80}_{-0.60}$	(1.3 σ)
$h^{(1)}_-$			$0.43^{+0.46}_{-0.26}$	(1.6 σ)	$0.19^{+0.66}_{-0.78}$	(0.2 σ)
$h^{(2)}_-$					$0.04^{+0.16}_{-0.07}$	(0.6 σ)
$h^{(1)}_0$			$0.31^{+1.03}_{-0.43}$	(0.7 σ)	$0.66^{+1.97}_{-0.60}$	(1.1 σ)
$h^{(2)}_0$					$-0.07^{+0.15}_{-0.10}$	(0.5 σ)

Table 6.6: Fit to $B \to K^*\mu^+\mu^-$ only, with $\mathcal{C}^{\rm NP}_{9\mu} = 0$, using LCSR results from Ref. [150] in the full-form-factor approach. All coefficients are given in units of 10^{-4}. Different orders n of the polynomial parametrisation of the long-distance charm-loop contribution are considered. If this contribution is set to zero, the fit yields $\chi^2_{\min;h=0} = 69.80$ for $N_{dof} = 59$.

coefficients $\mathcal{C}_7$ and $\mathcal{C}_9$.

In Refs. [144, 145] a different q^2-dependence was advocated referring to the parameter $h^{(2)}_-$ which showed a $\lesssim 2\sigma$ deviation from $h^{(2)}_- = 0$. We would like to emphasize that it is impossible to draw conclusions from a single parameter and that a global assessment of the whole fit is required. For instance, from our tables one can see that increasing the order of the expansion can lead to a reshuffling of the overall deviation from zero of the functions $h_\lambda(q^2)$ among the various expansion parameters, even in the case that no significant improvement of the fit is obtained. For instance, in the SM fit (Tab. 6.4) the parameter $h^{(0)}_+$ deviates from zero by 1.3σ at the order $n = 2$, but by 2.8σ at $n = 3$. We would expect a similar analysis to be possible in the Bayesian framework proposed in Ref. [144], by comparing the information criteria for the two hypotheses "no constraint for $q^2 \leq 1$ GeV^2 and $h^{(2)}_\lambda$ left free" and "no constraint for $q^2 \leq 1$ GeV^2 and $h^{(2)}_\lambda = 0$", which is unfortunately not provided in Ref. [144].

In the SM fit we find the pattern

$$h^{(0)}_+ \geq 0, \qquad h^{(0)}_- \geq 0, \qquad h^{(1)}_0 \simeq 0, \qquad h^{(1)}_+ \leq 0, \qquad h^{(1)}_- \simeq 0, \tag{6.3.5}$$

while higher orders are compatible with zero. These findings are in rough agreement with Refs. [144, 145] for the $\lambda = 0, +$ helicities. The differences can be attributed to the different treatment and input for the form factors and to the differences in the statistical approach. The comparison cannot be done easily for the $\lambda = -$ helicity, as large phases were found in Ref. [144] whereas we considered only real $c\bar{c}$ contributions.

Setting $\mathcal{C}^{\mu,\rm NP}_9 = -1.1$ improves the $\chi^2_{\min}$ significantly without modifying the above conclusions (see Tab. 6.5). As mentioned before, it is not strictly equivalent to modify $h^{(1)}$ or $\mathcal{C}_9$ since the latter is multiplied by a q^2-dependent form factor. Therefore the results of the fits are not exactly identical, both for the $\chi^2_{\min}$ and the values of the expansion coefficients $h^{(n)}$ (this explains why the addition of $h^{(1)}$ still brings some improvement to the fit with $\mathcal{C}^{\mu,\rm NP}_9 = -1.1$, although more modestly than in the SM case). In Tab. 6.6, we present the same fit as in Tab. 6.4 ($B \to K^*\mu^+\mu^-$ only, no NP contributions to the Wilson coefficients), taking the LCSR results from Ref. [150] within the full-form factor approach. As can be seen from the comparison of the two tables, the

n	0		1		2	
$\chi^{2(n)}_{\rm min}$	96.50		75.50		75.50	
$\chi^{2(n-1)}_{\rm min} - \chi^{2(n)}_{\rm min}$	1.53	(0.4 σ)	20.90	(3.9 σ)	0.10	(0.0 σ)
$h_+^{(0)}$	$0.39^{+1.00}_{-0.52}$	(0.7 σ)	$1.19^{+1.29}_{-0.42}$	(2.8 σ)	$1.16^{+1.04}_{-0.27}$	(4.3 σ)
$h_+^{(1)}$			$-0.45^{+0.66}_{-0.48}$	(0.7 σ)	$-0.29^{+0.83}_{-0.94}$	(0.4 σ)
$h_+^{(2)}$					$0.02^{+0.17}_{-0.17}$	(0.1 σ)
$h_-^{(0)}$	$0.72^{+1.12}_{-0.67}$	(1.1 σ)	$-0.21^{+1.05}_{-0.37}$	(0.2 σ)	$0.19^{+0.87}_{-0.60}$	(0.3 σ)
$h_-^{(1)}$			$0.29^{+0.53}_{-0.17}$	(1.7 σ)	$-0.58^{+1.18}_{-0.17}$	(0.5 σ)
$h_-^{(2)}$					$0.12^{+0.06}_{-0.13}$	(1.0 σ)
$h_0^{(1)}$			$1.54^{+0.75}_{-0.48}$	(3.2 σ)	$1.66^{+0.50}_{-1.08}$	(1.5 σ)
$h_0^{(2)}$					$0.01^{+0.13}_{-0.08}$	(0.1 σ)

Table 6.7: Fit to exclusive $b \to s e^+ e^-$ and $b \to s\mu^+\mu^-$ observables with $\mathcal{C}_{9\mu}^{\rm NP} = 0$, using the same approach as in Ref. [113]. All coefficients are given in units of 10^{-4}. Different orders n of the polynomial parametrisation of the long-distance charm-loop contribution for $B \to V\ell^+\ell^-$ are considered. If this contribution is set to zero, the fit yields $\chi^2_{{\rm min};h=0} = 98.00$ for $N_{dof} = 81$.

same conclusions hold independently of the specific input for the form factors.

We also performed another fit (Tab. 6.7) where we consider the SM case but include all the exclusive $b \to se^+e^-$ and $b \to s\mu^+\mu^-$ observables discussed in Ref. [113]. We take the same parameters for the charm-loop contributions in $B_s \to \phi\ell^+\ell^-$ and $B \to K^*\ell^+\ell^-$ (i.e., we assume an $SU(3)$ flavour symmetry for this long-distance contribution), but we neglect the effect of charm loops in $B \to K\ell^+\ell^-$ (in agreement with Ref. [148]). We see again that there is no strong for quadratic h terms: $h_-^{(2)}$ prefers to be slightly different from zero (positive), but the data can also be described equivalently well using only constant and linear contributions.

At this stage, we see that the data require constant and linear contributions, as expected also from Ref. [148]. On the other hand, the data do not require additional quadratic or cubic contributions, contrary to the claim made in Ref. [144]. This claim was later amended in Ref. [145], indicating that a solution with $h^{(2)} = 0$ also leads to acceptable Bayesian fits. Our own fits indicate that the current data do not show signs of a large and unaccounted for hadronic contribution from charm loops.

Chapter 7

Observables without charm

The $B \to K^*\mu\mu$ decay exhibits deviations with respect to Standard Model expectations and the measurement of the ratio R_K hints at a violation of lepton-flavour universality in $B \to K\ell\ell$ transitions. Both effects can be understood in model-independent fits as a short-distance contribution to the Wilson coefficient $\mathcal{C}_{9\mu}$, with some room for similar contributions in other Wilson coefficients for $b \to s\mu\mu$ transitions. We discuss how a full angular analysis of $B \to K^*ee$ and its comparison with $B \to K^*\mu\mu$ could improve our understanding of these anomalies and help confirming their interpretation in terms of short-distance New Physics. We discuss several observables of interest in this context and provide predictions for them within the Standard Model as well as within several New Physics benchmark scenarios. We pay special attention to the sensitivity of these observables to hadronic uncertainties from SM contributions with charm loops.

7.1 $B \to K^*\ell\ell$ observables assessing lepton flavour universality

Global analyses of the deviations in $b \to s\ell\ell$ transitions point towards a large additional contribution to the Wilson coefficient $\mathcal{C}_{9\mu}$ of the semileptonic operator in the effective Hamiltonian [30] for $b \to s\mu\mu$, as initially discussed in Ref. [153] and later confirmed by several works [113, 163, 164, 166, 168, 169]. Even though such a contribution to $\mathcal{C}_{9\mu}$ in $b \to s\mu\mu$ appears as a rather economical way of explaining a large set of deviations with respect to SM expectations, theory predictions for some $b \to s\mu\mu$ observables may also get a better agreement with data once additional contributions are allowed in other Wilson coefficients (such as $\mathcal{C}_{9'\mu}$ or $\mathcal{C}_{10\mu}$) [113]. On the other hand, $B \to K^*ee$ observables and the R_K ratio suggest that $b \to see$ transitions agree well with the SM [170], pointing to explanations with New Physics (NP) models with a maximal violation of LFU, affecting only muon and not electron modes.

As discussed in several works [110, 144, 148, 157, 171, 172], long-distance SM contributions from diagrams involving charm loops enter the computation of $b \to s\ell\ell$ processes, acting as additional contributions to the Wilson coefficient $\mathcal{C}_9$. These contributions are process-dependent and they must be estimated through different theoretical methods according to the dilepton invariant mass q^2. The latest estimates of these contributions [148, 157] have been included in the global fits for $B \to K^*\mu\mu$ [113, 164, 166], providing the consistent picture described above. In particular, bin-by-bin fits indicate that the data agrees well with a single, process-independent contribution to $\mathcal{C}_{9\mu}$, independent of the dimuon invariant mass, and present only in muon modes, as expected from a short-distance (NP) flavour-non-universal contribution. In order to confirm this pattern, it would be very desirable to design observables probing:

- only the short-distance part of $\mathcal{C}_{9\ell}$,
- other Wilson coefficients, such as $\mathcal{C}_{10\ell}$, which do not receive long-distance contributions from the SM,
- the amount of lepton-flavour non-universality between electron and muon modes.

In all cases, hadronic uncertainties should remain controlled: while non-universality is a smoking-gun-signal of NP (the SM predictions being very precise), the *measurement* of the effect is affected by the same hadronic uncertainties as the individual $b \to s\ell\ell$ modes.

The purpose of this chapter is to investigate which observables can be built that match these criteria, once a full angular analysis of $B \to K^*ee$, with an accuracy comparable to that of $B \to K^*\mu\mu$, is available. If the most obvious quantity consists in comparing branching ratios though the ratio R_{K^*} (similar to R_K) (see Ref. [113] for predictions for these ratios for different NP scenarios), it is also interesting to consider other ratios probing the violation of LFU using the angular coefficients J_i describing the whole angular kinematics of these decays. In this note, we will discuss observables that can measure LFUV in $B \to K^*\ell\ell$. Some of them are variations around the basis of optimised observables introduced in Refs. [103, 115] and others can be built directly by combining angular coefficients from muon and electron modes. We will discuss the advantages of these observables in the context of hadronic uncertainties, and provide predictions in the SM and in several benchmark scenarios corresponding to the best-fit points obtained in our recent global analysis of $b \to s\ell\ell$ modes [113].

We begin with a presentation of the observables of interest in Section 7.1. In addition to observables naturally derived from the angular coefficients J_i and the optimised observables $P_i^{(\prime)}$, we consider other observables, namely B_i and M (and $\widetilde{B}_i$, $\widetilde{M}$) which have a reduced sensitivity to charm contributions in some NP scenarios. In Section 7.2 we present our predictions in the SM and in several NP benchmark points, illustrating how these observables can help in discerning among NP scenarios and how (in)sensitive they are with respect to hadronic uncertainties. We present our conclusions in Section 4. In the appendices we discuss the dependence of M and $\widetilde{M}$ observables on charm contributions, we recall the definition of binned observables, and we provide further predictions for the various observables within the different benchmark scenarios.

7.1.1 Observables derived from J_i, P_i and S_i

We want to exploit the angular analyses of both $B \to K^*\mu\mu$ and $B \to K^*ee$ decays in order to build observables that will probe the violation of LFU, the short-distance part of $\mathcal{C}_{9\mu}$ and/or the other Wilson coefficients, with limited hadronic uncertainties. Natural combinations are [1]

$$Q_{F_L} = F_L^\mu - F_L^e\,, \quad Q_i = P_i^\mu - P_i^e\,, \quad T_i = \frac{S_i^\mu - S_i^e}{S_i^\mu + S_i^e}\,, \quad B_i = \frac{J_i^\mu}{J_i^e} - 1\,, \quad \widetilde{B}_i = \frac{\beta_e^2}{\beta_\mu^2}\frac{J_i^\mu}{J_k^e} - 1\,, \quad (7.1.1)$$

where P_i should be replaced by P_i' for $Q_{i=4,5,6,8}$. B_i and $\widetilde{B}_i$ differ mostly at very low q^2 and become almost identical for large q^2, where $\beta_\ell = \sqrt{1 - 4m_\ell^2/q^2} \simeq 1$ for both electrons and muons. The optimised observables $P_i^{(\prime)}$ have already a limited sensitivity to hadronic uncertainties [103, 112,

[1] In the following, we always consider quantities obtained by combining CP-averaged angular coefficients.

113, 115, 147], contrary to the angular averages S_i [31, 103, 115, 146, 147, 151]. We thus expect the Q_i observables to exhibit a correspondingly low sensitivity to hadronic uncertainties. [2] Moreover, these observables are protected from long-distance charm-loop contributions in the SM.

A measurement of Q_i different from zero would point to NP in an unambiguous way, confirming the violation of LFU observed in R_K. A second step would then consist in identifying the pattern of NP, which requires to separate the residual hadronic uncertainties (in particular, charm-loop contributions) from the NP contributions. The set of observables Q_i, T_i and B_k ($\widetilde{B}_k$) can be particularly instrumental at this second stage, with a sensitivity to the various Wilson coefficients depending on the particular angular coefficients considered.

We have already investigated this sensitivity [112, 113, 147], but we would like to highlight the difference of behaviour in the case of two of the relevant observables P_4' and P_5', directly related to Q_4 and Q_5 respectively. Both LHCb and Belle collaborations [176–178] observed the same pattern, i.e., a significant deviation from the SM for P_5' for q^2 between 4 and 8 GeV^2 and a result consistent with the SM within errors for P_4'. This behaviour is expected in the presence of NP in the Wilson coefficient $\mathcal{C}_9$. From the large-recoil expressions of $A^{L,R}_{\perp,\|,0}$ (see Eqs. (3.8)-(3.10) of Ref. [83]) one finds that the right-handed amplitudes $|A^R_{0,\perp,\|}| \propto (\mathcal{C}_9^{\rm eff} + \mathcal{C}_{10}) + ...$ are suppressed compared to the left-handed ones in the SM, due to the approximated cancellation $\mathcal{C}_9^{\rm eff} + \mathcal{C}_{10} \simeq 0$. This cancellation is not so effective in the presence of a negative NP contribution to $\mathcal{C}_9$, and $A^R_{0,\|}$, $|A^R_\perp|$ increase while $|A^L_{0,\|}|$, $A^L_\perp$ decrease. Both effects add up coherently in the numerator of $P_5' \propto {\rm Re}(A^L_0 A^{L*}_\perp - A^R_0 A^{R*}_\perp)$ due to the relative minus sign, and the effect is to reduce the value of $|P_5'|$ in the region far up from the photon pole, in agreement with the experimental observation. In $P_4' \propto {\rm Re}(A^L_0 A^{L*}_\| + A^R_0 A^{R*}_\|)$, however, an increase in the right-handed amplitudes will compensate a decrease in the left-handed ones, due to the relative positive sign. For this reason, no deviation is expected in P_4' in the presence of NP in $\mathcal{C}_9$ (but in the absence of right-handed currents). The same mechanism is at work for Q_4 and Q_5.

As discussed in Sec 2.3.1 of Ref. [113], LHCb currently determines the polarisation fraction F_T and F_L using a simplified description of the angular kinematics. This means that these two quantities are actually measured from J_{1c} rather than J_{2s} and J_{2c} respectively. Both determinations are equivalent in the massless limit, and therefore this only has a limited impact, apart from the first bin [0.1,0.98]. In order to interpret the actual measurements more precisely, we define the $\hat{P}_i$ observables involving $\hat{F}_T$ and $\hat{F}_L$, as measured currently by LHC:

$$F_L = \frac{-J_{2c}}{d\Gamma/dq^2} \to \hat{F}_L = \frac{J_{1c}}{d\Gamma/dq^2} \qquad F_T = \frac{4J_{2s}}{d\Gamma/dq^2} \to \hat{F}_T = 1 - \hat{F}_L \tag{7.1.2}$$

$$P_1 = \frac{J_3}{2J_{2s}} \to \hat{P}_1 = \frac{J_3}{2\hat{J}_{2s}} \qquad P_2 = \frac{J_{6s}}{8J_{2s}} \to \hat{P}_2 = \frac{J_{6s}}{8\hat{J}_{2s}} \tag{7.1.3}$$

$$P_3 = -\frac{J_9}{4J_{2s}} \to \hat{P}_3 = -\frac{J_9}{4\hat{J}_{2s}} \qquad P_4' = \frac{J_4}{\sqrt{-J_{2s}J_{2c}}} \to \hat{P}_4' = \frac{J_4}{\sqrt{\hat{J}_{2s}J_{1c}}} \tag{7.1.4}$$

$$P_5' = \frac{J_5}{2\sqrt{-J_{2s}J_{2c}}} \to \hat{P}_5' = \frac{J_5}{2\sqrt{\hat{J}_{2s}J_{1c}}} \qquad P_6' = -\frac{J_7}{2\sqrt{-J_{2s}J_{2c}}} \to \hat{P}_6' = -\frac{J_7}{2\sqrt{\hat{J}_{2s}J_{1c}}} \tag{7.1.5}$$

$$P_8' = -\frac{J_8}{\sqrt{-J_{2s}J_{2c}}} \to \hat{P}_8' = -\frac{J_8}{\sqrt{\hat{J}_{2s}J_{1c}}} \qquad \text{with } \hat{J}_{2s} = \frac{1}{16}(6J_{1s} - J_{1c} - 2J_{2s} - J_{2c}) \tag{7.1.6}$$

and we will provide predictions for both Q_i and $\hat{Q}_i$ observables, in order to illustrate the differences in the first bin, as well as the insensitivity of the effect in higher bins.

[2] We also expect a reduced sensitivity to $K\pi$ S-wave contributions (see *e.g.* [173–175]).

In the case of the S_i, the consideration of the T_i ratio is also natural, but unfortunately these quantities are quite sensitive to hadronic uncertainties. They depend on soft form factors even in the large recoil limit due to lepton mass effects at very low q^2, related to differences between muon and electron contributions in the normalization. Finally, the ratios B_i that are soft-form-factor independent at leading order in the large-recoil limit will be shown to complement the observables Q_i in an interesting way.

7.1.2 Observables with reduced sensitivity to charm effects

In the presence of NP, all observables Q_i, T_i and B_i are in principle affected by long-distance charm loop contributions in $\mathcal{C}_9$, both transversity-independent and transversity-dependent. We define these two terms in the following way: transversity-independent long-distance charm corresponds to an identical contribution to all $B \to K^*\ell\ell$ transversity amplitudes, whereas transversity-dependent contributions differ for each amplitude. Both of them are expected to exhibit a q^2-dependence in general. The explicit computation of charm-loop contributions performed in Ref. [148] using light-cone sum rules indicates that they are transversity-dependent, in agreement with general expectations that such hadronic contributions are different for different external hadronic states (including different K^* helicities). It is interesting to investigate these issues by considering specific observables with different sensitivity to transversity-dependent and independent long-distance charm contributions, as well as to LFUV New Physics.

One can think of exploiting the angular coefficients in electron and muon modes in order to build observables only sensitive to some of the Wilson coefficients, and in some cases, insensitive to transversity-independent long-distance charm contributions. It is easy to check that in the large-recoil limit and in the absence of right-handed or scalar operators, four angular coefficients exhibit a linear sensitivity to $\mathcal{C}_9$. Taking the results from Refs. [83, 103] we have:

$$\beta_\ell J_{6s} - 2iJ_9 = 16\beta_\ell^2 N^2 m_B^2 (1-\hat{s})^2 \mathcal{C}_{10\ell} \left[2\mathcal{C}_7 \frac{\hat{m}_b}{\hat{s}} + \mathcal{C}_{9\ell}\right] \xi_\perp^2 + \dots \quad (7.1.7)$$

$$\beta_\ell J_5 - 2iJ_8 = 8\beta_\ell^2 N^2 m_B^2 (1-\hat{s})^3 \frac{\hat{m}_{K^*}}{\sqrt{\hat{s}}} \mathcal{C}_{10\ell} \left[\mathcal{C}_7 \hat{m}_b \left(\frac{1}{\hat{s}} + 1\right) + \mathcal{C}_{9\ell}\right] \xi_\perp \xi_{||} + \dots \quad (7.1.8)$$

where $\hat{s} = q^2/m_B^2$ and $\hat{m}_b = m_b/m_B$, $\xi_\perp$ and $\xi_{||}$ correspond to the soft form factors [30], and the ellipses indicate terms suppressed in the large-recoil limit (including terms of order m_ℓ^2/q^2). If we limit ourselves to real NP contributions, it is interesting to consider B_5 and B_{6s} (and $\widetilde{B}_5$ and $\widetilde{B}_{6s}$) in Eq. (7.1.1), as well as a combination of them in the form [3]

$$M = \frac{(J_5^\mu - J_5^e)(J_{6s}^\mu - J_{6s}^e)}{J_{6s}^\mu J_5^e - J_{6s}^e J_5^\mu}, \quad \widetilde{M} = \frac{(\beta_e^2 J_5^\mu - \beta_\mu^2 J_5^e)(\beta_e^2 J_{6s}^\mu - \beta_\mu^2 J_{6s}^e)}{\beta_e^2 \beta_\mu^2 (J_{6s}^\mu J_5^e - J_{6s}^e J_5^\mu)}. \quad (7.1.9)$$

By construction, B_5 and $\widetilde{B}_5$ have a pole at the position of the zero of J_5^e in the SM (around $q^2 = 2$ GeV^2) and B_{6s}, $\widetilde{B}_{6s}$ have a pole at the position of the zero of $A_{\rm FB}$ in the SM (around $q^2 = 4$ GeV^2). We expect large uncertainties for these observables in the corresponding bins. On the contrary, M is well behaved in the same bins, but it will have large uncertainties when $B_5 \simeq B_{6s}$. In this sense, the observable M is well suited for NP scenarios and energy regions that

[3] The definitions of $B_{5,6s}$ ($\widetilde{B}_{5,6s}$) and M ($\widetilde{M}$) could be adapted to the imaginary contributions $J_{8,9}$. However the latter vanish in the case of real NP contributions. Since current data does not indicate any need for complex NP contributions, we will not include these additional observables here.

yield very different contributions to B_5 and B_{6s}. While the B_i have a value in the SM slightly different from zero (specially the first bin) due to β_μ/β_e kinematic effects, the $\widetilde{B}_i$ observables vanish by construction in the SM. [4]

Even more interesting is the case of $\widetilde{M}$, constructed in the same spirit as $\widetilde{B}_i$, *i.e.* to cancel the dependence of the angular coefficients on β_ℓ. Its first bin can be accurately predicted even in the presence of NP, while its M counterpart suffers from large uncertainties in that bin. In the next section we will discuss some NP scenarios and show how these set of observables can become instrumental to disentangle them.

Let us write $\mathcal{C}_{ie} = \mathcal{C}_i$ and $\mathcal{C}_{i\mu} = \mathcal{C}_i + \delta\mathcal{C}_i$ for $i \neq 9$, so that $\delta\mathcal{C}_i$ measure the LFU violation, whereas $\mathcal{C}_{ie}$ can include LFU-NP effects. Furthermore, for $i = 9$ we take $\mathcal{C}_{9e} = \mathcal{C}_9 + \Delta\mathcal{C}_9$ and $\mathcal{C}_{9\mu} = \mathcal{C}_9 + \delta\mathcal{C}_9 + \Delta\mathcal{C}_9$ where $\Delta\mathcal{C}_9$ is a long-distance charm contribution. In order to illustrate the relevant aspects of the various observables, within this Section we will give analytic formulas assuming the contribution $\Delta\mathcal{C}_9$ is transversity independent and neglecting imaginary parts. But all our numerical evaluations will be based on complete expressions, as computed in Ref. [113] where transversity-dependent charm contributions are included following Ref. [148], and imaginary parts are properly accounted for. We see that $\delta\mathcal{C}_{7,7'} = 0$ [5] and $\delta\mathcal{C}_9$ are directly related to short-distance physics, while $\Delta\mathcal{C}_9$ comes from long-distance contributions from $c\bar{c}$ loops where the lepton pair is created by an electromagnetic current, and thus identical for $\mathcal{C}_{9e}$ and $\mathcal{C}_{9\mu}$. Any $\delta\mathcal{C}_i \neq 0$ indicates the presence of LFUV New Physics.

In the large-recoil limit and in the absence of right-handed or scalar operators, we have:

$$B_5 = \frac{\beta_\mu^2 - \beta_e^2}{\beta_e^2} + \frac{\beta_\mu^2}{\beta_e^2}\frac{\delta\mathcal{C}_{10}}{\mathcal{C}_{10}} + \frac{\beta_\mu^2}{\beta_e^2}\frac{(\mathcal{C}_{10}+\delta\mathcal{C}_{10})\delta\mathcal{C}_9\hat{s}}{\mathcal{C}_{10}(\mathcal{C}_7\hat{m}_b(1+\hat{s})+(\mathcal{C}_9+\Delta\mathcal{C}_9)\hat{s})} + \dots \tag{7.1.10}$$

$$B_{6s} = \frac{\beta_\mu^2 - \beta_e^2}{\beta_e^2} + \frac{\beta_\mu^2}{\beta_e^2}\frac{\delta\mathcal{C}_{10}}{\mathcal{C}_{10}} + \frac{\beta_\mu^2}{\beta_e^2}\frac{(\mathcal{C}_{10}+\delta\mathcal{C}_{10})\delta\mathcal{C}_9\hat{s}}{\mathcal{C}_{10}(2\mathcal{C}_7\hat{m}_b+(\mathcal{C}_9+\Delta\mathcal{C}_9)\hat{s})} + \dots \tag{7.1.11}$$

$$M = \widetilde{M} + \Delta M + \mathcal{A}\Delta\mathcal{C}_9 + \mathcal{B}\Delta\mathcal{C}_9^2 + \dots \tag{7.1.12}$$

$$\widetilde{M} = \widetilde{M}_0 + \mathcal{A}'\delta\mathcal{C}_{10}\Delta\mathcal{C}_9 + \mathcal{B}'\delta\mathcal{C}_{10}^2\Delta\mathcal{C}_9^2 + \dots \tag{7.1.13}$$

where $\widetilde{M}_0$, ΔM, $\mathcal{A}^{(\prime)}$ and $\mathcal{B}^{(\prime)}$ are defined in App. B, and the ellipsis denote again terms neglected in Eqs. (7.1.7) and (7.1.8) and suppressed in the large-recoil limit. The difference between the muon and electron masses relative to q^2, induces a non-vanishing SM value for the B_i observables at low q^2. $\widetilde{B}_i$ are exactly zero in the SM, and can be obtained from Eqs. (7.1.10), (7.1.11) in the limit $\beta_\ell \to 1$. Note that the B_i observables always have a residual charm dependence $\Delta\mathcal{C}_9$ in the denominator in the presence of NP.

From Eq. (7.1.12), M appears sensitive to the muon-electron mass difference via ΔM, $\mathcal{A}$ and $\mathcal{B}$, and the last two terms introduce a sensitivity to charm effects through $\Delta\mathcal{C}_9$. Moreover, the first bin of M is very sensitive to this mass difference and will be affected by very large uncertainties in some NP scenarios. On the contrary, $\widetilde{M}$ is blind to such mass effects. In addition, if there is no NP in $\delta\mathcal{C}_{10}$ then $\widetilde{M}$ becomes also insensitive to transversity-independent charm effects at leading order and at large recoil. This means that $\widetilde{M}$ is particularly clean at low q^2 (where large-recoil expressions are relevant), especially in the presence of NP in $\delta\mathcal{C}_9$. For larger values of q^2 and/or in the presence of NP in $\mathcal{C}_{10}$, subleading charm effects are present and will enlarge the uncertainties,

[4] The measurement of $\widetilde{B}_i$ requires the measurement of the quantities $\langle J_i^\ell/\beta_\ell^2\rangle$. Experimentally, this can be done by assigning a β_ℓ^2 factor to the data on an event-by-event basis.

[5] $\mathcal{C}_7$ includes both the SM $\mathcal{C}_7^{\text{eff}}$ plus possible LFU-NP (the same applies to $\mathcal{C}_9$).

even though the impact of NP on this observable remains very large. $\widetilde{M}$ at low q^2 will turn out to be very efficient to disentangle NP scenarios.

We have the following behaviour for $\delta\mathcal{C}_9 = 0$:

$$B_5 = B_{6s} = \frac{\beta_\mu^2 - \beta_e^2}{\beta_e^2} + \frac{\beta_\mu^2}{\beta_e^2}\frac{\delta\mathcal{C}_{10}}{\mathcal{C}_{10}} \,. \tag{7.1.14}$$

For B_5 and B_{6s}, the limit of very small q^2 is equivalent to $\delta\mathcal{C}_9 = 0$, and M is not well predicted in this limit (subleading effects dominate the computation). This is however not a problem in the current context where global analyses point towards a large NP contribution to $\mathcal{C}_9$. On the other hand, if $\delta\mathcal{C}_{10} = 0$, we have [6]

$$B_5 = \frac{\beta_\mu^2 - \beta_e^2}{\beta_e^2} + \frac{\beta_\mu^2}{\beta_e^2}\frac{\delta\mathcal{C}_9 \hat{s}}{(\mathcal{C}_7 \hat{m}_b(1+\hat{s}) + (\mathcal{C}_9 + \Delta\mathcal{C}_9)\hat{s})} + \dots \tag{7.1.15}$$

$$B_{6s} = \frac{\beta_\mu^2 - \beta_e^2}{\beta_e^2} + \frac{\beta_\mu^2}{\beta_e^2}\frac{\delta\mathcal{C}_9 \hat{s}}{(2\mathcal{C}_7 \hat{m}_b + (\mathcal{C}_9 + \Delta\mathcal{C}_9)\hat{s})} + \dots \tag{7.1.16}$$

$$\widetilde{M} = -\frac{\delta\mathcal{C}_9 \hat{s}}{\mathcal{C}_7 \hat{m}_b(1-\hat{s})} + \dots \tag{7.1.17}$$

B_5 and B_{6s} contain then a residual charm sensitivity through $\Delta\mathcal{C}_9$, while $\widetilde{M}$ is totally free from this transversity-independent long-distance charm at leading order. This is a very specific property of $\widetilde{M}$ which is independent of transversity-independent charm contributions in the presence of New Physics in $\mathcal{C}_9$ only. Transversity-dependent charm effects are kinematically suppressed at very low q^2 in these observables as it will be shown later on.

In the case where both $\delta\mathcal{C}_9$ and $\delta\mathcal{C}_{10}$ are non-zero, a precise interpretation of these observables requires a more detailed study (including an assessment of all $c\bar{c}$ contributions to $\mathcal{C}_9$). We see therefore that some of these observables will have a limited sensitivity to charm-loop contributions in some cases (SM, NP only in $\mathcal{C}_{9\mu}$), but not in other cases (NP also in $\mathcal{C}_{10,\mu}$ for instance).

As a conclusion, the behaviour of B_5 ($\widetilde{B}_5$), B_{6s} ($\widetilde{B}_{6s}$) and M ($\widetilde{M}$) in specific q^2-regions should provide powerful tests of physics beyond the SM, with a limited sensitivity to hadronic uncertainties.

7.2 Predictions in the SM and in typical NP benchmark scenarios

7.2.1 Observables and scenarios

The above discussion assumed that one can determine exactly the value of the angular coefficients J_i differentially in q^2. This is in principle possible using the method of amplitudes in Ref. [179] even if for electrons it could be particularly difficult. The other methods (likelihood fit and method of moments) lead to binned observables, where the cancellations advocated above hold only in an approximate way, for bins small enough so that the angular coefficients do not exhibit steep variations. The modifications due to binning for the predictions of observables were described in detail in Ref. [112], and are also recalled in App. B for the observables described above. They will obviously have an impact on the previous discussion concerning the cancellation of hadronic uncertainties, which will then be only approximate.

[6] The corresponding expressions for $\widetilde{B}_{5,6s}$ when $\delta\mathcal{C}_{10} = 0$ can be easily obtained from Eqs.(7.1.15)-(7.1.16) by taking $\beta \to 1$ and the one of M can be obtained from App.B.

In order to illustrate the interest of the various observables, in addition to the SM, we consider several NP benchmark scenarios corresponding to the best-fit points for hypotheses with a large pull in the global analysis of Ref. [113] (with NP contributions in $b \to s\mu\mu$ but not in $b \to see$). We follow the same approach as in Ref. [113] and compute the various observables following the definition of binned observables in App. C. The results are shown in App. D and in Figs. 7.1-7.8.

In the SM, Q_i, T_i and B_i are expected to be close to zero, as shown in App. D. The binned observables B_5 and B_{6s} are actually different from zero due to the kinematic factors β_μ^2 and β_e^2 in the transversity amplitudes – one could imagine measuring the binned values of $J^\ell_{5,6s}/\beta_\ell^2$ and checking that the values for both lepton flavours are indeed identical. The difference between β_μ and β_e becomes less relevant for large q^2 (above 2.5 GeV^2), leading to B_5 and B_{6s} decreasing in magnitude and getting closer to each other. In the same region, M becomes larger as it involves the difference $B_5 - B_{6s}$ in the denominator. In the presence of NP affecting differently $\mathcal{C}_{9\mu}$ and $\mathcal{C}_{9e}$, B_5 and B_{6s} are different over the whole kinematic range. In the SM, the binned version of M is charm dependent due to β_μ/β_e terms. In the presence of LFUV in $\mathcal{C}_9$, it is interesting to focus instead on the observable $\widetilde{M}$, which is not affected by lepton-mass effects and is essentially charm independent at very low-q^2. If there are NP contributions in other Wilson coefficients, the situation becomes more complicated concerning the charm dependence of the observables. In the remainder of this Section we will identify patterns based on the set of Q_i and $\hat{Q}_i$, and we will describe a very promising test based on B_5, B_{6s} and M.

The observables $\hat{Q}_i$ (see Figs. 7.1-7.8) show specific patterns for the different scenarios considered here:

- **Scenario 1: $\mathcal{C}_{9\mu}^{\rm NP} = -1.1$.** Both $\hat{Q}_2$ and $\hat{Q}_5$ are affected significantly, especially the latter. The most interesting region is $q^2 \gtrsim 6$GeV^2, taking into account that these observables receive essentially no charm contributions in the SM. No deviation should be observed in $\hat{Q}_1$ or $\hat{Q}_4$ in the same region within this scenario (see the discussion in Section 7.1 concerning the sensitivity of P_4' to $\mathcal{C}_9$).

- **Scenario 2: $\mathcal{C}_{9\mu}^{\rm NP} = -\mathcal{C}_{10\mu}^{\rm NP} = -0.65$.** Within this scenario $\hat{Q}_2$ and $\hat{Q}_5$ show milder deviations, especially in the bin 6-8 GeV^2 where they are expected to be SM-like (contrary to Scenario 1). Indeed, the constraint from $B_s \to \mu\mu$ on $\mathcal{C}_{10\mu}$ reduces the allowed size of the deviation in $\mathcal{C}_{9\mu}$ in this particular scenario. On the contrary, $\hat{Q}_4$ could be particularly interesting in the region below 6 GeV^2 with a q^2-dependence rather different from Scenario 1. No deviation is expected in $\hat{Q}_1$.

- **Scenarios 3 and 4: $\mathcal{C}_{9\mu}^{\rm NP} = -\mathcal{C}_{9\mu}' = -1.07$ and $\mathcal{C}_{9\mu}^{\rm NP} = \mathcal{C}_{9\mu}' = -1.18$, $\mathcal{C}_{10\mu}^{\rm NP} = \mathcal{C}_{10\mu}' = 0.38$ respectively.** Both scenarios are quite difficult to distinguish using these observables. They have implications in all four relevant observables $\hat{Q}_{1,2,4,5}$. The behaviour of $\hat{Q}_2$ and $\hat{Q}_5$ is similar to Scenario 1, making the three scenarios difficult to disentangle when looking only to these observables. $\hat{Q}_1$, which is designed to test the presence of right-handed currents, is affected significantly. Finally, $\hat{Q}_4$ both at very low- and large-q^2 (but within the large recoil region) could be useful if accurate measurements are obtained. In particular, above 6 GeV^2 this observable is only sensitive to right handed currents.

The same discussion applies to the observables Q_i. We note that $\hat{Q}_i$ (Q_i) in the bin [6-8], which have no charm uncertainties in the SM, may play a central role in disentangling the first

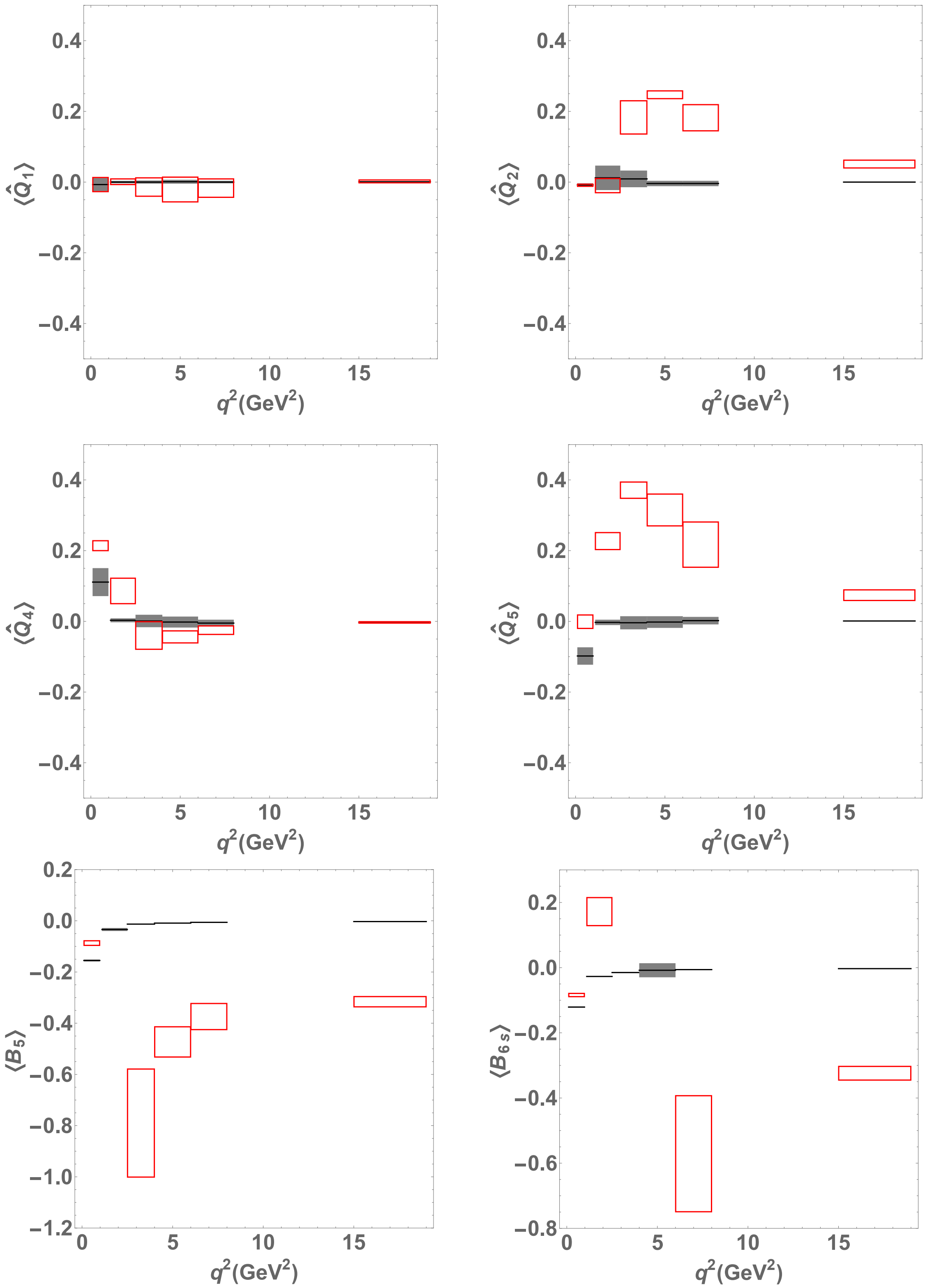

Figure 7.1: *Scenario 1.* SM predictions (grey boxes) and NP predictions (red boxes), assuming $\mathcal{C}_{9\mu}^{\rm NP} = -1.11$.

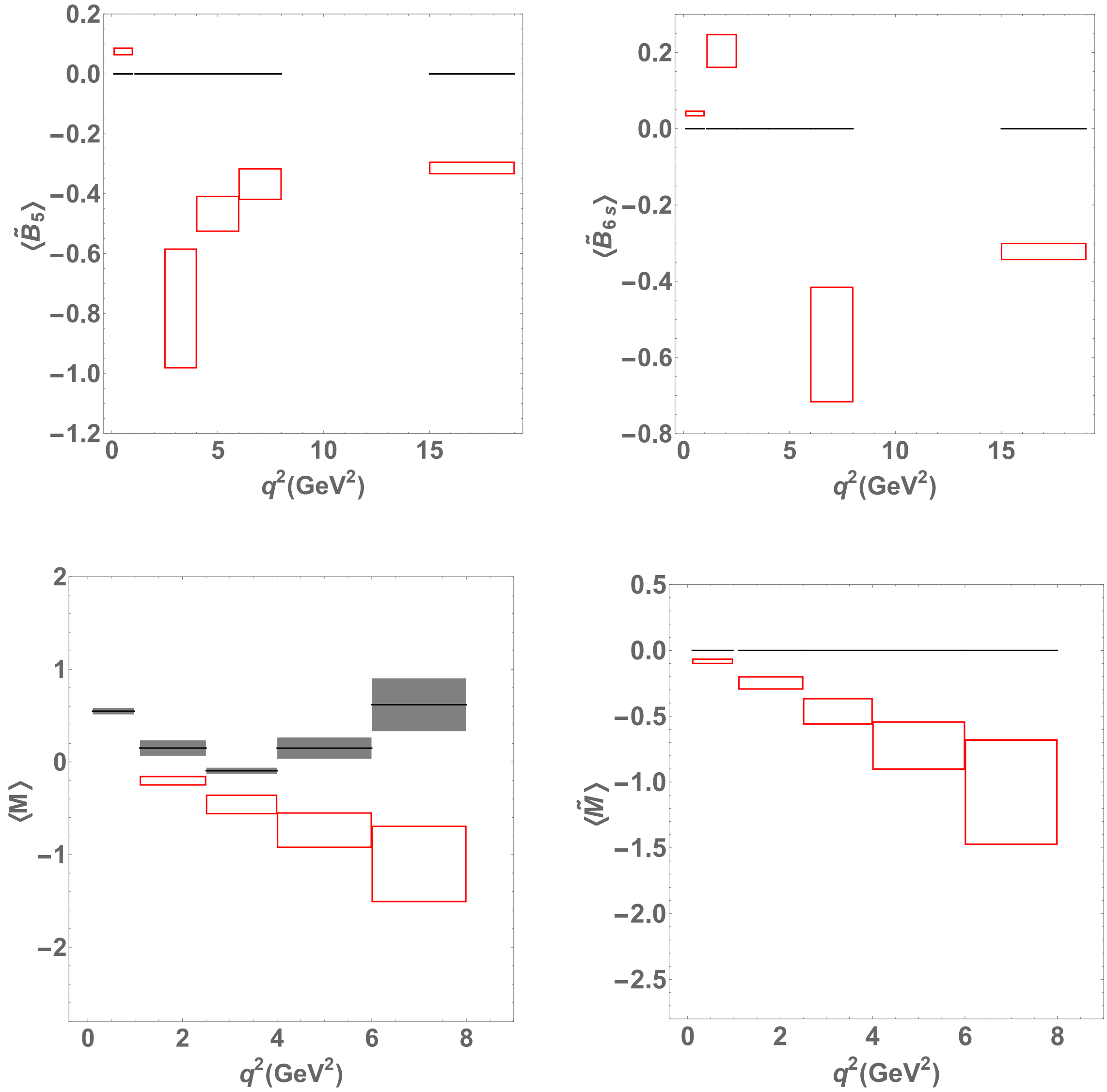

Figure 7.2: *Scenario 1.* SM predictions (grey boxes) and NP predictions (red boxes), assuming $\mathcal{C}_{9\mu}^{\rm NP} = -1.11$.

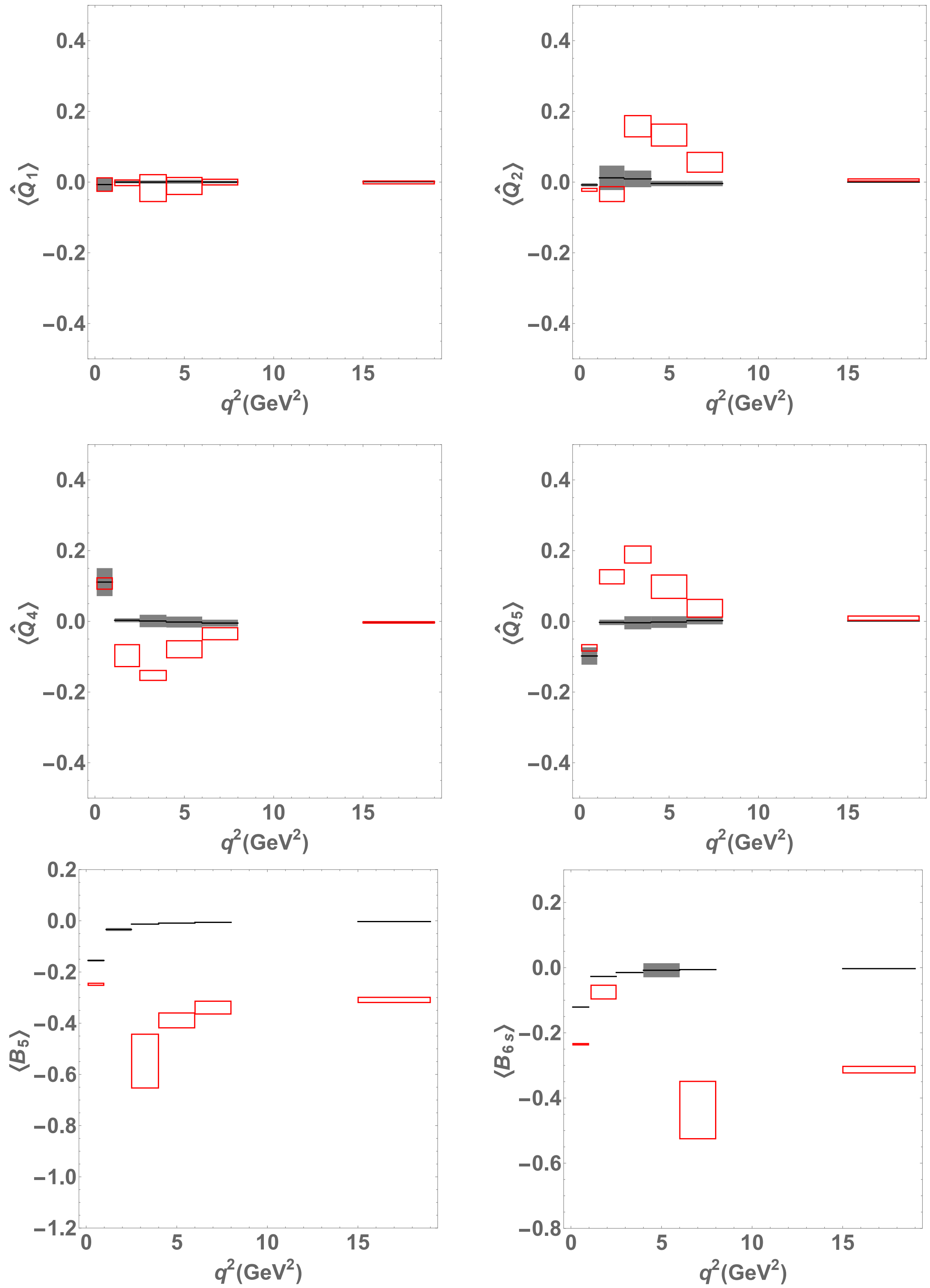

Figure 7.3: *Scenario 2.* SM predictions (grey boxes) and NP predictions (red boxes), assuming $\mathcal{C}_{9\mu}^{\rm NP} = -\mathcal{C}_{10\mu}^{\rm NP} = -0.65$.

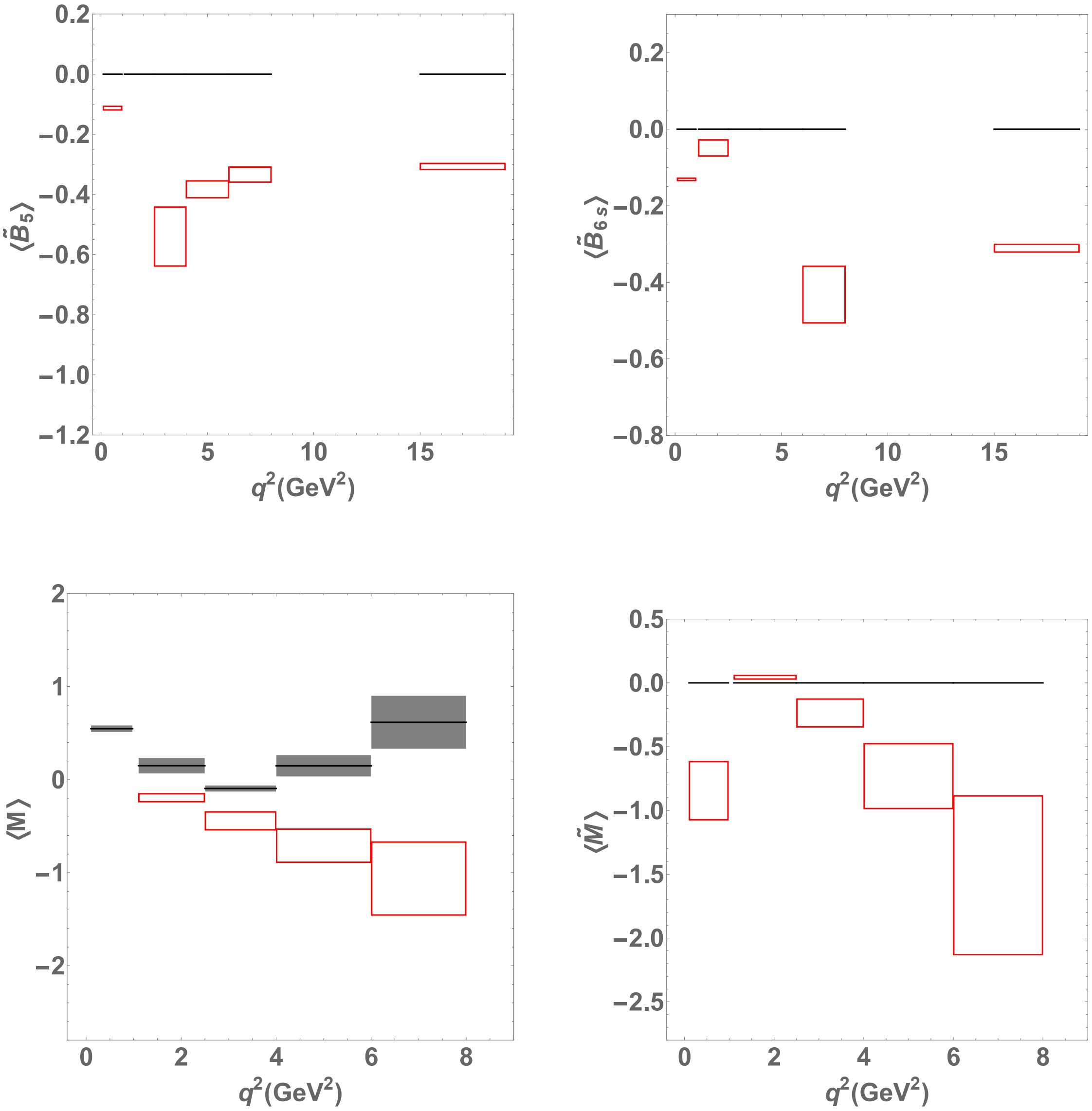

Figure 7.4: *Scenario 2.* SM predictions (grey boxes) and NP predictions (red boxes), assuming $\mathcal{C}_{9\mu}^{\rm NP} = -\mathcal{C}_{10\mu}^{\rm NP} = -0.65$.

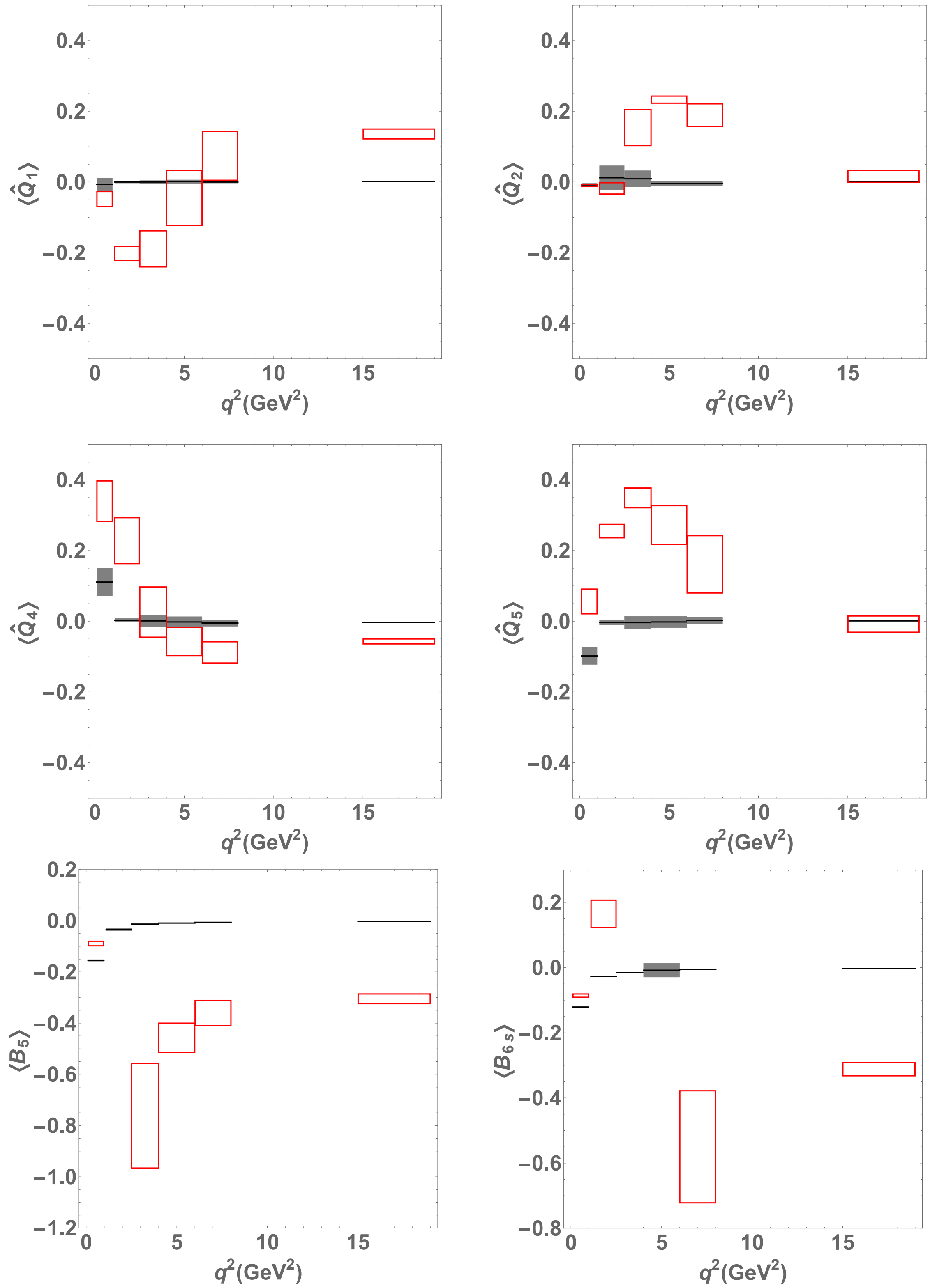

Figure 7.5: *Scenario 3*. SM predictions (grey boxes) and NP predictions (red boxes), assuming $\mathcal{C}_{9\mu}^{\mathrm{NP}} = -\mathcal{C}_{9'\mu}^{\mathrm{NP}} = -1.07$

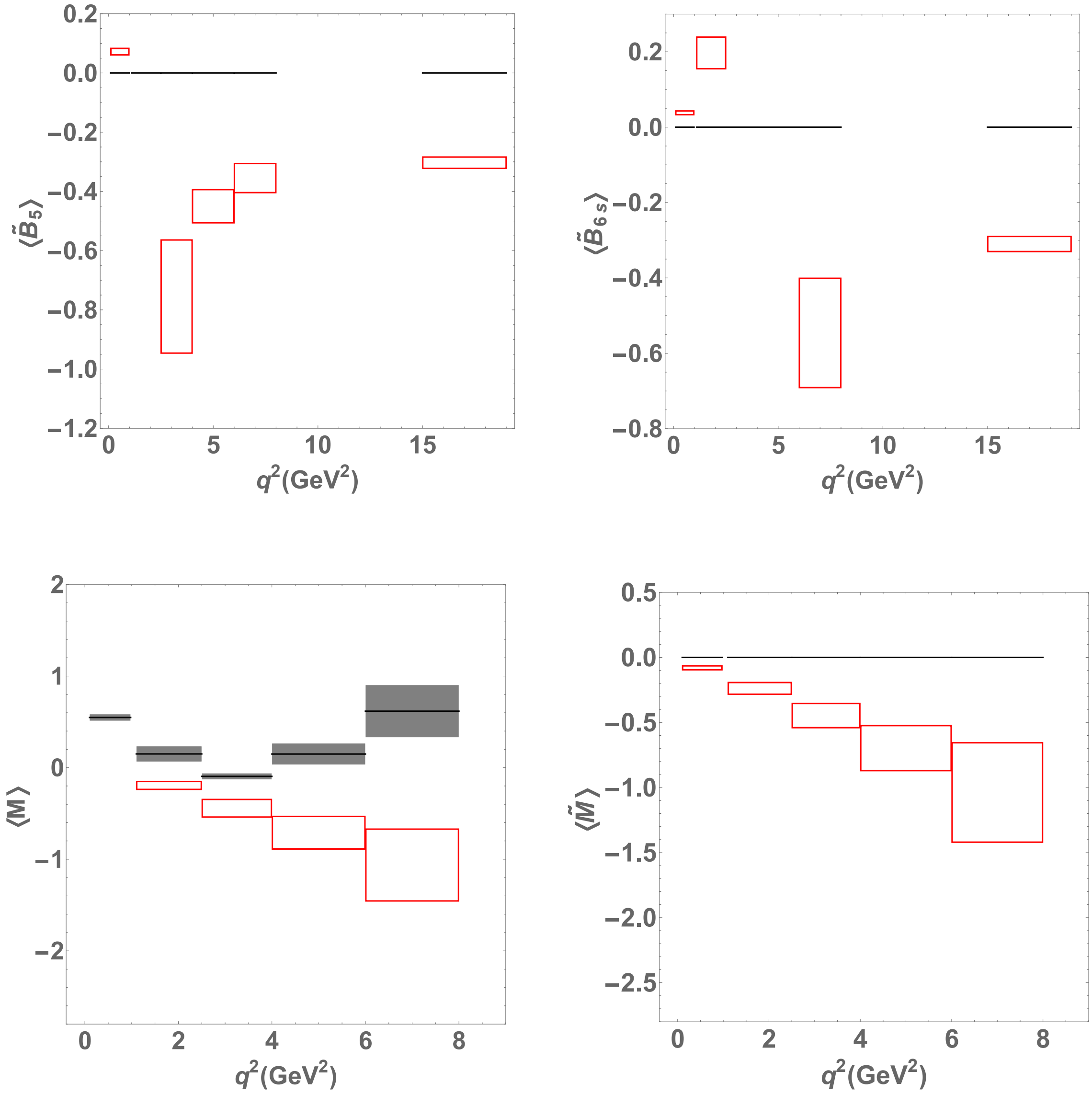

Figure 7.6: *Scenario 3*. SM predictions (grey boxes) and NP predictions (red boxes), assuming $\mathcal{C}_{9\mu}^{\rm NP} = -\mathcal{C}_{9'\mu}^{\rm NP} = -1.07$

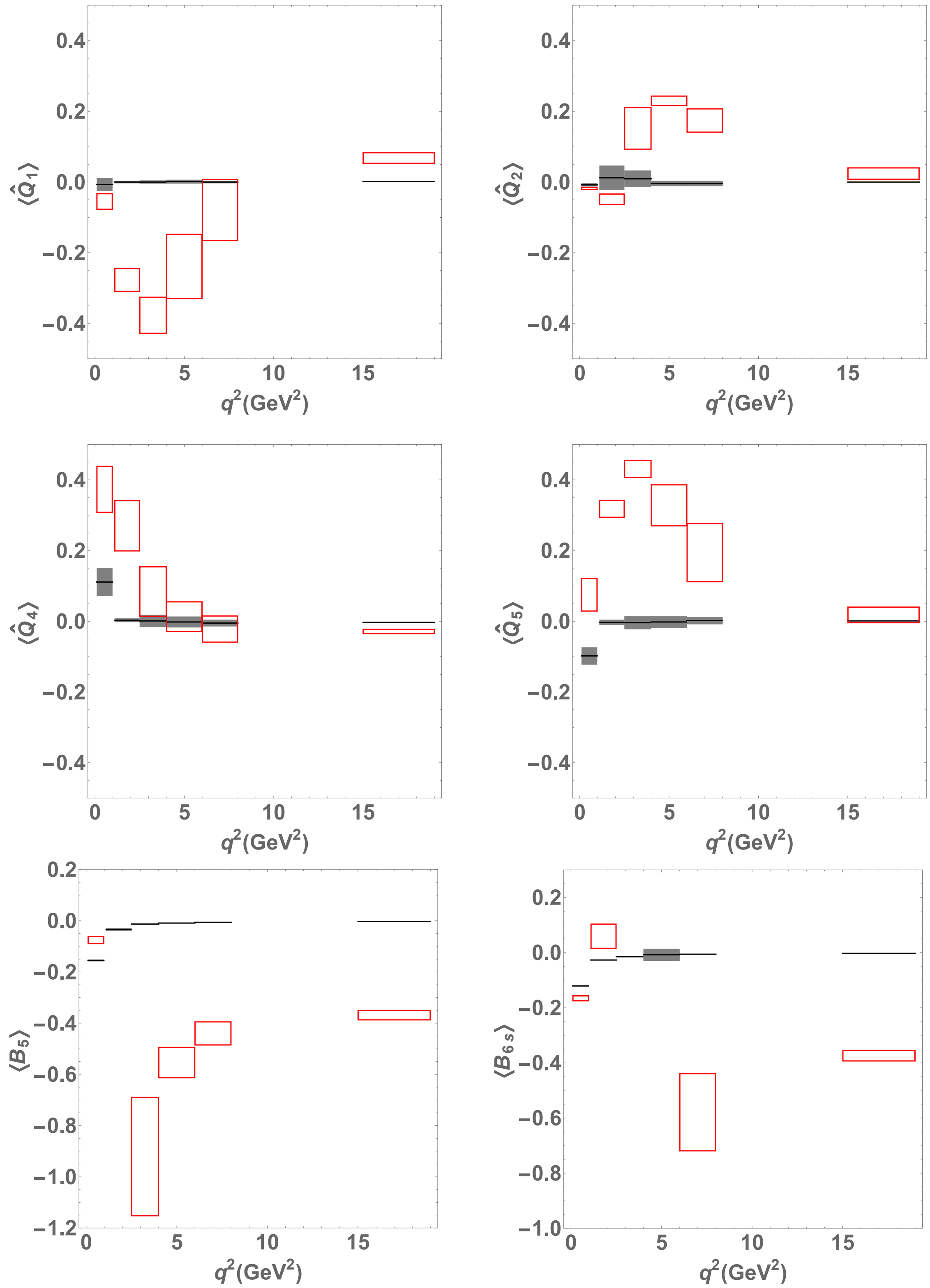

Figure 7.7: *Scenario 4.* SM predictions (grey boxes) and NP predictions (red boxes), assuming $\mathcal{C}_{9\mu}^{\rm NP} = -\mathcal{C}_{9'\mu}^{\rm NP} = -1.18$ and $\mathcal{C}_{10\mu}^{\rm NP} = \mathcal{C}_{10'\mu}^{\rm NP} = 0.38$

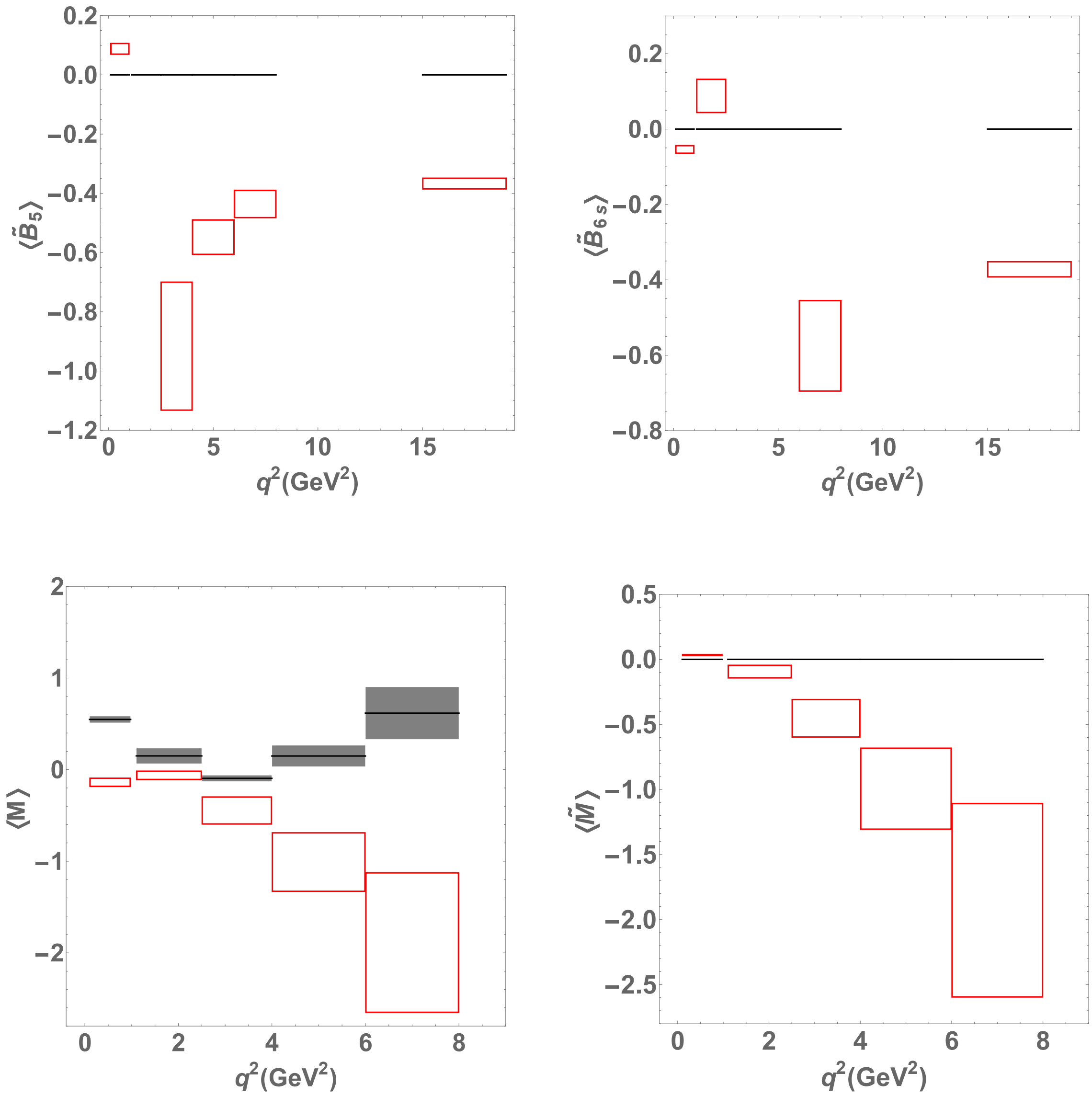

Figure 7.8: *Scenario 4.* SM predictions (grey boxes) and NP predictions (red boxes), assuming $\mathcal{C}_{9\mu}^{\rm NP} = -\mathcal{C}_{9'\mu}^{\rm NP} = -1.18$ and $\mathcal{C}_{10\mu}^{\rm NP} = \mathcal{C}_{10'\mu}^{\rm NP} = 0.38$

two scenarios.

These observables are quite complementary to R_{K^*}, for which we provide predictions in App. D. Indeed, the value of R_{K^*} is very similar (within uncertainties) in the first two scenarios, whereas a larger suppression is expected for the other scenarios at moderately large q^2, illustrating the complementarity with the $\hat{Q}_i$ (Q_i) observables. For completeness we also present predictions for the observables T_i in the same appendix.

7.2.2 B and $\widetilde{B}$ observables

We also give predictions for the B_i observables in App. D and in Figs. 7.1-7.8 within each scenario. In the plots we have not shown the predictions in the bins where B_5 or B_{6s} have a pole ([1.1,2.5] for B_5, [2.5,4] and [4,6] for B_{6s}) and cannot be predicted accurately. All scenarios give very similar predictions, apart from the first bin of B_5 and the two first bins of B_{6s}.

The first bin of these observables is predicted accurately both in the SM and in the presence of NP. Not only it is insensitive to form factors in the large-recoil limit at leading order, but it is also protected from long-distance charm contributions due to a kinematical suppression of the charm-dependent contribution at low q^2 (see also Ref. [1]). The analysis of this bin in the SM and in the scenarios presented above is particularly interesting. As explained in the previous section, the SM predictions $B_5^{\rm SM} = -0.155 \pm 0.003$ and $B_{6s}^{\rm SM} = -0.121 \pm 0.001$ are only different from zero due to β_μ/β_e effects integrated over the bin. This can be checked through the corresponding prediction for the $\widetilde{B}_i$ observables, which are free from these effects and equal to zero in the SM. In the case of a negative NP contribution to $\mathcal{C}_{9\mu}$, both B_5 and B_{6s} receive a positive contribution that pushes them towards zero in the first bin. If there is a positive NP contribution in $\mathcal{C}_{10\mu}$, the contribution to both observables is negative and large (of size $\mathcal{C}_{10\mu}^{\rm NP}/\mathcal{C}_{10\mu}$). In summary, a contribution close to zero will favour a scenario with NP only in $\mathcal{C}_{9\mu} < 0$, whereas values of B_5 and B_{6s} lower than the SM will signal NP in $\mathcal{C}_{10\mu}$ (NP in $\mathcal{C}_{9\mu}$ is better discriminated by other observables). In both cases B_5 and B_{6s} are almost equal, while a contribution to $\mathcal{C}'_{10\mu}$ would break this degeneracy. The second bin of B_{6s} exhibits a similar pattern (above the SM in Scenario 1, below in Scenario 2).

The same discussion applies to $\widetilde{B}_i$, which have a similar behaviour in those bins, the only difference being that they are centered around zero (SM prediction). For instance, the first bin of $\widetilde{B}_5$ and $\widetilde{B}_{6s}$ in the Scenario 1 (Scenario 2) receives a positive (negative) contribution. The second bin of $\widetilde{B}_{6s}$ follows the same rules as B_{6s}.

The low-recoil behaviour of the B_i and $\widetilde{B}_i$ observables is particularly interesting because it points to large deviations that cannot be seen easily in the Q_i observables. Unfortunately, they are not useful in distinguishing Scenarios 1 and 2, except if compared together with the corresponding Q_i at low recoil, which show a slightly different behaviour in that region.

7.2.3 M and $\widetilde{M}$ observables

M is also an interesting observable to get information on the existence of NP contributions and identifying their nature. This can be seen from the results in App. C and Figs. 7.1-7.8 by looking at the third bin, where it can be noted that this observable can help to disentangle Scenario 2 from Scenarios 1 and 3, thus testing for the presence of NP in $\mathcal{C}_{10\mu}$.

However in the first bin, where $B_5 \simeq B_{6s}$, M is poorly predicted. In these region it proves instead very useful to exploit the alternative observable $\widetilde{M}$, where effects related to β_ℓ are removed.

This observable then gives additional information in discerning between Scenario 2 and Scenarios 1 and 3. The effects in this first bin can also be confirmed by looking at the second bin (notice that $\widetilde{M}$ is well defined in its second bin even if $\widetilde{B}_5$ has a pole in its second bin).

7.2.4 LFUV observables and hadronic uncertainties

The observables presented here, specially Q_i, B_i and $\widetilde{B}_i$, are built to be very accurate in the SM, and almost insensitive to long-distance charm contributions. Moreover, whether NP is present or not, these observables are built to have no dependence on soft form factors at leading order in the large-recoil limit. In the presence of NP, these observables become again sensitive to charm-loop contributions, but in a very specific way that we discuss now.

Let us first recall that we introduced the observables $\hat{Q}_i$ in order to provide predictions taking into account how LHC measures F_L currently. Here the cancellation of soft form factors between numerator and denominator is not fully operative and these observables are thus sensitive to soft form factors arising in J_{1c} but suppressed by powers of m_ℓ^2/q^2. This explains why the errors of $\hat{Q}_i$ are larger (but still small in most of the bins) than for Q_i. The observables T_i exhibit a residual sensitivity to soft form factors in most of the bins. Finally, the observable M suffers from large uncertainties when $B_5 \simeq B_{6s}$, even though it is designed to have no dependence on soft form factors at leading order in the large-recoil limit.

Concerning long-distance charm-loop contributions, the most interesting observables are B_i ($\widetilde{B}_i$) and M ($\widetilde{M}$). In the analytic expressions provided in Section 7.1.2, we have assumed that the charm contribution $\Delta\mathcal{C}_9$ entered all transversity amplitudes in the same way. One can generalize the expressions for $B_{5,6s}$ and $\widetilde{M}$ in Eqs. (7.1.10,7.1.11) and allow for transversity-dependent charm contributions $\Delta\mathcal{C}_9^{\perp,\|,0}(q^2)$ associated to each amplitude:

$$B_5 = \frac{\beta_\mu^2-\beta_e^2}{\beta_e^2} + \frac{\beta_\mu^2}{\beta_e^2}\frac{\delta\mathcal{C}_{10}}{\mathcal{C}_{10}} + \frac{\beta_\mu^2}{\beta_e^2}\frac{2(\mathcal{C}_{10}+\delta\mathcal{C}_{10})\delta\mathcal{C}_9\hat{s}}{\mathcal{C}_{10}\left(2\mathcal{C}_7\hat{m}_b(1+\hat{s})+(2\mathcal{C}_9+\Delta\mathcal{C}_{9,0}+\Delta\mathcal{C}_{9,\perp})\hat{s}\right)} \tag{7.2.1}$$

$$B_{6s} = \frac{\beta_\mu^2-\beta_e^2}{\beta_e^2} + \frac{\beta_\mu^2}{\beta_e^2}\frac{\delta\mathcal{C}_{10}}{\mathcal{C}_{10}} + \frac{\beta_\mu^2}{\beta_e^2}\frac{2(\mathcal{C}_{10}+\delta\mathcal{C}_{10})\delta\mathcal{C}_9\hat{s}}{\mathcal{C}_{10}\left(4\mathcal{C}_7\hat{m}_b+(2\mathcal{C}_9+\Delta\mathcal{C}_{9,\perp}+\Delta\mathcal{C}_{9,\|})\hat{s}\right)} \tag{7.2.2}$$

$$\begin{aligned}\widetilde{M} = \ &\frac{\left(2\mathcal{C}_{10}\delta\mathcal{C}_9\hat{s}+\delta\mathcal{C}_{10}\left(2\mathcal{C}_7\hat{m}_b(1+\hat{s})+(2\mathcal{C}_9+2\delta\mathcal{C}_9+\Delta\mathcal{C}_{9,\perp}+\Delta\mathcal{C}_{9,0})\hat{s}\right)\right)}{2\mathcal{C}_{10}(\mathcal{C}_{10}+\delta\mathcal{C}_{10})\delta\mathcal{C}_9\left(2\mathcal{C}_7\hat{m}_b(\hat{s}-1)+(\Delta\mathcal{C}_{9,0}-\Delta\mathcal{C}_{9,\|})\hat{s}\right)\hat{s}}\\ &\times\left(2\mathcal{C}_{10}\delta\mathcal{C}_9\hat{s}+\delta\mathcal{C}_{10}\left(4\mathcal{C}_7\hat{m}_b+(2\mathcal{C}_9+2\delta\mathcal{C}_9+\Delta\mathcal{C}_{9,\perp}+\Delta\mathcal{C}_{9,\|})\hat{s}\right)\right)\end{aligned} \tag{7.2.3}$$

The corresponding expressions for the $\widetilde{B}_{5,6s}$ are obtained in the limit $\beta_\ell \to 1$. In the case of NP only in $\delta\mathcal{C}_9$ they simplify to

$$B_5 = \frac{\beta_\mu^2-\beta_e^2}{\beta_e^2} + \frac{\beta_\mu^2}{\beta_e^2}\frac{\delta\mathcal{C}_9\hat{s}}{(\mathcal{C}_7\hat{m}_b(1+\hat{s})+(\mathcal{C}_9+(\Delta\mathcal{C}_9^0+\Delta\mathcal{C}_9^\perp)/2)\hat{s})} + \ldots \tag{7.2.4}$$

$$B_{6s} = \frac{\beta_\mu^2-\beta_e^2}{\beta_e^2} + \frac{\beta_\mu^2}{\beta_e^2}\frac{\delta\mathcal{C}_9\hat{s}}{(2\mathcal{C}_7\hat{m}_b+(\mathcal{C}_9+(\Delta\mathcal{C}_9^\|+\Delta\mathcal{C}_9^\perp)/2)\hat{s})} + \ldots \tag{7.2.5}$$

$$\widetilde{M} = -\frac{\delta\mathcal{C}_9\hat{s}}{\mathcal{C}_7\hat{m}_b(1-\hat{s})-(\Delta\mathcal{C}_9^0-\Delta\mathcal{C}_9^\|)\hat{s}/2} + \ldots \tag{7.2.6}$$

The observable $\widetilde{M}$ was designed to cancel exactly a transversity-independent charm contribution $\Delta\mathcal{C}_9$ at leading order in the large recoil limit, which occurs in the denominator of the B_i observables. The above expressions indicate that for B_i, all the long-distance charm dependence is contained in the denominator, and its numerical impact is somehow reduced by a large $\mathcal{C}_9$, which explains their reduced sensitivity to $\Delta\mathcal{C}_9$ (this is even more efficient at very low q^2 due to the photon pole). In the case of $\widetilde{M}$, $\mathcal{C}_9$ cancels, leaving only the photon pole to tame the sensitivity to transversity-dependent charm-loop contributions. For this reason at higher q^2 values, where the photon pole contribution is smaller, the sensitivity to this transversity-dependent charm contribution is maximal in $\widetilde{M}$ as can be seen in App. D and in Figs. 7.1-7.8. In addition, looking at Eq. (7.2.3), it is interesting to note that $\widetilde{M}$ is sensitive to charm contributions only if *a)* there is LFUV New Physics in $\mathcal{C}_{10}$ or right handed operators, or *b)* there are transversity-dependent charm-loop contributions (such that $\Delta\mathcal{C}_9^0 \neq \Delta\mathcal{C}_9^{\|}$).

We should finally comment on the fact that our predictions do not include any evaluation of Bremsstrahlung effects. Naively one expects these effects to be of order $\alpha \log(m_e^2/m_\mu^2) \sim 8\%$ [180]. Part of these effects are taken into account at the level of the experimental analysis by means of a Montecarlo simulation with PHOTOS [181], which accounts for soft-photon emission from the leptons. Other contributions (e.g., real emission from the mesons, virtual photons) should still be estimated by separating in the theoretical computations the radiative corrections already implemented experimentally and those to be estimated theoretically (see Refs. [182, 183] for a discussion of this issue in the context of $K_{\ell 4}$ decays). Such a work goes far beyond the present note, but the impact of such effects should be expected to be of a few percent.

Part III

Results and implications of our Global Fits

Chapter 8

Global Fits to the B Anomalies

Over the last few years, many observables related to $b \to s\ell\ell$ flavour-changing neutral-current transitions have exhibited deviations from SM expectations. Due to their suppression within the SM, these transitions are well known to have a high sensitivity to potential NP contributions. In order to evaluate the significance and coherence of these deviations, a global model-independent fit is the most efficient tool to determine if they contain patterns explained by NP in a consistent way.

The present situation is *exceptional* in the sense that we have found that the observed deviations form coherent patterns within the model-independent approach of the effective Hamiltonian governing the $b \to s\ell\ell$ transitions. Already in 2013 first hints of this consistency were pointed out in Ref. [153] (using only $B \to K^*\mu^+\mu^-$) and later on in Ref. [113] (with all LHCb data available at that time) showing that a very economical mechanism, namely a negative contribution of the order of -25% to the short-distance coefficient of the effective operator $\mathcal{O}_{9\mu}$ in Eq. (4.1.15), is sufficient to alleviate all above-mentioned tensions, whereas the data allowed for NP contributions to other operators. This picture was later confirmed by other global analyses [163, 166] using different observables, hadronic inputs and theory approaches for their computations. Recent experiment results have shown additional hints of NP, indicating a violation of Lepton Flavour Universality (LFU) between $b \to see$ and $b \to s\mu\mu$ processes.

In this chapter we will discuss our most recent global analyses, including the most updated experimental and theoretical information on $b \to s\ell\ell$ processes. Additionally, model-building implications of the most significant results of our global fits and the potential of LFUV observables to disentangle scenarios will be also discussed.

8.1 Review of the experimental situation

We start by briefly discussing the recent experimental activity concerning $b \to s\ell\ell$ transitions. In 2013, using the 1 fb^{-1} dataset, the LHCb experiment measured the basis of optimised observables defined in Section 5.1.4 for $B \to K^*\mu^+\mu^-$ [176], observing the so-called P_5' anomaly [153], i.e. a sizeable 3.7σ discrepancy between the measurement and the SM prediction in one bin of the aforementioned angular observable [115]. In 2015, using the 3 fb^{-1} dataset, LHCb confirmed this discrepancy and reported a 3σ deviation in each of two adjacent bins at large K^* recoil [184]. LHCb also observed a systematic deficit with respect to SM predictions for the branching ratios of several decays [121, 185]. In 2016, the Belle experiment presented an independent analysis of

P_5' [178, 186] confirming the LHCb measurements in a very different experimental setting.

A conceptually new element arose when a discrepancy in the LFUV ratio R_K (see Section 5.3) was also observed by LHCb [187], hinting at NP signals with a LFUV signature such that it predominantly affects $b \to s\mu^+\mu^-$ transitions but not $b \to se^+e^-$ ones. Complementary LFUV tests were also presented by Belle, being the first experiment to measure the observables $Q_{4,5}$, proposed in Ref. [2] and reviewed in the previous chapter. Even if not yet statistically significant, these results point towards LFUV in Q_5, consistently with the deviation in R_K.

Further tests of the angular distribution of the $B \to K^*\mu^+\mu^-$ mode were performed by the ATLAS and CMS collaborations: the former measured the whole set of angular observables as well as F_L at large K^* recoil [188], whereas the latter presented results only for P_1 and P_5' at low and large recoils [189]. These results show a good (but not perfect) overall agreement with the LHCb results.

In 2017, the LHCb updated the $B \to K^*\mu^+\mu^-$ differential branching ratio [190] and released a striking new measurement of the LFUV ratio $R_{K^*} = \mathcal{B}(B \to K^*\mu^+\mu^-)\ /\mathcal{B}(B \to K^*e^+e^-)$ at large K^* recoil [191], exhibiting significant deviations from SM expectations. LFUV ratios are particularly interesting due to their lack of sensitivity to hadronic uncertainties in the SM, making any significant deviation from their SM value a clear sign of NP [192, 193]. Moreover, the tensions in R_{K^*} denote that hadronic uncertainties in the theoretical predictions are not sufficient to explain all the anomalies observed in $b \to s\ell^+\ell^-$ transitions, and that alternative explanations must be searched for.

This was the experimental situation as of mid 2017, which led to our global analysis of Ref. [136]. More recently, the LHCb collaboration announced a new measurement of R_K [194] using part of the full Run-2 data set. The average of the former Run-1 measurement and the new result moves the central value of the combination closer to the standard model prediction but, as the error has experienced a significant reduction too, only a minimal change in the significance can be observed: 2.5σ instead of the previous 2.6σ below the SM.

Finally, new Belle measurements on the LFUV ratios R_K and R_{K^*} have also been released earlier this year in several q^2 bins [195, 196]. However, these measurements have a very limited impact on the global fits, as their associated errors are still large.

8.2 Global analyses of $b \to s\ell\ell$ data

In order to combine all measurements and evaluate their impact, importance and consistency, one has to perform a global fit to all available data. Global analyses discussed here follow the guidelines of previous fits performed within the same framework [113, 115]. In this section we will review the general statistical framework used, including a description of both our fit strategy and the statistical measures we employ for the characterisation of our estimates, and we will present the main results of our most updated state-of-the-art global analyses [197], stating the relevant differences between them and our previous fits in Refs. [113, 136].

The starting point of our analyses is the effective Hamiltonian of Eq. (4.1.1) in which heavy degrees of freedom (the top quark, the W and Z bosons, the Higgs and any potential heavy new particles) have been integrated out in short-distance Wilson coefficients $\mathcal{C}_i$. In the SM, the Hamiltonian contains 10 main operators with specific chiralities due to the $V-A$ structure of the weak interactions, as discussed in Section 4.1.1. In presence of NP, additional operators may become of importance (see Eqs (4.1.29)-(4.1.32)). For the processes considered here, we will focus our attention only on the operators $\mathcal{O}_{7^{(\prime)}}$, $\mathcal{O}_{9^{(\prime)}\ell}$ and $\mathcal{O}_{10^{(\prime)}\ell}$ (being $\ell = e$ or μ), with their associated Wilson coefficients $\mathcal{C}_7, \mathcal{C}_{9^{(\prime)}\ell}, \mathcal{C}_{10^{(\prime)}\ell}$. These Wilson coefficients are equal for muons and electrons in the SM but NP can add very different contributions in muons compared to electrons. In order to estimate the aforementioned NP contributions to the Wilson coefficients, we parametrise them by splitting their SM and NP contributions

$$\mathcal{C}_{i\ell} = \mathcal{C}_{i\ell}^{\rm SM} + \mathcal{C}_{i\ell}^{\rm NP}, \tag{8.2.1}$$

where $i = 7^{(\prime)}$, $9^{(\prime)}$, $10^{(\prime)}$, being the SM contributions to chirally-flipped operators negligible. This defines one possible basis for assessing the impact of NP on the relevant Wilson coefficients of the underlying effective theory, but this choice is not unique. Indeed, we will show that interesting patterns can also be unveiled using a different basis based on a parametrisation in terms of LFU and LFUV-NP contributions to the Wilson coefficients, instead of NP contributions with a specific flavour attached. Fit results corresponding to the first NP parametrisation can be found in Section 8.2.1, while the second is explored in Section 8.2.2.

The full fit includes all available results for the following decay channels[1]:

- $B^{(0,+)} \to K^{*(0,+)}\mu^+\mu^-$, $B^{(0,+)} \to K^{*(0,+)}e^+e^-$, $B^{(0,+)} \to K^{*(0,+)}\gamma$,
- $B^{(0,+)} \to K^{(0,+)}\mu^+\mu^-$, $B^+ \to K^+e^+e^-$,
- $B_s \to \phi\mu^+\mu^-$, $B_s \to \phi\gamma$,
- $B \to X_s\mu^+\mu^-$, $B \to X_s\gamma$ and $B_s \to \mu^+\mu^-$.

More specifically, for the angular observables in $B \to K^*\mu^+\mu^-$, $B \to K^*e^+e^-$ and $B_s \to \phi\mu^+\mu^-$, we use the optimised observables $P_i^{(\prime)}$ obtained from LHCb's likelihood fit [184]. Concerning the q^2 binning we use the finest bins at large recoil (below the J/ψ), including the first bin in the low-q^2 region and the $[6, 8]$ GeV^2 bin, but the widest bins in the low-recoil region to ensure quark-hadron duality (see the discussion in 6.1.2). For the $b \to s\gamma$ radiative decays, we include in our fit the whole set of observables discussed in Section 5.4.2.

Although experimental data on the baryonic decay $\Lambda_b \to \Lambda\mu^+\mu^-$ is available, it is not included in the fit because for the low-q^2 region QCDf is poorly understood in this channel [198], while at high-q^2, where a recent determination of the $\Lambda_b \to \Lambda$ form factors from lattice QCD [199] reduces theory uncertainties, experimental errors are large [200]. Further considerations about this decay channel can be found in Refs. [113, 201]).

In addition, and following the discussion of the previous section, we add to the fit all the new measurements made available since Ref. [113]:

- The $B^0 \to K^{\star 0}\mu^+\mu^-$ differential branching fraction measured by LHCb [190] based on the full Run 1 dataset, superseding the results in Ref. [117]. We use the most recent update of Ref. [190] that led to a reduction of the branching ratio by about 20% in magnitude.

[1]See Appendix E for the full list of the 180 observables included in the global fit, with both their SM predictions and their associated most updated experimental measurements.

- The Belle measurements [186] for the isospin-averaged but lepton flavour dependent $B \to K^\star \ell^+\ell^-$ observables $P'^{e}_{4,5}$ and $P'^{\mu}_{4,5}$. The isospin average is given by the following expression,

$$P'^{\ell}_i = \sigma_+ \, P'^{\ell}_i(B^+) + (1-\sigma_+) \, P'^{\ell}_i(\bar{B}^0). \tag{8.2.2}$$

  Since σ_+ describing the relative weight of each isospin component in the average is not public, we treat it as a nuisance parameter $\sigma_+ = 0.5 \pm 0.5$. This will not have a significant effect in our results, since the isospin breaking in the SM is small (but accounted for in our analysis), and we do not consider NP contributions to four-quark operators.

- The ATLAS measurements [188] of the angular observables P_1, $P'_{4,5,6,8}$ in $B^0 \to K^{*0}\mu^+\mu^-$ as well as F_L in the large recoil region.

- The CMS measurements [189] of the angular observables P_1 and P'_5 in $B^0 \to K^{*0}\mu^+\mu^-$, both at large and low recoils (we consider only the long bin at low recoil). We take F_L and A_{FB} from an earlier analysis [202] and we also include the data from an earlier analysis at 7 TeV [203]. A very welcome check of the stability of the CMS results would consist in performing a simultaneous extraction of F_L, P_1 and P'_5, using the same folding distribution as ATLAS, LHCb and Belle.

- The 2017 measurement of the lepton-flavour non-universality ratio R_{K^*} in two large recoil bins by the LHCb collaboration [191]. The likelihood of these measurements is asymmetric, and dominated by statistical uncertainties. We thus take the two measurements as uncorrelated, and for each of the two bins, we take a symmetric Gaussian error that is the larger of the two asymmetric uncertainties (while keeping the central value unchanged). This approach will underestimate the impact of these measurements on our fit, but we prefer to remain conservative on this point until the likelihood is known in detail.

- The new ATLAS result for the branching ratio of the leptonic decay $B_s \to \mu^+\mu^-$ [204], combined with previous CMS [205] and LHCb [206] measurements. Two likelihood-based combinations can be found in the literature [207, 208], with similar results. We quote the first one for definiteness

$$\mathcal{B}(B_s \to \mu^+\mu^-) = \left(2.67^{+0.45}_{-0.35}\right) \times 10^{-9} \qquad \text{(with } \mathcal{B}(B^0 \to \mu^+\mu^-) \text{ profiled)}, \tag{8.2.3}$$

$$\mathcal{B}(B_s \to \mu^+\mu^-) = \left(2.67^{+0.45}_{-0.35}\right) \times 10^{-9} \qquad \text{(with } \mathcal{B}(B^0 \to \mu^+\mu^-) \text{ SM-like)} \tag{8.2.4}$$

  These combinations are based on a composition of the experimental two-dimensional likelihoods without accounting for the asymmetries in parameter space caused by the fact that both ATLAS and LHCb have only been able to provide upper bounds on $\mathcal{B}(B^0 \to \mu^+\mu^-)$. Therefore, unlike the analyses of Refs. [207, 208] and until the likelihoods of these measurements are better understood, we prefer to take a more conservative approach and use a naive weighted average [197]

$$\mathcal{B}(B_s \to \mu^+\mu^-) = (2.94 \pm 0.43) \times 10^{-9}. \tag{8.2.5}$$

- The average of the two LHCb measurements of the LFUV ratio R_K in the long large recoil q^2 bin [1, 6] GeV^2 [194]. Corresponding measurements of this observable performed by the Belle collaboration are also included [195].

- The Belle update of the R_{K^*} observable [196]. Similarly to the case of $P'^{\ell}_{4,5}$, Belle measured R_{K^*} as an isospin average of the neutral $B \to K^{*0}$ and charged $B \to K^{*+}$ channels. Hence, following Eq. (8.2.2), we introduce the following model for this observable in order to account for isospin breaking effects

$$R_{K^*} = \sigma_+ R_{K^*}(B^+) + (1 - \sigma_+) R_{K^*}(\bar{B}^0), \tag{8.2.6}$$

where σ_+ denotes a new nuisance parameter, which we assume to be uncorrelated with respect to the same parameter quantifying isospin breaking in $P'^{\ell}_{4,5}$. Again, isospin effects are expected to be negligible for this observable.

Regarding the theory computation of all observables, we work within the framework described between Chapters 4 and 6, taking into account the theoretical updates for the branching ratios of $B \to X_s\gamma$, $B \to X_s\mu\mu$ and $B_s \to \mu\mu$ described in Section 5.4. Furthermore, we update the value of the theory prediction for the leptonic branching ratio $\mathcal{B}(B_s \to \mu\mu)$ with the most recent lattice result for f_{B_s} obtained from simulations with $N_f = 2 + 1 + 1$ flavours [209]. As we already discussed in previous chapters, for the $B \to K^*$ form factors at large recoil we use the calculation in Ref. [148], which has more conservative uncertainties than the ones in Ref. [150], obtained with a different method. Since the corresponding calculation is not available for $B_s \to \phi$, we thus use Ref. [150]. This leads to smaller hadronic uncertainties quoted for $B_s \to \phi\ell\ell$ (see the corresponding branching ratios in Appendix E), but we stress that this is only due to the choice of input.

8.2.1 Fits results in presence of LFUV-NP

First, we consider fits to NP scenarios which affect muon modes only. In Tables 8.1 and 8.2, we give the fit results for several one- or two-dimensional hypothesis for NP contributions to the various operators, with two different datasets: either we include all available data from muon and electron channels presented in the previous section (column "All", 180 measurements), or we include only LFUV observables, i.e. R_K and R_{K^*} from LHCb and Belle and Q_i $(i = 4, 5)$ from Belle (column "LFUV", 22 measurements). In both cases, we include also the $b \to s\gamma$ observables, as well as $\mathcal{B}(B \to X_s\mu^+\mu^-)$ and $\mathcal{B}(B_s \to \mu^+\mu^-)$. The SM point yields a χ^2 corresponding to a p-value of 11.0% for the fit "All" and 8.0% for the fit "LFUV" [197].

	All				LFUV			
1D Hyp.	Best fit	$1\,\sigma/2\,\sigma$	Pull$_{\rm SM}$	p-value	Best fit	$1\,\sigma/\,2\,\sigma$	Pull$_{\rm SM}$	p-value
$\mathcal{C}_{9\mu}^{\rm NP}$	-0.98	$[-1.15, -0.81]$ $[-1.31, -0.64]$	5.6	65.4 %	-0.89	$[-1.23, -0.59]$ $[-1.60, -0.32]$	3.3	52.2 %
$\mathcal{C}_{9\mu}^{\rm NP} = -\mathcal{C}_{10\mu}^{\rm NP}$	-0.46	$[-0.56, -0.37]$ $[-0.66, -0.28]$	5.2	55.6 %	-0.40	$[-0.53, -0.29]$ $[-0.63, -0.18]$	4.0	74.0 %
$\mathcal{C}_{9\mu}^{\rm NP} = -\mathcal{C}_{9'\mu}$	-0.99	$[-1.15, -0.82]$ $[-1.31, -0.64]$	5.5	62.9 %	-1.61	$[-2.13, -0.96]$ $[-2.54, -0.41]$	3.0	42.5 %
$\mathcal{C}_{9\mu}^{\rm NP} = -3\mathcal{C}_{9e}^{\rm NP}$	-0.87	$[-1.03, -0.71]$ $[-1.19, -0.55]$	5.5	61.9 %	-0.66	$[-0.90, -0.44]$ $[-1.17, -0.24]$	3.3	52.2 %

Table 8.1: Most prominent 1D patterns of NP in $b \to s\mu^+\mu^-$. Pull$_{\rm SM}$ is quoted in units of standard deviation.

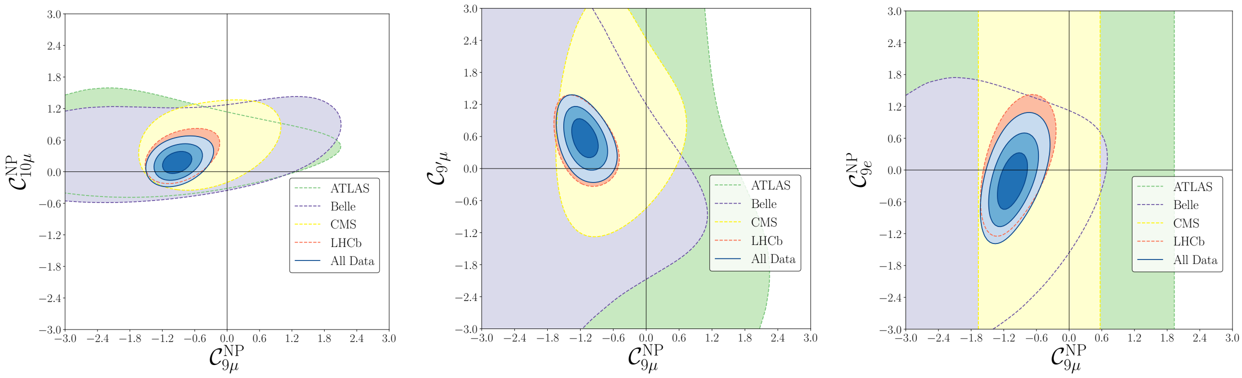

Figure 8.1: From left to right: Allowed regions in the $(\mathcal{C}_{9\mu}^{\rm NP}, \mathcal{C}_{10\mu}^{\rm NP})$, $(\mathcal{C}_{9\mu}^{\rm NP}, \mathcal{C}_{9'\mu})$ and $(\mathcal{C}_{9\mu}^{\rm NP}, \mathcal{C}_{9e}^{\rm NP})$ planes for the corresponding two-dimensional hypotheses, using all available data (fit "All"). We also show the 3 σ regions for the data subsets corresponding to specific experiments. Constraints from $b \to s\gamma$ observables, $\mathcal{B}(B \to X_s\mu\mu)$ and $\mathcal{B}(B_s \to \mu\mu)$ are included in each case (see text).

We start by discussing NP hypotheses for the fit "All". New available experimental data have further increased the significance of already prominent hypotheses in previous studies, namely, the first three hypotheses ($\mathcal{C}_{9\mu}^{\rm NP}$, $\mathcal{C}_{9\mu}^{\rm NP} = -\mathcal{C}_{10\mu}^{\rm NP}$ and $\mathcal{C}_{9\mu}^{\rm NP} = -\mathcal{C}_{9'\mu}$) already identified in Refs. [113, 153]. The $\text{Pull}_{\rm SM}$ of current estimates exceeds 5σ in each case, however hypotheses can hardly be distinguished on this criterion, and as we will discuss in Section 8.5, the Q_i observables will be very powerful tools to lift this quasi-degeneracy. We do not observe any significant differences in the 1D scenarios with "All" data compared to our previous analysis in Ref. [136].

Further scrutiny of the differences between our current most updated fits and the results from our earlier analysis [136], reveals that the scenario $\mathcal{C}_{9\mu}^{\rm NP} = -\mathcal{C}_{9'\mu}$, which would predict $R_K = 1$ and $R_{K^*} < 1$ [113, 192, 193, 211, 212], has an increased significance in the "All" fit. Also, the best-fit point for the scenario $\mathcal{C}_{9\mu}^{\rm NP}$ now coincides in the "All" and LFUV fits, as opposed to our previous conclusions in Ref. [136]. On the other hand, NP solutions based on $\mathcal{C}_{10\mu}^{\rm NP}$ only show a significance in the "All" fit at the level of 4.0σ (3.9σ for the LFUV fit), which explains its absence from Tab. 8.1 as in Ref. [136].

Besides providing the results for "simple" one- and two-dimensional hypotheses, we discuss five additional illustrative examples of NP hypotheses with specific chiral structures, leading to correlated shifts in Wilson coefficients. These hypotheses are:

1. $(\mathcal{C}_{9\mu}^{\rm NP} = -\mathcal{C}_{9'\mu}, \mathcal{C}_{10\mu}^{\rm NP} = \mathcal{C}_{10'\mu})$,
2. $(\mathcal{C}_{9\mu}^{\rm NP} = -\mathcal{C}_{9'\mu}, \mathcal{C}_{10\mu}^{\rm NP} = -\mathcal{C}_{10'\mu})$,
3. $(\mathcal{C}_{9\mu}^{\rm NP} = -\mathcal{C}_{10\mu}^{\rm NP}, \mathcal{C}_{9'\mu} = \mathcal{C}_{10'\mu})$,
4. $(\mathcal{C}_{9\mu}^{\rm NP} = -\mathcal{C}_{10\mu}^{\rm NP}, \mathcal{C}_{9'\mu} = -\mathcal{C}_{10'\mu})$,
5. $(\mathcal{C}_{9\mu}^{\rm NP}, \mathcal{C}_{9'\mu} = -\mathcal{C}_{10'\mu})$.

Concerning the 2D scenarios collected in Tab. 8.2, no significant changes can be be identified with respect to Ref. [136]. Nevertheless, with an R_K value closer to one, scenarios with right-handed currents (RHC) seem to emerge. Indeed, hypothesis 5 has now the highest $\text{Pull}_{\rm SM}$, indicating that small contributions to RHC are slightly favoured ($\mathcal{C}_{9'\mu} > 0, \mathcal{C}_{10'\mu} < 0$) [2]. Note that these RHC contributions tend to increase the value of R_K while $\mathcal{C}_{9\mu}^{\rm NP} < 0$ tend to decrease it. From a model-independent point of view, the also very competitive Hypothesis 1 is particularly interesting to yield a low value for R_{K^*} (especially if a contribution $\mathcal{C}_7^{\rm NP} > 0$ is allowed). Taking $\mathcal{C}_{10\mu}^{\rm NP} = -\mathcal{C}_{10'\mu}$ (i.e. Hypothesis 2) reduces the significance from 5.9σ to 5.3σ, similarly to Hypotheses 3 and 4 with the signature structure $\mathcal{C}_{9\mu}^{\rm NP} = -\mathcal{C}_{10\mu}^{\rm NP}$ (irrespective of the relative sign taken to constrain $\mathcal{C}_{9'\mu} = \pm\mathcal{C}_{10'\mu}$). Finally, the comparison between Hyps. 4 and 5 shows that the scenario $\mathcal{C}_{9'\mu} = -\mathcal{C}_{10'\mu}$ (left-handed lepton coupling for right-handed quarks) prefers to be associated with $\mathcal{C}_{9\mu}^{\rm NP}$ (vector lepton coupling for left-handed quarks) rather than $\mathcal{C}_{9\mu}^{\rm NP} = -\mathcal{C}_{10\mu}^{\rm NP}$ (left-handed lepton coupling for left-handed quarks).

Up to now, we have discussed scenarios where NP contributions occur only in $b \to s\mu\mu$ transitions. It is also interesting to consider scenarios with NP in both muon and electron channels, in particular ($\mathcal{C}_{9\mu}^{\rm NP}, \mathcal{C}_{9e}^{\rm NP}$), with a SM pull of 5.3σ and a p-value of 66.2%. While $\mathcal{C}_{9\mu}^{\rm NP} \sim -1$ is preferred over the SM with a significance around 5σ, $\mathcal{C}_{9e}$ is compatible with the SM already at 1σ, in agreement with the LFUV data included in the fit. New data included in our updated analysis [197] has induced a change on the central value of $\mathcal{C}_{9e}$: whereas the fit of Ref. [136] suggested a pattern $\mathcal{C}_{9e} > 0$, now we observe $\mathcal{C}_{9e} \lesssim 0$.

	All			LFUV		
2D Hyp.	Best fit	$\text{Pull}_{\rm SM}$	p-value	Best fit	$\text{Pull}_{\rm SM}$	p-value
($\mathcal{C}_{9\mu}^{\rm NP}, \mathcal{C}_{10\mu}^{\rm NP}$)	(-0.91,0.18)	5.4	68.7 %	(-0.16,0.56)	3.4	76.9 %
($\mathcal{C}_{9\mu}^{\rm NP}, \mathcal{C}_{7'}$)	(-1.00,0.02)	5.4	67.9 %	(-0.90,-0.04)	2.9	55.1 %
($\mathcal{C}_{9\mu}^{\rm NP}, \mathcal{C}_{9'\mu}$)	(-1.10,0.55)	5.7	75.1 %	(-1.79,1.14)	3.4	76.1 %
($\mathcal{C}_{9\mu}^{\rm NP}, \mathcal{C}_{10'\mu}$)	(-1.14,-0.35)	5.9	78.6 %	(-1.88,-0.62)	3.8	91.3 %
($\mathcal{C}_{9\mu}^{\rm NP}, \mathcal{C}_{9e}^{\rm NP}$)	(-1.05,-0.23)	5.3	66.2 %	(-0.73,0.16)	2.8	52.3 %
Hyp. 1	(-1.06,0.26)	5.7	75.7 %	(-1.62,0.29)	3.4	77.6 %
Hyp. 2	(-0.97,0.09)	5.3	65.2 %	(-1.95,0.25)	3.2	66.6 %
Hyp. 3	(-0.47,0.06)	4.8	55.7 %	(-0.39,-0.13)	3.4	76.2 %
Hyp. 4	(-0.49,0.12)	5.0	59.3 %	(-0.48,0.17)	3.6	84.3 %
Hyp. 5	(-1.14,0.24)	5.9	78.7 %	(-2.07,0.52)	3.9	92.5 %

Table 8.2: Most prominent 2D patterns of NP in $b \to s\mu^+\mu^-$. The last five rows correspond to Hypothesis 1: ($\mathcal{C}_{9\mu}^{\rm NP} = -\mathcal{C}_{9'\mu}, \mathcal{C}_{10\mu}^{\rm NP} = \mathcal{C}_{10'\mu}$), 2: ($\mathcal{C}_{9\mu}^{\rm NP} = -\mathcal{C}_{9'\mu}, \mathcal{C}_{10\mu}^{\rm NP} = -\mathcal{C}_{10'\mu}$), 3: ($\mathcal{C}_{9\mu}^{\rm NP} = -\mathcal{C}_{10\mu}^{\rm NP}, \mathcal{C}_{9'\mu} = \mathcal{C}_{10'\mu}$), 4: ($\mathcal{C}_{9\mu}^{\rm NP} = -\mathcal{C}_{10\mu}^{\rm NP}, \mathcal{C}_{9'\mu} = -\mathcal{C}_{10'\mu}$) and 5: ($\mathcal{C}_{9\mu}^{\rm NP}, \mathcal{C}_{9'\mu} = -\mathcal{C}_{10'\mu}$).

In Fig. 8.1 we show the corresponding constraints for the fit "All" under the three hypotheses ($\mathcal{C}_{9\mu}^{\rm NP}$, $\mathcal{C}_{10\mu}^{\rm NP}$), ($\mathcal{C}_{9\mu}^{\rm NP}, \mathcal{C}_{9\mu'}$) and ($\mathcal{C}_{9\mu}^{\rm NP}, \mathcal{C}_{9e}^{\rm NP}$), as well as the 3σ regions according to the results from individual experiments (for each region, we add the constraints from $b \to s\gamma$ observables, $\mathcal{B}(B \to X_s\mu^+\mu^-)$ and the average for $\mathcal{B}(B_s \to \mu^+\mu^-)$). As expected, the LHCb results drive most of the effect, with a clear exclusion of the origin, i.e. the SM point.

We can now move to the LFUV fit in Fig. 8.2, where we consider the same hypotheses favoured by global analyses. Note that this restricted subset of observables excludes the SM point with a higher significance, even though the p-value of the SM has increased with respect to Ref. [136] as a result of including new data points with little resolution (Belle measurements of R_K and

[2] Interestingly, these small contributions also reduce slightly the mild tension between P_5' at large and low recoils pointed out in Ref. [212] compared to the scenario with only $\mathcal{C}_{9\mu}^{\rm NP}$.

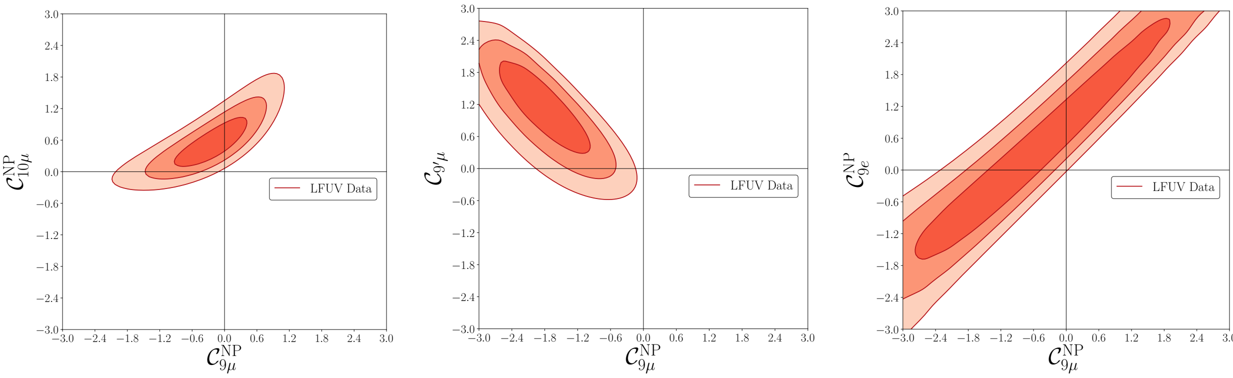

Figure 8.2: From left to right: Allowed regions in the $(\mathcal{C}_{9\mu}^{\rm NP}, \mathcal{C}_{10\mu}^{\rm NP})$, $(\mathcal{C}_{9\mu}^{\rm NP}, \mathcal{C}_{9'\mu})$ and $(\mathcal{C}_{9\mu}^{\rm NP}, \mathcal{C}_{9e}^{\rm NP})$ planes for the corresponding two-dimensional hypotheses, using only LFUV observables (fit "LFUV"). Constraints from $b \to s\gamma$ observables, $\mathcal{B}(B \to X_s\mu\mu)$ and $\mathcal{B}(B_s \to \mu\mu)$ are included in each case (see text).

R_{K^*}). Contrarily, the p-value of the SM for the fit "All" has not followed the same trend and currently stays at the same level as in 2017, hence no overall improvement of the SM in describing current data. While the same pattern of hierarchies is observed for this fit compared to our 2017 analysis [136], the $\text{Pulls}_{\rm SM}$ for some of 1D fits get reduced by half a standard deviation. It is important to stress that this fit favours regions similar to the fit "All" dominated by different $b \to s\mu\mu$-related observables ($B \to K^*\mu\mu$ optimised angular observables as well as low- and large-recoil branching ratios for $B \to K\mu\mu$, $B \to K^*\mu\mu$ and $B_s \to \phi\mu\mu$). This is also shown in Tabs. 8.1 and 8.2, where the scenarios with the highest pulls are confirmed with significances between 3 and 4σ, but get harder to distinguish on the basis of their significance.

	$\mathcal{C}_7^{\rm NP}$	$\mathcal{C}_{9\mu}^{\rm NP}$	$\mathcal{C}_{10\mu}^{\rm NP}$	$\mathcal{C}_{7'}$	$\mathcal{C}_{9'\mu}$	$\mathcal{C}_{10'\mu}$
Best fit	+0.01	-1.10	+0.15	+0.02	+0.36	-0.16
1σ	$[-0.01, +0.05]$	$[-1.28, -0.90]$	$[-0.00, +0.36]$	$[-0.00, +0.05]$	$[-0.14, +0.87]$	$[-0.39, +0.13]$
2σ	$[-0.03, +0.06]$	$[-1.44, -0.68]$	$[-0.12, +0.56]$	$[-0.02, +0.06]$	$[-0.49, +1.23]$	$[-0.58, +0.33]$

Table 8.3: 1 and 2σ confidence intervals for the NP contributions to Wilson coefficients in the 6D hypothesis allowing for NP in $b \to s\mu^+\mu^-$ operators dominant in the SM and their chirally-flipped counterparts, for the fit "All". The $\text{Pull}_{\rm SM}$ is 5.1 σ and the p-value is 81.6%.

Finally, we extend our analyses to include a six-dimensional fit allowing for NP contributions to all relevant Wilson coefficients $\mathcal{C}_{7('),9(')\mu,10(')\mu}$. The associated SM pull to this fit has shifted from 3.6σ in Ref. [113] to 5.1 σ, if one considers the fit "All" described above. Corresponding 1 and 2σ CL intervals are given in Tab. 8.3, with the pattern:

$$\mathcal{C}_7^{\rm NP} \gtrsim 0,\ \mathcal{C}_{9\mu}^{\rm NP} < 0,\ \mathcal{C}_{10\mu}^{\rm NP} > 0,\ \mathcal{C}_{7'} \gtrsim 0,\ \mathcal{C}_{9'\mu} > 0,\ \mathcal{C}_{10'\mu} \lesssim 0 \qquad (8.2.7)$$

where $\mathcal{C}_{9\mu}$ is compatible with the SM beyond 3σ and all the other coefficients at 1σ. No significant changes are observed in the updated 6D fit with respect to the result of the same fit in Ref. [136], except for a slight increase in the $\text{Pull}_{\rm SM}$ and the preference for a negative $\mathcal{C}_{10'\mu}$.

Scenario		Best-fit point	1σ	2σ	Pull_{SM}	p-value
Scenario 5	$\mathcal{C}^{\rm V}_{9\mu}$	-0.36	$[-0.86, +0.10]$	$[-1.41, +0.52]$	5.2	71.2 %
	$\mathcal{C}^{\rm V}_{10\mu}$	$+0.67$	$[+0.24, +1.03]$	$[-1.73, +1.36]$		
	$\mathcal{C}^{\rm U}_{9} = \mathcal{C}^{\rm U}_{10}$	-0.59	$[-0.90, -0.12]$	$[-1.13, +0.68]$		
Scenario 6	$\mathcal{C}^{\rm V}_{9\mu} = -\mathcal{C}^{\rm V}_{10\mu}$	-0.50	$[-0.61, -0.38]$	$[-0.72, -0.28]$	5.5	71.0 %
	$\mathcal{C}^{\rm U}_{9} = \mathcal{C}^{\rm U}_{10}$	-0.38	$[-0.52, -0.22]$	$[-0.64, -0.06]$		
Scenario 7	$\mathcal{C}^{\rm V}_{9\mu}$	-0.78	$[-1.11, -0.47]$	$[-1.45, -0.18]$	5.3	66.2 %
	$\mathcal{C}^{\rm U}_{9}$	-0.20	$[-0.57, +0.18]$	$[-0.92, +0.55]$		
Scenario 8	$\mathcal{C}^{\rm V}_{9\mu} = -\mathcal{C}^{\rm V}_{10\mu}$	-0.30	$[-0.42, -0.20]$	$[-0.53, -0.10]$	5.7	75.2 %
	$\mathcal{C}^{\rm U}_{9}$	-0.74	$[-0.96, -0.51]$	$[-1.15, -0.25]$		
Scenario 9	$\mathcal{C}^{\rm V}_{9\mu} = -\mathcal{C}^{\rm V}_{10\mu}$	-0.57	$[-0.73, -0.41]$	$[-0.87, -0.28]$	5.0	60.2 %
	$\mathcal{C}^{\rm U}_{10}$	-0.34	$[-0.60, -0.07]$	$[-0.84, +0.18]$		
Scenario 10	$\mathcal{C}^{\rm V}_{9\mu}$	-0.95	$[-1.13, -0.76]$	$[-1.30, -0.57]$	5.5	69.5 %
	$\mathcal{C}^{\rm U}_{10}$	$+0.27$	$[0.08, 0.47]$	$[-0.09, 0.66]$		
Scenario 11	$\mathcal{C}^{\rm V}_{9\mu}$	-1.03	$[-1.22, -0.84]$	$[-1.38, -0.65]$	5.6	73.6 %
	$\mathcal{C}^{\rm U}_{10'}$	-0.29	$[-0.47, -0.12]$	$[-0.63, 0.05]$		
Scenario 12	$\mathcal{C}^{\rm V}_{9'\mu}$	-0.03	$[-0.22, 0.15]$	$[-0.40, 0.32]$	1.6	15.7 %
	$\mathcal{C}^{\rm U}_{10}$	$+0.41$	$[0.21, 0.63]$	$[0.02, 0.83]$		
Scenario 13	$\mathcal{C}^{\rm V}_{9\mu}$	-1.11	$[-1.28, -0.91]$	$[-1.41, -0.71]$	5.4	78.7 %
	$\mathcal{C}^{\rm V}_{9'\mu}$	$+0.53$	$[0.24, 0.83]$	$[-0.10, 1.11]$		
	$\mathcal{C}^{\rm U}_{10}$	$+0.24$	$[0.01, 0.48]$	$[-0.21, 0.69]$		
	$\mathcal{C}^{\rm U}_{10'}$	-0.04	$[-0.28, 0.20]$	$[-0.48, 0.42]$		

Table 8.4: Most prominent patterns for LFU and LFUV-NP contributions from Fit "All". Scenarios 5 to 8 were introduced in Ref. [211]. Scenarios 9 (motivated by 2HDMs [213]) and 10 to 13 (motivated by Z' models with vector-like quarks [214]) are new.

8.2.2 Fits results in presence of LFUV and LFU-NP

Our previous global analyses assumed different NP contributions for muons and electrons, as the parametrisation in Eq. (8.2.1) suggests. Hence, all above-mentioned NP determinations were performed under the implicit hypothesis of LFUV-NP. In Ref. [211], assuming that hadronic contributions are properly assessed [1, 215], we considered for the first time the possibility that short-distance Wilson coefficients could receive NP contributions that are not only LFUV, but also lepton flavour universal or LFU. Indeed, whereas LFUV-NP contributions are mandatory to explain R_K and R_{K^*}, $b \to s\ell\ell$ processes are not restricted to such NP contributions alone. This idea was implemented by allowing two NP contributions inside the semileptonic Wilson coefficients [211]:

$$\mathcal{C}^{\rm NP}_{i\ell} = \mathcal{C}^{\rm V}_{i\ell} + \mathcal{C}^{\rm U}_{i} \tag{8.2.8}$$

with $\ell = e, \mu, \tau$ and where $\mathcal{C}^{\rm V}_{i\ell}$ stands for LFUV-NP and $\mathcal{C}^{\rm U}_{i}$ for LFU-NP contributions. We distinguish the two contributions by imposing that $\mathcal{C}^{\rm V}_{ie} = 0$[3]. It is important at this point to emphasize the difference between simply allowing the presence of NP in both muons and electrons or allowing for LFU and LFUV-NP contributions. The case of simply allowing NP in the electron channel has been discussed quite extensively in Refs. [208, 216] (see also Refs. [217, 218] for a smaller subset of scenarios with and without including low-recoil observables), but no further

[3]There is no loss of generality here, since this term can always be absorbed in such a way that $\mathcal{C}^{\rm V}_{i\mu}$ can be interpreted as the difference of NP contributions to muons and electrons.

structure emerged from these analyses. On the contrary, our approach provides a concrete NP structure, namely, that the $b \to s\ell\ell$ transitions get a common Lepton Flavour Universal (LFU) NP contribution for all charged leptons (electrons, muons and tau leptons), opening new ideas for model building and extending the possible interpretations of our global fits. Performing fits with this new setting [197], we recovered our previous results in Ref. [136] but also obtained new scenarios different from Refs. [208, 216–218]. This can be seen by translating LFU and LFUV contributions into NP contributions to muons and electrons (leaving τ aside at this stage)

$$\mathcal{C}_{9\mu}^{\rm NP} = \mathcal{C}_{9\mu}^{\rm V} + \mathcal{C}_{9}^{\rm U}\,, \quad \mathcal{C}_{10\mu}^{\rm NP} = \mathcal{C}_{10\mu}^{\rm V} + \mathcal{C}_{10}^{\rm U}, \quad \mathcal{C}_{9e}^{\rm NP} = \mathcal{C}_{9}^{\rm U}\,, \quad \mathcal{C}_{10e}^{\rm NP} = \mathcal{C}_{10}^{\rm U}\,. \tag{8.2.9}$$

This seemingly innocuous redefinition yields interesting consequences, as it provides new perspectives to explain with different mechanisms the anomalies coming purely from the muon sector (like $\langle P_5'\rangle_{[4,6]}$) and the ones describing the violation of lepton flavour universality (like $\langle R_K\rangle_{[1.1,6]}$). It is important to stress that this approach is different from all the analyses including NP in electrons [208, 216–219] where the muonic NP contribution is not correlated in any way with the electronic one.

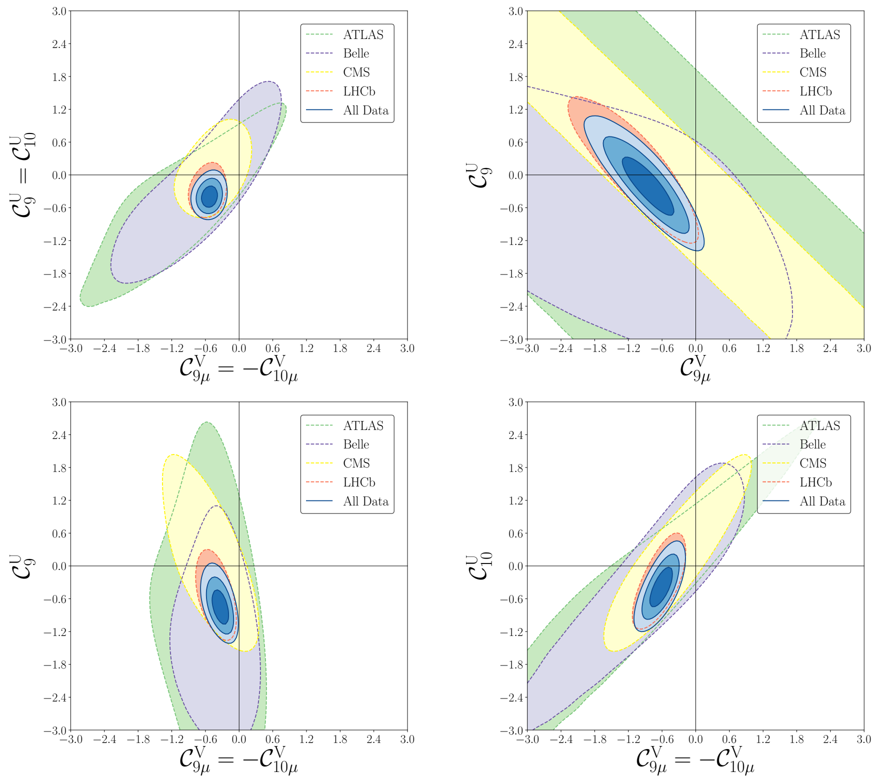

Figure 8.3: Updated plots of Ref. [211] corresponding to Scenarios 6,7,8 and the new Scenario 9.

In this section, we will discuss the update of the results in [211] with the new data made available since then. Furthermore, motivated by the results of the previous section, we extend the aforementioned analysis by allowing for LFUV and LFU-NP solutions with RHC, with particular emphasis on scenarios that could be easily obtained in NP models (see Section 8.3 for a discussion on the model-building implications). New fit results within this framework can be found in Table 8.4.

With the updated experimental inputs, we confirm our earlier observation [211] that a LFUV left-handed lepton coupling structure (corresponding to $\mathcal{C}_9^{\rm V} = -\mathcal{C}_{10}^{\rm V}$ and preferred from a model-building point of view) yields a better description of data with the addition of LFU-NP in the coefficients $\mathcal{C}_{9,10}$, as shown by scenarios 6 and 8 in Tab. 8.4 with p-values larger than 70%. On the other hand, we note a very slight decrease in significance for the scenarios 5–7, with the exception of scenario 8 which exhibits one of the most significant pulls with respect to the SM. The comparison of scenarios 10 and 12 illustrates that $\mathcal{C}^{\mathrm{V}}_{9\mu}$ plays an important role in LFU-NP scenarios and cannot be swapped for its chirally-flipped counterpart without consequences.

Finally, updated plots of the 2D LFU-LFUV scenarios discussed in Ref. [211] are shown in Fig. 8.3, with the allowed regions for the newly proposed LFU scenarios also being displayed in Fig. 8.4.

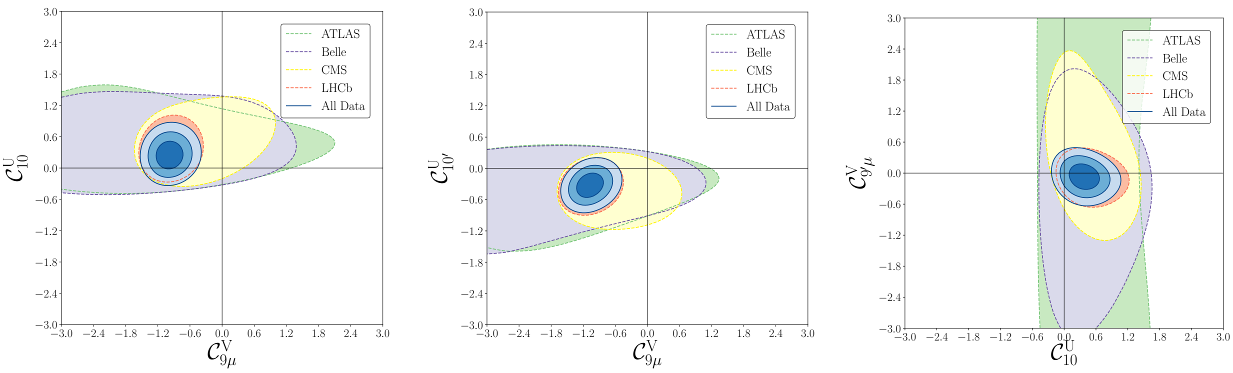

Figure 8.4: Updated plots of Ref. [211] corresponding to the new Scenarios 10,11,12.

8.2.3 Correlations among fit parameters

In addition to confidence intervals and regions, we provide the correlation matrices for the most interesting NP scenarios considered in our fits.

Correlation Matrices of Fits to LFUV-NP

First, we present the correlations between fit parameters of the NP scenarios defined in Tab. II and Tab. III. These are all NP solutions whose parameters assess LFUV-NP. By order of appearance in Tab. II, the correlations between the coefficients of all 2D scenarios with $\mathrm{Pull}_{\mathrm{SM}} \gtrsim 5.3\sigma$ are,

$$\mathrm{Corr}(\mathcal{C}^{\mathrm{NP}}_{9\mu}, \mathcal{C}^{\mathrm{NP}}_{10\mu}) = \begin{pmatrix} 1.00 & 0.30 \\ 0.30 & 1.00 \end{pmatrix}$$

$$\mathrm{Corr}(\mathcal{C}^{\mathrm{NP}}_{9\mu}, \mathcal{C}_{9'\mu}) = \begin{pmatrix} 1.00 & -0.39 \\ -0.39 & 1.00 \end{pmatrix}$$

$$\mathrm{Corr}(\mathcal{C}^{\mathrm{NP}}_{9\mu}, \mathcal{C}_{10'\mu}) = \begin{pmatrix} 1.00 & 0.33 \\ 0.33 & 1.00 \end{pmatrix}$$

$$\mathrm{Corr}(\mathcal{C}^{\mathrm{NP}}_{9\mu}, \mathcal{C}^{\mathrm{NP}}_{9e}) = \begin{pmatrix} 1.00 & 0.51 \\ 0.51 & 1.00 \end{pmatrix}$$

$$\mathrm{Corr}(\mathcal{C}^{\mathrm{NP}}_{9\mu} = -\mathcal{C}_{9'\mu}, \mathcal{C}^{\mathrm{NP}}_{10\mu} = \mathcal{C}_{10'\mu}) = \begin{pmatrix} 1.00 & -0.17 \\ -0.17 & 1.00 \end{pmatrix}$$

$$\mathrm{Corr}(\mathcal{C}_{9\mu}^{\mathrm{NP}}, \mathcal{C}_{9'\mu} = -\mathcal{C}_{10'\mu}) = \begin{pmatrix} 1.00 & -0.34 \\ -0.34 & 1.00 \end{pmatrix}$$

The last two matrices correspond to Hyp. 1 and Hyp. 5 as defined in Tab. II. Despite the high $\mathrm{Pull}_{\mathrm{SM}}$ of the 2D scenario $\{\mathcal{C}_{9\mu}^{\mathrm{NP}}, \mathcal{C}_{7'}\}$ (5.4σ), its correlation matrix is not collected here due to the central value of $\mathcal{C}_{7'}$ being negligible, with small errors.

Regarding the 6D fit of Tab. III,

$$\mathrm{Corr}_{6\mathrm{D}} = \begin{pmatrix} 1.00 & -0.34 & -0.07 & 0.06 & 0.02 & -0.03 \\ -0.34 & 1.00 & 0.24 & -0.06 & 0.04 & 0.24 \\ -0.07 & 0.24 & 1.00 & -0.13 & 0.61 & 0.59 \\ 0.06 & -0.06 & -0.13 & 1.00 & -0.13 & -0.08 \\ 0.02 & 0.04 & 0.61 & -0.13 & 1.00 & 0.85 \\ -0.03 & 0.24 & 0.59 & -0.08 & 0.85 & 1.00 \end{pmatrix}$$

where the columns are ordered as $\{\mathcal{C}_7^{\mathrm{NP}}, \mathcal{C}_{9\mu}^{\mathrm{NP}}, \mathcal{C}_{10\mu}^{\mathrm{NP}}, \mathcal{C}_{7'}, \mathcal{C}_{9'\mu}, \mathcal{C}_{10'\mu}\}$.

Interesting information can be extracted from $\mathrm{Corr}_{6\mathrm{D}}$. Most of the coefficients do not show particularly strong correlations with the others except for the pairs $\{\mathcal{C}_{10\mu}^{\mathrm{NP}}, \mathcal{C}_{9'\mu}\}$, $\{\mathcal{C}_{10\mu}^{\mathrm{NP}}, \mathcal{C}_{10'\mu}\}$ and $\{\mathcal{C}_{9'\mu}, \mathcal{C}_{10'\mu}\}$, being the latter the highest in correlation. While $\mathcal{C}_{9\mu}^{\mathrm{NP}}$ and $\mathcal{C}_{9'\mu}$ show a non-negligible correlation in the fit to these coefficients only, in the 6D fit the aforementioned parameters are uncorrelated to a large extent. On the contrary, the correlation between $\mathcal{C}_{9\mu}^{\mathrm{NP}}$ and $\mathcal{C}_{10\mu}^{\mathrm{NP}}$ is very similar for both the global 6D and the 2D fit to these parameters alone.

Correlation Matrices of Fits to LFUV-LFU NP

Second, the correlations between fit parameters of scenarios with both LFUV and LFU-NP have also been considered. Below one can find the correlation matrices of scenarios 5 to 11, in that order.

$$\mathrm{Corr}(\mathcal{C}_{9\mu}^{\mathrm{V}}, \mathcal{C}_9^{\mathrm{U}} = \mathcal{C}_{10}^{\mathrm{U}}, \mathcal{C}_{10\mu}^{\mathrm{V}}) = \begin{pmatrix} 1.00 & -0.93 & 0.91 \\ -0.93 & 1.00 & -0.94 \\ 0.91 & -0.94 & 1.00 \end{pmatrix}$$

$$\mathrm{Corr}(\mathcal{C}_{9\mu}^{\mathrm{V}} = -\mathcal{C}_{10\mu}^{\mathrm{V}}, \mathcal{C}_9^{\mathrm{U}} = \mathcal{C}_{10}^{\mathrm{U}}) = \begin{pmatrix} 1.00 & 0.17 \\ 0.17 & 1.00 \end{pmatrix}$$

$$\mathrm{Corr}(\mathcal{C}_{9\mu}^{\mathrm{V}}, \mathcal{C}_9^{\mathrm{U}}) = \begin{pmatrix} 1.00 & -0.85 \\ -0.85 & 1.00 \end{pmatrix}$$

$$\mathrm{Corr}(\mathcal{C}_{9\mu}^{\mathrm{V}} = -\mathcal{C}_{10\mu}^{\mathrm{V}}, \mathcal{C}_9^{\mathrm{U}}) = \begin{pmatrix} 1.00 & -0.44 \\ -0.44 & 1.00 \end{pmatrix}$$

$$\mathrm{Corr}(\mathcal{C}_{9\mu}^{\mathrm{V}} = -\mathcal{C}_{10\mu}^{\mathrm{V}}, \mathcal{C}_{10}^{\mathrm{U}}) = \begin{pmatrix} 1.00 & 0.69 \\ 0.69 & 1.00 \end{pmatrix}$$

$$\mathrm{Corr}(\mathcal{C}_{9\mu}^{\mathrm{V}}, \mathcal{C}_{10}^{\mathrm{U}}) = \begin{pmatrix} 1.00 & 0.05 \\ 0.05 & 1.00 \end{pmatrix}$$

$$\mathrm{Corr}(\mathcal{C}_{9\mu}^{\mathrm{V}}, \mathcal{C}_{10'}^{\mathrm{U}}) = \begin{pmatrix} 1.00 & 0.20 \\ 0.20 & 1.00 \end{pmatrix}$$

No significant changes can be observed when comparing with the results in App. 2 of Ref. [211]. As expected, $\mathcal{C}_{9\mu}^{\rm V}$ and $\mathcal{C}_{9}^{\rm U}$ are highly anti-correlated, with its nominal value somewhat smaller than in [211]. Fit estimates of the parameters in scenario $\{\mathcal{C}_{9\mu}^{\rm V} = -\mathcal{C}_{10\mu}^{\rm V}, \mathcal{C}_{9}^{\rm U} = \mathcal{C}_{10}^{\rm U}\}$ are now slightly correlated, while before their correlation was negligible. Interestingly, however, we find the parameters of the new scenario $\{\mathcal{C}_{9\mu}^{\rm V}, \mathcal{C}_{10}^{\rm U}\}$ statistically independent to a large extent.

8.3 Implications for models

Our most updated model-independent fits to available $b \to s\ell\ell$ and $b \to s\gamma$ data in Ref. [197] strongly favour several patterns of NP, with either purely LFUV or LFU and LFUV signatures. As it was already identified in previous analyses [113, 115, 136], the strongest signal of NP takes the form of an LFUV contribution to the coefficient $\mathcal{C}_9$ affecting mainly $b \to s\mu\mu$ transitions. However, more complex NP solutions with additional structures, involving either LFU types of NP or RHC, seem to emerge from the most recent data. This has important implications for some popular ultraviolet-complete models which we briefly discuss.

- **LFUV**: Given that leptoquarks (LQs) should posses very small couplings to electrons in order to avoid dangerous effects in $\mu \to e\gamma$, they naturally violate LFU. While Z' models can easily accommodate LFUV data [220], variants based on the assumption of LFU [221, 222] are now disfavoured. The same is true if one aims at explaining P_5' via NP in four-quark operators leading to a NP (q^2-dependent) contribution from charm loops [223].

- $\boldsymbol{\mathcal{C}_{9\mu}^{\rm NP}}$: Z' models with fundamental (gauge) couplings to leptons preferably yield $\mathcal{C}_{9\mu}^{\rm NP}$-like solutions in order to avoid gauge anomalies. In this context, $L_\mu - L_\tau$ models [224–227] are popular since they do not generate effects in electron channels. The new fit including R_{K^*} is also very favourable to models predicting $\mathcal{C}_{9\mu}^{\rm NP} = -3\mathcal{C}_{9e}^{\rm NP}$ [228]. Interestingly, such a symmetry pattern is in good agreement with the structure of the PMNS matrix. Concerning LQs, a $\mathcal{C}_{9\mu}^{\rm NP}$-like solution can only be generated by adding two scalar (an $SU(2)_L$ triplet and an $SU(2)_L$ doublet with $Y = 7/6$) or two vector representations (an $SU(2)_L$ singlet with $Y = 2/3$ and an $SU(2)_L$ doublet with $Y = 5/6$).

- $\boldsymbol{\mathcal{C}_{9\mu}^{\rm NP} = -\mathcal{C}_{10\mu}^{\rm NP}}$: This pattern can be achieved in Z' models with loop-induced couplings [229] or in Z' models with heavy vector-like fermions [180, 230] which posses also LFUV. Concerning LQs, here a single representation (the scalar $SU(2)_L$ triplet or the vector $SU(2)_L$ singlet with $Y = 2/3$) can generate a $\mathcal{C}_{9\mu} = -\mathcal{C}_{10\mu}$ like solution [231–237] and this pattern can also be obtained in models with loop contributions from three heavy new scalars and fermions [238–240]. Composite Higgs models are also able to achieve this pattern of deviations [241].

- **RHC:** with an R_K value closer to one, scenarios with right-handed currents, namely $\mathcal{C}_{9\mu}^{\rm NP} = -\mathcal{C}_{9'\mu}$, $(\mathcal{C}_{9\mu}^{\rm NP}, \mathcal{C}_{9'\mu})$ and $(\mathcal{C}_{9\mu}^{\rm NP}, \mathcal{C}_{10'\mu})$, seem to emerge. The first two scenarios are naturally generated in Z' models with certain assumptions on its couplings to right-handed and left-handed quarks, as it was shown in Ref. [224] within the context of a gauged $L_\mu - L_\tau$ symmetry with vector-like quarks. One could also obtain $\mathcal{C}_{9\mu}^{\rm NP} = -\mathcal{C}_{9'\mu}$ by adding a third Higgs doublet to the model of Ref. [226] with opposite $U(1)$ charge. On the other hand, generating the aforementioned contribution in LQ models requires one to add four scalar representations or three vector ones.

- $\boldsymbol{\mathcal{C}^{\mathrm{V}}_{9\mu} = -\mathcal{C}^{\mathrm{V}}_{10\mu}}$ **&** $\boldsymbol{\mathcal{C}^{\mathrm{U}}_{9}}$: Scenario 8 of Ref. [211] can be realized via off-shell photon penguins [242] in a leptoquark model explaining also $b \to c\tau\nu$ data (we will return to this point below).

- $\boldsymbol{\mathcal{C}^{\mathrm{U}}_{10(\prime)}}$: The new scenarios 9–13 are characterized by a $\mathcal{C}^{\mathrm{U}}_{10(\prime)}$ contribution. This arises naturally in models with modified Z couplings (to a good approximation $\mathcal{C}^{\mathrm{U}}_{9(\prime)}$ can be neglected). The pattern of scenario 9 occurs in Two-Higgs-Doublet models where this flavour universal effect can be supplemented by a $\mathcal{C}^{\mathrm{V}}_{9} = -\mathcal{C}^{\mathrm{V}}_{10}$ effect [213].

- **More LFU-LFUV:** In case of scenarios 11 to 13, one can invoke models with vector-like quarks where modified Z couplings are even induced at tree level. The LFU effect in $\mathcal{C}^{\mathrm{U}}_{10(\prime)}$ can be accompanied by a $\mathcal{C}^{\mathrm{V}}_{9,10(\prime)}$ effect from Z' exchanges [214]. Vector-like quarks with the quantum numbers of right-handed down quarks (left-handed quarks doublets) generate effects in $\mathcal{C}^{\mathrm{U}}_{10}$ and $\mathcal{C}^{\mathrm{V}}_{9'}$ ($\mathcal{C}^{\mathrm{U}}_{10(\prime)}$ and $\mathcal{C}^{\mathrm{V}}_{9}$) for a Z' boson with vector couplings to muons [214].

Concerning Hyps. 1 to 5 of Tab. 8.2, only two of them (2 and 4) can be explained within a Z' model, while hypotheses 1 and 3 violate the relationship $\mathcal{C}^{\mathrm{NP}}_{9\mu} \times \mathcal{C}_{10'\mu} = \mathcal{C}^{\mathrm{NP}}_{10\mu} \times \mathcal{C}_{9'\mu}$ [113] that minimal Z' models should obey. One would have to turn to other models (like LQs with a sufficient number of representations) to explain the hypothesis with the highest pull (Hyp. 1).

8.3.1 Model-independent connection to $b \to c\ell\nu$

We close our discussion of models by commenting on the model-independent connection between the anomalies in $b \to s\ell\ell$ neutral currents and those in $b \to c\tau\nu$ charged currents (i.e. R_D and R_{D^*}), which are now at the 3.1σ level [243]. Such a connection, however, requires further hypotheses. A solution of the $R_{D^{(*)}}$ anomaly can naturally be achieved with a NP contribution to the SM operator $(\bar{c}\gamma^{\mu}P_L b)(\bar{\tau}\gamma_{\mu}P_L\nu)$, as it complies with the B_c lifetime [244] and q^2 distributions [245–247]. Assuming $SU(2)$ invariance, the effect in $R_{D^{(*)}}$ is correlated to $b \to s\ell\ell$ and/or to $b \to s\nu\bar{\nu}$, following the pattern $\mathcal{C}_{9\mu} = -\mathcal{C}_{10\mu}$. From model-independent arguments, $b \to s\tau\tau$ must then be significantly enhanced, as we will discuss at length in Chapter 9. Indeed, since $b \to c\ell\nu$ processes are mediated already at tree level in the SM, one needs large NP contributions in order to explain the anomalies in R_D and R_{D^*}. In principle, these large NP effects would also generate large contributions to $b \to s\nu\bar{\nu}$ processes, due to $SU(2)$ invariance, however contributions to this channel are strongly constrained by $B \to K^{(*)}\nu\bar{\nu}$. A possible way to bypass this problem is to impose a coupling structure that is mainly aligned to the third generation, but this disagrees with direct LHC searches [248] and electroweak precision observables [249]. Another alternative, which yields no effects in $b \to s\nu\bar{\nu}$ processes, arises from the Standard Model Effective Theory (SMEFT) scenario where $\mathcal{C}^{(1)} = \mathcal{C}^{(3)}$ expressed in terms of gauge-invariant dimension-6 operators [3, 250, 251]. The operator involving-third generation leptons explains $R_{D^{(*)}}$ and the one involving the second generation gives a LFUV effect in $b \to s\mu\mu$ processes. Form a model-building perspective, this scenario stems naturally from models with an $SU(2)$ singlet vector LQ [234, 235, 252] or with a combination of two scalar LQs [253]. Both the two aforementioned models are predicted to induce large effects in $b \to s\tau\tau$ (of the order of 10^{-3} for $B_s \to \tau^+\tau^-$) [253, 254].

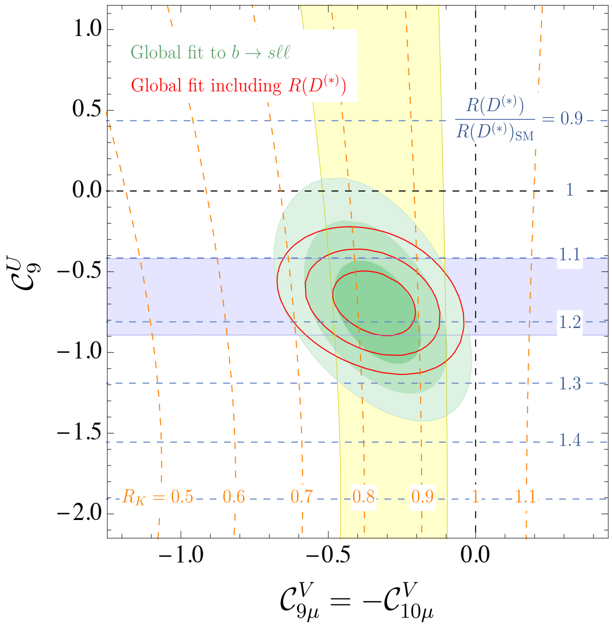

Figure 8.5: Preferred regions at the 1, 2 and 3σ level (green) in the ($\mathcal{C}_{9\mu}^{\rm V} = -\mathcal{C}_{10\mu}^{\rm V}$, $\mathcal{C}_9^{\rm U}$) plane from $b \to s\ell^+\ell^-$ data. The red contour lines show the corresponding regions once $R_{D^{(*)}}$ is included in the fit (for $\Lambda = 2$ TeV). The horizontal blue (vertical yellow) band is consistent with $R_{D^{(*)}}$ (R_K) at the 2$\,\sigma$ level and the contour lines show the predicted values for these ratios.

Assuming that the coupling to the second generation is sizeable in order to avoid the bounds from direct LHC searches and electroweak precision observables one finds

$$\mathcal{C}_{9(10)\tau} \approx \mathcal{C}_{9(10)}^{SM} - (+)2\frac{\pi}{\alpha}\frac{V_{cb}}{V_{ts}^*}\left(\sqrt{\frac{R_{D^{(*)}}}{R_{D^{(*)}}^{\rm SM}}} - 1\right) . \tag{8.3.1}$$

Notice that our discussion above, implicitly assumes LFUV-NP contributions to $b \to s\mu\mu$, as we only consider effects modifying the muonic Wilson coefficients through $\mathcal{C}_{9\mu} = -\mathcal{C}_{10\mu}$. However, the same SMEFT $\mathcal{C}^{(1)} = \mathcal{C}^{(3)}$ scenario also provides an interpretation of Scenario 8 in Table 8.4, based on both LFU and LFUV types of NP, that jointly accounts for the anomalies in $b \to s\mu\mu$ and $b \to c\tau\nu$. As we mentioned, the constraint from $b \to c\tau\nu$ and $SU(2)$ invariance generally leads to large contributions to the operator $(\bar{s}\gamma^\mu P_L b)\,(\bar{\tau}\gamma_\mu P_L \tau)$, which enhances $b \to s\tau\tau$ processes (see Chapter 9), but also mixes into $\mathcal{O}_9$ and generates $\mathcal{C}_9^{\rm U}$ at $\mu = m_b$ [242]. Note that not all models addressing the charged and neutral current anomalies simultaneously have an anarchic flavour structure. In fact, in the case of alignment in the down-sector [255, 256] one does not find large effects in $b \to s\tau\tau$ or $\mathcal{C}_9^{\rm U}$.

Therefore, Scenario 8 is reproduced in this setup with an additional correlation between $\mathcal{C}_9^{\rm U}$ and $R_{D^{(*)}}$. Assuming a generic flavour structure so that small CKM elements can be neglected [3, 242], we get

$$\mathcal{C}_9^{\rm U} \approx 7.5\left(1 - \sqrt{\frac{R_{D^{(*)}}}{R_{D^{(*)}\rm SM}}}\right)\left(1 + \frac{\log(\Lambda^2/(1{\rm TeV}^2))}{10.5}\right) . \tag{8.3.2}$$

Realizations of this scenario in specific NP models also usually yield an effect in $\mathcal{C}_7$ [242]. However, since this effect is model dependent (and in fact small in some UV complete models [257, 258]), we neglect it here, leading to the plot in Fig. 8.5, where we include the recent update of Ref. [259] to draw the band for $R_{D^{(*)}}$. Note that this scenario has a pull of 7.0σ due to the inclusion of $R_{D^{(*)}}$, which increases our $\Delta\chi^2$ by ~ 20.

In addition to the above-mentioned effects, in LQ models able to generate the effects described one expects sizeable branching ratios for $b \to s\tau\mu$ processes, reaching the level of 10^{-5} [253].

8.4 Inner tensions of the global fit

In Section 8.2, we have seen that different NP scenarios involving $\mathcal{C}_{9\mu}^{\rm NP}$ (or its LFU-LFUV variant $\mathcal{C}_{9\mu}^{\rm V}$) lead to a much better description of the data than the SM, with fits reaching p-values around 60-80% (the SM being around 10%) and providing pulls with respect to the SM above 5σ. The overall agreement is thus already very good within these NP scenarios and from a purely statistical point of view, it should be expected that these fits exhibit slight tensions. It is however interesting to look at these remaining tensions in more detail in order to determine where statistical fluctuations may be reduced with more data or where improved measurements might help to lift the degeneracy among NP scenarios. We focus on three main tensions that we consider particularly relevant in the current global fit.

8.4.1 R_{K^*} in the first bin

A first tension related to R_{K^*} occurs in the global fit and it proves interesting to consider both R_{K^*} and $\mathcal{B}(B \to K^*\mu^+\mu^-)$ as measured by LHCb in order to understand its nature (see Fig. 8.6).

Let us first consider the second bin (from 1 to 6 GeV^2) for R_{K^*}. Even though the deficit could be consistent with an excess in the electron channel with respect to the muon one, the study of the corresponding bins of $\mathcal{B}(B \to K^*\mu^+\mu^-)$ points towards a deficit of muons. The mechanism that explains the deviation with respect to the SM in the long second bin of R_{K^*} is consistent with all the deviations that have been observed in other channels and different invariant di-lepton mass square regions.

The situation is different for the first bin of R_{K^*}, where $\mathcal{B}(B \to K^*\mu^+\mu^-)$ is clearly compatible with the SM (see Fig. 8.6). An excess in the electron channel would then be needed in order to explain the observed deficit in $\langle R_{K^*}\rangle_{[1.1,6]}$. This difference of mechanism between the first and the second bins of R_{K^*} can be understood in two ways: i) a specific NP effect [260, 261] localised at very low q^2 and able to compete with the dominant Wilson coefficient $\mathcal{C}_7$ (well determined to be in agreement with the SM expectations from $\mathcal{B}(B \to X_s\gamma)$) [85, 92, 131, 136, 197, 262]; ii) some experimental issue in measuring di-electron pairs at very small invariant mass, close to the photon pole. It would be very interesting that LHCb keep on their efforts to understand the systematics in this bin. Interestingly the recent Belle measurement [195] indicates also a low central value in the same bin, even though the large uncertainty affecting the measurement prevents us from drawing any definite conclusion and makes it compatible also with the SM.

Another approach to slightly reduce the tension between data and SM in the first bin of R_{K^*} through a NP explanation consists in including NP contributions to the $b \to see$ channel, in particular, considering right-handed currents affecting electrons, as discussed in Ref. [219]. In the scenarios S8-S11 (using the notation of Ref. [219]) the prediction of $\langle R_{K^*}\rangle_{[0.045,1.1]}$ is found to be within $\sim 1\sigma$ range of the current measurement. This could open a new window to explore the existence of right-handed currents and to explain some of the tensions found, even though more

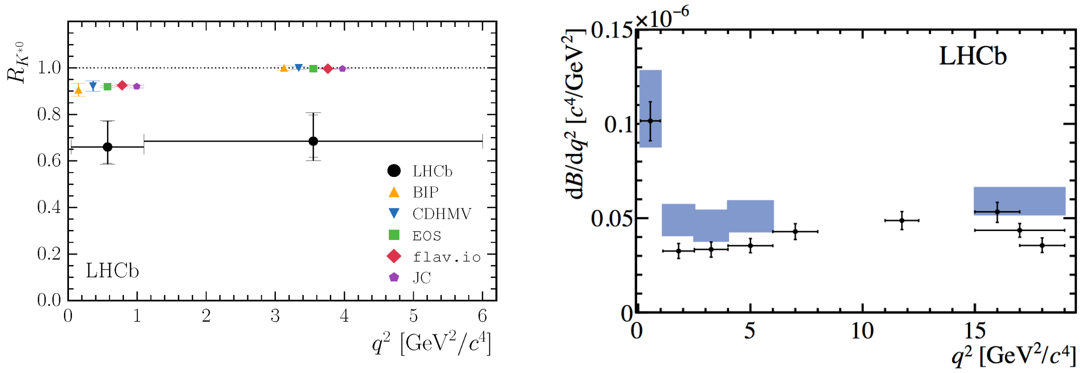

Figure 8.6: R_{K^*} (left panel) and $\mathcal{B}(B \to K^* \mu^+\mu^-)$ (right panel) measured by LHCb. Figures extracted from Refs. [191] and [190] respectively.

data is required in order to be conclusive.

8.4.2 $B_s \to \phi\mu^+\mu^-$ versus $B \to K^*\mu^+\mu^-$

Another tension in the fit concerns the branching ratio for $B_s \to \phi\mu^+\mu^-$, in particular when compared with the related decay $B \to K^*\mu^+\mu^-$.

The prediction for the branching ratio $\mathcal{B}(B \to K^*\mu^+\mu^-)$ involves hadronic form factors to be determined using different theoretical approaches, depending on the di-lepton invariant mass region analysed: at large recoil, one can use light-cone sum-rules based on light-meson distribution amplitudes [150], while lattice form factors are available at low recoil. Due to the difficulty to assess precisely the uncertainties attached to light-cone sum rules, we perform our computations using the more conservative framework described in Chapter 6. We checked that our results are compatible with those obtained in Ref. [150] and that the two approaches yield very similar results for the fits [113, 136, 263, 264].

Contrary to the case of $\mathcal{B}(B \to K^*\mu^+\mu^-)$, there are no computations available using the B-meson light cone sum rules of Refs. [148, 149] for $B_s \to \phi\mu^+\mu^-$, and one must rely on the estimates given in Ref. [150]. One can see in Fig. 8.7 that at low recoil, where lattice form factors are used, the prediction for $\mathcal{B}(B \to K^*\mu^+\mu^-)$ is expected to be slightly larger than $\mathcal{B}(B_s \to \phi\mu^+\mu^-)$ and indeed data (with large error bars) follows the same trend. On the contrary, in the large-recoil region where the light-cone sum rules results of Ref. [150] are used, the SM predictions lead to a larger value for $\mathcal{B}(B_s \to \phi\mu^+\mu^-)$ than for $\mathcal{B}(B \to K^*\mu^+\mu^-)$. Surprisingly, data shows the opposite trend, which may come from a statistical fluctuation of the data leading to an inversion of the experimental measurements of both modes at large recoil. Alternatively, this issue may signal a problem in the theoretical prediction of the form factors of Ref. [150]. Firstly, these predictions are obtained by combining results in different kinematic regions (light-cone sum rules and lattice QCD) which do not fully agree with each other when they are extrapolated: the fit to a common parametrisation over the whole kinematic space leads to a fit with uncertainties that may be artificially small due to these incompatibilities of the inputs. Moreover, the choice of the z parametrisation [148, 150] used to describe the form factors over the whole kinematic range has interesting properties of convergence, but it may in some cases lead to potential unitarity violations [265].

Finally, another issue that specifically affects $\mathcal{B}(B_s \to \phi\mu^+\mu^-)$ is the B_s-$\bar{B}_s$ mixing. As we

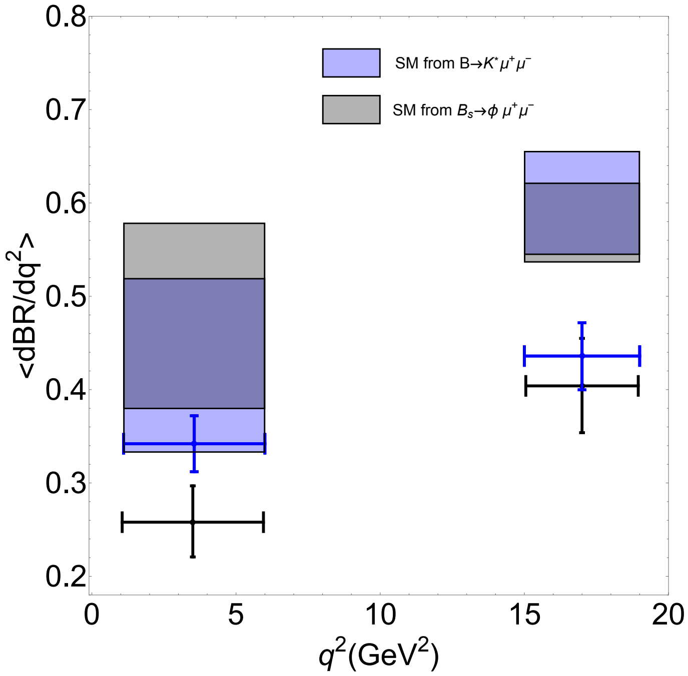

Figure 8.7: Theoretical predictions for $\mathcal{B}(B_s \to \phi\mu^+\mu^-)$ and $\mathcal{B}(B \to K^*\mu^+\mu^-)$ within the SM along with their corresponding experimental measurement. The results at large recoil are presented here only for illustrative purposes and are based on the form factors presented in Ref. [150] (these results are not used in our global analyses). The results at low recoil are indeed used in Ref. [113] and are based on available lattice QCD inputs for the form factors.

discussed in Section 5.2, the neat effect of the evolution between the two mass states on the time-integrated branching ratio is a correction of $O(\Delta\Gamma_s/\Gamma_s)$ in the relation between its theoretical computation and its measurement at LHCb [122, 266–268]. This effect is taken into account in the global fit [113] as an additional source of uncertainty for the theoretical estimate of the branching ratios.

The experimental efficiencies should also be corrected for this effect, which depend on the CP-asymmetry $A_{\Delta\Gamma}$ that can also be affected by NP contributions. It should thus be kept free within a large range in the absence of measurements. Neglecting this effect and assuming a SM value for this asymmetry may lead to an underestimation of some systematics on the efficiencies. For instance, Ref. [269] showed that this issue can lead to an additional systematic effect of 10% in the $B_s \to \mu^+\mu^-$ systematics. The impact on efficiencies from NP effects was indeed considered in Ref. [121] for $B_s \to \phi\mu^+\mu^-$ by varying $\mathcal{C}_{9\mu}$ in the underlying physics model used to compute signal efficiencies, leading to a much smaller effect in this case (of a few percent, in line with back-of-the-envelope estimates).

8.4.3 Tensions between large and low recoil in angular observables

We discuss for the first time here a rather different type of tension, concerning the $B \to K^*\mu^+\mu^-$ angular observables at large and low recoil. On the one hand, we observe that branching ratios exhibit the same discrepancy pattern between theory and experiment at low and large recoil [4]. On the other hand, the current deviations at LHCb in P_5' require NP contributions with opposite sign in the two kinematic regions. Indeed, the pull between the SM value and the LHCb experimental measurement in $\langle P_5' \rangle_{[15,19]}$ has the opposite sign (albeit the significance is only 1.2σ) w.r.t. its large-recoil bins, in particular $\langle P_5' \rangle_{[4,6]}$ and $\langle P_5' \rangle_{[6,8]}$. This very slight tension is not there in the case of the Belle data where same-sign deviations are observed, even though the error bars are rather large in this case.

For the purposes of illustration, let us consider the NP scenario where there is no LFU contribution and NP occurs only in $\mathcal{C}_{9\mu}^{\rm V}$ and $\mathcal{C}_{10\mu}^{\rm V}$. This is illustrated in Fig. 8.8 where the constraints for these observables (as well as other relevant observables that will be listed below) are shown at 68.3% (left) and 95% (right) CL. One can notice their milder sensitivity to $\mathcal{C}_{10\mu}^{\rm V}$. $\langle P_5' \rangle_{[4,6]}$ (blue region) would prefer a negative $\mathcal{C}_{9\mu}^{\rm V}$ while $\langle P_5' \rangle_{[15,19]}$ (green region) would favour a positive $\mathcal{C}_{9\mu}^{\rm V}$ at 68.3% CL.

Black dots indicate the particular solutions $(-1.02, 0)$ and $(-0.45, 0.45)$ corresponding to the best-fit points of the 1D scenarios $\mathcal{C}_{9\mu}^{\rm V}$ and $\mathcal{C}_{9\mu}^{\rm V} = -\mathcal{C}_{10\mu}^{\rm V}$ in Ref. [197], where 2017 data was used for our analyses. We also indicate the constraints from $\langle P_2 \rangle_{[4,6]}$, $\langle P_2 \rangle_{[15,19]}$, and $\langle R_K \rangle_{[1.1,6]}$ $\langle \mathcal{B}(B^0 \to K^{*0}\mu^+\mu^-) \rangle_{[15,19]}$ since we believe that they are representative of the set of observables driving our global fit [5]. The former pair of observables ($\langle P_2 \rangle_{[4,6]}$, $\langle P_2 \rangle_{[15,19]}$) has a large overlap region compatible with the SM while the latter one ($\langle R_K \rangle_{[1.1,6]}$, $\langle \mathcal{B}(B^0 \to K^{*0}\mu^+\mu^-) \rangle_{[15,19]}$) overlaps far from the SM point. While P_5' and R_K strongly constrain NP solutions, the P_2 bins are weakly constraining. Finally, the yellow region in the right panel in Fig. 8.8 is the overlap of the regions from the five observables obtained after considering the data regions at 95% CL.

In summary, an interesting tension between low- and large-recoil regions for P_5' is observed at the 2-sigma level, favouring $\mathcal{C}_{9\mu}$ contributions of different signs in the two kinematic regions. Although not statistically significant, this inner tension seems to require either different sources of NP or a shift in the data once more statistics is added.

8.5 Assessing the potential of R_K (and Q_5) to disentangle NP hypotheses

The goal of this final section is to scrutinize the results of the fit from a different perspective to prepare the next step, i.e. to discriminate the most relevant NP scenario among the ones already favoured, complementing the results of our global analyses. Currently, the most significant patterns identified exhibit a pull w.r.t. the SM very close to each other (within a range of half a σ). We explore strategies to disentangle different scenarios and to identify the impact of a more precise measurement of R_K. We then combine information on R_K and Q_5 in order to illustrate that R_K by itself will not be sufficient to disentangle clearly one or a small subset of scenarios, but that a combination of R_K and Q_5 can be useful, depending on the (future) measured value

More precisely, here we discuss the potential impact of prospective new measurements of $\langle R_K \rangle_{[1.1,6]}$ and $\langle Q_5 \rangle_{[1.1,6]}$ on the global fits in order to distinguish NP hypotheses. We perform the

[4] This is true for all $b \to s\ell\ell$ modes, apart from the decay $\Lambda_b^0 \to \Lambda\mu^+\mu^-$, where the experimental errors at low recoil are very large and the normalisation chosen prevents further interpretation [200, 270].

[5] P_1 and P_4' observables are known to behave in a more SM like way than the ones selected here, thus providing weaker constraints.

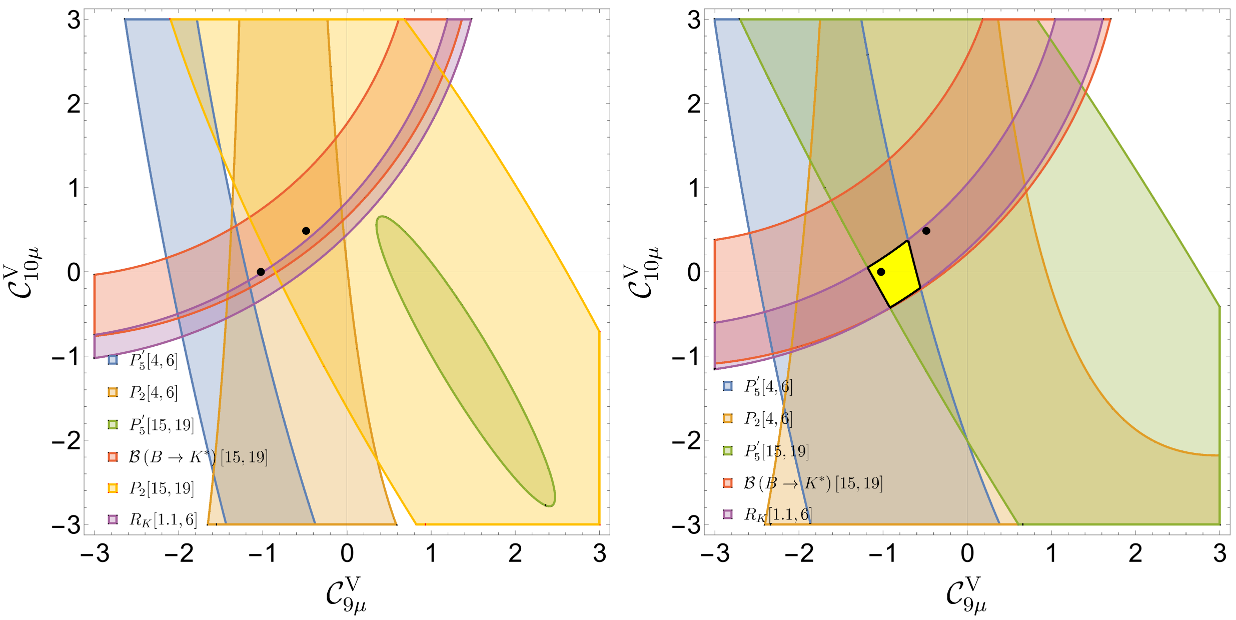

Figure 8.8: 68.3% (left) and 95% (right) CL solutions regions for the observables discussed in the main text in the $(\mathcal{C}^{\rm V}_{9\mu}, \mathcal{C}^{\rm V}_{10\mu})$ plane. The yellow region corresponds to the overlap region. $\langle P_2 \rangle_{[15,19]}$ is only shown in the left panel.

following illustrative exercise: we vary the experimental values of $\langle R_K \rangle_{[1.1,6]}$ and $\langle Q_5 \rangle_{[1.1,6]}$ within suitable ranges, and we perform fits according to these values taken as actual measurements. First only $\langle R_K \rangle_{[1.1,6]}$ is allowed to vary before we consider the combined impact of $\langle R_K \rangle_{[1.1,6]}$ and $\langle Q_5 \rangle_{[1.1,6]}$. The "pseudo-data" for $\langle R_K \rangle_{[1.1,6]}$ takes into account the expected increase in statistics soon available for this observable. For this exercise we assume a reduction by a factor $\sqrt{2}$ on the statistical error of $\langle R_K \rangle_{[1.1,6]}$ [194]. Indeed, according to the latter reference, this would amount to the inclusion of the data sets of 2017 and 2018 which are said to have the same statistical power as the combined data set of Run 1, 2015 and 2016.

For each fit (corresponding to a given hypothesis and set of data), both the pull of the hypothesis w.r.t. the SM (Pull_{SM}) and the best-fit-point (b.f.p) are computed, which we plot as functions of either $\langle R_K \rangle_{[1.1,6]}$ or $\langle Q_5 \rangle_{[1.1,6]}$. However, in this Thesis, we will only show plots of the Pull_{SM} for the different hypotheses considered with the value of the aforementioned observables, as this is the most relevant information. We refer the interested reader to our article in Ref. [212] for analogous plots for the b.f.p.s.

Before discussing the results of our analysis, we first state our assumptions:

- We follow the same approach described in Section 8.2 regarding the statistical framework and anatomy of our fits.

- We consider two different kinds of fits with different subsets of observables: on one side, the global fit (or Fit "All", as we called it above, to all available observables) and on the other one, the LFUV fit. When several experiments have measured the same observable, we do not average the results but we include all these measurements in the χ^2 taking into account their (theoretical) correlations.

- Any variation of the experimental value of $\langle R_K\rangle_{[1.1,6]}$ could manifest itself also in a change in the branching ratios $\mathcal{B}(B^+\to K^+\mu^+\mu^-)$ and/or $\mathcal{B}(B^+\to K^+e^+e^-)$. However, the update of $\langle R_K\rangle_{[1.1,6]}$ in Ref. [194] has not led to significant changes in these branching ratios, and we will assume that this will also occur in the forthcoming updates, so that we modify only the value of $\langle R_K\rangle_{[1.1,6]}$

- $\langle R_K\rangle_{[1.1,6]}$ is freely varied within a 2σ range from its current experimental value. It represents a good compromise between a high coverage of the true value and a span compatible with our computational means. $\langle Q_5\rangle_{[1.1,6]}$ is varied within the range $[-0.5, 1.0]$ in order to ensure that we scan over values corresponding to the most relevant NP scenarios (see Fig. 2 of Ref. [211]).

- With the increased statistics available at Run 2, it will be possible for experiments to provide more precise determinations of key observables. Therefore, besides the reduction in the error of $\langle R_K\rangle_{[1.1,6]}$, we assume a guesstimated uncertainty of order 0.1 for $\langle Q_5\rangle_{[1.1,6]}$.

In this study, we take the most relevant 1D and 2D scenarios with purely LFUV-NP contributions and also allowing for LFU-NP, as suggested by our global fits of Section 8.2. When translated from one language to the other, these scenarios become, for the purely LFUV cases:

$$\begin{array}{lrcl}
\text{[Hyp. I]} & \{\mathcal{C}^{\rm V}_{9\mu}\} & \to & \{\mathcal{C}^{\rm NP}_{9\mu}\} \\
\text{[Hyp. II]} & \{\mathcal{C}^{\rm V}_{9\mu}=-\mathcal{C}^{\rm V}_{10\mu}\} & \to & \{\mathcal{C}^{\rm NP}_{9\mu}=-\mathcal{C}^{\rm NP}_{10\mu}\} \\
\text{[Hyp. III]} & \{\mathcal{C}^{\rm V}_{9\mu}=-\mathcal{C}^{\rm V}_{9'\mu}\} & \to & \{\mathcal{C}^{\rm NP}_{9\mu}=-\mathcal{C}^{\rm NP}_{9'\mu}\} \\
\text{[Hyp. IV]} & \{\mathcal{C}^{\rm V}_{9\mu},\mathcal{C}^{\rm V}_{10\mu}\} & \to & \{\mathcal{C}^{\rm NP}_{9\mu},\mathcal{C}^{\rm NP}_{10\mu}\} \\
\text{[Hyp. V]} & \{\mathcal{C}^{\rm V}_{9\mu},\mathcal{C}^{\rm V}_{9'\mu}\} & \to & \{\mathcal{C}^{\rm NP}_{9\mu},\mathcal{C}^{\rm NP}_{9'\mu}\} \\
\text{[Hyp. VI]} & \{\mathcal{C}^{\rm V}_{9\mu},\mathcal{C}^{\rm V}_{10'\mu}\} & \to & \{\mathcal{C}^{\rm NP}_{9\mu},\mathcal{C}^{\rm NP}_{10'\mu}\} \\
\text{[Hyp. VII]} & \{\mathcal{C}^{\rm V}_{9\mu}=-\mathcal{C}^{\rm V}_{9'\mu},\mathcal{C}^{\rm V}_{10\mu}=\mathcal{C}^{\rm V}_{10'\mu}\} & \to & \{\mathcal{C}^{\rm NP}_{9\mu}=-\mathcal{C}_{9'\mu},\mathcal{C}^{\rm NP}_{10\mu}=\mathcal{C}_{10'\mu}\} \\
\text{[Hyp. VIII]} & \{\mathcal{C}^{\rm V}_{9\mu},\mathcal{C}^{\rm V}_{9'\mu}=-\mathcal{C}^{\rm V}_{10'\mu}\} & \to & \{\mathcal{C}^{\rm NP}_{9\mu},\mathcal{C}^{\rm NP}_{9'\mu}=-\mathcal{C}_{10'\mu}\}
\end{array} \tag{8.5.1}$$

and the scenarios allowing both LFUV and LFU contributions

$$\begin{array}{lrcl}
\text{[Hyp.IX]} & \{\mathcal{C}^{\rm V}_{9\mu}=-\mathcal{C}^{\rm V}_{10\mu},\mathcal{C}^{\rm U}_{9}=\mathcal{C}^{\rm U}_{10}\} & \to & \{\mathcal{C}^{\rm NP}_{9\mu}=-\mathcal{C}^{\rm NP}_{10\mu}+2\mathcal{C}^{\rm NP}_{9e},\mathcal{C}^{\rm NP}_{9e}=\mathcal{C}^{\rm NP}_{10e}\} \\
\text{[Hyp.X]} & \{\mathcal{C}^{\rm V}_{9\mu},\mathcal{C}^{\rm U}_{9}\} & \to & \{\mathcal{C}^{\rm NP}_{9\mu},\mathcal{C}^{\rm NP}_{9e}\} \\
\text{[Hyp.XI]} & \{\mathcal{C}^{\rm V}_{9\mu}=-\mathcal{C}^{\rm V}_{10\mu},\mathcal{C}^{\rm U}_{9}\} & \to & \{\mathcal{C}^{\rm NP}_{9\mu}=-\mathcal{C}^{\rm NP}_{10\mu}+\mathcal{C}^{\rm NP}_{9e},\mathcal{C}^{\rm NP}_{10\mu},\mathcal{C}^{\rm NP}_{9e}\} \\
\text{[Hyp.XII]} & \{\mathcal{C}^{\rm V}_{9\mu}=-\mathcal{C}^{\rm V}_{10\mu},\mathcal{C}^{\rm U}_{10}\} & \to & \{\mathcal{C}^{\rm NP}_{9\mu},\mathcal{C}^{\rm NP}_{10\mu}=-\mathcal{C}^{\rm NP}_{9\mu}+\mathcal{C}^{\rm NP}_{10e},\mathcal{C}^{\rm NP}_{10e}\} \\
\text{[Hyp.XIII]} & \{\mathcal{C}^{\rm V}_{9\mu},\mathcal{C}^{\rm U}_{10}\} & \to & \{\mathcal{C}^{\rm NP}_{9\mu},\mathcal{C}^{\rm NP}_{10\mu}=\mathcal{C}^{\rm NP}_{10e}\} \\
\text{[Hyp.XIV]} & \{\mathcal{C}^{\rm V}_{9\mu},\mathcal{C}^{\rm U}_{10'}\} & \to & \{\mathcal{C}^{\rm NP}_{9\mu},\mathcal{C}^{\rm NP}_{10'\mu}=\mathcal{C}^{\rm NP}_{10'e}\}
\end{array} \tag{8.5.2}$$

Hypotheses VII and VIII correspond to Hypotheses 1 and 5 first defined in Refs. [136]. Hypotheses IX to XIV correspond to Scenarios 6 to 11 in Ref. [211] (Scenarios 5 and 13 are also interesting in terms of their ability to explain the deviations observed, but they require three or four free parameters and will not be considered in the following).

The purpose of this analysis is not to provide precise determinations of the pull of the SM and the b.f.p.s for different values of $\langle R_K\rangle_{[1.1,6]}$ and $\langle Q_5\rangle_{[1.1,6]}$ but rather to gain qualitative knowledge on how experimental measurements of these two observables will drive the analyses.

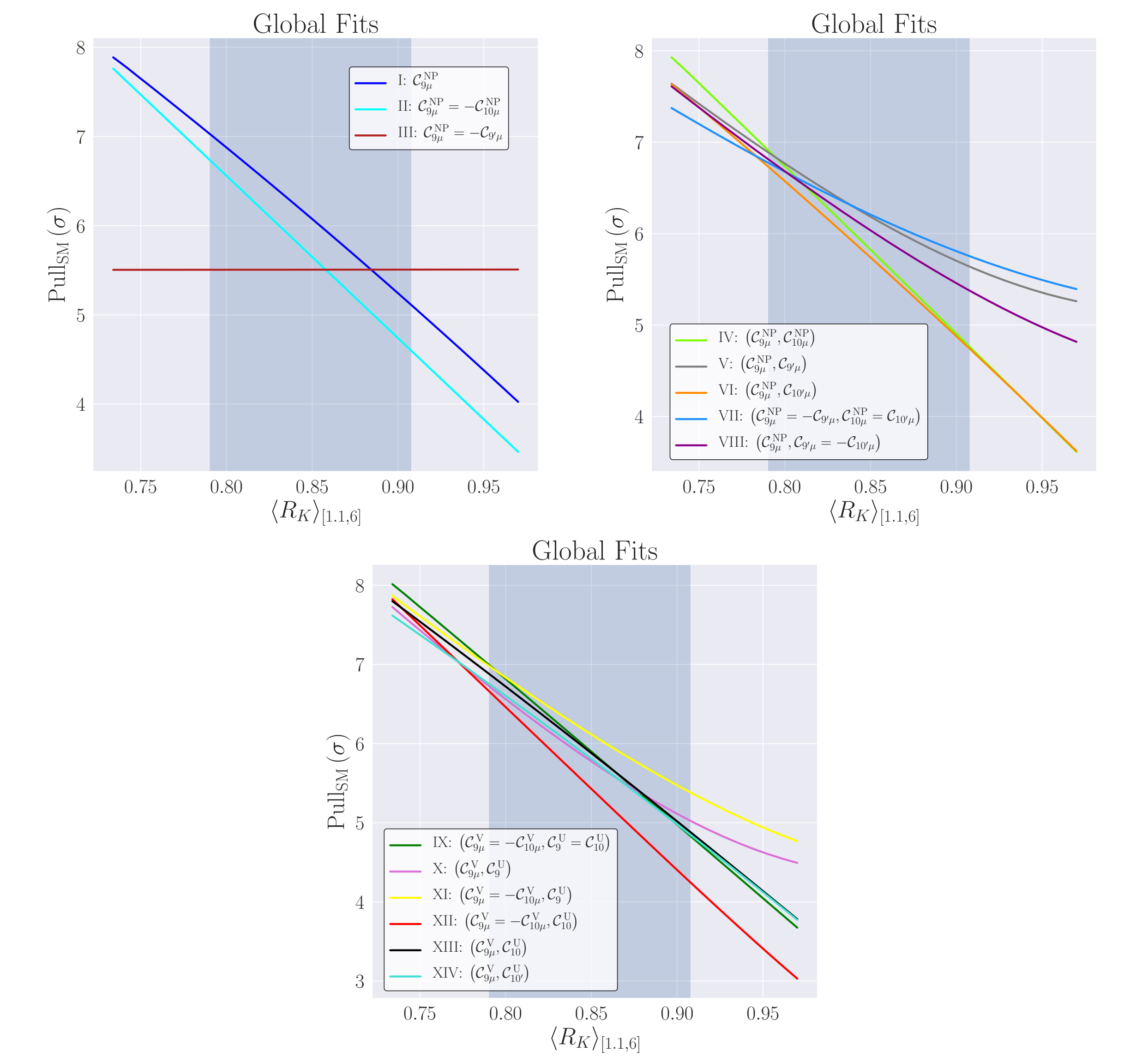

Figure 8.9: Global fit: Impact of the central value of $\langle R_K \rangle_{[1.1,6]}$ on the $\text{Pull}_{\rm SM}$ of the NP scenarios under consideration.

8.5.1 Global Fits

Figure 8.9 displays the outcome of the global fit (or fit "All", involving 178 observables) for the pulls with respect of the SM, assuming different experimental central values of $\langle R_K \rangle_{[1.1,6]}$ and different NP hypotheses varied according to the procedure described above. The shaded vertical band in the plots of Figures 8.9 highlights the current experimental 1σ confidence interval for the LHCb average of $\langle R_K \rangle_{[1.1,6]}$.

Figure 8.9 illustrates the relevance of $\langle R_K \rangle_{[1.1,6]}$ on the global fits. For all the NP scenarios considered, except for Hyp. III, $\mathcal{C}_{9\mu}^{\rm V} = -\mathcal{C}_{9'\mu}^{\rm V}$, we observe that their corresponding $\text{Pull}_{\rm SM}$ undergoes a $\sim 3-4\sigma$ variation from one end of the range of variation of $\langle R_K \rangle_{[1.1,6]}$ to the other. If we restrict the variation of $\langle R_K \rangle_{[1.1,6]}$ to only 1σ, one can see differences of $\sim 2\sigma$ between the two extremes, as expected from the linearity of $\text{Pull}_{\rm SM}$ on $\langle R_K \rangle_{[1.1,6]}$ seen in the plots.

The flatness of the $\text{Pull}_{\rm SM}$ under the hypothesis III, $\mathcal{C}_{9\mu}^{\rm V} = -\mathcal{C}_{9'\mu}^{\rm V}$, can be easily understood. The theoretical prediction of $\langle R_K \rangle_{[1.1,6]}$ is insensitive to the value of $\mathcal{C}_{9\mu}^{\rm V} = -\mathcal{C}_{9'\mu}^{\rm V}$, so that it remains constant and equal to 1 to a very high accuracy. Therefore the difference between the theoretical and experimental values of $\langle R_K\rangle_{[1.1,6]}$ does not play any role in the minimisation of the χ^2 function. As a consequence, the b.f.p. is determined using the other observables of the fit, regardless of the experimental value for $\langle R_K\rangle_{[1.1,6]}$, and the contribution of $\langle R_K\rangle_{[1.1,6]}$ cancels in the $\Delta\chi^2 = \chi^2_{\rm SM} - \chi^2_{\rm min}$ statistic. This explains the observed flat curve for the $\text{Pull}_{\rm SM}$, up to small variations linked to the numerical minimisation of the χ^2 function.

The results in Figure 8.9 show that, for most of the values of $\langle R_K\rangle_{[1.1,6]}$ scanned, it is not possible to fully disentangle all the NP scenarios, with the exception of Hyp III: $\mathcal{C}^{\rm V}_{9\mu} = -\mathcal{C}^{\rm V}_{9'\mu}$. However, large values of $\langle R_K\rangle_{[1.1,6]}$ (around 0.90 or above) provide the potential to disentangle some of the LFUV-NP scenarios. Many scenarios get their significances down to the range $\sim 3.8\sigma - 4.8\sigma$, apart from scenarios with right-handed currents like Hyps. V, VII, VIII. Indeed, if a new measurement of $\langle R_K\rangle_{[1.1,6]}$ is found in better agreement with its SM prediction, this favours right-handed currents for $\mathcal{C}^{\rm V}_{9'\mu}$ cancelling the contribution for $\mathcal{C}^{\rm V}_{9\mu}$, but there is still an important number of other tensions (i.e. R_{K^*}, $P'_{5\mu}$ and $\mathcal{B}(B_s \to \phi\mu^+\mu^-)$) that require NP contributions in order to be explained. Large values of $\langle R_K\rangle_{[1.1,6]}$ would help also to distinguish among NP scenarios featuring both LFUV and LFU NP, separating Hyps. X and XI from the others).

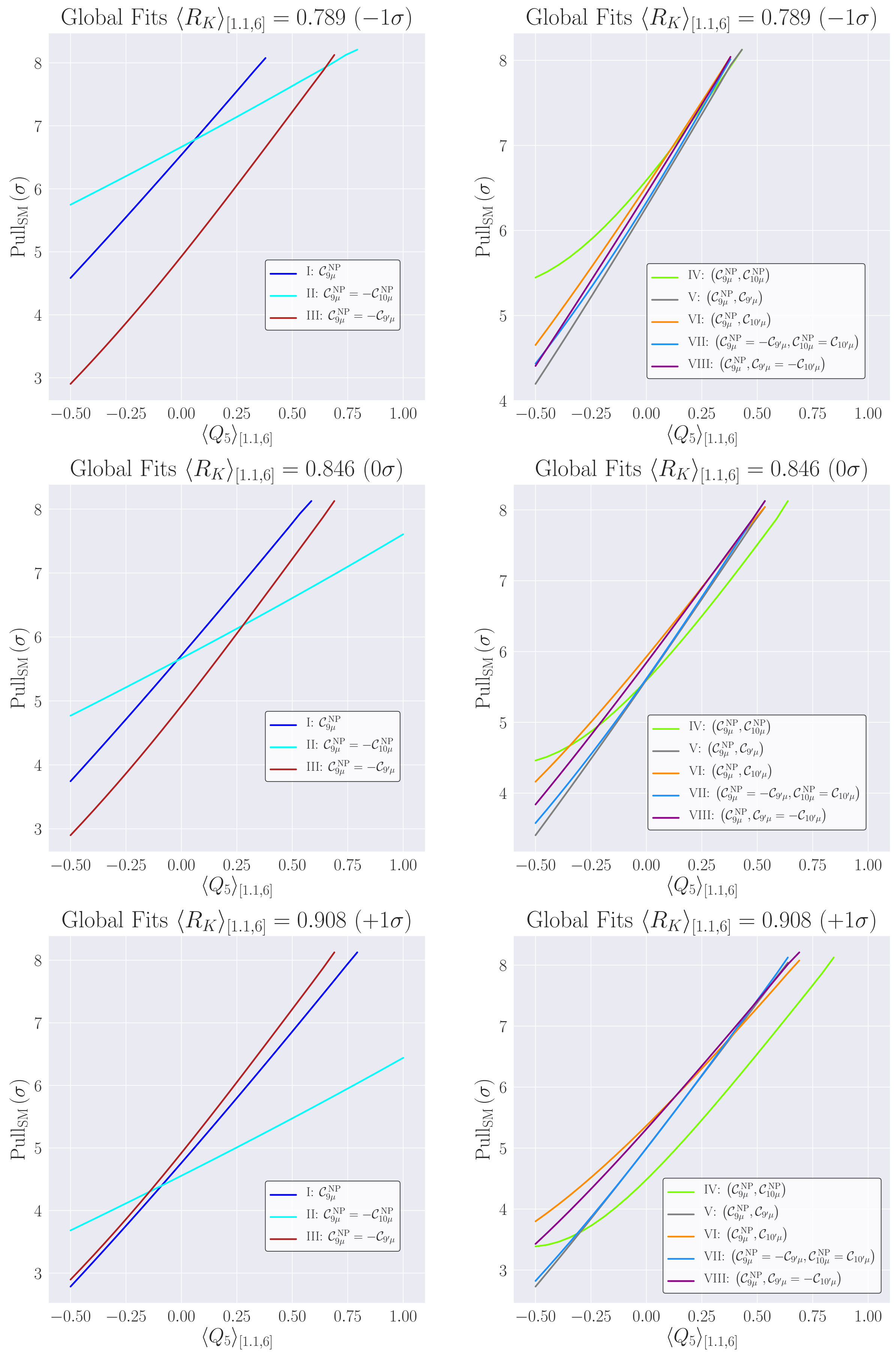

Figure 8.10: Global fit: Impact of $\langle Q_5 \rangle_{[1.1,6]}$ on the $\mathrm{Pull_{SM}}$ of the NP scenarios under consideration for different values of $\langle R_K \rangle_{[1.1,6]}$.

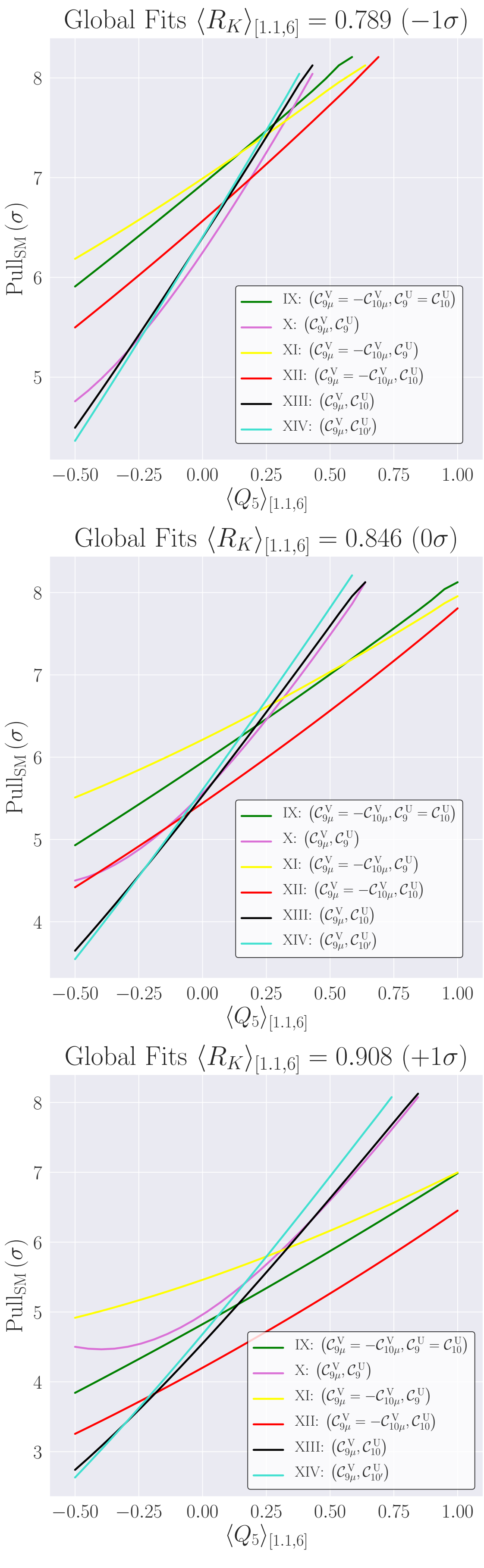

Figure 8.11: Global fit: Impact of $\langle Q_5 \rangle_{[1.1,6]}$ on the $\mathrm{Pull}_{\mathrm{SM}}$ of the NP scenarios under consideration for different values of $\langle R_K \rangle_{[1.1,6]}$.

We then study the combined influence of $\langle R_K\rangle_{[1.1,6]}$ and $\langle Q_5\rangle_{[1.1,6]}$. The value of $\langle Q_5\rangle_{[1.1,6]}$ is varied as explained above and we repeat the analysis for three different values of $\langle R_K\rangle_{[1.1,6]}$: its current experimental value and the ends of its 1σ range. Figs. 8.10 and 8.11 show how the Pull_{SM} varies with different experimental values of $\langle Q_5\rangle_{[1.1,6]}$ and $\langle R_K\rangle_{[1.1,6]}$.

We observe that most of the hypotheses see their Pull_{SM} increase for larger values of $\langle Q_5\rangle_{[1.1,6]}$. One can separate the discussion according to the value of $\langle R_K\rangle_{[1.1,6]}$

- $\langle R_K\rangle_{[1.1,6]} \simeq 0.8$: The pulls are larger than in the current case. The rather low value of R_K disfavours in general scenarios with right-handed currents with respect to scenarios involving only SM vector operators. A large value of $\langle Q_5\rangle_{[1.1,6]}$ (close to 1) favours $\mathcal{C}_{9\mu}^{\text{NP}}$, whereas a low value supports NP in both $\mathcal{C}_{9\mu}^{\text{NP}}$ and $\mathcal{C}_{10\mu}^{\text{NP}}$ either from LFUV NP only (Hyps. II, IV) or from a combination of LFU and LFUV-NP (Hyp. XI).

- $\langle R_K\rangle_{[1.1,6]} \simeq 0.85$: The new determination of $\langle R_K\rangle_{[1.1,6]}$ is then nominally close to its current experimental value but with smaller errors. Therefore, the values for the b.f.p.s are numerically similar to the b.f.p.s reported in Ref. [136, 197]. On one hand, low and large values of $\langle Q_5\rangle_{[1.1,6]}$ provide both a rather clear separation between Hyps. II, IX, X, XI and Hyps. I, III, XIII, XIV. On the other hand, it does not help to separate a set of hypotheses with LFUV NP only (IV to VIII).

- $\langle R_K\rangle_{[1.1,6]} \simeq 0.9$: The pulls are lower with respect to their present values. Large values of $\langle Q_5\rangle_{[1.1,6]}$ allow one to disfavour Hyp II, and low and large values of $\langle Q_5\rangle_{[1.1,6]}$ provide still both a rather clear separation among hypotheses combining LFU and LFUV-NP (Hyps. IX, X, XI on one hand and Hyps. XIII, XIV on the other). However, it does not help to separate a set of hypotheses with LFUV NP only (IV to VIII).

In summary, if the update of $\langle R_K\rangle_{[1.1,6]}$ is larger than its current value, it can help distinguishing among various NP hypotheses, with a preference for hypotheses involving right-handed currents in $\mathcal{C}_{9'\mu}^{\text{V}}$. A value of $\langle R_K\rangle_{[1.1,6]}$ similar or smaller than the current value would clearly disfavour the hypothesis $\mathcal{C}_{9\mu}^{\text{V}} = -\mathcal{C}_{9'\mu}^{\text{V}}$, but many other NP hypotheses (with LFUV only or with a combination of LFU and LFUV) cannot be separated. The observable $\langle Q_5\rangle_{[1.1,6]}$ is an excellent candidate to separate among some of these possibilities. Depending on the situation, low and/or large values of this observables provide a good separation in terms of pulls.

8.5.2 LFUV fits

It is also interesting to address the impact of the observables $\langle R_K\rangle_{[1.1,6]}$ and $\langle Q_5\rangle_{[1.1,6]}$ on the LFUV fits. For them, we follow the same guidelines as for the global fits.

Most of the features observed in the global fit are also observed in the LFUV fit, although with lower pulls, so we refrain from showing the corresponding plots here (one can find these plots in Ref. [212]). For different values of $\langle R_K\rangle_{[1.1,6]}$, the separation among hypotheses can be improved if one measures either low or large values of $\langle Q_5\rangle_{[1.1,6]}$. One can in particular notice that the separation between the LFUV NP hypotheses (IV to VIII) seems easier for low values of $\langle Q_5\rangle_{[1.1,6]}$ compared to the fit “All”. This means that the observables in the LFUV fit are more sensitive to details of this scenario, but this gets compensated by other observables in the fit “All” so that the sensitivity is reduced in the more complete fit.

LFUV fits lead us to draw similar conclusions to the ones extracted from the global fits. However they exhibit a stronger clustering of the pulls, especially if only $\langle R_K \rangle_{[1.1,6]}$ is used to discriminate them. Moreover, if we take a given hypothesis with LFUV-NP only, and consider hypotheses obtained by adding further LFU-NP contributions, we obtain very similar pulls. Therefore, the only way to distinguish among different LFU-NP hypotheses consists in performing the global fits and having access to both muonic and electronic branching ratios. The addition of $\langle Q_5 \rangle_{[1.1,6]}$ allows for strategies that enable the discrimination of various scenarios in a similar way to the case of the global fits.

Chapter 9

Exploring NP in processes with τ leptons

Measurements of the $b \to c\ell\nu_\ell$ charged current have also shown interesting patterns of deviations, even though these are tree-level processes in the SM which are in general less sensitive to NP. As we mentioned in Chapter 8, the ratios $R_{D^{(*)}}$, which measure LFU violation in the charged current by comparing the tau mode to light lepton (e, μ) modes, differ from their SM predictions by a combined significance of approximately 3.1σ [243]. The effect related to tau leptons in $R_{D^{(*)}}$ corresponds to an $O(10\%)$ effect at the amplitude level, assuming its interference with the SM. Recently, LHCb released results for the ratio $R_{J/\psi}$ [271] which measures LFU violation in $b \to c\ell^-\bar{\nu}_\ell$ as well. Again, even though the error is large, the experimental central value exceeds the SM prediction in agreement with the expectations from $R_{D^{(*)}}$ [272–275].

9.1 Implications for $b \to s\tau\tau$

Taking into account the above-mentioned hints for NP, we might expect to have a large LFU violation in the neutral current involving tau leptons, i.e. $b \to s\tau^+\tau^-$ transitions. In fact, it has been shown in Refs. [234, 253, 257] that one can expect an enhancement of up to three orders of magnitude compared to the SM predictions in $b \to s\tau^+\tau^-$ processes if one aims at explaining the central value of $R_{D^{(*)}}$. So far, among the possible processes, only LHCb searched for $B_s \to \tau^+\tau^-$ [276]

$$\mathrm{Br}\big(B_s \to \tau^+\tau^-\big)_{\mathrm{EXP}} \leq 6.8 \times 10^{-3}\,, \tag{9.1.1}$$

and BaBar performed an analysis of $B \to K\tau^+\tau^-$ [277]

$$\mathrm{Br}\big(B \to K\tau^+\tau^-\big)_{\mathrm{EXP}} \leq 2.25 \times 10^{-3}\,. \tag{9.1.2}$$

A search for $B \to K^{(*)}\tau^+\tau^-$ or $B_s \to \phi\tau^+\tau^-$ should be possible at LHCb: compared to the case of $B_s \to \tau^+\tau^-$, these analyses involve more tracks (originating from the K, K^* or ϕ mesons) that can be reconstructed. In addition, the Belle experiment has not analysed their data for $b \to s\tau^+\tau^-$ transitions yet and the upcoming Belle II experiment should be able to improve significantly on the measurement of $B \to K^{(*)}\tau^+\tau^-$ decays: an e^+e^- experiment such as Belle II can be expected to be more efficient in reconstructing B decays to tau leptons than LHCb. Since Belle II is expected to run at the $\Upsilon(4S)$ resonance, it will not study $B_s \to \tau^+\tau^-$ whereas $B \to K^{(*)}\tau^+\tau^-$

are golden modes for finding NP at this facility. There are thus good experimental prospects for these transitions in the coming years.

On the theory side, $b \to s\tau^+\tau^-$ processes have received a limited attention so far. Within the SM, the $B_s \to \tau^+\tau^-$ branching ratio is known very precisely [139, 278]

$$\mathrm{Br}\big(B_s \to \tau^+\tau^-\big)_{\mathrm{SM}} = (7.73 \pm 0.49) \times 10^{-7}\,, \tag{9.1.3}$$

whereas the $b \to s\tau^+\tau^-$ processes $B \to K^*\tau^+\tau^-$, $B \to K\tau^+\tau^-$ and $B_s \to \phi\tau^+\tau^-$ have not been considered in detail until recently, especially concerning the impact of NP contributions. Only the branching ratio for $B \to K\tau^+\tau^-$ was estimated in Ref. [279] including NP effects. Recently, an analysis of branching ratios and tau polarisations in $b \to s\tau^+\tau^-$ was performed to determine the sensitivity to NP contributions to the Wilson coefficients [280].

Within the SM, the branching ratios for $B \to K^*\tau^+\tau^-$ and $B_s \to \phi\tau^+\tau^-$ are known to be of $O(10^{-7})$ [280–282] and the inclusive $B \to X_s\tau^+\tau^-$ process was assessed in Refs. [134, 279]. Ref. [279] also studied the indirect constraints on $b \to s\tau^+\tau^-$ operators, finding that the constraints on NP contributions are very loose once the effects in $b \to s\tau^+\tau^-$ and $b \to d\tau^+\tau^-$ transitions are correlated such that the stringent bounds from $\Delta\Gamma_s/\Delta\Gamma_d$ are avoided. Interestingly, sizable effects in analogous $b \to d\tau^+\tau^-$ operators [283] could help solving the long-standing anomaly in the like-sign dimuon asymmetry measured by the DØ experiment [284, 285].

In this chapter we look in detail at the $b \to s\tau^+\tau^-$ processes $B_s \to \tau^+\tau^-$, $B \to K^*\tau^+\tau^-$, $B \to K\tau^+\tau^-$ and $B_s \to \phi\tau^+\tau^-$. We will express their branching ratios in terms of the Wilson coefficients $\mathcal{C}_{9^{(\prime)}}$ and $\mathcal{C}_{10^{(\prime)}}$. In order to compute these processes we will use the same approach as in Chapters 4, 5 and 6 to compute $b \to s\mu\mu$ observables, substituting muons by taus and taking the relevant form factors in the q^2-region for the $\tau^+\tau^-$ invariant mass where these decays are allowed kinematically. Since the mass of the tau leptons cannot be neglected compared to the B meson, this region is much smaller than for decays to light leptons and we will consider the branching ratios only in the equivalent of the high-q^2 region (or low recoil) for lighter leptons.

9.2 EFT approach

In this section we express the branching ratios for our $b \to s\tau^+\tau^-$ processes as functions of $\mathcal{C}_{9^{(\prime)}}^{\tau\tau}$ and $\mathcal{C}_{10^{(\prime)}}^{\tau\tau}$ and calculate the SM predictions. We define our effective Hamiltonian in the following way, focusing on the relevant operators for our discussion

$$H_{\mathrm{eff}}(b \to s\tau\tau) = -\frac{4G_F}{\sqrt{2}} V_{tb}V_{ts}^* \sum_a \mathcal{C}_a O_a\,, \tag{9.2.1}$$

$$O_{9(10)}^{\tau\tau} = \frac{\alpha}{4\pi}[\bar{s}\gamma^\mu P_L b]\,[\bar{\tau}\gamma_\mu(\gamma^5)\tau]\,, \tag{9.2.2}$$

$$O_{9'(10')}^{\tau\tau} = \frac{\alpha}{4\pi}[\bar{s}\gamma^\mu P_R b]\,[\bar{\tau}\gamma_\mu(\gamma^5)\tau]\,, \tag{9.2.3}$$

where $\mathcal{C}_9^{\mathrm{SM}} \approx 4.1$ and $\mathcal{C}_{10}^{\mathrm{SM}} \approx -4.3$ at the scale $\mu = 4.8$ GeV [85, 89, 93], $P_{L,R} = (1 \mp \gamma_5)/2$, and the chirality-flipped coefficients have negligible contributions in the SM.

Besides $\mathrm{Br}\,(B_s \to \tau^+\tau^-)_{\mathrm{SM}}$ given in Eq. (9.1.3) we use the approach and inputs of Chapter 6 (see also Refs. [112, 113, 136, 147]) to compute the other processes of interest. Averaging over the charged and the neutral modes for $B \to K^{(*)}\tau^+\tau^-$ we find

$$\mathrm{Br}\left(B \to K\tau^+\tau^-\right)^{[15,22]}_{\mathrm{SM}} = (1.20 \pm 0.12) \times 10^{-7}\,, \tag{9.2.4}$$

$$\mathrm{Br}\left(B \to K^*\tau^+\tau^-\right)^{[15,19]}_{\mathrm{SM}} = (0.98 \pm 0.10) \times 10^{-7}\,, \tag{9.2.5}$$

$$\mathrm{Br}\left(B_s \to \phi\tau^+\tau^-\right)^{[15,18.8]}_{\mathrm{SM}} = (0.86 \pm 0.06) \times 10^{-7} \tag{9.2.6}$$

The superscript denotes the q^2-range for the dilepton invariant mass. This broad bin is chosen to leave out the $\psi(2S)$ resonance allowing the use of quark-hadron duality. As discussed in our previous works, our error budget includes in particular a conservative estimate of 10% for duality violation effects, while estimates based on resonance models [157] yield violations around 2%.

In order to assess the structure of the branching ratios including beyond the SM effects, we parametrise both the central value and uncertainty of the branching ratio in each channel as quadratic polynomials in $\mathcal{C}_9^{\mathrm{NP}}$, $\mathcal{C}_{10}^{\mathrm{NP}}$, $\mathcal{C}_{9'}$ and $\mathcal{C}_{10'}$. The values of the polynomial coefficients are estimated by performing a fit to our theoretical predictions computed on an evenly spaced grid in the parameter space $\{\mathcal{C}_9^{\mathrm{NP}}, \mathcal{C}_{10}^{\mathrm{NP}}, \mathcal{C}_{9'}, \mathcal{C}_{10'}\}$, with 300 points each in the ranges [-2,2], [-2,2], [-1,1] and [-0.2,0.2], respectively.

$$\begin{aligned} 10^7 \times \mathrm{Br}\left(B \to K\tau^+\tau^-\right)^{[15,22]} &= \big(1.20 + 0.15\,\mathcal{C}_9^{\mathrm{NP}} - 0.42\,\mathcal{C}_{10}^{\mathrm{NP}} + 0.15\,\mathcal{C}'_9 - 0.42\,\mathcal{C}'_{10} + 0.04\,\mathcal{C}_9^{\mathrm{NP}}\mathcal{C}'_9 \\ &\quad +0.10\,\mathcal{C}_{10}^{\mathrm{NP}}\mathcal{C}'_{10} + 0.02\,\mathcal{C}_9^{\mathrm{NP}\,2} + 0.05\,\mathcal{C}_{10}^{\mathrm{NP}\,2} + 0.02\,\mathcal{C}'^{2}_9 + 0.05\,\mathcal{C}'^{2}_{10}\big) \\ &\quad \pm\big(0.12 + 0.02\,\mathcal{C}_9^{\mathrm{NP}} - 0.04\,\mathcal{C}_{10}^{\mathrm{NP}} + 0.01\,\mathcal{C}'_9 - 0.04\,\mathcal{C}'_{10} \\ &\quad +0.01\,\mathcal{C}_{10}^{\mathrm{NP}}\mathcal{C}'_{10} + 0.01\,\mathcal{C}_{10}^{\mathrm{NP}\,2} + 0.08\,\mathcal{C}'^{2}_{10}\big)\,, \end{aligned} \tag{9.2.7}$$

$$\begin{aligned} 10^7 \times \mathrm{Br}\left(B \to K^*\tau^+\tau^-\right)^{[15,19]} &= \big(0.98 + 0.38\,\mathcal{C}_9^{\mathrm{NP}} - 0.14\,\mathcal{C}_{10}^{\mathrm{NP}} - 0.30\,\mathcal{C}'_9 + 0.12\,\mathcal{C}'_{10} - 0.08\,\mathcal{C}_9^{\mathrm{NP}}\mathcal{C}'_9 \\ &\quad -0.03\,\mathcal{C}_{10}^{\mathrm{NP}}\mathcal{C}'_{10} + 0.05\,\mathcal{C}_9^{\mathrm{NP}\,2} + 0.02\,\mathcal{C}_{10}^{\mathrm{NP}\,2} + 0.05\,\mathcal{C}'^{2}_9 + 0.02\,\mathcal{C}'^{2}_{10}\big) \\ &\quad \pm\big(0.09 + 0.03\,\mathcal{C}_9^{\mathrm{NP}} - 0.01\,\mathcal{C}_{10}^{\mathrm{NP}} - 0.03\,\mathcal{C}'_9 - 0.01\,\mathcal{C}_9^{\mathrm{NP}}\mathcal{C}'_9 \\ &\quad -0.01\,\mathcal{C}'_9\mathcal{C}'_{10} + 0.01\,\mathcal{C}'^{2}_9 - 0.01\,\mathcal{C}'^{2}_{10}\big)\,, \end{aligned} \tag{9.2.8}$$

$$\begin{aligned} 10^7 \times \mathrm{Br}\left(B_s \to \phi\tau^+\tau^-\right)^{[15,18.8]} &= \big(0.86 + 0.34\,\mathcal{C}_9^{\mathrm{NP}} - 0.11\,\mathcal{C}_{10}^{\mathrm{NP}} - 0.28\,\mathcal{C}'_9 + 0.10\,\mathcal{C}'_{10} - 0.08\,\mathcal{C}_9^{\mathrm{NP}}\mathcal{C}'_9 \\ &\quad -0.02\,\mathcal{C}_{10}^{\mathrm{NP}}\mathcal{C}'_{10} + 0.05\,\mathcal{C}_9^{\mathrm{NP}\,2} + 0.01\,\mathcal{C}_{10}^{\mathrm{NP}\,2} + 0.05\,\mathcal{C}'^{2}_9 + 0.01\,\mathcal{C}'^{2}_{10}\big) \\ &\quad \pm\big(0.06 + 0.02\,\mathcal{C}_9^{\mathrm{NP}} - 0.02\,\mathcal{C}'_9 + 0.02\,\mathcal{C}'^{2}_{10}\big) \end{aligned} \tag{9.2.9}$$

As expected, there is a limited dependence of the uncertainties on the values of the Wilson coefficients. In order to shorten the equations, we dropped the superscript $\tau\tau$ in the Wilson coefficients here. Comparing our results with Ref. [280], we find slightly lower central values for the SM (Eqs. (9.2.4)-(9.2.6)). On the other hand, we obtain the same dependence of the central values on the NP contributions to the Wilson coefficients (Eqs. (9.2.7)-(9.2.9)).

In this analysis we neglect the effects of scalar and tensor operators. This is justified since the current global analyses of $b \to s\ell^+\ell^-$ anomalies do not favour such contributions [113, 153, 164, 166]. Moreover, the indirect bounds on the Wilson coefficients of scalar operators from $B_s \to \tau^+\tau^-$ are much stronger than for $\mathcal{C}_{9^{(\prime)}}$ and $\mathcal{C}_{10^{(\prime)}}$ [279] and therefore they cannot lead to comparably large and observable effects in $B \to K^{(*)}\tau^+\tau^-$ or $B_s \to \phi\tau^+\tau^-$. We also neglect tensor operators since they are not generated at the dimension-6 level for $b \to s\ell^+\ell^-$[286, 287].

9.3 Correlation with $R_{D^{(*)}}$ and $R_{J/\psi}$

It is interesting to correlate these results with the tree-level $b \to c\tau^-\bar{\nu}_\tau$ transition. A solution of the $\sim 3\sigma$ anomaly in $R_{D^{(*)}}$ and $R_{J/\psi}$ requires a NP contribution of $\mathcal{O}(20\%)$ to the branching ratio of $B \to D^{(*)}\tau^-\bar{\nu}_\tau$, which is rather large given that these decays are mediated in the SM already at tree level. In order to comply with the B_c lifetime [244] and the q^2 distribution of $R_{D^{(*)}}$ [245–247], a contribution to the SM operator $[\bar{c}\gamma^\mu P_L b][\bar{\tau}\gamma_\mu P_L \nu_\tau]$ is favoured such that there is interference with the SM. In principle, these constraints can be avoided with right-handed couplings (including possibly right-handed neutrinos [288]). However, no interference with the SM appears for such solutions, which require very large couplings close to the perturbativity limit, and we will not consider such solutions any further.

Since a NP contribution to the Wilson coefficient of the SM $V-A$ operator amounts only to changing the normalisation of the Fermi constant for $b \to s\tau^+\tau^-$ transitions, one predicts in this case:

$$R_{J/\psi}/R_{J/\psi}^{\rm SM} = R_D/R_D^{\rm SM} = R_{D^*}/R_{D^*}^{\rm SM}\,, \tag{9.3.1}$$

which agrees well with the current measurements.

If NP generates this contribution from a scale much larger than the electroweak symmetry breaking scale [250, 289], the semileptonic decays involving only left-handed quarks and leptons are described by the two $SU(2)_L$-invariant operators

$$\begin{aligned} \mathcal{O}^{(1)}_{ijkl} &= [\bar{Q}_i\gamma_\mu Q_j][\bar{L}_k\gamma^\mu L_l], \\ \mathcal{O}^{(3)}_{ijkl} &= [\bar{Q}_i\gamma_\mu \sigma^I Q_j][\bar{L}_k\gamma^\mu \sigma^I L_l], \end{aligned} \tag{9.3.2}$$

where the Pauli matrices σ^I act on the weak-isospin components of the quark (lepton) doublets Q (L). Note that there are no further dimension-six operators involving only left-handed fields and that dimension-eight operators can be neglected for NP around the TeV scale. This approach has been used to correlate Wilson coefficients of the effective Hamiltonian for both charged- and neutral-current transitions in various broad classes of NP models (some examples are found in Refs. [234, 235, 251, 290]).

After electroweak symmetry breaking, these operators contribute to semileptonic $b \to c(s)$ decays involving charged tau leptons and tau neutrinos. Working in the down basis when writing the $SU(2)$ components of the operators in Eq. (9.3.2) (i.e., in the field basis with diagonal down quark mass matrices) we obtain

$$\mathcal{C}^{(1)}\mathcal{O}^{(1)} \to \mathcal{C}^{(1)}_{23}\left([\bar{s}_L\gamma_\mu b_L][\bar{\tau}_L\gamma^\mu\tau_L] + [\bar{s}_L\gamma_\mu b_L][\bar{\nu}_\tau\gamma^\mu\nu_\tau]\right), \tag{9.3.3}$$

$$\begin{aligned} \mathcal{C}^{(3)}\mathcal{O}^{(3)} \to\ & \mathcal{C}^{(3)}_{23}\left(2V_{cs}[\bar{c}_L\gamma_\mu b_L][\bar{\tau}_L\gamma^\mu\nu_\tau] + [\bar{s}_L\gamma_\mu b_L][\bar{\tau}_L\gamma^\mu\tau_L]\right. \\ & \left.-[\bar{s}_L\gamma_\mu b_L][\bar{\nu}_\tau\gamma^\mu\nu_\tau]\right) + \mathcal{C}^{(3)}_{33}\left(2V_{cb}[\bar{c}_L\gamma_\mu b_L][\bar{\tau}_L\gamma^\mu\nu_\tau]\right). \end{aligned} \tag{9.3.4}$$

where $\mathcal{C}^{(n)}_{ij}$ denote the Wilson coefficients for $\mathcal{O}^{(n)}_{ij33}$.

We neglect the effect of $\mathcal{C}^{(3)}_{13}$ which would enter $b \to c\tau\nu_\tau$ processes with a factor proportional to V_{cd}. But it would contribute even more dominantly to $b \to d\tau\tau$ and $b \to u\tau\nu_\tau$ processes such as $B^- \to \tau^-\bar{\nu}_\tau$, where no deviation from the SM is observed [291, 292]. We will thus not consider this contribution any more.

As a consequence, we see that $b \to c\tau\nu_\tau$ processes receive a NP contribution from $\mathcal{C}^{(3)}_{33}$ also in scenarios with a flavour-diagonal alignment to the third generation, which would avoid any effects in down-quark FCNCs. However, due to the CKM suppression of this contribution, a solution

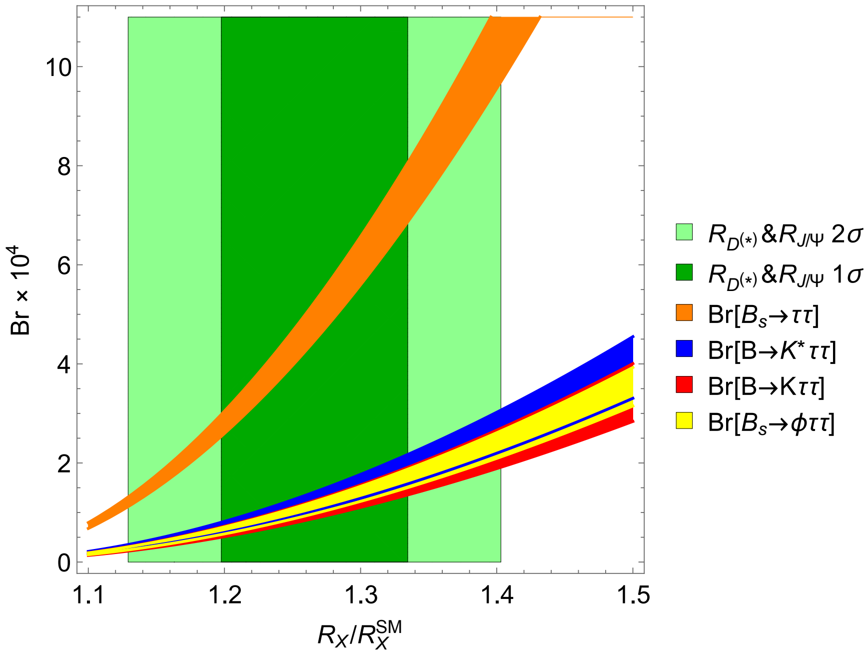

Figure 9.1: Predictions of the branching ratios of the $b \to s\tau^+\tau^-$ processes (including uncertainties) as a function of $R_X/R_X^{\rm SM}$.

of the $R_{D^{(*)}}$ anomaly via this contribution requires a rather large $\mathcal{C}_{33}^{(3)}$ coming into conflict with bounds from electroweak precision data [249] and direct LHC searches for $\tau^+\tau^-$ final states [248].

The $R_{D^{(*)}}$ anomaly can thus only be solved via $\mathcal{C}_{23}^{(1,3)}$ which then must generate huge contributions to $b \to s\tau\tau$ and/or $b \to s\nu_\tau\bar{\nu}_\tau$ processes. The severe bounds on NP from $B \to K^{(*)}\nu\bar{\nu}$ (e.g., Ref. [293]) rule out large effects in $b \to s\nu\bar{\nu}$ and they can only be accommodated if the contribution from $\mathcal{C}_{23}^{(3)}$ is approximately cancelled by the one from $\mathcal{C}_{23}^{(1)}$, implying $\mathcal{C}_{23}^{(1)} \approx C23^{(3)}$ [290]. Such a situation can for instance be realized by a vector leptoquark singlet [234, 235, 256, 257, 294] or by combining two scalar leptoquarks [253]. Neglecting small CKM factors, the assumption $C_{23}^{(1)} \approx C_{23}^{(3)}$ implies that contributions to $b \to c\tau^-\bar{\nu}_\tau$ and $b \to s\tau^+\tau^-$ are generated together in the combination

$$[\bar{c}_L\gamma_\mu b_L][\bar{\tau}_L\gamma^\mu\nu_\tau] + [\bar{s}_L\gamma_\mu b_L][\bar{\tau}_L\gamma^\mu\tau_L]. \tag{9.3.5}$$

This correlation means that effects in $b \to s\tau\tau$ are of the same order as the ones required to explain $R_{D^{(*)}}$, i.e., of the order of a tree-level SM process. We may neglect Cabibbo-suppressed contributions and assume that the NP contribution to $b \to c\tau\nu_\tau$ is small compared to the SM one, so that we keep only the SM contribution and the SM-NP interference terms in $b \to c\tau\nu_\tau$ decay rates. We find the relation

$$\mathcal{C}_{9(10)}^{\tau\tau} \approx \mathcal{C}_{9(10)}^{\rm SM} - (+)\Delta\,, \tag{9.3.6}$$

with

$$\Delta = \frac{2\pi}{\alpha}\frac{V_{cb}}{V_{tb}V_{ts}^*}\left(\sqrt{\frac{R_X}{R_X^{\rm SM}}} - 1\right). \tag{9.3.7}$$

In our framework, Δ is independent of the exclusive $b \to c\ell^-\bar{\nu}_\ell$ channel chosen X, see Eq. (9.3.1). Note that this prediction for the Wilson coefficients $\mathcal{C}_9^{\tau\tau}$ and $\mathcal{C}_{10}^{\tau\tau}$ is model independent, in the sense that the only ingredients in the derivation are the assumptions that NP only affects left-handed quarks and leptons and that it couples significantly to the second generation in such a way that experimental constraints can be avoided.

We stress that the factor multiplying the bracket in Eq. (9.3.7) is very large (around 860). Using the current values for $R_{D^{(*)}}$, we obtain a positive (respectively negative) NP contribution to the Wilson coefficient $\mathcal{C}_9^{\tau\tau}$ (respectively $\mathcal{C}_{10}^{\tau\tau}$) parametrised by $\Delta = O(100)$ which overwhelms completely the SM contribution to these Wilson coefficients. Such large values of the Wilson coefficients are not in contradiction with the constraints obtained in Ref. [279] (when comparing with the results of this reference, one must be aware of the different normalisations of the operators in the effective Hamiltonian).

In view of these huge coefficients, we provide predictions for the relevant decay rates assuming that they are completely dominated by the NP contribution Δ, and thus neglecting both short- and long-distance SM contributions. We obtain the branching ratios of the various $b \to s\tau^+\tau^-$ channels

$$\text{Br}\left(B_s \to \tau^+\tau^-\right) = \left(\frac{\Delta}{C_{10}^{\text{SM}}}\right)^2 \text{Br}\left(B_s \to \tau^+\tau^-\right)_{\text{SM}} \tag{9.3.8}$$

$$\begin{aligned}
\text{Br}\left(B \to K\tau^+\tau^-\right) &= (8.8 \pm 0.8) \times 10^{-9}\Delta^2\,, && (9.3.9)\\
\text{Br}\left(B \to K^*\tau^+\tau^-\right) &= (10.1 \pm 0.8) \times 10^{-9}\Delta^2\,, && (9.3.10)\\
\text{Br}\left(B_s \to \phi\tau^+\tau^-\right) &= (9.1 \pm 0.5) \times 10^{-9}\Delta^2\,, && (9.3.11)
\end{aligned}$$

where the last three branching ratios are considered over the whole kinematic range for the lepton pair invariant mass q^2 (i.e., from $4m_\tau^2$ up to the low-recoil endpoint). We neglect the contributions only due to the SM. In the above expressions, the uncertainties quoted come from hadronic contributions multiplied by the short-distance NP contribution Δ. A naive estimate suggests that the contribution of the $\psi(2S)$ resonance to this branching ratio amounts to 2×10^{-6}, which is negligible in the limit of very large NP contributions considered here. We thus may calculate the branching ratios for the whole kinematically allowed q^2 region, from the vicinity of the $\psi(2S)$ resonance up to the low-recoil endpoint, assuming that the result is completely dominated by the NP contribution.

Since we neglected all errors related to the SM contribution for the semileptonic processes, we should do the same for $B_s \to \tau^+\tau^-$. For $\text{Br}\,(B_s \to \tau^+\tau^-)_{\text{SM}}$ in Eq. (9.3.8), we should only consider the uncertainties coming from the B_s decay constant and decay width as well as the different scales used to compute the Wilson coefficients here and in Ref. [139], leading to a relative uncertainty of 4.7% (to be compared with the larger 6.4% uncertainty in Eq. (9.1.3) that includes other sources of uncertainties irrelevant under our current assumptions).

In Fig. 9.1, we indicate the corresponding predictions as a function of R_X/R_X^{SM} (assumed to be independent of the $b \to c\ell\nu_\ell$ hadronic decay channel X in our approach). We have also indicated the current experimental range for R_X/R_X^{SM}, obtained by performing the weighted average of R_D, R_{D^*} and $R_{J/\psi}$ without taking into account correlations. We see that the branching ratios for semileptonic decays can easily reach 3×10^{-4}, whereas $B_s \to \tau^+\tau^-$ can be increased up to 10^{-3}.

Up to now, we have discussed the correlation between NP in $b \to c\tau\bar{\nu}_\tau$ and $b \to s\tau\tau$ under a limited set of assumptions that are fairly model independent. A comment is in order concerning the implications of these assumptions for $b \to s\mu\mu$. If we assume that the same mechanism is at work for muons and taus, we obtain also a correlation between $b \to s\mu\mu$ and $b \to c\mu\nu_\mu$: the $O(25\%)$ shift needed in $\mathcal{C}_9^{\mu\mu}$ and $\mathcal{C}_{10}^{\mu\mu}$ to describe $b \to s\mu^+\mu^-$ data [136] translates into a very small positive Δ and a decrease of $b \to c\mu\nu_\mu$ decay rates compared to the SM by a negligible amount of only a few per mille, so that there would be no measurable differences between electron and muon semileptonic decays.

Conclusions

Over the last years, a very interesting pattern of deviations has emerged in $b \to s\ell\ell$ transitions. After the initial P_5' anomaly identified in $B \to K^*\mu\mu$ by the LHCb experiment, several systematic deviations have been observed in various branching ratios. At the same time, new observables comparing electron and muon modes have been measured at LHCb (R_K) and Belle ($Q_{4,5}$) hinting at a violation of lepton flavour universality. Global analyses of all these deviations find a preference for NP solutions with respect to the SM with high significances (above 5σ) with distinctive features: i) the dominant NP contribution enters the semileptonic operator $\mathcal{O}_{9\mu}$, ii) NP affects $b \to s\mu\mu$ transitions much more noticeably than $b \to see$ ones and iii) strong consistency between the pattern of deviations in $b \to s\mu\mu$ and LFUV observables.

In Part I we have discussed the basics needed for performing global analyses of $b \to s\ell\ell$ data. These include the use of an effective Hamiltonian for the description of the underlying $b \to s$ quark level transition, the leading order parametrisation of matrix elements in terms of form factors, the development of a factorisation formula for the computation of $O(\alpha_s)$ corrections to the amplitude in a systematic way (which emerges from the simplified dynamics one obtains at the heavy quark and large energy limits) and the construction of a basis of optimised observables where most of hadronic information cancels at leading order.

On the theoretical side, we have seen in Chapter 6 that hadronic uncertainties conform to theoretical expectations and unexpectedly large effects (power corrections to form factors, charm-loop contributions) are disfavoured, in particular by the significant amount of LFUV observed. However, it would be very useful to have more determinations of the form factors involved, both at low and large meson recoils, as well as refined estimates of charm-loop contributions, in order to improve the accuracy of theoretical predictions.

In Chapter 7 we have discussed how angular analyses of $B \to K^*ee$ and $B \to K^*\mu\mu$ decay modes can be combined to understand better the pattern of anomalies observed and to get a solid handle on the size of some SM long-distance contributions.We have proposed different sets of observables comparing $B \to K^*ee$ and $B \to K^*\mu\mu$, discussing their respective merits. A first set of observables is obtained directly from the observables that have been introduced for $B \to K^*\mu\mu$, namely Q_i (related to the optimised observables P_i), T_i (related to the angular averages S_i) and B_i (related to the angular coefficients J_i), measuring in each case the differences between muon and electron modes.

As the analysis in Chapter 8 demonstrates, recent experimental updates (R_K, R_{K^*} and $\mathcal{B}(B_s \to \mu^+\mu^-)$) yield a very similar picture to the one previously found in Refs. [136, 211] for the various NP scenarios of interest with some important peculiarities. In presence of LFUV NP contributions only, the 1D fits to "All" observables remain basically unchanged showing the preference for $\mathcal{C}_{9\mu}^{\rm NP}$ scenario over $\mathcal{C}_{9\mu}^{\rm NP} = -\mathcal{C}_{10\mu}^{\rm NP}$. If only LFUV observables are considered the situation is reversed, as already found in Ref. [136], but now with an increased gap between the significances. This difference between the preferred hypotheses, depending on the data set used, can be solved introducing LFU NP contributions [211].

The main differences arise for the 2D scenarios: the cases including RHC, $(\mathcal{C}_{9\mu}^{\rm NP}, \mathcal{C}_{10'\mu})$, $(\mathcal{C}_{9\mu}^{\rm NP}, \mathcal{C}_{9'\mu})$ or $(\mathcal{C}_{9\mu}^{\rm NP}, \mathcal{C}_{9'\mu} = -\mathcal{C}_{10'\mu})$, can accommodate better the recent updates, which enhances the significance of these scenarios compared to Ref. [136], pointing to new patterns including RHC. A more precise experimental measurement of the observable P_1[83, 103] would be very useful to confirm or not the presence of RHC NP encoded in $\mathcal{C}_{9'\mu}$ and $\mathcal{C}_{10'\mu}$.

We also observe interesting changes in the 2D fits in the presence of LFU NP, where new scenarios (not considered in Ref. [211]) give a good fit to data with $\mathcal{C}_{10^{(\prime)}}^{\rm U}$ and additional LFUV contributions. For example scenario 11 $(\mathcal{C}_{9\mu}^{\rm V}, \mathcal{C}_{10'\mu})$ can accommodate $b \to s\ell^+\ell^-$ data very well, at the same level as scenario 8. Scenarios including LFU NP in left-handed currents (discussed in Ref. [211]) stay practically unchanged but with some preference for scenarios 6 and 8, which have a $(V-A)$ structure for the LFUV-NP and a V or $(V+A)$ structure for the LFU-NP. Furthermore, we have included additional scenarios 9 and 10 that exhibit a significance of 5.0σ and 5.5σ respectively.

We note that the amount of LFU NP is sensitive to the structure of the LFUV component. For instance, in scenario 7 ($\mathcal{C}_{9\mu}^{\rm V}$ and $\mathcal{C}_{9}^{\rm U}$) the LFU component is negligible at its best fit point. On the contrary, if the LFUV-NP has a $(V-A)$ structure, the LFU-NP component ($\mathcal{C}_{9}^{\rm U}$) is large, as illustrated by scenarios 6, 8 and 9. Scenarios with NP in RHC (either LFU or LFUV) prefer such contributions at the 2σ level (see scenarios 11 and 13) with the exception of scenario 12 with negligible $\mathcal{C}_{9'\mu}^{\rm V}$. The new values of R_K and R_{K^*} seem thus to open a window for RHC contributions while the new $\mathcal{B}(B_s \to \mu\mu)$ update (theory and experiment) helps only marginally scenarios with $\mathcal{C}_{10\mu}^{\rm NP}$.

Then, we have discussed the impact of forthcoming measurements of $\langle R_K\rangle_{[1.1,6]}$ and $\langle Q_5\rangle_{[1.1,6]}$ to disentangle NP hypotheses. We considered various central values for these two measurements and we assumed some reduction in the experimental uncertainties in order to study how pulls w.r.t. SM and best-fit points would evolve. $\langle R_K\rangle_{[1.1,6]}$ alone proves to have only a limited ability to separate the various NP hypotheses: $\mathcal{C}_{9\mu}^{\rm V} = -\mathcal{C}_{9'\mu}^{\rm V}$ is the only hypothesis strongly affected. On the other hand, the combination of $\langle R_K\rangle_{[1.1,6]}$ and $\langle Q_5\rangle_{[1.1,6]}$ proves much more efficient to separate various favoured hypotheses, either with only LFUV-NP contributions or with both LFUV and LFU contributions.

Finally, in Chapter 9 we have also analysed the correlation between NP contributions to $b \to s\tau^+\tau^-$ and $b \to c\tau^-\bar{\nu}_\tau$ under general assumptions in agreement with experimental indications: the deviations in $b \to c\tau^-\bar{\nu}_\tau$ decays come from a NP contribution to the left-handed four-fermion vector operator, this NP contribution is due to physics coming from a scale significantly larger than the electroweak scale, and the resulting contribution to $b \to s\nu_\tau\bar{\nu}_\tau$ is suppressed. Under these assumptions, an explanation of $R_{D^{(*)}}$ requires an enhancement of all $b \to s\tau^+\tau^-$ processes by approximately three orders of magnitude compared to the SM, confirming the potential of $b \to s\tau^+\tau^-$ decays to look for NP in the context of the measurements searching for violation of LFU in semileptonic b-decays.

Therefore, we consider our analyses in solid grounds, both from a theoretical perspective and from the point of view of our data analysis strategies, being our approach characterised for always using the most conservative estimation of errors. Hence, if new data from LHCb and, more importantly, results from a completely independent experiment such as Belle II, confirm the same picture we have already observed, there are arguments enough for taking the B-anomalies as the new guideline to follow in the short- and mid-term future in the research field of fundamental Particle Physics. In this context, the B-anomalies can potentially play the role of the Higgs boson during the LEP to LHC transition for the new experiments to come.

Appendix A

Some kinematics for $B \to K^* \ell^+ \ell^-$

This appendix is a compilation of the most relevant definitions and results concerning the kinematics of four-body decays. Our notation is going to be general ($X \to Y(\to ab)Z(\to cd)$), so that it can be applied to any decay, but at the end of the appendix you can also find a translation table between the notation used here and the one in Chapter 3 for the $B \to K^*(\to K\pi)\ell^+\ell^-$ mode.

The dimension of the four-body phase space is 4×4. However, because of the on-shell and 4-momentum conservation conditions (four constraints each), the dimension is reduced to 4×2. Moreover, exploiting isotropic symmetry, one can fix three Euler angles and ends up with 5 physical degrees of freedom. Following [295], the typical five independent kinematical degrees of freedom are portrayed by

- m_{ab}^2, the effective mass squared of the ab system, $m_a + m_b < m_{ab} < m_X - m_c - m_d$.
- m_{cd}^2, the effective mass squared of the cd system, $m_c + m_d < m_{ab} < m_X - m_a - m_b$.
- θ_Y, the angle of the a particle in the C.M. system of the particles a and b with respect to the direction of flight of (a, b) in the X rest system $(0 < \theta_Y < \pi)$.
- θ_Z, the angle of the c particle in the C.M. system of the particles c and d with respect to the direction of flight of (c, d) in the X rest system $(0 < \theta_Y < \pi)$.
- θ_X, the angle between the plane formed by the decay products (a, b) and the corresponding plane of (c, d) in the X rest frame $(-\pi < \theta_X < \pi)$.

More than the individual momenta of each of the particles, it is usual to work with the following combinations

$$P_{ab} = p_a + p_b, \qquad Q_{ab} = p_a - p_b,$$

$$P_{cd} = p_c + p_d, \qquad Q_{cd} = p_c - p_d,$$

Then, the diparticle masses read

$$P_{ab}^2 = m_{ab}^2 \qquad P_{cd}^2 = m_{cd}^2 \tag{A.0.1}$$

The three kinematical angles introduced before can be expressed in terms of momenta in the following way

$$\cos\theta_Y = -\frac{\mathbf{Q}_{ab}\cdot\mathbf{P}_{cd}}{|\mathbf{Q}_{ab}||\mathbf{P}_{cd}|}, \qquad \cos\theta_Z = -\frac{\mathbf{Q}_{cd}\cdot\mathbf{P}_{ab}}{|\mathbf{Q}_{cd}||\mathbf{P}_{ab}|} \tag{A.1}$$

$$\sin\theta_X = \frac{(\mathbf{P}_{ab}\times\mathbf{Q}_{ab})\times(\mathbf{P}_{cd}\times\mathbf{Q}_{cd})}{|\mathbf{P}_{ab}\times\mathbf{Q}_{ab}||\mathbf{P}_{cd}\times\mathbf{Q}_{cd}|} \tag{A.2}$$

where all these quantities must be evaluated, respectively, at the Y, Z and X rest frames.

Using the five independent variables θ_X, θ_Y, θ_Z, m^2_{ab} and m^2_{cd}, the invariant products of the vectors P_{ab}, P_{cd}, Q_{ab} and Q_{cd} write as [31]

$$\begin{aligned}
P_{ab}\,Q_{ab} &= m_a^2 - m_b^2,\\
P_{ab}\,P_{cd} &= \bar{p},\\
P_{ab}\,Q_{cd} &= \frac{m_c^2 - m_d^2}{m_{cd}^2}\bar{p} + \frac{2}{m_{cd}^2}\sigma\sigma_{cd}\cos\theta_Z,\\
Q_{ab}\,Q_{ab} &= \frac{1}{m_{ab}^2 m_{cd}^2}[(m_a^2 - m_b^2)(m_c^2 - m_d^2)\bar{p}\\
&+ 2\sigma\sigma_{ab}(m_c^2 - m_d^2)\cos\theta_Y\\
&+ 2\sigma\sigma_{cd}(m_a^2 - m_b^2)\cos\theta_Z\\
&+ 4\sigma_{ab}\sigma_{cd}\bar{p}\cos\theta_Y\cos\theta_Z\\
&+ 4\sigma_{ab}\sigma_{cd}m_{ab}m_{cd}\sin\theta_Y\sin\theta_Z\cos\theta_X],\\
\epsilon_{\alpha\beta\gamma\delta}P^\alpha_{ab}Q^\beta_{ab}P^\gamma_{cd}Q^\delta_{cd} &= -\frac{4\sigma\sigma_{ab}\sigma_{cd}}{m_{ab}m_{cd}}\sin\theta_Y\sin\theta_Z\sin\theta_X
\end{aligned}$$

with the quantities

$$\begin{aligned}
\bar{p} &= \frac{1}{2}(M_X^2 - m_{ab}^2 - m_{cd}^2),\\
\sigma &= \sqrt{\bar{p}^2 - m_{ab}^2 m_{cd}^2},\\
\bar{p}_{ab} &= \frac{1}{2}(m_{ab}^2 - m_a^2 - m_b^2)\\
\sigma_{ab} &= \sqrt{\bar{p}_{ab}^2 - m_a^2 - m_b^2}
\end{aligned}$$

General	$B \to K^*(\to K\pi)\ell^+\ell^-$
(ab)	$(K\pi)$
(cd)	$(\ell^+\ell^-)$
m_{ab}	m_{K^*}
m_{cd}	$\sqrt{q^2}$
σ_X	ϕ
σ_Y	θ_{K^*}
σ_Z	θ_ℓ
σ^2_{ab}	$m^4_{K^*}\beta^2/4$
σ^2_{cd}	$q^4\beta^2_\ell/4$
σ^2	$\lambda/4$
$\bar{p}$	$(p_{K^*} \cdot q)$

Table A.1: Translation table between the general $X \to Y(\to ab)Z(\to cd)$ variables and the particular notation used for the decay $B \to K^*(\to K\pi)\ell^+\ell^-$ in chapter 3.

Appendix B

Large-recoil expressions for M and $\widetilde{M}$

Under the notation and hypotheses in Section 7.1.2, we can separate the charm contributions from the rest of the $\widetilde{M}$ observable

$$\widetilde{M} = \widetilde{M}_0 + \mathcal{A}'\delta\mathcal{C}_{10}\Delta\mathcal{C}_9 + \mathcal{B}'\delta\mathcal{C}_{10}^2\Delta\mathcal{C}_9^2 \tag{B.0.1}$$

with

$$\begin{aligned}
\widetilde{M}_0 &= \frac{(2\mathcal{C}_7\delta\mathcal{C}_{10}\hat{m}_b + \delta\mathcal{C}_9\mathcal{C}_{10}\hat{s} + \delta\mathcal{C}_{10}(\mathcal{C}_9+\delta\mathcal{C}_9)\hat{s})}{\mathcal{C}_7\delta\mathcal{C}_9\mathcal{C}_{10}(\mathcal{C}_{10}+\delta\mathcal{C}_{10})\hat{m}_b(\hat{s}-1)\hat{s}} \\
&\quad \times (\mathcal{C}_7\delta\mathcal{C}_{10}\hat{m}_b + \delta\mathcal{C}_9\mathcal{C}_{10}\hat{s} + \delta\mathcal{C}_{10}(\mathcal{C}_7\hat{m}_b + \mathcal{C}_9 + \delta\mathcal{C}_9)\hat{s}) && \text{(B.0.2)} \\
\mathcal{A}' &= \frac{2\delta\mathcal{C}_9\mathcal{C}_{10}\hat{s} + \delta\mathcal{C}_{10}\left(2(\mathcal{C}_9+\delta\mathcal{C}_9)\hat{s} + \mathcal{C}_7\hat{m}_b(3+\hat{s})\right)}{\mathcal{C}_7\delta\mathcal{C}_9\mathcal{C}_{10}(\mathcal{C}_{10}+\delta\mathcal{C}_{10})\hat{m}_b(\hat{s}-1)} && \text{(B.0.3)} \\
\mathcal{B}' &= \frac{\hat{s}}{\mathcal{C}_7\delta\mathcal{C}_9\mathcal{C}_{10}(\mathcal{C}_{10}+\delta\mathcal{C}_{10})\hat{m}_b(\hat{s}-1)} && \text{(B.0.4)}
\end{aligned}$$

M can be expressed in terms of $\widetilde{M}$ and considering all the lepton mass effects coming from $\beta_\ell = \sqrt{1-4m_\ell^2/s}$ in the large recoil limit and up to leading order

$$M = \widetilde{M} + \Delta M + \mathcal{A}\Delta\mathcal{C}_9 + \mathcal{B}\Delta\mathcal{C}_9^2 \tag{B.0.5}$$

$$\begin{aligned}
\Delta M &= -\frac{\beta_e^2-\beta_\mu^2}{\beta_e^2\beta_\mu^2}\frac{1}{\mathcal{C}_7\delta\mathcal{C}_9\mathcal{C}_{10}(\mathcal{C}_{10}+\delta\mathcal{C}_{10})\hat{m}_b(\hat{s}-1)\hat{s}} \\
&\quad \times\Big[-\mathcal{C}_{10}^2(2\mathcal{C}_7\hat{m}_b+\mathcal{C}_9\hat{s})(\mathcal{C}_9\hat{s}+\mathcal{C}_7\hat{m}_b(1+\hat{s}))\beta_e^2 && \text{(B.0.6)} \\
&\quad +(\mathcal{C}_{10}+\delta\mathcal{C}_{10})^2\left(2\mathcal{C}_7\hat{m}_b+(\mathcal{C}_9+\delta\mathcal{C}_9)\hat{s}\right)\left((\mathcal{C}_9+\delta\mathcal{C}_9)\hat{s}+\mathcal{C}_7\hat{m}_b(1+\hat{s})\right)\beta_\mu^2\Big] \\
\mathcal{A} &= \frac{\beta_e^2-\beta_\mu^2}{\beta_e^2\beta_\mu^2}\frac{1}{\mathcal{C}_7\delta\mathcal{C}_9\mathcal{C}_{10}(\mathcal{C}_{10}+\delta\mathcal{C}_{10})\hat{m}_b(\hat{s}-1)} && \text{(B.0.7)} \\
&\quad \times\left[\mathcal{C}_{10}^2\left(2\mathcal{C}_9\hat{s}+\mathcal{C}_7\hat{m}_b(3+\hat{s})\right)\beta_e^2-(\mathcal{C}_{10}+\delta\mathcal{C}_{10})^2\left(2(\mathcal{C}_9+\delta\mathcal{C}_9)\hat{s}+\mathcal{C}_7\hat{m}_b(3+\hat{s})\right)\beta_\mu^2\right] \\
\mathcal{B} &= \frac{\beta_e^2-\beta_\mu^2}{\beta_e^2\beta_\mu^2}\frac{\hat{s}\left(\mathcal{C}_{10}^2\beta_e^2-(\mathcal{C}_{10}+\delta\mathcal{C}_{10})^2\beta_\mu^2\right)}{\mathcal{C}_7\delta\mathcal{C}_9\mathcal{C}_{10}(\mathcal{C}_{10}+\delta\mathcal{C}_{10})\hat{m}_b(\hat{s}-1)} && \text{(B.0.8)}
\end{aligned}$$

Appendix C

Definition of binned observables

The binned observables are defined following the same rules as in Ref. [112]:

$$\langle Q_i\rangle = \langle P_i^\mu\rangle - \langle P_i^e\rangle \qquad \langle \hat{Q}_i\rangle = \langle \hat{P}_i^\mu\rangle - \langle \hat{P}_i^e\rangle \qquad \langle T_i\rangle = \frac{\langle S_i^\mu\rangle - \langle S_i^e\rangle}{\langle S_i^\mu\rangle + \langle S_i^e\rangle} \tag{C.0.1}$$

$$\langle B_i\rangle = \frac{\langle J_i^\mu\rangle}{\langle J_i^e\rangle} - 1 \qquad \langle \widetilde{B}_i\rangle = \frac{\langle J_i^\mu/\beta_\mu^2\rangle}{\langle J_i^e/\beta_e^2\rangle} - 1 \tag{C.0.2}$$

$$\langle M\rangle = \frac{(\langle J_5^\mu\rangle - \langle J_5^e\rangle)\,(\langle J_{6s}^\mu\rangle - \langle J_{6s}^e\rangle)}{\langle J_{6s}^\mu\rangle\langle J_5^e\rangle - \langle J_{6s}^e\rangle\langle J_5^\mu\rangle} \tag{C.0.3}$$

$$\langle \widetilde{M}\rangle = \frac{\left(\langle J_5^\mu/\beta_\mu^2\rangle - \langle J_5^e/\beta_e^2\rangle\right)\left(\langle J_{6s}^\mu/\beta_\mu^2\rangle - \langle J_{6s}^e/\beta_e^2\rangle\right)}{\langle J_{6s}^\mu/\beta_\mu^2\rangle\langle J_5^e/\beta_e^2\rangle - \langle J_{6s}^e/\beta_e^2\rangle\langle J_5^\mu/\beta_\mu^2\rangle} \tag{C.0.4}$$

where $\langle P_i^\ell\rangle$ and $\langle S_i^\ell\rangle$ correspond to the observables defined in Ref. [112] with $\ell = e$ or μ. Similarly, the $\langle \hat{P}_i^\ell\rangle$ are obtained from Eqs. (7.1.2)-(7.1.6), substituting $J_i^\ell \to \langle J_i^\ell\rangle$.

Appendix D

Predictions for the observables in various benchmark scenarios

Our predictions are obtained following Ref. [113]. We quote two uncertainties, the second corresponding to the charm contributions, the first to all other sources of uncertainties. Bars denote predictions affected by a very large uncertainty (presence of a pole).

D.1 SM

Bin	Q_{F_L}	Q_1	Q_2	Q_3
$[0.1, 0.98]$	$-0.041 \pm 0.044 \pm 0.010$	$-0.001 \pm 0.001 \pm 0.001$	$0.019 \pm 0.003 \pm 0.001$	$0.000 \pm 0.000 \pm 0.000$
$[1.1, 2.5]$	$-0.027 \pm 0.014 \pm 0.001$	$-0.000 \pm 0.000 \pm 0.000$	$0.007 \pm 0.000 \pm 0.000$	$0.000 \pm 0.000 \pm 0.000$
$[2.5, 4.]$	$-0.016 \pm 0.009 \pm 0.000$	$0.000 \pm 0.000 \pm 0.000$	$0.001 \pm 0.001 \pm 0.000$	$0.000 \pm 0.000 \pm 0.000$
$[4., 6.]$	$-0.010 \pm 0.008 \pm 0.000$	$0.000 \pm 0.000 \pm 0.000$	$-0.001 \pm 0.000 \pm 0.000$	$0.000 \pm 0.000 \pm 0.000$
$[6., 8.]$	$-0.006 \pm 0.006 \pm 0.000$	$0.000 \pm 0.000 \pm 0.000$	$-0.001 \pm 0.000 \pm 0.000$	$0.000 \pm 0.000 \pm 0.000$
$[15., 19.]$	$-0.001 \pm 0.000 \pm 0.000$	$-0.000 \pm 0.000 \pm 0.000$	$-0.000 \pm 0.000 \pm 0.000$	$0.000 \pm 0.000 \pm 0.000$

Bin	Q_4	Q_5	Q_6	Q_8
$[0.1, 0.98]$	$0.005 \pm 0.002 \pm 0.004$	$0.047 \pm 0.003 \pm 0.008$	$-0.005 \pm 0.002 \pm 0.001$	$0.001 \pm 0.000 \pm 0.000$
$[1.1, 2.5]$	$0.002 \pm 0.000 \pm 0.000$	$0.001 \pm 0.002 \pm 0.001$	$-0.001 \pm 0.000 \pm 0.000$	$0.000 \pm 0.000 \pm 0.000$
$[2.5, 4.]$	$0.000 \pm 0.000 \pm 0.000$	$-0.004 \pm 0.001 \pm 0.000$	$-0.000 \pm 0.000 \pm 0.000$	$-0.000 \pm 0.000 \pm 0.000$
$[4., 6.]$	$0.000 \pm 0.000 \pm 0.000$	$-0.004 \pm 0.000 \pm 0.000$	$-0.000 \pm 0.000 \pm 0.000$	$0.000 \pm 0.000 \pm 0.000$
$[6., 8.]$	$0.000 \pm 0.000 \pm 0.000$	$-0.003 \pm 0.000 \pm 0.000$	$-0.000 \pm 0.000 \pm 0.000$	$0.000 \pm 0.000 \pm 0.000$
$[15., 19.]$	$0.000 \pm 0.000 \pm 0.000$	$-0.001 \pm 0.000 \pm 0.000$	$0.000 \pm 0.000 \pm 0.000$	$0.000 \pm 0.000 \pm 0.000$

Bin	$\hat{Q}_{F_L}$	$\hat{Q}_1$	$\hat{Q}_2$	$\hat{Q}_3$
$[0.1, 0.98]$	$0.018 \pm 0.017 \pm 0.004$	$-0.007 \pm 0.006 \pm 0.018$	$-0.008 \pm 0.004 \pm 0.001$	$0.000 \pm 0.001 \pm 0.001$
$[1.1, 2.5]$	$0.014 \pm 0.002 \pm 0.000$	$-0.000 \pm 0.003 \pm 0.000$	$0.013 \pm 0.032 \pm 0.002$	$0.000 \pm 0.000 \pm 0.000$
$[2.5, 4.]$	$0.010 \pm 0.002 \pm 0.000$	$0.000 \pm 0.003 \pm 0.000$	$0.010 \pm 0.025 \pm 0.001$	$0.000 \pm 0.001 \pm 0.000$
$[4., 6.]$	$0.008 \pm 0.001 \pm 0.000$	$0.001 \pm 0.006 \pm 0.000$	$-0.004 \pm 0.005 \pm 0.000$	$0.000 \pm 0.000 \pm 0.000$
$[6., 8.]$	$0.006 \pm 0.002 \pm 0.000$	$0.000 \pm 0.003 \pm 0.000$	$-0.004 \pm 0.007 \pm 0.000$	$0.000 \pm 0.000 \pm 0.000$
$[15., 19.]$	$0.001 \pm 0.000 \pm 0.000$	$0.001 \pm 0.000 \pm 0.000$	$-0.000 \pm 0.000 \pm 0.000$	$0.000 \pm 0.000 \pm 0.000$
Bin	$\hat{Q}_4$	$\hat{Q}_5$	$\hat{Q}_6$	$\hat{Q}_8$
$[0.1, 0.98]$	$0.111 \pm 0.007 \pm 0.037$	$-0.097 \pm 0.013 \pm 0.019$	$0.008 \pm 0.003 \pm 0.001$	$-0.004 \pm 0.004 \pm 0.003$
$[1.1, 2.5]$	$0.003 \pm 0.005 \pm 0.002$	$-0.003 \pm 0.007 \pm 0.001$	$0.001 \pm 0.003 \pm 0.000$	$-0.001 \pm 0.002 \pm 0.000$
$[2.5, 4.]$	$0.001 \pm 0.016 \pm 0.001$	$-0.005 \pm 0.017 \pm 0.001$	$-0.001 \pm 0.003 \pm 0.000$	$0.000 \pm 0.002 \pm 0.000$
$[4., 6.]$	$-0.002 \pm 0.015 \pm 0.000$	$-0.002 \pm 0.017 \pm 0.000$	$-0.000 \pm 0.001 \pm 0.000$	$-0.000 \pm 0.001 \pm 0.000$
$[6., 8.]$	$-0.005 \pm 0.009 \pm 0.001$	$0.002 \pm 0.010 \pm 0.000$	$0.000 \pm 0.000 \pm 0.000$	$-0.000 \pm 0.000 \pm 0.000$
$[15., 19.]$	$-0.003 \pm 0.000 \pm 0.000$	$0.001 \pm 0.000 \pm 0.000$	$0.000 \pm 0.000 \pm 0.000$	$0.000 \pm 0.000 \pm 0.000$

Bin	T_3	T_4	T_5
$[0.1, 0.98]$	$--$	$-0.116 \pm 0.002 \pm 0.005$	$-0.075 \pm 0.003 \pm 0.001$
$[1.1, 2.5]$	$--$	$--$	$-0.017 \pm 0.004 \pm 0.001$
$[2.5, 4.]$	$--$	$-0.010 \pm 0.003 \pm 0.000$	$-0.006 \pm 0.003 \pm 0.000$
$[4., 6.]$	$-0.007 \pm 0.006 \pm 0.000$	$-0.007 \pm 0.003 \pm 0.000$	$-0.004 \pm 0.003 \pm 0.000$
$[6., 8.]$	$-0.005 \pm 0.004 \pm 0.060$	$-0.005 \pm 0.002 \pm 0.000$	$-0.003 \pm 0.002 \pm 0.000$
$[15., 19.]$	$-0.001 \pm 0.000 \pm 0.000$	$-0.001 \pm 0.000 \pm 0.000$	$-0.000 \pm 0.000 \pm 0.000$
Bin	T_7	T_8	T_9
$[0.1, 0.98]$	$-0.067 \pm 0.003 \pm 0.000$	$-0.081 \pm 0.025 \pm 0.051$	$--$
$[1.1, 2.5]$	$-0.013 \pm 0.003 \pm 0.000$	$-0.020 \pm 0.003 \pm 0.000$	$--$
$[2.5, 4.]$	$-0.007 \pm 0.003 \pm 0.000$	$-0.010 \pm 0.003 \pm 0.000$	$-0.010 \pm 0.027 \pm 0.000$
$[4., 6.]$	$-0.005 \pm 0.003 \pm 0.000$	$-0.007 \pm 0.003 \pm 0.000$	$-0.007 \pm 0.003 \pm 0.000$
$[6., 8.]$	$-0.003 \pm 0.002 \pm 0.000$	$-0.005 \pm 0.002 \pm 0.000$	$-0.005 \pm 0.004 \pm 0.000$
$[15., 19.]$	$-0.000 \pm 0.000 \pm 0.000$	$-0.001 \pm 0.001 \pm 0.004$	$-0.001 \pm 0.002 \pm 0.001$

Bin	B_5	B_{6s}	M
$[0.1, 0.98]$	$-0.155 \pm 0.002 \pm 0.002$	$-0.121 \pm 0.001 \pm 0.000$	$0.548 \pm 0.021 \pm 0.024$
$[1.1, 2.5]$	$-0.034 \pm 0.005 \pm 0.002$	$-0.027 \pm 0.000 \pm 0.000$	$0.150 \pm 0.071 \pm 0.037$
$[2.5, 4.]$	$-0.013 \pm 0.000 \pm 0.000$	$-0.015 \pm 0.001 \pm 0.000$	$-0.095 \pm 0.033 \pm 0.007$
$[4., 6.]$	$-0.009 \pm 0.000 \pm 0.000$	$-0.008 \pm 0.021 \pm 0.000$	$0.149 \pm 0.122 \pm 0.019$
$[6., 8.]$	$-0.006 \pm 0.000 \pm 0.000$	$-0.006 \pm 0.000 \pm 0.000$	$0.617 \pm 0.253 \pm 0.204$
$[15., 19.]$	$-0.003 \pm 0.000 \pm 0.000$	$-0.003 \pm 0.000 \pm 0.000$	$--$

Bin	$\widetilde{B}_5$	$\widetilde{B}_{6s}$	$\widetilde{M}$
$[0.1, 0.98]$	$0.000 \pm 0.000 \pm 0.000$	$0.000 \pm 0.000 \pm 0.000$	$0.000 \pm 0.000 \pm 0.000$
$[1.1, 2.5]$	$0.000 \pm 0.000 \pm 0.000$	$0.000 \pm 0.000 \pm 0.000$	$0.000 \pm 0.000 \pm 0.000$
$[2.5, 4.]$	$0.000 \pm 0.000 \pm 0.000$	$0.000 \pm 0.000 \pm 0.000$	$0.000 \pm 0.000 \pm 0.000$
$[4., 6.]$	$0.000 \pm 0.000 \pm 0.000$	$0.000 \pm 0.000 \pm 0.000$	$0.000 \pm 0.000 \pm 0.000$
$[6., 8.]$	$0.000 \pm 0.000 \pm 0.000$	$0.000 \pm 0.000 \pm 0.000$	$0.000 \pm 0.000 \pm 0.000$
$[15., 19.]$	$0.000 \pm 0.000 \pm 0.000$	$0.000 \pm 0.000 \pm 0.000$	$0.000 \pm 0.000 \pm 0.000$

D.2 Scenario 1: $\mathcal{C}_{9\mu}^{\rm NP} = -1.11$

Bin	Q_{F_L}	Q_1	Q_2	Q_3
[0.1, 0.98]	$-0.085 \pm 0.073 \pm 0.021$	$-0.001 \pm 0.002 \pm 0.003$	$0.017 \pm 0.002 \pm 0.001$	$0.000 \pm 0.000 \pm 0.000$
[1.1, 2.5]	$-0.122 \pm 0.032 \pm 0.001$	$0.001 \pm 0.008 \pm 0.003$	$-0.008 \pm 0.010 \pm 0.001$	$-0.000 \pm 0.001 \pm 0.000$
[2.5, 4.]	$-0.086 \pm 0.037 \pm 0.002$	$-0.013 \pm 0.026 \pm 0.007$	$0.174 \pm 0.058 \pm 0.006$	$-0.001 \pm 0.002 \pm 0.000$
[4., 6.]	$-0.051 \pm 0.016 \pm 0.002$	$-0.022 \pm 0.038 \pm 0.010$	$0.246 \pm 0.009 \pm 0.002$	$-0.000 \pm 0.001 \pm 0.000$
[6., 8.]	$-0.027 \pm 0.008 \pm 0.003$	$-0.017 \pm 0.028 \pm 0.009$	$0.184 \pm 0.036 \pm 0.009$	$0.000 \pm 0.000 \pm 0.000$
[15., 19.]	$-0.002 \pm 0.000 \pm 0.003$	$0.002 \pm 0.001 \pm 0.004$	$0.051 \pm 0.004 \pm 0.010$	$0.000 \pm 0.000 \pm 0.003$
Bin	Q_4	Q_5	Q_6	Q_8
[0.1, 0.98]	$0.136 \pm 0.011 \pm 0.049$	$0.172 \pm 0.004 \pm 0.016$	$-0.011 \pm 0.004 \pm 0.001$	$-0.012 \pm 0.004 \pm 0.003$
[1.1, 2.5]	$0.087 \pm 0.033 \pm 0.019$	$0.241 \pm 0.021 \pm 0.013$	$-0.002 \pm 0.001 \pm 0.000$	$-0.018 \pm 0.007 \pm 0.001$
[2.5, 4.]	$-0.037 \pm 0.035 \pm 0.010$	$0.370 \pm 0.017 \pm 0.014$	$-0.003 \pm 0.001 \pm 0.000$	$-0.014 \pm 0.007 \pm 0.001$
[4., 6.]	$-0.041 \pm 0.008 \pm 0.008$	$0.312 \pm 0.044 \pm 0.017$	$-0.006 \pm 0.002 \pm 0.000$	$-0.006 \pm 0.004 \pm 0.000$
[6., 8.]	$-0.020 \pm 0.005 \pm 0.010$	$0.212 \pm 0.056 \pm 0.029$	$-0.004 \pm 0.003 \pm 0.000$	$-0.002 \pm 0.002 \pm 0.001$
[15., 19.]	$-0.001 \pm 0.000 \pm 0.002$	$0.073 \pm 0.007 \pm 0.013$	$-0.001 \pm 0.000 \pm 0.020$	$-0.001 \pm 0.000 \pm 0.004$

Bin	$\hat{Q}_{F_L}$	$\hat{Q}_1$	$\hat{Q}_2$	$\hat{Q}_3$
[0.1, 0.98]	$-0.037 \pm 0.022 \pm 0.011$	$-0.007 \pm 0.007 \pm 0.019$	$-0.009 \pm 0.003 \pm 0.000$	$0.000 \pm 0.001 \pm 0.001$
[1.1, 2.5]	$-0.086 \pm 0.049 \pm 0.001$	$0.001 \pm 0.008 \pm 0.003$	$-0.010 \pm 0.019 \pm 0.002$	$-0.000 \pm 0.001 \pm 0.000$
[2.5, 4.]	$-0.060 \pm 0.046 \pm 0.002$	$-0.014 \pm 0.026 \pm 0.007$	$0.183 \pm 0.048 \pm 0.006$	$-0.001 \pm 0.002 \pm 0.000$
[4., 6.]	$-0.033 \pm 0.021 \pm 0.002$	$-0.021 \pm 0.036 \pm 0.011$	$0.247 \pm 0.011 \pm 0.002$	$-0.000 \pm 0.001 \pm 0.000$
[6., 8.]	$-0.015 \pm 0.008 \pm 0.003$	$-0.017 \pm 0.026 \pm 0.009$	$0.182 \pm 0.035 \pm 0.009$	$0.000 \pm 0.000 \pm 0.000$
[15., 19.]	$-0.001 \pm 0.000 \pm 0.002$	$0.002 \pm 0.001 \pm 0.004$	$0.051 \pm 0.004 \pm 0.010$	$0.000 \pm 0.000 \pm 0.003$
Bin	$\hat{Q}_4$	$\hat{Q}_5$	$\hat{Q}_6$	$\hat{Q}_8$
[0.1, 0.98]	$0.214 \pm 0.008 \pm 0.010$	$-0.000 \pm 0.011 \pm 0.014$	$0.003 \pm 0.001 \pm 0.001$	$-0.014 \pm 0.007 \pm 0.001$
[1.1, 2.5]	$0.086 \pm 0.035 \pm 0.016$	$0.227 \pm 0.021 \pm 0.010$	$0.000 \pm 0.002 \pm 0.001$	$-0.019 \pm 0.007 \pm 0.001$
[2.5, 4.]	$-0.040 \pm 0.042 \pm 0.009$	$0.370 \pm 0.017 \pm 0.013$	$-0.003 \pm 0.002 \pm 0.000$	$-0.014 \pm 0.006 \pm 0.001$
[4., 6.]	$-0.045 \pm 0.016 \pm 0.008$	$0.314 \pm 0.043 \pm 0.017$	$-0.005 \pm 0.003 \pm 0.000$	$-0.006 \pm 0.004 \pm 0.000$
[6., 8.]	$-0.025 \pm 0.007 \pm 0.009$	$0.216 \pm 0.054 \pm 0.029$	$-0.004 \pm 0.003 \pm 0.000$	$-0.002 \pm 0.002 \pm 0.001$
[15., 19.]	$-0.003 \pm 0.000 \pm 0.002$	$0.074 \pm 0.007 \pm 0.013$	$-0.001 \pm 0.000 \pm 0.020$	$-0.001 \pm 0.000 \pm 0.004$

Bin	T_3	T_4	T_5
[0.1, 0.98]	−−	−−	$-0.026 \pm 0.038 \pm 0.011$
[1.1, 2.5]	−−	−−	$0.402 \pm 0.152 \pm 0.076$
[2.5, 4.]	−−	$0.005 \pm 0.072 \pm 0.008$	$-0.608 \pm 0.295 \pm 0.121$
[4., 6.]	−−	$-0.010 \pm 0.031 \pm 0.004$	$-0.224 \pm 0.061 \pm 0.026$
[6., 8.]	−−	$-0.009 \pm 0.014 \pm 0.004$	$-0.126 \pm 0.042 \pm 0.025$
[15., 19.]	$-0.001 \pm 0.001 \pm 0.004$	$-0.002 \pm 0.000 \pm 0.001$	$-0.069 \pm 0.006 \pm 0.015$

Bin	T_7	T_8	T_9
[0.1, 0.98]	$-0.056 \pm 0.038 \pm 0.011$	−−	−−
[1.1, 2.5]	$0.029 \pm 0.071 \pm 0.010$	$-0.244 \pm 0.137 \pm 0.073$	−−
[2.5, 4.]	$0.065 \pm 0.050 \pm 0.005$	$-0.143 \pm 0.075 \pm 0.023$	−−
[4., 6.]	$0.087 \pm 0.028 \pm 0.003$	$-0.091 \pm 0.050 \pm 0.016$	−−
[6., 8.]	$0.102 \pm 0.015 \pm 0.004$	$-0.067 \pm 0.083 \pm 0.025$	−−
[15., 19.]	$0.118 \pm 0.001 \pm 0.003$	−−	−−

Bin	B_5	B_{6s}	M
[0.1, 0.98]	$-0.087 \pm 0.008 \pm 0.004$	$-0.084 \pm 0.005 \pm 0.001$	−−
[1.1, 2.5]	−−	$0.172 \pm 0.047 \pm 0.006$	$-0.203 \pm 0.049 \pm 0.012$
[2.5, 4.]	$-0.785 \pm 0.181 \pm 0.078$	−−	$-0.459 \pm 0.106 \pm 0.026$
[4., 6.]	$-0.472 \pm 0.051 \pm 0.026$	−−	$-0.736 \pm 0.188 \pm 0.062$
[6., 8.]	$-0.372 \pm 0.040 \pm 0.027$	$-0.569 \pm 0.150 \pm 0.032$	$-1.101 \pm 0.328 \pm 0.242$
[15., 19.]	$-0.316 \pm 0.007 \pm 0.018$	$-0.324 \pm 0.008 \pm 0.019$	−−

Bin	$\widetilde{B}_5$	$\widetilde{B}_{6s}$	$\widetilde{M}$
[0.1, 0.98]	$0.075 \pm 0.010 \pm 0.006$	$0.040 \pm 0.006 \pm 0.001$	$-0.083 \pm 0.017 \pm 0.006$
[1.1, 2.5]	−−	$0.204 \pm 0.048 \pm 0.006$	$-0.247 \pm 0.049 \pm 0.015$
[2.5, 4.]	$-0.783 \pm 0.184 \pm 0.079$	−−	$-0.463 \pm 0.102 \pm 0.027$
[4., 6.]	$-0.467 \pm 0.051 \pm 0.026$	−−	$-0.723 \pm 0.182 \pm 0.061$
[6., 8.]	$-0.368 \pm 0.040 \pm 0.027$	$-0.566 \pm 0.151 \pm 0.032$	$-1.077 \pm 0.319 \pm 0.238$
[15., 19.]	$-0.314 \pm 0.007 \pm 0.018$	$-0.322 \pm 0.008 \pm 0.019$	−−

D.3 Scenario 2: $\mathcal{C}_{9\mu}^{\rm NP} = -\mathcal{C}_{10\mu}^{\rm NP} = -0.65$

Bin	Q_{F_L}	Q_1	Q_2	Q_3
[0.1, 0.98]	$-0.096 \pm 0.081 \pm 0.013$	$-0.001 \pm 0.001 \pm 0.002$	$0.001 \pm 0.000 \pm 0.000$	$0.000 \pm 0.000 \pm 0.000$
[1.1, 2.5]	$-0.107 \pm 0.027 \pm 0.007$	$-0.002 \pm 0.008 \pm 0.002$	$-0.032 \pm 0.015 \pm 0.002$	$-0.000 \pm 0.001 \pm 0.000$
[2.5, 4.]	$-0.043 \pm 0.014 \pm 0.003$	$-0.017 \pm 0.039 \pm 0.008$	$0.148 \pm 0.037 \pm 0.003$	$0.000 \pm 0.001 \pm 0.000$
[4., 6.]	$-0.009 \pm 0.012 \pm 0.002$	$-0.011 \pm 0.027 \pm 0.005$	$0.134 \pm 0.029 \pm 0.006$	$0.001 \pm 0.001 \pm 0.000$
[6., 8.]	$0.003 \pm 0.011 \pm 0.003$	$-0.001 \pm 0.008 \pm 0.001$	$0.059 \pm 0.029 \pm 0.007$	$0.001 \pm 0.001 \pm 0.000$
[15., 19.]	$0.001 \pm 0.000 \pm 0.003$	$-0.002 \pm 0.001 \pm 0.005$	$0.005 \pm 0.001 \pm 0.003$	$0.000 \pm 0.000 \pm 0.003$

Bin	Q_4	Q_5	Q_6	Q_8
[0.1, 0.98]	$-0.003 \pm 0.007 \pm 0.027$	$0.078 \pm 0.007 \pm 0.029$	$-0.005 \pm 0.002 \pm 0.002$	$-0.005 \pm 0.001 \pm 0.003$
[1.1, 2.5]	$-0.102 \pm 0.028 \pm 0.014$	$0.136 \pm 0.017 \pm 0.012$	$-0.000 \pm 0.001 \pm 0.001$	$-0.005 \pm 0.002 \pm 0.001$
[2.5, 4.]	$-0.152 \pm 0.013 \pm 0.010$	$0.188 \pm 0.021 \pm 0.010$	$-0.007 \pm 0.002 \pm 0.001$	$0.002 \pm 0.003 \pm 0.001$
[4., 6.]	$-0.078 \pm 0.031 \pm 0.009$	$0.096 \pm 0.032 \pm 0.010$	$-0.008 \pm 0.004 \pm 0.000$	$0.005 \pm 0.004 \pm 0.000$
[6., 8.]	$-0.031 \pm 0.021 \pm 0.009$	$0.033 \pm 0.021 \pm 0.011$	$-0.004 \pm 0.003 \pm 0.000$	$0.004 \pm 0.003 \pm 0.001$

[15., 19.]	$0.000 \pm 0.000 \pm 0.002$	$0.007 \pm 0.001 \pm 0.006$	$-0.001 \pm 0.000 \pm 0.015$	$-0.001 \pm 0.001 \pm 0.005$

Bin	$\hat{Q}_{F_L}$	$\hat{Q}_1$	$\hat{Q}_2$	$\hat{Q}_3$
[0.1, 0.98]	$-0.051 \pm 0.031 \pm 0.003$	$-0.007 \pm 0.006 \pm 0.019$	$-0.022 \pm 0.004 \pm 0.001$	$0.000 \pm 0.001 \pm 0.001$
[1.1, 2.5]	$-0.071 \pm 0.043 \pm 0.008$	$-0.002 \pm 0.008 \pm 0.002$	$-0.034 \pm 0.020 \pm 0.003$	$-0.000 \pm 0.001 \pm 0.000$
[2.5, 4.]	$-0.017 \pm 0.020 \pm 0.003$	$-0.017 \pm 0.040 \pm 0.008$	$0.159 \pm 0.028 \pm 0.003$	$0.000 \pm 0.001 \pm 0.000$
[4., 6.]	$0.009 \pm 0.007 \pm 0.002$	$-0.011 \pm 0.024 \pm 0.005$	$0.133 \pm 0.032 \pm 0.006$	$0.001 \pm 0.002 \pm 0.000$
[6., 8.]	$0.016 \pm 0.006 \pm 0.003$	$-0.000 \pm 0.005 \pm 0.001$	$0.056 \pm 0.027 \pm 0.007$	$0.001 \pm 0.002 \pm 0.000$
[15., 19.]	$0.002 \pm 0.001 \pm 0.004$	$-0.001 \pm 0.001 \pm 0.005$	$0.006 \pm 0.001 \pm 0.003$	$0.000 \pm 0.000 \pm 0.003$
Bin	$\hat{Q}_4$	$\hat{Q}_5$	$\hat{Q}_6$	$\hat{Q}_8$
[0.1, 0.98]	$0.107 \pm 0.007 \pm 0.015$	$-0.075 \pm 0.008 \pm 0.005$	$0.008 \pm 0.003 \pm 0.000$	$-0.008 \pm 0.004 \pm 0.001$
[1.1, 2.5]	$-0.097 \pm 0.030 \pm 0.012$	$0.126 \pm 0.017 \pm 0.009$	$0.002 \pm 0.002 \pm 0.000$	$-0.006 \pm 0.002 \pm 0.001$
[2.5, 4.]	$-0.154 \pm 0.009 \pm 0.010$	$0.189 \pm 0.022 \pm 0.010$	$-0.007 \pm 0.003 \pm 0.001$	$0.002 \pm 0.003 \pm 0.001$
[4., 6.]	$-0.079 \pm 0.023 \pm 0.008$	$0.098 \pm 0.030 \pm 0.010$	$-0.008 \pm 0.004 \pm 0.000$	$0.005 \pm 0.004 \pm 0.000$
[6., 8.]	$-0.035 \pm 0.015 \pm 0.008$	$0.037 \pm 0.021 \pm 0.011$	$-0.004 \pm 0.003 \pm 0.000$	$0.004 \pm 0.003 \pm 0.001$
[15., 19.]	$-0.003 \pm 0.000 \pm 0.002$	$0.009 \pm 0.001 \pm 0.006$	$-0.001 \pm 0.000 \pm 0.015$	$-0.001 \pm 0.001 \pm 0.005$

Bin	T_3	T_4	T_5
[0.1, 0.98]	−−	$-0.158 \pm 0.050 \pm 0.043$	$-0.101 \pm 0.046 \pm 0.005$
[1.1, 2.5]	−−	−−	$0.276 \pm 0.131 \pm 0.056$
[2.5, 4.]	−−	$-0.156 \pm 0.118 \pm 0.023$	$-0.234 \pm 0.100 \pm 0.039$
[4., 6.]	−−	$-0.057 \pm 0.033 \pm 0.008$	$-0.070 \pm 0.022 \pm 0.008$
[6., 8.]	−−	$-0.026 \pm 0.023 \pm 0.007$	$-0.026 \pm 0.015 \pm 0.005$
[15., 19.]	$-0.001 \pm 0.001 \pm 0.005$	$-0.000 \pm 0.000 \pm 0.001$	$-0.007 \pm 0.002 \pm 0.006$
Bin	T_7	T_8	T_9
[0.1, 0.98]	$-0.116 \pm 0.047 \pm 0.005$	−−	−−
[1.1, 2.5]	$0.015 \pm 0.056 \pm 0.002$	$-0.050 \pm 0.084 \pm 0.029$	−−
[2.5, 4.]	$0.069 \pm 0.014 \pm 0.003$	$0.037 \pm 0.029 \pm 0.006$	−−
[4., 6.]	$0.089 \pm 0.008 \pm 0.003$	$0.073 \pm 0.022 \pm 0.003$	−−
[6., 8.]	$0.095 \pm 0.012 \pm 0.006$	$0.138 \pm 0.042 \pm 0.005$	−−
[15., 19.]	$0.094 \pm 0.002 \pm 0.004$	−−	−−

Bin	B_5	B_{6s}	M
[0.1, 0.98]	$-0.248 \pm 0.003 \pm 0.002$	$-0.235 \pm 0.002 \pm 0.001$	−−
[1.1, 2.5]	−−	$-0.075 \pm 0.023 \pm 0.003$	$0.062 \pm 0.011 \pm 0.004$
[2.5, 4.]	$-0.546 \pm 0.090 \pm 0.039$	−−	$-0.231 \pm 0.126 \pm 0.015$
[4., 6.]	$-0.389 \pm 0.025 \pm 0.013$	−−	$-0.750 \pm 0.280 \pm 0.061$
[6., 8.]	$-0.338 \pm 0.020 \pm 0.013$	$-0.436 \pm 0.074 \pm 0.016$	$-1.550 \pm 0.570 \pm 0.305$
[15., 19.]	$-0.309 \pm 0.003 \pm 0.009$	$-0.313 \pm 0.004 \pm 0.009$	−−

Bin	$\widetilde{B}_5$	$\widetilde{B}_{6s}$	$\widetilde{M}$
[0.1, 0.98]	$-0.113 \pm 0.005 \pm 0.003$	$-0.131 \pm 0.003 \pm 0.001$	$-0.845 \pm 0.182 \pm 0.136$
[1.1, 2.5]	−−	$-0.049 \pm 0.024 \pm 0.003$	$0.044 \pm 0.016 \pm 0.002$
[2.5, 4.]	$-0.540 \pm 0.091 \pm 0.039$	−−	$-0.236 \pm 0.120 \pm 0.014$
[4., 6.]	$-0.383 \pm 0.025 \pm 0.013$	−−	$-0.731 \pm 0.269 \pm 0.059$
[6., 8.]	$-0.334 \pm 0.020 \pm 0.013$	$-0.432 \pm 0.075 \pm 0.016$	$-1.508 \pm 0.551 \pm 0.297$
[15., 19.]	$-0.307 \pm 0.003 \pm 0.009$	$-0.311 \pm 0.004 \pm 0.009$	−−

D.4 Scenario 3: $\mathcal{C}_{9\mu}^{\rm NP} = -\mathcal{C}_{9'\mu}^{\rm NP} = -1.07$

Bin	Q_{F_L}	Q_1	Q_2	Q_3
[0.1, 0.98]	$-0.109 \pm 0.094 \pm 0.034$	$-0.055 \pm 0.009 \pm 0.003$	$0.017 \pm 0.002 \pm 0.001$	$0.002 \pm 0.001 \pm 0.000$
[1.1, 2.5]	$-0.164 \pm 0.044 \pm 0.007$	$-0.204 \pm 0.024 \pm 0.005$	$-0.014 \pm 0.007 \pm 0.002$	$0.009 \pm 0.004 \pm 0.001$
[2.5, 4.]	$-0.133 \pm 0.060 \pm 0.003$	$-0.186 \pm 0.050 \pm 0.005$	$0.148 \pm 0.062 \pm 0.006$	$0.013 \pm 0.006 \pm 0.000$
[4., 6.]	$-0.106 \pm 0.037 \pm 0.004$	$-0.045 \pm 0.083 \pm 0.012$	$0.232 \pm 0.011 \pm 0.001$	$0.011 \pm 0.006 \pm 0.000$
[6., 8.]	$-0.089 \pm 0.021 \pm 0.007$	$0.074 \pm 0.072 \pm 0.015$	$0.190 \pm 0.032 \pm 0.008$	$0.007 \pm 0.005 \pm 0.000$
[15., 19.]	$-0.022 \pm 0.003 \pm 0.009$	$0.136 \pm 0.013 \pm 0.007$	$0.016 \pm 0.007 \pm 0.016$	$-0.017 \pm 0.007 \pm 0.007$

Bin	Q_4	Q_5	Q_6	Q_8
[0.1, 0.98]	$0.295 \pm 0.023 \pm 0.107$	$0.246 \pm 0.003 \pm 0.017$	$-0.017 \pm 0.007 \pm 0.002$	$-0.025 \pm 0.009 \pm 0.006$
[1.1, 2.5]	$0.233 \pm 0.050 \pm 0.045$	$0.271 \pm 0.016 \pm 0.013$	$-0.008 \pm 0.004 \pm 0.001$	$-0.030 \pm 0.012 \pm 0.003$
[2.5, 4.]	$0.031 \pm 0.068 \pm 0.021$	$0.347 \pm 0.021 \pm 0.017$	$-0.007 \pm 0.003 \pm 0.001$	$-0.025 \pm 0.013 \pm 0.001$
[4., 6.]	$-0.052 \pm 0.035 \pm 0.014$	$0.267 \pm 0.054 \pm 0.021$	$-0.008 \pm 0.003 \pm 0.000$	$-0.015 \pm 0.010 \pm 0.001$
[6., 8.]	$-0.082 \pm 0.022 \pm 0.017$	$0.153 \pm 0.071 \pm 0.038$	$-0.006 \pm 0.003 \pm 0.000$	$-0.008 \pm 0.008 \pm 0.001$
[15., 19.]	$-0.055 \pm 0.006 \pm 0.003$	$-0.009 \pm 0.008 \pm 0.021$	$-0.002 \pm 0.001 \pm 0.034$	$0.027 \pm 0.011 \pm 0.011$

Bin	$\hat{Q}_{F_L}$	$\hat{Q}_1$	$\hat{Q}_2$	$\hat{Q}_3$
[0.1, 0.98]	$-0.067 \pm 0.046 \pm 0.027$	$-0.048 \pm 0.011 \pm 0.019$	$-0.010 \pm 0.003 \pm 0.000$	$0.002 \pm 0.001 \pm 0.001$
[1.1, 2.5]	$-0.130 \pm 0.062 \pm 0.006$	$-0.202 \pm 0.021 \pm 0.005$	$-0.018 \pm 0.015 \pm 0.002$	$0.009 \pm 0.004 \pm 0.001$
[2.5, 4.]	$-0.108 \pm 0.070 \pm 0.003$	$-0.189 \pm 0.055 \pm 0.005$	$0.154 \pm 0.053 \pm 0.006$	$0.013 \pm 0.006 \pm 0.000$
[4., 6.]	$-0.089 \pm 0.045 \pm 0.004$	$-0.045 \pm 0.083 \pm 0.012$	$0.233 \pm 0.008 \pm 0.001$	$0.011 \pm 0.006 \pm 0.000$
[6., 8.]	$-0.076 \pm 0.025 \pm 0.007$	$0.075 \pm 0.071 \pm 0.015$	$0.189 \pm 0.031 \pm 0.008$	$0.007 \pm 0.006 \pm 0.000$
[15., 19.]	$-0.022 \pm 0.003 \pm 0.008$	$0.136 \pm 0.013 \pm 0.007$	$0.016 \pm 0.007 \pm 0.016$	$-0.017 \pm 0.007 \pm 0.007$

Bin	$\hat{Q}_4$	$\hat{Q}_5$	$\hat{Q}_6$	$\hat{Q}_8$
[0.1, 0.98]	$0.340 \pm 0.015 \pm 0.052$	$0.056 \pm 0.012 \pm 0.031$	$-0.002 \pm 0.002 \pm 0.003$	$-0.024 \pm 0.011 \pm 0.002$
[1.1, 2.5]	$0.227 \pm 0.053 \pm 0.041$	$0.255 \pm 0.015 \pm 0.010$	$-0.006 \pm 0.004 \pm 0.001$	$-0.031 \pm 0.013 \pm 0.003$
[2.5, 4.]	$0.025 \pm 0.074 \pm 0.020$	$0.348 \pm 0.021 \pm 0.017$	$-0.007 \pm 0.003 \pm 0.001$	$-0.025 \pm 0.013 \pm 0.001$
[4., 6.]	$-0.058 \pm 0.040 \pm 0.014$	$0.271 \pm 0.052 \pm 0.021$	$-0.008 \pm 0.003 \pm 0.000$	$-0.015 \pm 0.010 \pm 0.001$
[6., 8.]	$-0.089 \pm 0.024 \pm 0.016$	$0.159 \pm 0.069 \pm 0.038$	$-0.006 \pm 0.003 \pm 0.000$	$-0.009 \pm 0.008 \pm 0.001$
[15., 19.]	$-0.057 \pm 0.006 \pm 0.003$	$-0.008 \pm 0.008 \pm 0.021$	$-0.002 \pm 0.001 \pm 0.033$	$0.027 \pm 0.011 \pm 0.011$

Bin	T_3	T_4	T_5
[0.1, 0.98]	$--$	$--$	$-0.007 \pm 0.061 \pm 0.021$
[1.1, 2.5]	$--$	$--$	$0.436 \pm 0.158 \pm 0.080$
[2.5, 4.]	$--$	$0.091 \pm 0.149 \pm 0.012$	$-0.528 \pm 0.296 \pm 0.122$
[4., 6.]	$--$	$0.004 \pm 0.087 \pm 0.006$	$-0.161 \pm 0.090 \pm 0.029$
[6., 8.]	$--$	$-0.031 \pm 0.066 \pm 0.006$	$-0.074 \pm 0.075 \pm 0.032$
[15., 19.]	$-0.103 \pm 0.021 \pm 0.011$	$-0.031 \pm 0.004 \pm 0.003$	$-0.002 \pm 0.008 \pm 0.017$

Bin	T_7	T_8	T_9
[0.1, 0.98]	$-0.036 \pm 0.062 \pm 0.021$	$--$	$--$
[1.1, 2.5]	$0.081 \pm 0.105 \pm 0.021$	$-0.514 \pm 0.246 \pm 0.198$	$--$
[2.5, 4.]	$0.121 \pm 0.086 \pm 0.011$	$-0.322 \pm 0.117 \pm 0.059$	$0.830 \pm 0.290 \pm 0.082$
[4., 6.]	$0.136 \pm 0.069 \pm 0.008$	$-0.283 \pm 0.112 \pm 0.045$	$0.791 \pm 0.276 \pm 0.080$
[6., 8.]	$0.144 \pm 0.058 \pm 0.012$	$-0.304 \pm 0.312 \pm 0.100$	$--$
[15., 19.]	$0.177 \pm 0.005 \pm 0.009$	$--$	$--$

Bin	B_5	B_{6s}	M
[0.1, 0.98]	$-0.089 \pm 0.008 \pm 0.004$	$-0.086 \pm 0.005 \pm 0.001$	−−
[1.1, 2.5]	−−	$0.165 \pm 0.045 \pm 0.006$	$-0.194 \pm 0.047 \pm 0.011$
[2.5, 4.]	$-0.758 \pm 0.175 \pm 0.075$	−−	$-0.443 \pm 0.102 \pm 0.026$
[4., 6.]	$-0.455 \pm 0.049 \pm 0.025$	−−	$-0.710 \pm 0.182 \pm 0.060$
[6., 8.]	$-0.359 \pm 0.039 \pm 0.026$	$-0.549 \pm 0.145 \pm 0.031$	$-1.063 \pm 0.317 \pm 0.234$
[15., 19.]	$-0.305 \pm 0.007 \pm 0.017$	$-0.312 \pm 0.007 \pm 0.018$	−−

Bin	$\widetilde{B}_5$	$\widetilde{B}_{6s}$	$\widetilde{M}$
[0.1, 0.98]	$0.072 \pm 0.010 \pm 0.005$	$0.038 \pm 0.006 \pm 0.001$	$-0.080 \pm 0.016 \pm 0.006$
[1.1, 2.5]	−−	$0.197 \pm 0.046 \pm 0.006$	$-0.238 \pm 0.047 \pm 0.015$
[2.5, 4.]	$-0.755 \pm 0.177 \pm 0.076$	−−	$-0.447 \pm 0.098 \pm 0.026$
[4., 6.]	$-0.450 \pm 0.050 \pm 0.025$	−−	$-0.697 \pm 0.176 \pm 0.059$
[6., 8.]	$-0.355 \pm 0.039 \pm 0.026$	$-0.546 \pm 0.146 \pm 0.031$	$-1.038 \pm 0.308 \pm 0.229$
[15., 19.]	$-0.303 \pm 0.007 \pm 0.018$	$-0.310 \pm 0.007 \pm 0.018$	−−

D.5 Scenario 4: $\mathcal{C}_{9\mu}^{\text{NP}} = -\mathcal{C}_{9'\mu}^{\text{NP}} = -1.18$, $\mathcal{C}_{10\mu}^{\text{NP}} = \mathcal{C}_{10'\mu}^{\text{NP}} = 0.38$

Bin	Q_{F_L}	Q_1	Q_2	Q_3
[0.1, 0.98]	$-0.113 \pm 0.097 \pm 0.037$	$-0.063 \pm 0.010 \pm 0.004$	$0.006 \pm 0.001 \pm 0.001$	$0.002 \pm 0.001 \pm 0.000$
[1.1, 2.5]	$-0.167 \pm 0.044 \pm 0.009$	$-0.280 \pm 0.037 \pm 0.006$	$-0.044 \pm 0.009 \pm 0.003$	$0.010 \pm 0.004 \pm 0.001$
[2.5, 4.]	$-0.120 \pm 0.052 \pm 0.004$	$-0.371 \pm 0.045 \pm 0.005$	$0.146 \pm 0.071 \pm 0.007$	$0.016 \pm 0.007 \pm 0.000$
[4., 6.]	$-0.084 \pm 0.027 \pm 0.005$	$-0.236 \pm 0.092 \pm 0.013$	$0.230 \pm 0.014 \pm 0.004$	$0.014 \pm 0.008 \pm 0.000$
[6., 8.]	$-0.064 \pm 0.014 \pm 0.009$	$-0.078 \pm 0.087 \pm 0.018$	$0.175 \pm 0.033 \pm 0.008$	$0.009 \pm 0.007 \pm 0.000$
[15., 19.]	$-0.013 \pm 0.002 \pm 0.010$	$0.068 \pm 0.008 \pm 0.011$	$0.024 \pm 0.006 \pm 0.015$	$-0.020 \pm 0.009 \pm 0.008$
Bin	Q_4	Q_5	Q_6	Q_8
[0.1, 0.98]	$0.336 \pm 0.025 \pm 0.118$	$0.271 \pm 0.005 \pm 0.026$	$-0.018 \pm 0.007 \pm 0.003$	$-0.028 \pm 0.010 \pm 0.007$
[1.1, 2.5]	$0.276 \pm 0.052 \pm 0.052$	$0.337 \pm 0.022 \pm 0.006$	$-0.011 \pm 0.005 \pm 0.002$	$-0.034 \pm 0.014 \pm 0.003$
[2.5, 4.]	$0.089 \pm 0.066 \pm 0.025$	$0.430 \pm 0.021 \pm 0.013$	$-0.012 \pm 0.004 \pm 0.001$	$-0.026 \pm 0.014 \pm 0.002$
[4., 6.]	$0.018 \pm 0.035 \pm 0.017$	$0.324 \pm 0.059 \pm 0.019$	$-0.012 \pm 0.005 \pm 0.000$	$-0.016 \pm 0.011 \pm 0.001$
[6., 8.]	$-0.016 \pm 0.028 \pm 0.021$	$0.187 \pm 0.074 \pm 0.035$	$-0.008 \pm 0.005 \pm 0.000$	$-0.009 \pm 0.009 \pm 0.001$
[15., 19.]	$-0.027 \pm 0.004 \pm 0.004$	$0.017 \pm 0.008 \pm 0.020$	$-0.002 \pm 0.001 \pm 0.039$	$0.031 \pm 0.013 \pm 0.013$

Bin	$\hat{Q}_{F_L}$	$\hat{Q}_1$	$\hat{Q}_2$	$\hat{Q}_3$
[0.1, 0.98]	$-0.072 \pm 0.051 \pm 0.031$	$-0.055 \pm 0.012 \pm 0.020$	$-0.018 \pm 0.003 \pm 0.001$	$0.002 \pm 0.001 \pm 0.001$
[1.1, 2.5]	$-0.133 \pm 0.062 \pm 0.009$	$-0.277 \pm 0.034 \pm 0.006$	$-0.048 \pm 0.014 \pm 0.003$	$0.010 \pm 0.004 \pm 0.001$
[2.5, 4.]	$-0.094 \pm 0.062 \pm 0.004$	$-0.378 \pm 0.054 \pm 0.005$	$0.153 \pm 0.062 \pm 0.007$	$0.016 \pm 0.008 \pm 0.000$
[4., 6.]	$-0.065 \pm 0.034 \pm 0.005$	$-0.239 \pm 0.097 \pm 0.013$	$0.231 \pm 0.010 \pm 0.004$	$0.014 \pm 0.008 \pm 0.000$
[6., 8.]	$-0.051 \pm 0.017 \pm 0.009$	$-0.079 \pm 0.087 \pm 0.018$	$0.173 \pm 0.032 \pm 0.008$	$0.009 \pm 0.007 \pm 0.000$
[15., 19.]	$-0.013 \pm 0.002 \pm 0.010$	$0.068 \pm 0.009 \pm 0.011$	$0.024 \pm 0.006 \pm 0.015$	$-0.020 \pm 0.009 \pm 0.008$
Bin	$\hat{Q}_4$	$\hat{Q}_5$	$\hat{Q}_6$	$\hat{Q}_8$
[0.1, 0.98]	$0.372 \pm 0.016 \pm 0.060$	$0.076 \pm 0.014 \pm 0.041$	$-0.002 \pm 0.002 \pm 0.003$	$-0.027 \pm 0.012 \pm 0.003$
[1.1, 2.5]	$0.269 \pm 0.055 \pm 0.047$	$0.319 \pm 0.023 \pm 0.006$	$-0.008 \pm 0.005 \pm 0.002$	$-0.034 \pm 0.014 \pm 0.003$
[2.5, 4.]	$0.083 \pm 0.072 \pm 0.024$	$0.431 \pm 0.020 \pm 0.013$	$-0.011 \pm 0.005 \pm 0.001$	$-0.027 \pm 0.014 \pm 0.002$
[4., 6.]	$0.012 \pm 0.040 \pm 0.017$	$0.327 \pm 0.056 \pm 0.019$	$-0.012 \pm 0.005 \pm 0.000$	$-0.016 \pm 0.011 \pm 0.001$
[6., 8.]	$-0.023 \pm 0.030 \pm 0.021$	$0.192 \pm 0.072 \pm 0.034$	$-0.008 \pm 0.005 \pm 0.000$	$-0.009 \pm 0.009 \pm 0.001$
[15., 19.]	$-0.029 \pm 0.004 \pm 0.004$	$0.018 \pm 0.008 \pm 0.020$	$-0.002 \pm 0.001 \pm 0.039$	$0.031 \pm 0.013 \pm 0.013$

Bin	T_3	T_4	T_5
$[0.1, 0.98]$	$--$	$--$	$0.002 \pm 0.065 \pm 0.027$
$[1.1, 2.5]$	$0.991 \pm 0.188 \pm 0.182$	$--$	$0.488 \pm 0.162 \pm 0.090$
$[2.5, 4.]$	$1.010 \pm 0.231 \pm 0.028$	$0.133 \pm 0.149 \pm 0.012$	$-0.809 \pm 0.524 \pm 0.177$
$[4., 6.]$	$--$	$0.040 \pm 0.074 \pm 0.007$	$-0.222 \pm 0.085 \pm 0.032$
$[6., 8.]$	$--$	$0.002 \pm 0.050 \pm 0.008$	$-0.101 \pm 0.063 \pm 0.030$
$[15., 19.]$	$-0.047 \pm 0.010 \pm 0.014$	$-0.016 \pm 0.002 \pm 0.004$	$-0.021 \pm 0.007 \pm 0.017$
Bin	T_7	T_8	T_9
$[0.1, 0.98]$	$-0.034 \pm 0.066 \pm 0.023$	$--$	$--$
$[1.1, 2.5]$	$0.094 \pm 0.107 \pm 0.023$	$-0.614 \pm 0.296 \pm 0.250$	$0.974 \pm 0.486 \pm 0.234$
$[2.5, 4.]$	$0.146 \pm 0.076 \pm 0.012$	$-0.371 \pm 0.120 \pm 0.072$	$0.849 \pm 0.264 \pm 0.074$
$[4., 6.]$	$0.170 \pm 0.053 \pm 0.009$	$-0.319 \pm 0.112 \pm 0.055$	$0.817 \pm 0.252 \pm 0.071$
$[6., 8.]$	$0.183 \pm 0.040 \pm 0.013$	$-0.346 \pm 0.371 \pm 0.126$	$--$
$[15., 19.]$	$0.205 \pm 0.004 \pm 0.011$	$--$	$--$

Bin	B_5	B_{6s}	M
$[0.1, 0.98]$	$-0.075 \pm 0.010 \pm 0.009$	$-0.166 \pm 0.009 \pm 0.003$	$-0.138 \pm 0.031 \pm 0.031$
$[1.1, 2.5]$	$--$	$0.059 \pm 0.048 \pm 0.005$	$-0.062 \pm 0.051 \pm 0.006$
$[2.5, 4.]$	$-0.916 \pm 0.202 \pm 0.077$	$--$	$-0.446 \pm 0.163 \pm 0.022$
$[4., 6.]$	$-0.552 \pm 0.052 \pm 0.024$	$--$	$-1.009 \pm 0.337 \pm 0.079$
$[6., 8.]$	$-0.439 \pm 0.038 \pm 0.021$	$-0.577 \pm 0.119 \pm 0.028$	$-1.888 \pm 0.668 \pm 0.376$
$[15., 19.]$	$-0.369 \pm 0.007 \pm 0.016$	$-0.374 \pm 0.007 \pm 0.017$	$--$

Bin	$\widetilde{B}_5$	$\widetilde{B}_{6s}$	$\widetilde{M}$
$[0.1, 0.98]$	$0.088 \pm 0.013 \pm 0.012$	$-0.054 \pm 0.011 \pm 0.003$	$0.033 \pm 0.003 \pm 0.002$
$[1.1, 2.5]$	$--$	$0.088 \pm 0.050 \pm 0.006$	$-0.094 \pm 0.054 \pm 0.007$
$[2.5, 4.]$	$-0.916 \pm 0.205 \pm 0.078$	$--$	$-0.453 \pm 0.159 \pm 0.023$
$[4., 6.]$	$-0.548 \pm 0.053 \pm 0.024$	$--$	$-0.994 \pm 0.328 \pm 0.078$
$[6., 8.]$	$-0.436 \pm 0.038 \pm 0.021$	$-0.575 \pm 0.119 \pm 0.028$	$-1.851 \pm 0.651 \pm 0.369$
$[15., 19.]$	$-0.367 \pm 0.007 \pm 0.016$	$-0.372 \pm 0.007 \pm 0.017$	$--$

D.6 R_{K^*}

R_{K^*}				
Bin	$[0.1, 2]$	$[2, 4.3]$	$[4.3, 8.68]$	$[16., 19.]$
SM	$0.988 \pm 0.007 \pm 0.001$	$1.000 \pm 0.006 \pm 0.000$	$1.000 \pm 0.005 \pm 0.000$	$0.998 \pm 0.000 \pm 0.000$
Scen.1	$0.951 \pm 0.096 \pm 0.021$	$0.871 \pm 0.093 \pm 0.009$	$0.813 \pm 0.026 \pm 0.029$	$0.786 \pm 0.001 \pm 0.004$
Scen.2	$0.889 \pm 0.102 \pm 0.008$	$0.737 \pm 0.028 \pm 0.005$	$0.701 \pm 0.016 \pm 0.045$	$0.701 \pm 0.003 \pm 0.006$
Scen.3	$0.898 \pm 0.142 \pm 0.039$	$0.780 \pm 0.142 \pm 0.018$	$0.747 \pm 0.090 \pm 0.045$	$0.692 \pm 0.006 \pm 0.013$
Scen.4	$0.890 \pm 0.149 \pm 0.043$	$0.742 \pm 0.123 \pm 0.019$	$0.690 \pm 0.059 \pm 0.052$	$0.655 \pm 0.005 \pm 0.015$

Appendix E

Full list of observables used in the fit

Fit to All Data			
$10^7 \times BR(B^+ \to K^+\mu^+\mu^-)$[LHCb]	Standard Model	Experiment	Pull
$[0.1, 0.98]$	0.31 ± 0.10	0.29 ± 0.02	$+0.2$
$[1.1, 2]$	0.32 ± 0.10	0.21 ± 0.02	$+1.1$
$[2, 3]$	0.35 ± 0.11	0.28 ± 0.02	$+0.6$
$[3, 4]$	0.35 ± 0.11	0.25 ± 0.02	$+0.8$
$[4, 5]$	0.34 ± 0.11	0.22 ± 0.02	$+1.1$
$[5, 6]$	0.34 ± 0.12	0.23 ± 0.02	$+0.9$
$[6, 7]$	0.34 ± 0.12	0.25 ± 0.02	$+0.8$
$[7, 8]$	0.34 ± 0.13	0.23 ± 0.02	$+0.8$
$[15, 22]$	0.97 ± 0.13	0.85 ± 0.05	$+0.9$
$10^7 \times BR(B^0 \to K^0\mu^+\mu^-)$[LHCb]	Standard Model	Experiment	Pull
$[0.1, 2]$	0.62 ± 0.19	0.23 ± 0.11	$+1.8$
$[2, 4]$	0.64 ± 0.20	0.37 ± 0.11	$+1.2$
$[4, 6]$	0.63 ± 0.21	0.35 ± 0.10	$+1.2$
$[6, 8]$	0.63 ± 0.23	0.54 ± 0.12	$+0.3$
$[15, 22]$	0.90 ± 0.12	0.67 ± 0.12	$+1.4$
$10^7 \times BR(B^0 \to K^{*0}\mu^+\mu^-)$[LHCb]	Standard Model	Experiment	Pull
$[0.1, 0.98]$	0.90 ± 0.83	0.89 ± 0.09	$+0.0$
$[1.1, 2.5]$	0.54 ± 0.34	0.46 ± 0.06	$+0.2$
$[2.5, 4]$	0.62 ± 0.43	0.50 ± 0.06	$+0.3$
$[4, 6]$	0.88 ± 0.65	0.71 ± 0.07	$+0.3$
$[6, 8]$	1.09 ± 0.89	0.86 ± 0.08	$+0.3$
$[15, 19]$	2.40 ± 0.23	1.74 ± 0.14	$+2.4$
$10^7 \times BR(B^+ \to K^{*+}\mu^+\mu^-)$[LHCb]	Standard Model	Experiment	Pull
$[0.1, 2]$	1.36 ± 1.10	1.12 ± 0.27	$+0.2$
$[2, 4]$	0.81 ± 0.55	1.12 ± 0.32	-0.5
$[4, 6]$	0.96 ± 0.71	0.50 ± 0.20	$+0.6$

$[6, 8]$	1.18 ± 0.96	0.66 ± 0.22	$+0.5$
$[15, 19]$	2.59 ± 0.25	1.60 ± 0.32	$+2.4$

$10^7 \times BR(B_s \to \phi\mu^+\mu^-)$[LHCb]	Standard Model	Experiment	Pull
$[0.1, 2.]$	1.55 ± 0.34	1.11 ± 0.16	$+1.2$
$[2., 5.]$	1.55 ± 0.32	0.77 ± 0.14	$+2.3$
$[5., 8.]$	1.88 ± 0.39	0.96 ± 0.15	$+2.2$
$[15, 18.8]$	2.20 ± 0.17	1.62 ± 0.20	$+2.2$

$F_L(B \to K^*\mu^+\mu^-)$[LHCb]	Standard Model	Experiment	Pull
$[0.1, 0.98]$	0.22 ± 0.24	0.26 ± 0.05	-0.2
$[1.1, 2.5]$	0.67 ± 0.28	0.66 ± 0.09	$+0.0$
$[2.5, 4]$	0.76 ± 0.24	0.88 ± 0.11	-0.4
$[4, 6]$	0.71 ± 0.29	0.61 ± 0.06	$+0.3$
$[6, 8]$	0.62 ± 0.33	0.58 ± 0.05	$+0.1$
$[15, 19]$	0.34 ± 0.03	0.34 ± 0.03	-0.1

$P_1(B \to K^*\mu^+\mu^-)$[LHCb]	Standard Model	Experiment	Pull
$[0.1, 0.98]$	0.03 ± 0.08	-0.10 ± 0.17	$+0.7$
$[1.1, 2.5]$	-0.00 ± 0.06	-0.45 ± 0.64	$+0.7$
$[2.5, 4]$	0.00 ± 0.06	0.57 ± 2.40	-0.2
$[4, 6]$	0.02 ± 0.12	0.18 ± 0.37	-0.4
$[6, 8]$	0.02 ± 0.13	-0.20 ± 0.28	$+0.7$
$[15, 19]$	-0.64 ± 0.06	-0.50 ± 0.11	-1.2

$P_2(B \to K^*\mu^+\mu^-)$[LHCb]	Standard Model	Experiment	Pull
$[0.1, 0.98]$	0.12 ± 0.02	0.00 ± 0.05	$+2.1$
$[1.1, 2.5]$	0.44 ± 0.02	0.37 ± 0.20	$+0.3$
$[2.5, 4]$	0.20 ± 0.12	0.64 ± 1.74	-0.2
$[4, 6]$	-0.19 ± 0.10	-0.04 ± 0.09	-1.1
$[6, 8]$	-0.38 ± 0.06	-0.24 ± 0.06	-1.5
$[15, 19]$	-0.36 ± 0.02	-0.36 ± 0.03	-0.0

$P_3(B \to K^*\mu^+\mu^-)$[LHCb]	Standard Model	Experiment	Pull
$[0.1, 0.98]$	-0.00 ± 0.00	-0.11 ± 0.08	$+1.4$
$[1.1, 2.5]$	0.00 ± 0.00	-0.35 ± 0.33	$+1.1$
$[2.5, 4]$	0.00 ± 0.01	-0.75 ± 2.59	$+0.3$
$[4, 6]$	0.00 ± 0.01	-0.08 ± 0.19	$+0.5$
$[6, 8]$	0.00 ± 0.00	-0.06 ± 0.15	$+0.4$
$[15, 19]$	0.00 ± 0.02	-0.08 ± 0.06	$+1.3$

$P_4'(B \to K^*\mu^+\mu^-)$[LHCb]	Standard Model	Experiment	Pull
$[0.1, 0.98]$	-0.49 ± 0.17	-0.37 ± 0.32	-0.3
$[1.1, 2.5]$	-0.06 ± 0.16	0.33 ± 0.48	-0.8
$[2.5, 4]$	0.55 ± 0.20	1.43 ± 2.61	-0.3

[4, 6]	0.82 ± 0.14	0.90 ± 0.35	-0.2
[6, 8]	0.93 ± 0.11	1.20 ± 0.27	-0.9
[15, 19]	1.28 ± 0.02	1.19 ± 0.17	$+0.5$

$P'_5(B \to K^* \mu^+ \mu^-)$[LHCb]	Standard Model	Experiment	Pull
[0.1, 0.98]	0.67 ± 0.14	0.39 ± 0.14	$+1.4$
[1.1, 2.5]	0.19 ± 0.12	0.29 ± 0.22	-0.4
[2.5, 4]	-0.49 ± 0.11	-0.07 ± 0.36	-1.1
[4, 6]	-0.82 ± 0.08	-0.30 ± 0.16	-2.9
[6, 8]	-0.94 ± 0.08	-0.51 ± 0.12	-3.0
[15, 19]	-0.57 ± 0.05	-0.68 ± 0.08	$+1.2$

$P'_6(B \to K^* \mu^+ \mu^-)$[LHCb]	Standard Model	Experiment	Pull
[0.1, 0.98]	-0.06 ± 0.02	0.03 ± 0.14	-0.7
[1.1, 2.5]	-0.07 ± 0.03	-0.46 ± 0.22	$+1.8$
[2.5, 4]	-0.06 ± 0.03	0.21 ± 0.96	-0.3
[4, 6]	-0.04 ± 0.02	-0.03 ± 0.17	-0.0
[6, 8]	-0.02 ± 0.01	-0.10 ± 0.17	$+0.4$
[15, 19]	-0.00 ± 0.07	0.10 ± 0.09	-0.9

$P'_8(B \to K^* \mu^+ \mu^-)$[LHCb]	Standard Model	Experiment	Pull
[0.1, 0.98]	0.02 ± 0.02	-0.36 ± 0.35	$+1.1$
[1.1, 2.5]	0.04 ± 0.03	0.42 ± 0.54	-0.7
[2.5, 4]	0.04 ± 0.02	-0.18 ± 1.30	$+0.2$
[4, 6]	0.03 ± 0.02	-0.68 ± 0.38	$+1.9$
[6, 8]	0.02 ± 0.01	0.34 ± 0.29	-1.1
[15, 19]	-0.00 ± 0.03	-0.12 ± 0.19	$+0.6$

$P_1(B_s \to \phi \mu^+ \mu^-)$[LHCb]	Standard Model	Experiment	Pull
[0.1, 2.]	0.11 ± 0.08	-0.13 ± 0.33	$+0.7$
[2., 5.]	-0.11 ± 0.10	-0.38 ± 1.47	$+0.2$
[5., 8.]	-0.21 ± 0.11	-0.44 ± 1.27	$+0.2$
[15, 18.8]	-0.69 ± 0.03	-0.25 ± 0.34	-1.3

$P'_4(B_s \to \phi \mu^+ \mu^-)$[LHCb]	Standard Model	Experiment	Pull
[0.1, 2.]	-0.28 ± 0.14	-1.35 ± 1.46	$+0.7$
[2., 5.]	0.81 ± 0.11	2.02 ± 1.84	-0.7
[5., 8.]	1.06 ± 0.06	0.40 ± 0.72	$+0.9$
[15, 18.8]	1.30 ± 0.01	0.62 ± 0.49	$+1.4$

$P'_6(B_s \to \phi \mu^+ \mu^-)$[LHCb]	Standard Model	Experiment	Pull
[0.1, 2.]	-0.07 ± 0.02	0.10 ± 0.30	-0.6
[2., 5.]	-0.05 ± 0.02	-0.06 ± 0.49	$+0.0$
[5., 8.]	-0.02 ± 0.01	0.08 ± 0.40	-0.2
[15, 18.8]	-0.00 ± 0.07	0.29 ± 0.24	-1.1

$F_L(B_s \to \phi\mu^+\mu^-)$[LHCb]	Standard Model	Experiment	Pull
$[0.1, 2.]$	0.43 ± 0.09	0.20 ± 0.09	$+1.8$
$[2., 5.]$	0.77 ± 0.05	0.68 ± 0.16	$+0.5$
$[5., 8.]$	0.61 ± 0.06	0.54 ± 0.10	$+0.6$
$[15, 18.8]$	0.36 ± 0.02	0.29 ± 0.07	$+0.9$

$B^0 \to K^{*0}e^+e^-$[LHCb]	Standard Model	Experiment	Pull
$F_L[0.0020, 1.120]$	0.11 ± 0.16	0.16 ± 0.07	-0.3
$P_1[0.0020, 1.120]$	0.03 ± 0.08	-0.23 ± 0.24	$+1.0$
$P_2[0.0020, 1.120]$	0.03 ± 0.00	0.05 ± 0.09	-0.2
$P_3[0.0020, 1.120]$	-0.00 ± 0.00	-0.07 ± 0.11	$+0.6$

R_K[LHCb Average]	Standard Model	Experiment	Pull
$[1.1, 6.0]$	1.00 ± 0.00	0.85 ± 0.06	$+2.5$

R_K[Belle]	Standard Model	Experiment	Pull
$[1.0, 6.0]$	1.00 ± 0.00	0.98 ± 0.28	$+0.1$
$[14.18, 22.90]$	1.00 ± 0.00	1.11 ± 0.30	-0.4

R_{K^*}[LHCb]	Standard Model	Experiment	Pull
$[0.045, 1.1]$	0.91 ± 0.02	0.66 ± 0.11	$+2.2$
$[1.1, 6.0]$	1.00 ± 0.01	0.69 ± 0.12	$+2.6$

R_{K^*}[Belle]	Standard Model	Experiment	Pull
$[0.045, 1.1]$	0.92 ± 0.02	0.52 ± 0.36	$+1.1$
$[1.1, 6.0]$	1.00 ± 0.01	0.96 ± 0.46	$+0.1$
$[15, 19]$	1.00 ± 0.00	1.18 ± 0.53	-0.5

$P_4'(B \to K^*e^+e^-)$[Belle]	Standard Model	Experiment	Pull
$[0.1, 4.]$	-0.09 ± 0.15	-0.68 ± 0.93	$+0.6$
$[4., 8.]$	0.88 ± 0.12	1.04 ± 0.48	-0.3
$[14.18, 19.]$	1.26 ± 0.03	0.30 ± 0.82	$+1.2$

$P_4'(B \to K^*\mu^+\mu^-)$[Belle]	Standard Model	Experiment	Pull
$[0.1, 4.]$	-0.05 ± 0.16	0.76 ± 1.03	-0.8
$[4., 8.]$	0.88 ± 0.12	0.14 ± 0.66	$+1.1$
$[14.18, 19.]$	1.26 ± 0.03	0.20 ± 0.79	$+1.3$

$P_5'(B \to K^*e^+e^-)$[Belle]	Standard Model	Experiment	Pull
$[0.1, 4.]$	0.18 ± 0.09	0.51 ± 0.47	-0.7
$[4., 8.]$	-0.88 ± 0.07	-0.52 ± 0.28	-1.3
$[14.18, 19.]$	-0.60 ± 0.05	-0.91 ± 0.36	$+0.8$

$P_5'(B \to K^*\mu^+\mu^-)$[Belle]	Standard Model	Experiment	Pull
$[0.1, 4.]$	0.17 ± 0.10	0.42 ± 0.41	-0.6
$[4., 8.]$	-0.89 ± 0.07	-0.03 ± 0.32	-2.7

[14.18, 19.]	-0.60 ± 0.05	-0.13 ± 0.39	-1.3

$F_L(B \to K^*\mu^+\mu^-)$[ATLAS]	Standard Model	Experiment	Pull
[0.04, 2.]	0.35 ± 0.31	0.44 ± 0.11	-0.3
[2., 4.]	0.75 ± 0.24	0.64 ± 0.12	$+0.4$
[4., 6.]	0.71 ± 0.29	0.42 ± 0.18	$+0.8$

$P_1(B \to K^*\mu^+\mu^-)$[ATLAS]	Standard Model	Experiment	Pull
[0.04, 2.]	0.02 ± 0.08	-0.06 ± 0.32	$+0.2$
[2., 4.]	-0.00 ± 0.05	-0.78 ± 0.66	$+1.2$
[4., 6.]	0.02 ± 0.12	0.00 ± 0.54	$+0.0$

$P_4'(B \to K^*\mu^+\mu^-)$[ATLAS]	Standard Model	Experiment	Pull
[0.04, 2.]	-0.35 ± 0.15	-0.78 ± 1.14	$+0.4$
[2., 4.]	0.44 ± 0.20	1.92 ± 0.94	-1.5
[4., 6.]	0.82 ± 0.14	-1.62 ± 0.97	$+2.5$

$P_5'(B \to K^*\mu^+\mu^-)$[ATLAS]	Standard Model	Experiment	Pull
[0.04, 2.]	0.50 ± 0.10	0.67 ± 0.31	-0.5
[2., 4.]	-0.36 ± 0.12	-0.33 ± 0.34	-0.1
[4., 6.]	-0.82 ± 0.08	0.26 ± 0.39	-2.7

$P_6'(B \to K^*\mu^+\mu^-)$[ATLAS]	Standard Model	Experiment	Pull
[0.04, 2.]	-0.06 ± 0.02	-0.18 ± 0.21	$+0.6$
[2., 4.]	-0.06 ± 0.03	0.31 ± 0.34	-1.1
[4., 6.]	-0.04 ± 0.02	0.06 ± 0.30	-0.3

$P_8'(B \to K^*\mu^+\mu^-)$[ATLAS]	Standard Model	Experiment	Pull
[0.04, 2.]	0.03 ± 0.02	0.44 ± 0.81	-0.5
[2., 4.]	0.05 ± 0.02	-1.68 ± 0.89	$+1.9$
[4., 6.]	0.03 ± 0.02	0.38 ± 0.67	-0.5

$P_1(B \to K^*\mu^+\mu^-)$[CMS 8 TeV]	Standard Model	Experiment	Pull
[1., 2.]	0.00 ± 0.06	0.12 ± 0.47	-0.3
[2., 4.3]	0.00 ± 0.05	-0.69 ± 0.59	$+1.2$
[4.3, 6.]	0.02 ± 0.12	0.53 ± 0.38	-1.3
[6., 8.68]	0.01 ± 0.14	-0.47 ± 0.30	$+1.5$
[16., 19.]	-0.69 ± 0.05	-0.53 ± 0.23	-0.7

$P_5'(B \to K^*\mu^+\mu^-)$[CMS 8 TeV]	Standard Model	Experiment	Pull
[1., 2.]	0.33 ± 0.11	0.10 ± 0.34	$+0.6$
[2., 4.3]	-0.41 ± 0.12	-0.57 ± 0.37	$+0.4$
[4.3, 6.]	-0.84 ± 0.07	-0.96 ± 0.27	$+0.4$
[6., 8.68]	-0.95 ± 0.08	-0.64 ± 0.24	-1.2
[16., 19.]	-0.53 ± 0.04	-0.56 ± 0.14	$+0.2$

$F_L(B \to K^*\mu^+\mu^-)$[CMS 8 TeV]	Standard Model	Experiment	Pull
$[1., 2.]$	0.62 ± 0.30	0.64 ± 0.12	-0.1
$[2., 4.3]$	0.75 ± 0.24	0.80 ± 0.10	-0.2
$[4.3, 6.]$	0.70 ± 0.30	0.62 ± 0.12	$+0.2$
$[6., 8.68]$	0.61 ± 0.33	0.50 ± 0.08	$+0.3$
$[16., 19.]$	0.34 ± 0.03	0.38 ± 0.07	-0.6

$A_{FB}(B \to K^*\mu^+\mu^-)$[CMS 8 TeV]	Standard Model	Experiment	Pull
$[1., 2.]$	-0.20 ± 0.19	-0.27 ± 0.41	$+0.2$
$[2., 4.3]$	-0.08 ± 0.08	-0.12 ± 0.18	$+0.2$
$[4.3, 6.]$	0.10 ± 0.12	0.01 ± 0.15	$+0.4$
$[6., 8.68]$	0.23 ± 0.21	0.03 ± 0.10	$+0.8$
$[16., 19.]$	0.34 ± 0.03	0.35 ± 0.07	-0.1

$10^7 \times BR(B \to K^*\mu^+\mu^-)$[CMS 8 TeV]	Standard Model	Experiment	Pull
$[1., 2.]$	0.40 ± 0.26	0.46 ± 0.08	-0.2
$[2., 4.3]$	0.86 ± 0.59	0.76 ± 0.12	$+0.2$
$[4.3, 6.]$	0.84 ± 0.63	0.58 ± 0.10	$+0.4$
$[6., 8.68]$	1.52 ± 1.26	1.26 ± 0.13	$+0.2$
$[16., 19.]$	1.65 ± 0.15	1.26 ± 0.13	$+2.0$

$F_L(B \to K^*\mu^+\mu^-)$[CMS 7 TeV]	Standard Model	Experiment	Pull
$[1., 2.]$	0.62 ± 0.30	0.60 ± 0.34	$+0.1$
$[2., 4.3]$	0.75 ± 0.24	0.65 ± 0.17	$+0.3$
$[4.3, 8.68]$	0.63 ± 0.33	0.81 ± 0.14	-0.5
$[16., 19.]$	0.34 ± 0.03	0.44 ± 0.08	-1.3

$A_{FB}(B \to K^*\mu^+\mu^-)$[CMS 7 TeV]	Standard Model	Experiment	Pull
$[1., 2.]$	-0.20 ± 0.19	-0.29 ± 0.41	$+0.2$
$[2., 4.3]$	-0.08 ± 0.08	-0.07 ± 0.20	-0.1
$[4.3, 8.68]$	0.19 ± 0.19	-0.01 ± 0.11	$+0.9$
$[16., 19.]$	0.34 ± 0.03	0.41 ± 0.06	-1.1

$10^7 \times BR(B \to K^*\mu^+\mu^-)$[CMS 7 TeV]	Standard Model	Experiment	Pull
$[1., 2.]$	0.40 ± 0.26	0.48 ± 0.15	-0.3
$[2., 4.3]$	0.86 ± 0.59	0.87 ± 0.18	-0.0
$[4.3, 8.68]$	2.60 ± 2.74	1.62 ± 0.35	$+0.4$
$[16., 19.]$	1.65 ± 0.15	1.56 ± 0.23	$+0.3$

$10^5 \times BR(B^0 \to K^{*0}\gamma)$[PDG]	Standard Model	Experiment	Pull
	4.53 ± 5.51	4.33 ± 0.15	$+0.0$

$10^5 \times BR(B^+ \to K^{*+}\gamma)$[PDG]	Standard Model	Experiment	Pull
	4.50 ± 5.70	4.21 ± 0.18	$+0.1$

$10^5 \times BR(B_s \to \phi\gamma)$[PDG]	Standard Model	Experiment	Pull

	4.66 ± 1.29	3.50 ± 0.40	$+0.9$

Bibliography

[1] B. Capdevila, S. Descotes-Genon, L. Hofer and J. Matias, *Hadronic uncertainties in $B \to K^*\mu^+\mu^-$: a state-of-the-art analysis*, *JHEP* **04** (2017) 016, [1701.08672].

[2] B. Capdevila, S. Descotes-Genon, J. Matias and J. Virto, *Assessing lepton-flavour non-universality from $B \to K^*\ell\ell$ angular analyses*, *JHEP* **10** (2016) 075, [1605.03156].

[3] B. Capdevila, A. Crivellin, S. Descotes-Genon, L. Hofer and J. Matias, *Searching for New Physics with $b \to s\tau^+\tau^-$ processes*, *Phys. Rev. Lett.* **120** (2018) 181802, [1712.01919].

[4] K. G. Wilson, *Nonlagrangian models of current algebra*, *Phys. Rev.* **179** (1969) 1499–1512.

[5] W. Zimmermann, *Composite operators in the perturbation theory of renormalizable interactions*, *Annals Phys.* **77** (1973) 536–569.

[6] E. Witten, *Short distance analysis of weak interactions*, *Nuclear Physics B* **122** (Apr., 1977) 109–143.

[7] G. Buchalla, A. J. Buras and M. E. Lautenbacher, *Weak decays beyond leading logarithms*, *Rev. Mod. Phys.* **68** (1996) 1125–1144, [hep-ph/9512380].

[8] M. Neubert, *Effective field theory and heavy quark physics*, in *Physics in $D \geq 4$. Proceedings, Theoretical Advanced Study Institute in elementary particle physics, TASI 2004, Boulder, USA, June 6-July 2, 2004*, pp. 149–194, 2005. hep-ph/0512222. DOI.

[9] A. Pich, *Effective field theory: Course*, in *Probing the standard model of particle interactions. Proceedings, Summer School in Theoretical Physics, NATO Advanced Study Institute, 68th session, Les Houches, France, July 28-September 5, 1997. Pt. 1, 2*, pp. 949–1049, 1998. hep-ph/9806303.

[10] C. P. Burgess, *Introduction to Effective Field Theory*, *Ann. Rev. Nucl. Part. Sci.* **57** (2007) 329–362, [hep-th/0701053].

[11] G. Buchalla, *Heavy quark theory*, in *Heavy flavor physics: Theory and experimental results in heavy quark physics and CP violation. Proceedings, 55th Scottish Universities Summer School in Physics, SUSSP 2001, St. Andrews, UK, August 7-23, 2001*, pp. 57–104, 2002. hep-ph/0202092.

[12] M. Neubert, *Heavy quark effective theory*, *Subnucl. Ser.* **34** (1997) 98–165, [hep-ph/9610266].

[13] M. Neubert, *Heavy quark symmetry*, *Phys. Rept.* **245** (1994) 259–396, [hep-ph/9306320].

[14] E. Eichten and F. Feinberg, *Spin Dependent Forces in QCD*, *Phys. Rev.* **D23** (1981) 2724.

[15] W. E. Caswell and G. P. Lepage, *Effective Lagrangians for Bound State Problems in QED, QCD, and Other Field Theories*, *Phys. Lett.* **167B** (1986) 437–442.

[16] E. Eichten, *Heavy Quarks on the Lattice*, *Nucl. Phys. Proc. Suppl.* **4** (1988) 170.

[17] E. Eichten and B. R. Hill, *An Effective Field Theory for the Calculation of Matrix Elements Involving Heavy Quarks*, *Phys. Lett.* **B234** (1990) 511–516.

[18] H. D. Politzer and M. B. Wise, *Leading Logarithms of Heavy Quark Masses in Processes with Light and Heavy Quarks*, *Phys. Lett.* **B206** (1988) 681–684.

[19] B. Grinstein, *The Static Quark Effective Theory*, *Nucl. Phys.* **B339** (1990) 253–268.

[20] A. F. Falk, H. Georgi, B. Grinstein and M. B. Wise, *Heavy Meson Form-factors From QCD*, *Nucl. Phys.* **B343** (1990) 1–13.

[21] T. Mannel, W. Roberts and Z. Ryzak, *A Derivation of the heavy quark effective Lagrangian from QCD*, *Nucl. Phys.* **B368** (1992) 204–217.

[22] N. Isgur and M. B. Wise, *Weak Decays of Heavy Mesons in the Static Quark Approximation*, *Phys. Lett.* **B232** (1989) 113–117.

[23] N. Isgur and M. B. Wise, *WEAK TRANSITION FORM-FACTORS BETWEEN HEAVY MESONS*, *Phys. Lett.* **B237** (1990) 527–530.

[24] J. Charles, A. Le Yaouanc, L. Oliver, O. Pene and J. C. Raynal, *Heavy to light form-factors in the heavy mass to large energy limit of QCD*, *Phys. Rev.* **D60** (1999) 014001, [hep-ph/9812358].

[25] M. J. Dugan and B. Grinstein, *QCD basis for factorization in decays of heavy mesons*, *Phys. Lett.* **B255** (1991) 583–588.

[26] E. de Rafael, *An Introduction to sum rules in QCD: Course*, in *Probing the standard model of particle interactions. Proceedings, Summer School in Theoretical Physics, NATO Advanced Study Institute, 68th session, Les Houches, France, July 28-September 5, 1997. Pt. 1, 2*, pp. 1171–1218, 1997. hep-ph/9802448.

[27] P. Colangelo and A. Khodjamirian, *QCD sum rules, a modern perspective*, hep-ph/0010175.

[28] A. Khodjamirian, *Applications of QCD Sum Rules to Heavy Quark Physics*, in *Proceedings, Helmholtz International Summer School on Physics of Heavy Quarks and Hadrons (HQ 2013): JINR, Dubna, Russia, July 15-28, 2013*, pp. 109–138, 2014. 1312.6480. DOI.

[29] M. Beneke and T. Feldmann, *Symmetry breaking corrections to heavy to light B meson form-factors at large recoil*, *Nucl. Phys.* **B592** (2001) 3–34, [hep-ph/0008255].

[30] M. Beneke, T. Feldmann and D. Seidel, *Systematic approach to exclusive $B \to V l^+ l^-$, $V\gamma$ decays*, *Nucl. Phys.* **B612** (2001) 25–58, [hep-ph/0106067].

[31] W. Altmannshofer, P. Ball, A. Bharucha, A. J. Buras, D. M. Straub and M. Wick, *Symmetries and Asymmetries of $B \to K^* \mu^+ \mu^-$ Decays in the Standard Model and Beyond*, *JHEP* **01** (2009) 019, [0811.1214].

[32] P. Ball and V. M. Braun, *Exclusive semileptonic and rare B meson decays in QCD*, *Phys. Rev.* **D58** (1998) 094016, [hep-ph/9805422].

[33] M. Beneke, T. Feldmann and D. Seidel, *Exclusive radiative and electroweak $b \to d$ and $b \to s$ penguin decays at NLO*, *Eur. Phys. J.* **C41** (2005) 173–188, [hep-ph/0412400].

[34] M. Neubert and B. Stech, *Nonleptonic weak decays of B mesons*, *Adv. Ser. Direct. High Energy Phys.* **15** (1998) 294–344, [hep-ph/9705292].

[35] M. Bauer and B. Stech, *Exclusive D-decays*, *Physics Letters B* **152** (1985) 380 – 384.

[36] M. Bauer, B. Stech and M. Wirbel, *Exclusive Nonleptonic Decays of D, D(s), and B Mesons*, *Z. Phys.* **C34** (1987) 103.

[37] M. Beneke, G. Buchalla, M. Neubert and C. T. Sachrajda, *QCD factorization for B —¿ pi pi decays: Strong phases and CP violation in the heavy quark limit*, *Phys. Rev. Lett.* **83** (1999) 1914–1917, [hep-ph/9905312].

[38] J. Virto, *Topics in Hadronic B Decays*. PhD thesis, Barcelona, IFAE, 2008. 0712.3367.

[39] M. Ramon, *Looking for new physics in the $\bar{B}_d^0 \to \bar{K}^{*0}(\to K\pi)\ell^+\ell^-$ decay mode at large recoil*. PhD thesis, Barcelona, IFAE.

[40] G. Bell, *Higher order QCD corrections in exclusive charmless B decays*. PhD thesis, Munich U., 2006. 0705.3133.

[41] S. W. Bosch, *Exclusive radiative decays of B mesons in QCD factorization*. PhD thesis, Munich, Max Planck Inst., 2002. hep-ph/0208203.

[42] J. D. Bjorken, *Topics in B Physics*, *Nucl. Phys. Proc. Suppl.* **11** (1989) 325–341.

[43] M. Neubert, *Aspects of QCD factorization*, *AIP Conf. Proc.* **602** (2001) 168–179, [hep-ph/0110093].

[44] J. M. Soares, *"Nonfactorizable" terms in hadronic B-meson weak decays*, *Phys. Rev. D* **51** (1995) 3518–3524.

[45] H.-Y. Cheng and B. Tseng, *Nonfactorizable effects in spectator and penguin amplitudes of hadronic charmless B decays*, *Phys. Rev.* **D58** (1998) 094005, [hep-ph/9803457].

[46] Y.-H. Chen, H.-Y. Cheng, B. Tseng and K.-C. Yang, *Charmless hadronic two-body decays of B(u) and B(d) mesons*, *Phys. Rev.* **D60** (1999) 094014, [hep-ph/9903453].

[47] A. Ali and C. Greub, *An Analysis of two-body nonleptonic B decays involving light mesons in the standard model*, *Phys. Rev.* **D57** (1998) 2996–3016, [hep-ph/9707251].

[48] A. Ali, G. Kramer and C.-D. Lu, *Experimental tests of factorization in charmless nonleptonic two-body B decays*, *Phys. Rev.* **D58** (1998) 094009, [hep-ph/9804363].

[49] A. J. Buras and L. Silvestrini, *Generalized factorization in nonleptonic two-body B decays: A Critical look*, *Nucl. Phys.* **B548** (1999) 293–308, [hep-ph/9806278].

[50] H.-Y. Cheng, *Nonfactorizable contributions to nonleptonic weak decays of heavy mesons*, *Physics Letters B* **335** (1994) 428 – 435.

[51] C.-H. V. Chang and H.-n. Li, *Three - scale factorization theorem and effective field theory*, *Phys. Rev.* **D55** (1997) 5577–5580, [hep-ph/9607214].

[52] H.-n. Li and G. F. Sterman, *The Perturbative pion form-factor with Sudakov suppression*, *Nucl. Phys.* **B381** (1992) 129–140.

[53] T.-W. Yeh and H.-n. Li, *Factorization theorems, effective field theory, and nonleptonic heavy meson decays*, *Phys. Rev.* **D56** (1997) 1615–1631, [hep-ph/9701233].

[54] H.-Y. Cheng, H.-n. Li and K.-C. Yang, *Gauge invariant and infrared finite theory of nonleptonic heavy meson decays*, *Phys. Rev.* **D60** (1999) 094005, [hep-ph/9902239].

[55] M. Beneke, G. Buchalla, M. Neubert and C. T. Sachrajda, *QCD factorization for exclusive, nonleptonic B meson decays: General arguments and the case of heavy light final states*, *Nucl. Phys.* **B591** (2000) 313–418, [hep-ph/0006124].

[56] M. Beneke, G. Buchalla, M. Neubert and C. T. Sachrajda, *QCD factorization in B —¿ pi K, pi pi decays and extraction of Wolfenstein parameters*, *Nucl. Phys.* **B606** (2001) 245–321, [hep-ph/0104110].

[57] M. Beneke and M. Neubert, *QCD factorization for B —¿ PP and B —¿ PV decays*, *Nucl. Phys.* **B675** (2003) 333–415, [hep-ph/0308039].

[58] S. W. Bosch and G. Buchalla, *The Radiative decays $B \to V\gamma$ at next-to-leading order in QCD*, *Nucl. Phys.* **B621** (2002) 459–478, [hep-ph/0106081].

[59] G. P. Lepage and S. J. Brodsky, *Exclusive Processes in Perturbative Quantum Chromodynamics*, *Phys. Rev.* **D22** (1980) 2157.

[60] J. C. Collins, D. E. Soper and G. F. Sterman, *Factorization of Hard Processes in QCD*, *Adv. Ser. Direct. High Energy Phys.* **5** (1989) 1–91, [hep-ph/0409313].

[61] J. C. Collins, *Light cone variables, rapidity and all that*, hep-ph/9705393.

[62] D. J. Gross and S. B. Treiman, *Light cone structure of current commutators in the gluon quark model*, *Phys. Rev.* **D4** (1971) 1059–1072.

[63] R. L. Jaffe and X.-D. Ji, *Chiral odd parton distributions and Drell-Yan processes*, *Nucl. Phys.* **B375** (1992) 527–560.

[64] P. Ball and V. M. Braun, *The Rho meson light cone distribution amplitudes of leading twist revisited*, *Phys. Rev.* **D54** (1996) 2182–2193, [hep-ph/9602323].

[65] S. Wandzura and F. Wilczek, *Sum Rules for Spin Dependent Electroproduction: Test of Relativistic Constituent Quarks*, *Phys. Lett.* **72B** (1977) 195–198.

[66] A. H. Mueller, *Perturbative QCD: Exclusive Processes in Quantum Chromodynamics by S.J. Brodsky and G.P. Lepage, World Scientific (Singapore)* (1989) 93.

[67] V. L. Chernyak and A. R. Zhitnitsky, *Asymptotics of Hadronic Form-Factors in the Quantum Chromodynamics. (In Russian)*, *Sov. J. Nucl. Phys.* **31** (1980) 544–552.

[68] V. M. Braun, *Light cone sum rules*, in *Progress in heavy quark physics. Proceedings, 4th International Workshop, Rostock, Germany, September 20-22, 1997*, pp. 105–118, 1997. hep-ph/9801222.

[69] D. S. Kim, T. Kim and S.-H. Rim, *Some identities involving Gegenbauer polynomials*, 2012.

[70] D. J. Gross and F. Wilczek, *ASYMPTOTICALLY FREE GAUGE THEORIES. 2.*, *Phys. Rev.* **D9** (1974) 980–993.

[71] M. A. Shifman and M. I. Vysotsky, *FORM-FACTORS OF HEAVY MESONS IN QCD*, *Nucl. Phys.* **B186** (1981) 475–518.

[72] M. Beneke, T. Huber and X.-Q. Li, *NNLO vertex corrections to non-leptonic B decays: Tree amplitudes*, *Nucl. Phys.* **B832** (2010) 109–151, [0911.3655].

[73] V. M. Braun, D. Yu. Ivanov and G. P. Korchemsky, *The B meson distribution amplitude in QCD*, *Phys. Rev.* **D69** (2004) 034014, [hep-ph/0309330].

[74] M. Beneke, V. M. Braun, Y. Ji and Y.-B. Wei, *Radiative leptonic decay $B \to \gamma \ell \nu_\ell$ with subleading power corrections*, *JHEP* **07** (2018) 154, [1804.04962].

[75] M. Neubert, *QCD factorization and CP asymmetries in hadronic B decays*, *Nucl. Phys. Proc. Suppl.* **99B** (2001) 113–120, [hep-ph/0011064].

[76] M. Beneke, G. Buchalla, M. Neubert and C. T. Sachrajda, *Penguins with Charm and Quark-Hadron Duality*, *Eur. Phys. J.* **C61** (2009) 439–449, [0902.4446].

[77] C. W. Bauer, D. Pirjol and I. W. Stewart, *Soft collinear factorization in effective field theory*, *Phys. Rev.* **D65** (2002) 054022, [hep-ph/0109045].

[78] C. W. Bauer, D. Pirjol, I. Z. Rothstein and I. W. Stewart, *B —¿ M(1) M(2): Factorization, charming penguins, strong phases, and polarization*, *Phys. Rev.* **D70** (2004) 054015, [hep-ph/0401188].

[79] M. Ciuchini, E. Franco, G. Martinelli and L. Silvestrini, *Charming penguins in B decays*, *Nucl. Phys.* **B501** (1997) 271–296, [hep-ph/9703353].

[80] M. Ciuchini, E. Franco, G. Martinelli, M. Pierini and L. Silvestrini, *Charming penguins strike back*, *Phys. Lett.* **B515** (2001) 33–41, [hep-ph/0104126].

[81] M. Beneke, G. Buchalla, M. Neubert and C. T. Sachrajda, *Comment on 'B —¿ M(1)M(2): Factorization, charming penguins, strong phases, and polarization'*, *Phys. Rev.* **D72** (2005) 098501, [hep-ph/0411171].

[82] F. Kruger and E. Lunghi, *Looking for novel CP violating effects in $\bar{B} \to K^* \ell^+$ lepton-*, *Phys. Rev.* **D63** (2001) 014013, [hep-ph/0008210].

[83] F. Kruger and J. Matias, *Probing new physics via the transverse amplitudes of $B^0 \to K^{*0}(\to K^-\pi^+)l^+l^-$ at large recoil*, Phys. Rev. **D71** (2005) 094009, [hep-ph/0502060].

[84] E. Lunghi and J. Matias, *Huge right-handed current effects in B-¿K*(K pi)l+l- in supersymmetry*, JHEP **04** (2007) 058, [hep-ph/0612166].

[85] S. Descotes-Genon, D. Ghosh, J. Matias and M. Ramon, *Exploring New Physics in the C7-C7' plane*, JHEP **06** (2011) 099, [1104.3342].

[86] G. C. Branco and L. Lavoura, *Wolfenstein-type parametrization of the quark mixing matrix*, Phys. Rev. D **38** (Oct, 1988) 2295–2298.

[87] K. G. Chetyrkin, M. Misiak and M. Munz, *Weak radiative B meson decay beyond leading logarithms*, Phys. Lett. **B400** (1997) 206–219, [hep-ph/9612313].

[88] K. G. Chetyrkin, M. Misiak and M. Munz, *$|\Delta F| = 1$ nonleptonic effective Hamiltonian in a simpler scheme*, Nucl. Phys. **B520** (1998) 279–297, [hep-ph/9711280].

[89] C. Bobeth, M. Misiak and J. Urban, *Photonic penguins at two loops and m_t dependence of $BR[B \to X_s l^+l^-]$*, Nucl. Phys. **B574** (2000) 291–330, [hep-ph/9910220].

[90] M. Beneke, *A Quark mass definition adequate for threshold problems*, Phys. Lett. **B434** (1998) 115–125, [hep-ph/9804241].

[91] M. Beneke and A. Signer, *The Bottom MS-bar quark mass from sum rules at next-to-next-to-leading order*, Phys. Lett. **B471** (1999) 233–243, [hep-ph/9906475].

[92] M. Misiak et al., *Estimate of $\mathcal{B}(\bar{B} \to X_s\gamma)$ at $O(\alpha_s^2)$*, Phys. Rev. Lett. **98** (2007) 022002, [hep-ph/0609232].

[93] T. Huber, E. Lunghi, M. Misiak and D. Wyler, *Electromagnetic logarithms in $\bar{B} \to X_s l^+l^-$*, Nucl. Phys. **B740** (2006) 105–137, [hep-ph/0512066].

[94] P. Gambino, M. Gorbahn and U. Haisch, *Anomalous dimension matrix for radiative and rare semileptonic B decays up to three loops*, Nucl. Phys. **B673** (2003) 238–262, [hep-ph/0306079].

[95] M. Gorbahn and U. Haisch, *Effective Hamiltonian for non-leptonic $|\Delta F| = 1$ decays at NNLO in QCD*, Nucl. Phys. **B713** (2005) 291–332, [hep-ph/0411071].

[96] C. Bobeth, P. Gambino, M. Gorbahn and U. Haisch, *Complete NNLO QCD analysis of anti-B —¿ X(s) l+ l- and higher order electroweak effects*, JHEP **04** (2004) 071, [hep-ph/0312090].

[97] A. J. Buras, M. Misiak, M. Munz and S. Pokorski, *Theoretical uncertainties and phenomenological aspects of B —¿ X(s) gamma decay*, Nucl. Phys. **B424** (1994) 374–398, [hep-ph/9311345].

[98] A. J. Buras and M. Munz, *Effective Hamiltonian for B —¿ X(s) e+ e- beyond leading logarithms in the NDR and HV schemes*, Phys. Rev. **D52** (1995) 186–195, [hep-ph/9501281].

[99] C. S. Kim, Y. G. Kim, C.-D. Lu and T. Morozumi, *Azimuthal angle distribution in $B \to K^*(\to K\pi)\ell^+\ell^-$ at low invariant $m(\ell + \ell-)$ region*, Phys. Rev. **D62** (2000) 034013, [hep-ph/0001151].

[100] F. Kruger, L. M. Sehgal, N. Sinha and R. Sinha, *Angular distribution and CP asymmetries in the decays $\bar{B} \to K^-\pi^+e^-e^+$ and $\bar{B} \to \pi^-\pi^+e^-e^+$*, Phys. Rev. **D61** (2000) 114028, [hep-ph/9907386].

[101] A. Faessler, T. Gutsche, M. A. Ivanov, J. G. Korner and V. E. Lyubovitskij, *The Exclusive rare decays $B \to K(K^*)\ \bar{\ell}\ell$ and $B_c \to D(D^*)\ \bar{\ell}\ell$ in a relativistic quark model*, Eur. Phys. J.direct **4** (2002) 18, [hep-ph/0205287].

[102] A. K. Alok, A. Datta, A. Dighe, M. Duraisamy, D. Ghosh and D. London, *New Physics in $b- > s\mu^+\mu^-$: CP-Conserving Observables*, JHEP **11** (2011) 121, [1008.2367].

[103] J. Matias, F. Mescia, M. Ramon and J. Virto, *Complete Anatomy of $\bar{B}_d- > \bar{K}^{*0}(- > K\pi)l^+l^-$ and its angular distribution*, JHEP **04** (2012) 104, [1202.4266].

[104] B. Grinstein, M. J. Savage and M. B. Wise, *B —¿ X(s) e+ e- in the Six Quark Model*, Nucl. Phys. **B319** (1989) 271–290.

[105] G. Burdman and G. Hiller, *Semileptonic form-factors from B —¿ K* gamma decays in the large energy limit*, Phys. Rev. **D63** (2001) 113008, [hep-ph/0011266].

[106] D. Seidel, *Analytic two loop virtual corrections to b —¿ d l+ l-*, Phys. Rev. **D70** (2004) 094038, [hep-ph/0403185].

[107] H. H. Asatrian, H. M. Asatrian, C. Greub and M. Walker, *Two loop virtual corrections to $B \to X_s l^+l^-$ in the standard model*, Phys. Lett. **B507** (2001) 162–172, [hep-ph/0103087].

[108] A. L. Kagan and M. Neubert, *Isospin breaking in $B \to K^*\gamma$ decays*, Phys. Lett. **B539** (2002) 227–234, [hep-ph/0110078].

[109] T. Feldmann and J. Matias, *Forward backward and isospin asymmetry for $B \to K^*l^+l^-$ decay in the standard model and in supersymmetry*, JHEP **01** (2003) 074, [hep-ph/0212158].

[110] B. Grinstein and D. Pirjol, *Exclusive rare $B \to K^*\ell^+\ell^-$ decays at low recoil: Controlling the long-distance effects*, Phys. Rev. **D70** (2004) 114005, [hep-ph/0404250].

[111] U. Egede, T. Hurth, J. Matias, M. Ramon and W. Reece, *New physics reach of the decay mode $\bar{B} \to \bar{K}^{*0}\ell^+\ell^-$*, JHEP **10** (2010) 056, [1005.0571].

[112] S. Descotes-Genon, T. Hurth, J. Matias and J. Virto, *Optimizing the basis of $B \to K^*ll$ observables in the full kinematic range*, JHEP **05** (2013) 137, [1303.5794].

[113] S. Descotes-Genon, L. Hofer, J. Matias and J. Virto, *Global analysis of $b \to s\ell\ell$ anomalies*, JHEP **06** (2016) 092, [1510.04239].

[114] D. Becirevic and E. Schneider, *On transverse asymmetries in B –¿ K* l+l-*, Nucl. Phys. **B854** (2012) 321–339, [1106.3283].

[115] S. Descotes-Genon, J. Matias, M. Ramon and J. Virto, *Implications from clean observables for the binned analysis of $B->K*\mu^+\mu^-$ at large recoil*, *JHEP* **01** (2013) 048, [1207.2753].

[116] W. Altmannshofer, P. Paradisi and D. M. Straub, *Model-Independent Constraints on New Physics in $b \to s$ Transitions*, *JHEP* **04** (2012) 008, [1111.1257].

[117] LHCb collaboration, R. Aaij et al., *Differential branching fraction and angular analysis of the decay $B^0 \to K^{*0}\mu^+\mu^-$*, *JHEP* **08** (2013) 131, [1304.6325].

[118] J. Gratrex, M. Hopfer and R. Zwicky, *Generalised helicity formalism, higher moments and the $B \to K_{J_K}(\to K\pi)\bar{\ell}_1\ell_2$ angular distributions*, *Phys. Rev.* **D93** (2016) 054008, [1506.03970].

[119] D. Bečirević, O. Sumensari and R. Zukanovich Funchal, *Lepton flavor violation in exclusive $b \to s$ decays*, *Eur. Phys. J.* **C76** (2016) 134, [1602.00881].

[120] Particle Data Group collaboration, J. Beringer, J. F. Arguin, R. M. Barnett, K. Copic, O. Dahl, D. E. Groom et al., *Review of particle physics*, *Phys. Rev. D* **86** (Jul, 2012) 010001.

[121] LHCb collaboration, R. Aaij et al., *Angular analysis and differential branching fraction of the decay $B^0_s \to \phi\mu^+\mu^-$*, *JHEP* **09** (2015) 179, [1506.08777].

[122] S. Descotes-Genon and J. Virto, *Time dependence in $B \to V\ell\ell$ decays*, *JHEP* **04** (2015) 045, [1502.05509].

[123] C. Bobeth, G. Hiller and G. Piranishvili, *CP Asymmetries in bar $B \to \bar{K}^*(\to \bar{K}\pi)\bar{\ell}\ell$ and Untagged $\bar{B}_s$, $B_s \to \phi(\to K^+K^-)\bar{\ell}\ell$ Decays at NLO*, *JHEP* **07** (2008) 106, [0805.2525].

[124] U. Nierste, *Three Lectures on Meson Mixing and CKM phenomenology*, in *Heavy quark physics. Proceedings, Helmholtz International School, HQP08, Dubna, Russia, August 11-21, 2008*, pp. 1–38, 2009. 0904.1869.

[125] C. Bobeth, T. Ewerth, F. Kruger and J. Urban, *Analysis of neutral Higgs boson contributions to the decays $\bar{B}(\ s) \to \ell^+\ell^-$ and $\bar{B} \to K\ell^+\ell^-$*, *Phys. Rev.* **D64** (2001) 074014, [hep-ph/0104284].

[126] C. Bobeth, G. Hiller and G. Piranishvili, *Angular distributions of $\bar{B} \to \bar{K}\ell^+\ell^-$ decays*, *JHEP* **12** (2007) 040, [0709.4174].

[127] BaBar collaboration, B. Aubert et al., *Measurements of branching fractions, rate asymmetries, and angular distributions in the rare decays $B \to K\ell^+\ell^-$ and $B \to K^*\ell^+\ell^-$*, *Phys. Rev.* **D73** (2006) 092001, [hep-ex/0604007].

[128] F. Beaujean, C. Bobeth and S. Jahn, *Constraints on tensor and scalar couplings from $B \to K\bar{\mu}\mu$ and $B_s \to \bar{\mu}\mu$*, *Eur. Phys. J.* **C75** (2015) 456, [1508.01526].

[129] G. Hiller and F. Kruger, *More model-independent analysis of $b \to s$ processes*, *Phys. Rev.* **D69** (2004) 074020, [hep-ph/0310219].

[130] B. Capdevila, U. Laa and G. Valencia, *Anatomy of a six-parameter fit to the $b \to s\ell^+\ell^-$ anomalies*, 1811.10793.

[131] M. Misiak and M. Steinhauser, *NNLO QCD corrections to the anti-B —¿ X(s) gamma matrix elements using interpolation in m(c)*, *Nucl. Phys.* **B764** (2007) 62–82, [hep-ph/0609241].

[132] M. Misiak and M. Steinhauser, *Large-m_c Asymptotic Behaviour of $O(\alpha_s^2)$ Corrections to $B \to X_s\gamma$*, *Nucl. Phys.* **B840** (2010) 271–283, [1005.1173].

[133] M. Misiak et al., *Updated NNLO QCD predictions for the weak radiative B-meson decays*, *Phys. Rev. Lett.* **114** (2015) 221801, [1503.01789].

[134] D. Guetta and E. Nardi, *Searching for new physics in rare B —¿ tau decays*, *Phys. Rev.* **D58** (1998) 012001, [hep-ph/9707371].

[135] T. Huber, T. Hurth and E. Lunghi, *Inclusive $\overline{B} \to X_s\ell^+\ell^-$: complete angular analysis and a thorough study of collinear photons*, *JHEP* **06** (2015) 176, [1503.04849].

[136] B. Capdevila, A. Crivellin, S. Descotes-Genon, J. Matias and J. Virto, *Patterns of New Physics in $b \to s\ell^+\ell^-$ transitions in the light of recent data*, *JHEP* **01** (2018) 093, [1704.05340].

[137] B. Grinstein and D. Pirjol, *The CP asymmetry in B0(t) —¿ K(S) pi0 gamma in the standard model*, *Phys. Rev.* **D73** (2006) 014013, [hep-ph/0510104].

[138] P. Ball, G. W. Jones and R. Zwicky, *$B \to V\gamma$ beyond QCD factorisation*, *Phys. Rev.* **D75** (2007) 054004, [hep-ph/0612081].

[139] C. Bobeth, M. Gorbahn, T. Hermann, M. Misiak, E. Stamou and M. Steinhauser, *$B_{s,d} \to l^+l^-$ in the Standard Model with Reduced Theoretical Uncertainty*, *Phys. Rev. Lett.* **112** (2014) 101801, [1311.0903].

[140] C. Bobeth, M. Gorbahn and E. Stamou, *Electroweak Corrections to $B_{s,d} \to \ell^+\ell^-$*, *Phys. Rev.* **D89** (2014) 034023, [1311.1348].

[141] T. Hermann, M. Misiak and M. Steinhauser, *Three-loop QCD corrections to $B_s \to \mu^+\mu^-$*, *JHEP* **12** (2013) 097, [1311.1347].

[142] M. Beneke, C. Bobeth and R. Szafron, *Enhanced electromagnetic correction to the rare B-meson decay $B_{s,d} \to \mu^+\mu^-$*, *Phys. Rev. Lett.* **120** (2018) 011801, [1708.09152].

[143] M. Beneke, C. Bobeth and R. Szafron, *Power-enhanced leading-logarithmic QED corrections to $B_q \to \mu^+\mu^-$*, *JHEP* **10** (2019) 232, [1908.07011].

[144] M. Ciuchini, M. Fedele, E. Franco, S. Mishima, A. Paul, L. Silvestrini et al., *$B \to K^*\ell^+\ell^-$ decays at large recoil in the Standard Model: a theoretical reappraisal*, *JHEP* **06** (2016) 116, [1512.07157].

[145] M. Ciuchini, M. Fedele, E. Franco, S. Mishima, A. Paul, L. Silvestrini et al., *$B \to K^*\ell^+\ell^-$ in the Standard Model: Elaborations and Interpretations*, *PoS* **ICHEP2016** (2016) 584, [1611.04338].

[146] S. Jäger and J. Martin Camalich, *Reassessing the discovery potential of the $B \to K^* \ell^+ \ell^-$ decays in the large-recoil region: SM challenges and BSM opportunities*, *Phys. Rev.* **D93** (2016) 014028, [1412.3183].

[147] S. Descotes-Genon, L. Hofer, J. Matias and J. Virto, *On the impact of power corrections in the prediction of $B \to K^* \mu^+ \mu^-$ observables*, *JHEP* **12** (2014) 125, [1407.8526].

[148] A. Khodjamirian, T. Mannel, A. A. Pivovarov and Y. M. Wang, *Charm-loop effect in $B \to K^{(*)} \ell^+ \ell^-$ and $B \to K^* \gamma$*, *JHEP* **09** (2010) 089, [1006.4945].

[149] N. Gubernari, A. Kokulu and D. van Dyk, *$B \to P$ and $B \to V$ Form Factors from B-Meson Light-Cone Sum Rules beyond Leading Twist*, *JHEP* **01** (2019) 150, [1811.00983].

[150] A. Bharucha, D. M. Straub and R. Zwicky, *$B \to V \ell^+ \ell^-$ in the Standard Model from light-cone sum rules*, *JHEP* **08** (2016) 098, [1503.05534].

[151] S. Jäger and J. Martin Camalich, *On $B \to V \ell \ell$ at small dilepton invariant mass, power corrections, and new physics*, *JHEP* **05** (2013) 043, [1212.2263].

[152] U. Egede, T. Hurth, J. Matias, M. Ramon and W. Reece, *New observables in the decay mode $\bar{B}_d \to \bar{K}^{*0} l^+ l^-$*, *JHEP* **11** (2008) 032, [0807.2589].

[153] S. Descotes-Genon, J. Matias and J. Virto, *Understanding the $B \to K^* \mu^+ \mu^-$ Anomaly*, *Phys. Rev.* **D88** (2013) 074002, [1307.5683].

[154] C. Bobeth, G. Hiller and D. van Dyk, *The Benefits of $\bar{B} -> \bar{K}^* l^+ l^-$ Decays at Low Recoil*, *JHEP* **07** (2010) 098, [1006.5013].

[155] C. Bobeth, G. Hiller and D. van Dyk, *More Benefits of Semileptonic Rare B Decays at Low Recoil: CP Violation*, *JHEP* **07** (2011) 067, [1105.0376].

[156] C. Bobeth, G. Hiller and D. van Dyk, *General analysis of $\bar{B} \to \bar{K}^{(*)} \ell^+ \ell^-$ decays at low recoil*, *Phys. Rev.* **D87** (2013) 034016, [1212.2321].

[157] M. Beylich, G. Buchalla and T. Feldmann, *Theory of $B \to K^{(*)} \ell^+ \ell^-$ decays at high q^2: OPE and quark-hadron duality*, *Eur. Phys. J.* **C71** (2011) 1635, [1101.5118].

[158] R. R. Horgan, Z. Liu, S. Meinel and M. Wingate, *Calculation of $B^0 \to K^{*0} \mu^+ \mu^-$ and $B_s^0 \to \phi \mu^+ \mu^-$ observables using form factors from lattice QCD*, *Phys. Rev. Lett.* **112** (2014) 212003, [1310.3887].

[159] C. Greub, V. Pilipp and C. Schupbach, *Analytic calculation of two-loop QCD corrections to $b \to s l^+ l^-$ in the high q^2 region*, *JHEP* **12** (2008) 040, [0810.4077].

[160] M. Beneke, A. P. Chapovsky, M. Diehl and T. Feldmann, *Soft collinear effective theory and heavy to light currents beyond leading power*, *Nucl. Phys.* **B643** (2002) 431–476, [hep-ph/0206152].

[161] M. Beneke and D. Yang, *Heavy-to-light B meson form-factors at large recoil energy: Spectator-scattering corrections*, *Nucl. Phys.* **B736** (2006) 34–81, [hep-ph/0508250].

[162] G. Bell, M. Beneke, T. Huber and X.-Q. Li, *Heavy-to-light currents at NNLO in SCET and semi-inclusive $\bar{B} \to X_s l^+ l^-$ decay*, Nucl. Phys. **B843** (2011) 143–176, [1007.3758].

[163] W. Altmannshofer and D. M. Straub, *New physics in $b \to s$ transitions after LHC run 1*, Eur. Phys. J. **C75** (2015) 382, [1411.3161].

[164] W. Altmannshofer and D. M. Straub, *Implications of $b \to s$ measurements*, in *Proceedings, 50th Rencontres de Moriond Electroweak Interactions and Unified Theories: La Thuile, Italy, March 14-21, 2015*, pp. 333–338, 2015. 1503.06199.

[165] P. Ball and R. Zwicky, *$B_{d,s} \to \rho, \omega, K^*, \phi$ decay form-factors from light-cone sum rules revisited*, Phys. Rev. **D71** (2005) 014029, [hep-ph/0412079].

[166] T. Hurth, F. Mahmoudi and S. Neshatpour, *On the anomalies in the latest LHCb data*, Nucl. Phys. **B909** (2016) 737–777, [1603.00865].

[167] T. Hurth, F. Mahmoudi and S. Neshatpour, *Global fits to $b \to s\ell\ell$ data and signs for lepton non-universality*, JHEP **12** (2014) 053, [1410.4545].

[168] W. Altmannshofer and D. M. Straub, *New Physics in $B \to K^* \mu\mu$?*, Eur. Phys. J. **C73** (2013) 2646, [1308.1501].

[169] F. Beaujean, C. Bobeth and D. van Dyk, *Comprehensive Bayesian analysis of rare (semi)leptonic and radiative B decays*, Eur. Phys. J. **C74** (2014) 2897, [1310.2478].

[170] LHCb collaboration, R. Aaij et al., *Angular analysis of the $B^0 \to K^{*0} e^+ e^-$ decay in the low q^2 region*, JHEP **04** (2015) 064, [1501.03038].

[171] A. Khodjamirian, T. Mannel and Y. M. Wang, *$B \to K \ell^+ \ell^-$ decay at large hadronic recoil*, JHEP **02** (2013) 010, [1211.0234].

[172] J. Lyon and R. Zwicky, *Resonances gone topsy turvy - the charm of QCD or new physics in $b \to s\ell^+\ell^-$?*, 1406.0566.

[173] D. Becirevic and A. Tayduganov, *Impact of $B \to K_0^* \ell^+ \ell^-$ on the New Physics search in $B \to K^* \ell^+ \ell^-$ decay*, Nucl. Phys. **B868** (2013) 368–382, [1207.4004].

[174] J. Matias, *On the S-wave pollution of B-¿ K* l+l- observables*, Phys. Rev. **D86** (2012) 094024, [1209.1525].

[175] T. Blake, U. Egede and A. Shires, *The effect of S-wave interference on the $B^0 \to K^{*0} \ell^+ \ell^-$ angular observables*, JHEP **03** (2013) 027, [1210.5279].

[176] LHCb collaboration, R. Aaij et al., *Measurement of Form-Factor-Independent Observables in the Decay $B^0 \to K^{*0} \mu^+ \mu^-$*, Phys. Rev. Lett. **111** (2013) 191801, [1308.1707].

[177] LHCb collaboration, R. Aaij et al., *Angular analysis of charged and neutral $B \to K \mu^+ \mu^-$ decays*, JHEP **05** (2014) 082, [1403.8045].

[178] Belle collaboration, A. Abdesselam et al., *Angular analysis of $B^0 \to K^*(892)^0 \ell^+ \ell^-$*, in *Proceedings, LHCSki 2016 - A First Discussion of 13 TeV Results: Obergurgl, Austria, April 10-15, 2016*, 2016. 1604.04042.

[179] U. Egede, M. Patel and K. A. Petridis, *Method for an unbinned measurement of the q^2 dependent decay amplitudes of $\overline{B}^0 \to K^{*0}\mu^+\mu^-$ decays*, JHEP **06** (2015) 084, [1504.00574].

[180] S. M. Boucenna, A. Celis, J. Fuentes-Martin, A. Vicente and J. Virto, *Non-abelian gauge extensions for B-decay anomalies*, Phys. Lett. **B760** (2016) 214–219, [1604.03088].

[181] E. Barberio and Z. Was, *PHOTOS: A Universal Monte Carlo for QED radiative corrections. Version 2.0*, Comput. Phys. Commun. **79** (1994) 291–308.

[182] P. Stoffer, *Isospin breaking effects in $K_{\ell 4}$ decays*, Eur. Phys. J. **C74** (2014) 2749, [1312.2066].

[183] V. Bernard, S. Descotes-Genon and M. Knecht, *On some aspects of isospin breaking in the decay $K^\pm \to \pi^0\pi^0 e^\pm \overset{(-)}{\nu}_e$*, Eur. Phys. J. **C75** (2015) 145, [1501.07102].

[184] LHCb collaboration, R. Aaij et al., *Angular analysis of the $B^0 \to K^{*0}\mu^+\mu^-$ decay using 3 fb^{-1} of integrated luminosity*, JHEP **02** (2016) 104, [1512.04442].

[185] LHCb collaboration, R. Aaij et al., *Differential branching fraction and angular analysis of the decay $B_s^0 \to \phi\mu^+\mu^-$*, JHEP **07** (2013) 084, [1305.2168].

[186] Belle collaboration, S. Wehle et al., *Lepton-Flavor-Dependent Angular Analysis of $B \to K^*\ell^+\ell^-$*, Phys. Rev. Lett. **118** (2017) 111801, [1612.05014].

[187] LHCb collaboration, R. Aaij et al., *Test of lepton universality using $B^+ \to K^+\ell^+\ell^-$ decays*, Phys. Rev. Lett. **113** (2014) 151601, [1406.6482].

[188] ATLAS collaboration, M. Aaboud et al., *Angular analysis of $B_d^0 \to K^*\mu^+\mu^-$ decays in pp collisions at $\sqrt{s} = 8$ TeV with the ATLAS detector*, JHEP **10** (2018) 047, [1805.04000].

[189] CMS collaboration, A. M. Sirunyan et al., *Measurement of angular parameters from the decay $\mathrm{B}^0 \to \mathrm{K}^{*0}\mu^+\mu^-$ in proton-proton collisions at $\sqrt{s} = 8$ TeV*, Phys. Lett. **B781** (2018) 517–541, [1710.02846].

[190] LHCb collaboration, R. Aaij et al., *Measurements of the S-wave fraction in $B^0 \to K^+\pi^-\mu^+\mu^-$ decays and the $B^0 \to K^*(892)^0\mu^+\mu^-$ differential branching fraction*, JHEP **11** (2016) 047, [1606.04731].

[191] LHCb collaboration, R. Aaij et al., *Test of lepton universality with $B^0 \to K^{*0}\ell^+\ell^-$ decays*, JHEP **08** (2017) 055, [1705.05802].

[192] G. Hiller and M. Schmaltz, *R_K and future $b \to s\ell\ell$ physics beyond the standard model opportunities*, Phys. Rev. **D90** (2014) 054014, [1408.1627].

[193] G. Hiller and M. Schmaltz, *Diagnosing lepton-nonuniversality in $b \to s\ell\ell$*, JHEP **02** (2015) 055, [1411.4773].

[194] LHCb collaboration, R. Aaij et al., *Search for lepton-universality violation in $B^+ \to K^+\ell^+\ell^-$ decays*, Phys. Rev. Lett. **122** (2019) 191801, [1903.09252].

[195] Belle collaboration, A. Abdesselam et al., *Test of lepton flavor universality in $B \to K^*\ell^+\ell^-$ decays at Belle*, 1904.02440.

[196] Belle collaboration, A. Abdesselam et al., *Test of lepton flavor universality in $B \to K\ell^+\ell^-$ decays*, 1908.01848.

[197] M. Algueró, B. Capdevila, A. Crivellin, S. Descotes-Genon, P. Masjuan, J. Matias et al., *Emerging patterns of New Physics with and without Lepton Flavour Universal contributions*, Eur. Phys. J. **C79** (2019) 714, [1903.09578].

[198] Y.-M. Wang and Y.-L. Shen, *Perturbative Corrections to $\Lambda_b \to \Lambda$ Form Factors from QCD Light-Cone Sum Rules*, JHEP **02** (2016) 179, [1511.09036].

[199] W. Detmold and S. Meinel, *$\Lambda_b \to \Lambda\ell^+\ell^-$ form factors, differential branching fraction, and angular observables from lattice QCD with relativistic b quarks*, Phys. Rev. **D93** (2016) 074501, [1602.01399].

[200] LHCb collaboration, R. Aaij et al., *Differential branching fraction and angular analysis of $\Lambda_b^0 \to \Lambda\mu^+\mu^-$ decays*, JHEP **06** (2015) 115, [1503.07138].

[201] S. Meinel and D. van Dyk, *Using $\Lambda_b \to \Lambda\mu^+\mu^-$ data within a Bayesian analysis of $|\Delta B| = |\Delta S| = 1$ decays*, Phys. Rev. **D94** (2016) 013007, [1603.02974].

[202] CMS collaboration, V. Khachatryan et al., *Angular analysis of the decay $B^0 \to K^{*0}\mu^+\mu^-$ from pp collisions at $\sqrt{s} = 8$ TeV*, Phys. Lett. **B753** (2016) 424–448, [1507.08126].

[203] CMS collaboration, S. Chatrchyan et al., *Angular analysis and branching fraction measurement of the decay $B^0 \to K^{*0}\mu^+\mu^-$*, Phys. Lett. **B727** (2013) 77–100, [1308.3409].

[204] ATLAS collaboration, M. Aaboud et al., *Study of the rare decays of B_s^0 and B^0 mesons into muon pairs using data collected during 2015 and 2016 with the ATLAS detector*, JHEP **04** (2019) 098, [1812.03017].

[205] CMS collaboration, S. Chatrchyan et al., *Measurement of the $B_s^0 \to \mu^+\mu^-$ Branching Fraction and Search for $B^0 \to \mu^+\mu^-$ with the CMS Experiment*, Phys. Rev. Lett. **111** (2013) 101804, [1307.5025].

[206] LHCb collaboration, R. Aaij et al., *Measurement of the $B_s^0 \to \mu^+\mu^-$ branching fraction and effective lifetime and search for $B^0 \to \mu^+\mu^-$ decays*, Phys. Rev. Lett. **118** (2017) 191801, [1703.05747].

[207] J. Aebischer, W. Altmannshofer, D. Guadagnoli, M. Reboud, P. Stangl and D. M. Straub, *B-decay discrepancies after Moriond 2019*, 1903.10434.

[208] A. Arbey, T. Hurth, F. Mahmoudi, D. M. Santos and S. Neshatpour, *Update on the $b \to s$ anomalies*, Phys. Rev. **D100** (2019) 015045, [1904.08399].

[209] Flavour Lattice Averaging Group collaboration, S. Aoki et al., *FLAG Review 2019*, 1902.08191.

[210] S. S. Wilks, *The Large-Sample Distribution of the Likelihood Ratio for Testing Composite Hypotheses*, Annals Math. Statist. **9** (1938) 60–62.

[211] M. Algueró, B. Capdevila, S. Descotes-Genon, P. Masjuan and J. Matias, *Are we overlooking Lepton Flavour Universal New Physics in* $b \to s\ell\ell$ *?*, 1809.08447.

[212] M. Algueró, B. Capdevila, S. Descotes-Genon, P. Masjuan and J. Matias, *What* R_K *and* Q_5 *can tell us about New Physics in* $b \to s\ell\ell$ *transitions?*, 1902.04900.

[213] A. Crivellin, D. Müller and C. Wiegand, $b \to s\ell^+\ell^-$ *transitions in two-Higgs-doublet models*, *JHEP* **06** (2019) 119, [1903.10440].

[214] C. Bobeth, A. J. Buras, A. Celis and M. Jung, *Patterns of Flavour Violation in Models with Vector-Like Quarks*, *JHEP* **04** (2017) 079, [1609.04783].

[215] A. Arbey, T. Hurth, F. Mahmoudi and S. Neshatpour, *Hadronic and New Physics Contributions to* $b \to s$ *Transitions*, *Phys. Rev.* **D98** (2018) 095027, [1806.02791].

[216] T. Hurth, F. Mahmoudi, D. Martinez Santos and S. Neshatpour, *Lepton nonuniversality in exclusive* $b{\to}s\ell\ell$ *decays*, *Phys. Rev.* **D96** (2017) 095034, [1705.06274].

[217] M. Ciuchini, A. M. Coutinho, M. Fedele, E. Franco, A. Paul, L. Silvestrini et al., *On Flavourful Easter eggs for New Physics hunger and Lepton Flavour Universality violation*, *Eur. Phys. J.* **C77** (2017) 688, [1704.05447].

[218] M. Ciuchini, A. M. Coutinho, M. Fedele, E. Franco, A. Paul, L. Silvestrini et al., *New Physics in* $b \to s\ell^+\ell^-$ *confronts new data on Lepton Universality*, *Eur. Phys. J.* **C79** (2019) 719, [1903.09632].

[219] J. Kumar and D. London, *New physics in* $b \to se^+e^-$ *?*, *Phys. Rev.* **D99** (2019) 073008, [1901.04516].

[220] A. Falkowski, M. Nardecchia and R. Ziegler, *Lepton Flavor Non-Universality in B-meson Decays from a U(2) Flavor Model*, *JHEP* **11** (2015) 173, [1509.01249].

[221] R. Gauld, F. Goertz and U. Haisch, *On minimal* Z' *explanations of the* $B \to K^*\mu^+\mu^-$ *anomaly*, *Phys. Rev.* **D89** (2014) 015005, [1308.1959].

[222] A. J. Buras, F. De Fazio and J. Girrbach, *331 models facing new* $b \to s\mu^+\mu^-$ *data*, *JHEP* **02** (2014) 112, [1311.6729].

[223] S. Jäger, M. Kirk, A. Lenz and K. Leslie, *Charming new physics in rare B-decays and mixing?*, *Phys. Rev.* **D97** (2018) 015021, [1701.09183].

[224] W. Altmannshofer, S. Gori, M. Pospelov and I. Yavin, *Quark flavor transitions in* $L_\mu - L_\tau$ *models*, *Phys. Rev.* **D89** (2014) 095033, [1403.1269].

[225] A. Crivellin, G. D'Ambrosio and J. Heeck, *Explaining* $h \to \mu^\pm\tau^\mp$, $B \to K^*\mu^+\mu^-$ *and* $B \to K\mu^+\mu^-/B \to Ke^+e^-$ *in a two-Higgs-doublet model with gauged* $L_\mu - L_\tau$, *Phys. Rev. Lett.* **114** (2015) 151801, [1501.00993].

[226] A. Crivellin, G. D'Ambrosio and J. Heeck, *Addressing the LHC flavor anomalies with horizontal gauge symmetries*, *Phys. Rev.* **D91** (2015) 075006, [1503.03477].

[227] A. Crivellin, J. Fuentes-Martin, A. Greljo and G. Isidori, *Lepton Flavor Non-Universality in B decays from Dynamical Yukawas*, *Phys. Lett.* **B766** (2017) 77–85, [1611.02703].

[228] D. Bhatia, S. Chakraborty and A. Dighe, *Neutrino mixing and R_K anomaly in $U(1)_X$ models: a bottom-up approach*, *JHEP* **03** (2017) 117, [1701.05825].

[229] G. Bélanger, C. Delaunay and S. Westhoff, *A Dark Matter Relic From Muon Anomalies*, *Phys. Rev.* **D92** (2015) 055021, [1507.06660].

[230] S. M. Boucenna, A. Celis, J. Fuentes-Martin, A. Vicente and J. Virto, *Phenomenology of an $SU(2) \times SU(2) \times U(1)$ model with lepton-flavour non-universality*, *JHEP* **12** (2016) 059, [1608.01349].

[231] B. Gripaios, M. Nardecchia and S. A. Renner, *Composite leptoquarks and anomalies in B-meson decays*, *JHEP* **05** (2015) 006, [1412.1791].

[232] S. Fajfer and N. Košnik, *Vector leptoquark resolution of R_K and $R_{D^{(*)}}$ puzzles*, *Phys. Lett.* **B755** (2016) 270–274, [1511.06024].

[233] I. de Medeiros Varzielas and G. Hiller, *Clues for flavor from rare lepton and quark decays*, *JHEP* **06** (2015) 072, [1503.01084].

[234] R. Alonso, B. Grinstein and J. Martin Camalich, *Lepton universality violation and lepton flavor conservation in B-meson decays*, *JHEP* **10** (2015) 184, [1505.05164].

[235] L. Calibbi, A. Crivellin and T. Ota, *Effective Field Theory Approach to $b \to s\ell\ell$('), $B \to K^{(*)}\nu\overline{\nu}$ and $B \to D^{(*)}\tau\nu$ with Third Generation Couplings*, *Phys. Rev. Lett.* **115** (2015) 181801, [1506.02661].

[236] R. Barbieri, G. Isidori, A. Pattori and F. Senia, *Anomalies in B-decays and $U(2)$ flavour symmetry*, *Eur. Phys. J.* **C76** (2016) 67, [1512.01560].

[237] S. Sahoo, R. Mohanta and A. K. Giri, *Explaining the R_K and $R_{D^{(*)}}$ anomalies with vector leptoquarks*, *Phys. Rev.* **D95** (2017) 035027, [1609.04367].

[238] B. Gripaios, M. Nardecchia and S. A. Renner, *Linear flavour violation and anomalies in B physics*, *JHEP* **06** (2016) 083, [1509.05020].

[239] P. Arnan, L. Hofer, F. Mescia and A. Crivellin, *Loop effects of heavy new scalars and fermions in $b \to s\mu^+\mu^-$*, *JHEP* **04** (2017) 043, [1608.07832].

[240] F. Mahmoudi, S. Neshatpour and J. Virto, *$B \to K^*\mu^+\mu^-$ optimised observables in the MSSM*, *Eur. Phys. J.* **C74** (2014) 2927, [1401.2145].

[241] C. Niehoff, P. Stangl and D. M. Straub, *Violation of lepton flavour universality in composite Higgs models*, *Phys. Lett.* **B747** (2015) 182–186, [1503.03865].

[242] A. Crivellin, C. Greub, D. Müller and F. Saturnino, *Importance of Loop Effects in Explaining the Accumulated Evidence for New Physics in B Decays with a Vector Leptoquark*, *Phys. Rev. Lett.* **122** (2019) 011805, [1807.02068].

[243] HFLAV collaboration, Y. Amhis et al., *Averages of b-hadron, c-hadron, and τ-lepton properties as of summer 2016*, Eur. Phys. J. **C77** (2017) 895, [1612.07233].

[244] R. Alonso, B. Grinstein and J. Martin Camalich, *Lifetime of B_c^- Constrains Explanations for Anomalies in $B \to D^{(*)}\tau\nu$*, Phys. Rev. Lett. **118** (2017) 081802, [1611.06676].

[245] M. Freytsis, Z. Ligeti and J. T. Ruderman, *Flavor models for $\bar{B} \to D^{(*)}\tau\bar{\nu}$*, Phys. Rev. **D92** (2015) 054018, [1506.08896].

[246] A. Celis, M. Jung, X.-Q. Li and A. Pich, *Scalar contributions to $b \to c(u)\tau\nu$ transitions*, Phys. Lett. **B771** (2017) 168–179, [1612.07757].

[247] M. A. Ivanov, J. G. Körner and C.-T. Tran, *Probing new physics in $\bar{B}^0 \to D^{(*)}\tau^-\bar{\nu}_\tau$ using the longitudinal, transverse, and normal polarization components of the tau lepton*, Phys. Rev. **D95** (2017) 036021, [1701.02937].

[248] D. A. Faroughy, A. Greljo and J. F. Kamenik, *Confronting lepton flavor universality violation in B decays with high-p_T tau lepton searches at LHC*, Phys. Lett. **B764** (2017) 126–134, [1609.07138].

[249] F. Feruglio, P. Paradisi and A. Pattori, *Revisiting Lepton Flavor Universality in B Decays*, Phys. Rev. Lett. **118** (2017) 011801, [1606.00524].

[250] B. Grzadkowski, M. Iskrzynski, M. Misiak and J. Rosiek, *Dimension-Six Terms in the Standard Model Lagrangian*, JHEP **10** (2010) 085, [1008.4884].

[251] A. Celis, J. Fuentes-Martin, A. Vicente and J. Virto, *Gauge-invariant implications of the LHCb measurements on lepton-flavor nonuniversality*, Phys. Rev. **D96** (2017) 035026, [1704.05672].

[252] A. Greljo, G. Isidori and D. Marzocca, *On the breaking of Lepton Flavor Universality in B decays*, JHEP **07** (2015) 142, [1506.01705].

[253] A. Crivellin, D. Müller and T. Ota, *Simultaneous explanation of $R(D^{(*)})$ and $b \to s\mu^+\mu^-$: the last scalar leptoquarks standing*, JHEP **09** (2017) 040, [1703.09226].

[254] I. Garcia Garcia, *LHCb anomalies from a natural perspective*, JHEP **03** (2017) 040, [1611.03507].

[255] M. Blanke and A. Crivellin, *B Meson Anomalies in a Pati-Salam Model within the Randall-Sundrum Background*, Phys. Rev. Lett. **121** (2018) 011801, [1801.07256].

[256] L. Di Luzio, A. Greljo and M. Nardecchia, *Gauge leptoquark as the origin of B-physics anomalies*, Phys. Rev. **D96** (2017) 115011, [1708.08450].

[257] L. Calibbi, A. Crivellin and T. Li, *Model of vector leptoquarks in view of the B-physics anomalies*, Phys. Rev. **D98** (2018) 115002, [1709.00692].

[258] M. Bordone, C. Cornella, J. Fuentes-Martin and G. Isidori, *A three-site gauge model for flavor hierarchies and flavor anomalies*, Phys. Lett. **B779** (2018) 317–323, [1712.01368].

[259] BELLE collaboration, A. Abdesselam et al., *Measurement of $\mathcal{R}(D)$ and $\mathcal{R}(D^*)$ with a semileptonic tagging method*, 1904.08794.

[260] A. Datta, J. Kumar, J. Liao and D. Marfatia, *New light mediators for the R_K and R_{K^*} puzzles*, *Phys. Rev.* **D97** (2018) 115038, [1705.08423].

[261] W. Altmannshofer, M. J. Baker, S. Gori, R. Harnik, M. Pospelov, E. Stamou et al., *Light resonances and the low-q^2 bin of R_{K^*}*, *JHEP* **03** (2018) 188, [1711.07494].

[262] HEAVY FLAVOR AVERAGING GROUP collaboration, D. Asner et al., *Averages of b-hadron, c-hadron, and τ-lepton properties*, 1010.1589.

[263] W. Altmannshofer, P. Stangl and D. M. Straub, *Interpreting Hints for Lepton Flavor Universality Violation*, *Phys. Rev.* **D96** (2017) 055008, [1704.05435].

[264] W. Altmannshofer, C. Niehoff, P. Stangl and D. M. Straub, *Status of the $B \to K^* \mu^+ \mu^-$ anomaly after Moriond 2017*, *Eur. Phys. J.* **C77** (2017) 377, [1703.09189].

[265] S. Gonzàlez-Solís and P. Masjuan, *Study of $B \to \pi \ell \nu_\ell$ and $B^+ \to \eta^{(\prime)} \ell^+ \nu_\ell$ decays and determination of $|V_{ub}|$*, *Phys. Rev.* **D98** (2018) 034027, [1805.11262].

[266] S. Descotes-Genon, J. Matias and J. Virto, *An analysis of $B_{d,s}$ mixing angles in presence of New Physics and an update of $B_s \to K^{0*} - K^{0*}$*, *Phys. Rev.* **D85** (2012) 034010, [1111.4882].

[267] K. De Bruyn, R. Fleischer, R. Knegjens, P. Koppenburg, M. Merk and N. Tuning, *Branching Ratio Measurements of B_s Decays*, *Phys. Rev.* **D86** (2012) 014027, [1204.1735].

[268] K. De Bruyn, R. Fleischer, R. Knegjens, M. Merk, M. Schiller and N. Tuning, *Exploring $B_s \to D_s^{(*)\pm} K^\mp$ Decays in the Presence of a Sizable Width Difference $\Delta\Gamma_s$*, *Nucl. Phys.* **B868** (2013) 351–367, [1208.6463].

[269] F. Dettori and D. Guadagnoli, *On the model dependence of measured B_s-meson branching fractions*, *Phys. Lett.* **B784** (2018) 96–100, [1804.03591].

[270] LHCB collaboration, R. Aaij et al., *Angular moments of the decay $\Lambda_b^0 \to \Lambda \mu^+ \mu^-$ at low hadronic recoil*, *JHEP* **09** (2018) 146, [1808.00264].

[271] LHCB collaboration, R. Aaij et al., *Measurement of the ratio of branching fractions $\mathcal{B}(B_c^+ \to J/\psi \tau^+ \nu_\tau)/\mathcal{B}(B_c^+ \to J/\psi \mu^+ \nu_\mu)$*, *Phys. Rev. Lett.* **120** (2018) 121801, [1711.05623].

[272] R. Watanabe, *New Physics effect on $B_c \to J/\psi \tau \bar{\nu}$ in relation to the $R_{D^{(*)}}$ anomaly*, *Phys. Lett.* **B776** (2018) 5–9, [1709.08644].

[273] B. Chauhan and B. Kindra, *Invoking Chiral Vector Leptoquark to explain LFU violation in B Decays*, 1709.09989.

[274] R. Dutta, *Exploring R_D, R_{D^*} and $R_{J/\Psi}$ anomalies*, 1710.00351.

[275] A. K. Alok, D. Kumar, J. Kumar, S. Kumbhakar and S. U. Sankar, *New physics solutions for R_D and R_{D^*}*, *JHEP* **09** (2018) 152, [1710.04127].

[276] LHCb collaboration, R. Aaij et al., *Search for the decays $B_s^0 \to \tau^+\tau^-$ and $B^0 \to \tau^+\tau^-$*, *Phys. Rev. Lett.* **118** (2017) 251802, [1703.02508].

[277] BaBar collaboration, J. P. Lees et al., *Search for $B^+ \to K^+\tau^+\tau^-$ at the BaBar experiment*, *Phys. Rev. Lett.* **118** (2017) 031802, [1605.09637].

[278] C. Bobeth, *Updated $B_q \to \bar{\ell}\ell$ in the standard model at higher orders*, in *Proceedings, 49th Rencontres de Moriond on Electroweak Interactions and Unified Theories: La Thuile, Italy, March 15-22, 2014*, pp. 75–80, 2014. 1405.4907.

[279] C. Bobeth and U. Haisch, *New Physics in Γ_{12}^s: $(\bar{s}b)(\bar{\tau}\tau)$ Operators*, *Acta Phys. Polon.* **B44** (2013) 127–176, [1109.1826].

[280] J. F. Kamenik, S. Monteil, A. Semkiv and L. V. Silva, *Lepton polarization asymmetries in rare semi-tauonic $b \to s$ exclusive decays at FCC-ee*, *Eur. Phys. J.* **C77** (2017) 701, [1705.11106].

[281] J. L. Hewett, *Tau polarization asymmetry in B —¿ X(s) tau+ tau-*, *Phys. Rev.* **D53** (1996) 4964–4969, [hep-ph/9506289].

[282] HPQCD collaboration, C. Bouchard, G. P. Lepage, C. Monahan, H. Na and J. Shigemitsu, *Standard Model Predictions for $B \to K\ell^+\ell^-$ with Form Factors from Lattice QCD*, *Phys. Rev. Lett.* **111** (2013) 162002, [1306.0434].

[283] C. Bobeth, U. Haisch, A. Lenz, B. Pecjak and G. Tetlalmatzi-Xolocotzi, *On new physics in $\Delta\Gamma_d$*, *JHEP* **06** (2014) 040, [1404.2531].

[284] A. Lenz, U. Nierste, J. Charles, S. Descotes-Genon, A. Jantsch, C. Kaufhold et al., *Anatomy of New Physics in $B - \bar{B}$ mixing*, *Phys. Rev.* **D83** (2011) 036004, [1008.1593].

[285] A. Lenz, U. Nierste, J. Charles, S. Descotes-Genon, H. Lacker, S. Monteil et al., *Constraints on new physics in $B - \bar{B}$ mixing in the light of recent LHCb data*, *Phys. Rev.* **D86** (2012) 033008, [1203.0238].

[286] R. Alonso, B. Grinstein and J. Martin Camalich, *$SU(2) \times U(1)$ gauge invariance and the shape of new physics in rare B decays*, *Phys. Rev. Lett.* **113** (2014) 241802, [1407.7044].

[287] J. Aebischer, A. Crivellin, M. Fael and C. Greub, *Matching of gauge invariant dimension-six operators for $b \to s$ and $b \to c$ transitions*, *JHEP* **05** (2016) 037, [1512.02830].

[288] D. Bečirević, S. Fajfer, N. Košnik and O. Sumensari, *Leptoquark model to explain the B-physics anomalies, R_K and R_D*, *Phys. Rev.* **D94** (2016) 115021, [1608.08501].

[289] W. Buchmuller and D. Wyler, *Effective Lagrangian Analysis of New Interactions and Flavor Conservation*, *Nucl. Phys.* **B268** (1986) 621–653.

[290] D. Buttazzo, A. Greljo, G. Isidori and D. Marzocca, *B-physics anomalies: a guide to combined explanations*, *JHEP* **11** (2017) 044, [1706.07808].

[291] J. Charles et al., *Current status of the Standard Model CKM fit and constraints on $\Delta F = 2$ New Physics*, *Phys. Rev.* **D91** (2015) 073007, [1501.05013].

[292] S. Descotes-Genon and P. Koppenburg, *The CKM Parameters*, *Ann. Rev. Nucl. Part. Sci.* **67** (2017) 97–127, [1702.08834].

[293] A. J. Buras, J. Girrbach-Noe, C. Niehoff and D. M. Straub, *$B \to K^{(*)}\nu\bar{\nu}$ decays in the Standard Model and beyond*, *JHEP* **02** (2015) 184, [1409.4557].

[294] R. Barbieri, C. W. Murphy and F. Senia, *B-decay Anomalies in a Composite Leptoquark Model*, *Eur. Phys. J.* **C77** (2017) 8, [1611.04930].

[295] N. Cabibbo and A. Maksymowicz, *Angular correlations in K_{e4} decays and determination of low-energy $\pi - \pi$ phase shifts*, *Phys. Rev.* **137** (Jan, 1965) B438–B443.